Iron Complexes for Hydrogen Activation and Catalytic Hydrogenation

THÈSE N° 6776 (2015)

PRÉSENTÉE LE 25 SEPTEMBRE 2015
À LA FACULTÉ DES SCIENCES DE BASE
LABORATOIRE DE SYNTHÈSE ET DE CATALYSE INORGANIQUE
PROGRAMME DOCTORAL EN CHIMIE ET GÉNIE CHIMIQUE

ÉCOLE POLYTECHNIQUE FÉDÉRALE DE LAUSANNE

POUR L'OBTENTION DU GRADE DE DOCTEUR ÈS SCIENCES

PAR

Simona MAZZA

acceptée sur proposition du jury:

Prof. K. Severin, président du jury
Prof. X. Hu, directeur de thèse
Prof. A. Mezzetti, rapporteur
Dr Ph. Dupau, rapporteur
Dr M. Mazzanti, rapporteuse

"Imagination is more important than knowledge.
Knowledge is limited.
Imagination encircles the world"
A. Einstein

Abstract

The activation of molecular hydrogen (H_2) via either homolytic or heterolytic cleavage is one of the most attractive subjects in sustainable chemistry. So far the cleavage of H-H bond is commonly achieved by using transition metal complexes based on precious metals such as ruthenium, rhodium, platinum, palladium or iridium. Due to the low availability and price issues in the last decades an unceasing amount of research has been carried out in order to find more attractive substitute metals. Looking at the first-row transition metals, iron is offering a good alternative being non-toxic, abundant, inexpensive and eco-friendly.

Inspired by Nature several groups have developed structural and functional iron complexes mimicking the active site of the iron-hydrogenases, which show high reactivity in the H_2 cleavage. Usually pendant bases have been incorporated onto families of Fe complexes in order to achieve active systems. In the view of these recent developments, in chapter two, we investigated the possibility of synthesizing novel iron (II) complexes bearing an amine internal base and providing an open site for substrate binding as catalysts for H_2 activation. Pentacoordinated Fe(II) low spin complexes [(^{Ph}PNP)Fe(CO)(bdt)] (**1**), [(^{Ph}PNP)Fe-(CO)(Nbt)] (**4**), [(^{Cy}PNP)Fe(CO)(Nbt)] (**5**), [(dppe)Fe(CO)(Nbt)] (**6**) and the paramagnetic complex [(^{Cy}PNP)FeCl$_2$] (**10**) have been synthesized and fully characterised. Unfortunately, when these complexes were tested as catalysts for hydrogenation reaction of a wide range of unsaturated substrates, no appreciable reactivity was observed. Same behaviour was observed in the case of complexes [(^{Cy}PNP)Fe(CO)(Cp)] (**11**) and [(^{Cy}PNP)Fe(CH$_3$CN)(Cp)] (**12**) where the Cp ligand was installed in order to modulate the electronic and steric properties on the iron center.

In chapter three, a new class of well-defined iron pincer complexes is reported. Several Fe(II) complexes supported by a 2,6-bis(phosphinito)pyridine ligand (PONOP) have been synthesized and fully characterised. In particular, the Fe-hydride complexes [(^{iPr}PONOP)-Fe(CO)(H)Br] (**14**) and [(^{iPr}PONOP)Fe(CO)(H)(CH$_3$CN)](OTf) (**15**) could activate H_2 at room temperature. Moreover, complexes **14** and **15** served as catalysts for the selective hydrogenation of aldehydes at room temperature. In presence of sodium formate as hydrogen donor, **14** and **15** showed an excellent reactivity in hydrogen transfer reaction of aldehydes. The mechanism of hydrogen activation and hydrogenation is discussed based on the observed reactivity of iron complexes. The feature of being chemoselective towards

aldehydes and a broad functional-group tolerance make these iron-hydride systems remarkable in the class of the earth-abundant-metal hydrogenation catalysts.

Chapter four is dedicated to the tuning of the Fe-PONOP systems reported in chapter three in order to synthesize similar iron(II) complexes exhibiting enhanced reactivity for H_2 activation and hydrogenation of unsaturated substrates. As first attempt, complexes [(^{Cy}PONOP)Fe(CO)Br$_2$] (**22**) and the analogous chloride [(^{Cy}PONOP)Fe(CO)Cl$_2$] (**23**) bearing the stronger donor ^{Cy}PONOP ligand were synthesized and tested as catalysts for hydrogenation reaction, but none of the substrates employed was reduced. As second attempt, the CO ligand was substituted with the better donor ligand *tert*-butyl isocyanide in presence of ^{iPr}PONOP as pincer ligand. Several Fe-PONOP complexes were synthesized and fully characterized. In particular the Fe-hydride complex [(^{iPr}PONOP)Fe(^{t}BuNC)(H)Br] (**25**) exhibited reactivity towards hydrogenation of aldehydes under the same reaction conditions reported for **14**. No reaction was observed in presence of acetophenone, cyclohexene and 1-decene demonstrating that, although spectroscopically different, **25** did not exhibit enhanced reactivity relative to **14**.

Résumé

L'activation d'hydrogène moléculaire (H_2) via un clivage homolytique ou un clivage hétérolytique est l'un des sujets les plus attractifs de la chimie durable. Jusqu'à présent, le clivage de la liaison H-H est communément réalisé par l'utilisation de complexes basés sur des métaux de transition tels que le ruthénium, le rhodium, le platine, le palladium ou l'iridium. A cause de leur faible disponibilité et de problèmes de coût ces dernières décennies, d'incessantes recherches ont été menées afin de trouver des métaux de substitution plus attractifs. Parmi les métaux de transition de la première rangée, le fer offre une bonne alternative tant par sa non-toxicité, son abondance, son bas coût que par son caractère écologique.

S'inspirant de la nature, plusieurs groupes de recherche ont développé des complexes de fer mimant par leur structure et par leur fonction le site actif des hydrogénases à fer, qui font preuve d'une réactivité élevée pour le clivage de H_2. Des bases pendantes ont été généralement incorporées dans les familles de ces complexes de fer afin d'obtenir des systèmes actifs. Dans l'optique de ces récents développements, le chapitre 2 présente les recherches sur la possibilité de synthétiser de nouveaux complexes de fer (II) portant une base amine interne et fournissant un site libre pour lier les substrats en tant que catalyseurs d'activation de H_2. Les complexes pentacoordinés de Fe(II) bas spin [(^{Ph}PNP)Fe(CO)(bdt)] (**1**), [(^{Ph}PNP)Fe(CO)(Nbt)] (**4**), [(^{Cy}PNP)Fe(CO)(Nbt)] (**5**), [(dppe)Fe(CO)(Nbt)] (**6**) et le complexe paramagnétique [(^{Cy}PNP)FeCl$_2$] (**10**) ont été synthétisés et entièrement caractérisés. Malheureusement, lorsque ces complexes ont été testés comme catalyseur des réactions d'hydrogénation d'une grande variété de substrats insaturés, aucune réactivité appréciable n'a été observée. Le même comportement a été observé dans le cas des complexes [(^{Cy}PNP)Fe(CO)(Cp)] (**11**) et [(^{Cy}PNP)Fe(CH$_3$CN)(Cp)] (**12**) dans lesquels le ligand Cp a été placé afin de moduler les propriétés électroniques et stériques du centre métallique fer.

Dans le chapitre 3, une nouvelle classe de complexes "pincer" de fer bien définis est exposée. Plusieurs complexes de Fe(II) supportés par un ligand 2,6-bis(phosphinito)pyridine (PONOP) ont été synthétisés et entièrement caractérisés. En particulier, les complexes d'hydrure de fer [(^{iPr}PONOP)-Fe(CO)(H)Br] (**14**) et [(^{iPr}PONOP)Fe(CO)(H)(CH$_3$CN)](OTf) (**15**) peuvent activer H_2 à température ambiante. De plus, les complexes **14** et **15** ont servi comme catalyseur pour l'hydrogénation sélective des aldéhydes à température ambiante. En présence de formate de sodium comme donneur d'hydrogène, **14** et **15** ont montré une

excellente réactivité pour la réaction de hydrogénation par transfert des aldéhydes. Le mécanisme d'activation de l'hydrogène et d'hydrogénation est discuté en se basant sur la réactivité observée de ces complexes de fer. Le caractère chémiosélectif envers les aldéhydes et une grande tolérance aux groupes fonctionnels rendent ces systèmes d'hydrure de fer remarquables dans la classe des catalyseurs d'hydrogénation à base de métaux abondants sur Terre.

Le chapitre 4 est consacré à la mise au point de systèmes Fe-PONOP décrits au chapitre 3 afin de synthétiser des complexes de fer (II) similaires exhibant une réactivité améliorée pour l'activation de H_2 et l'hydrogénation de substrats insaturés. Comme premiers essais, les complexes $[(^{Cy}PONOP)Fe(CO)Br_2]$ (**22**) et l'analogue chloré $[(^{Cy}PONOP)Fe(CO)Cl_2]$ (**23**) portant le ligand $^{Cy}PONOP$ plus fortement donneur ont été synthétisés et testés comme catalyseurs pour la réaction d'hydrogénation mais aucun des substrats employés n'a été réduits. En deuxièmes essais, le ligand CO a été substitué par le ligand *tert*-butyle isocyanide, meilleur donneur, en présence du ligand "pincer" $^{iPr}PONOP$. Plusieurs complexes Fe-PONOP ont été synthétisés et entièrement caractérisés. En particulier, le complexe d'hydrure de fer $[(^{iPr}PONOP)Fe(^{t}BuNC)(H)Br]$ (**25**) a montré une certaine réactivité pour l'hydrogénation des aldéhydes sous les mêmes conditions rapportées pour le complexe **14**. Aucune réaction n'a été observée en présence d'acétophénone, de cyclohexène et de 1-décène, ce qui démontre que le complexe **25**, bien que différent par analyse spectroscopique, ne fait pas preuve d'une réactivité améliorée par rapport au complexe **14**.

Mots-clés: activation de l'hydrogène, réaction d'hydrogénation, réaction de transfert d'hydrogène, complexe d'hydrure de fer, hydrogénase, ligands "pincer", catalyse homogène, aldéhyde

Riassunto

L'attivazione di idrogeno molecolare (H_2) tramite sia scissione omolitica che eterolitica è uno dei temi più affascinanti della chimica verde. Normalmente, la scissione del legame H-H avviene utilizzando catalizzatori a base di metalli di transizione come rutenio, rodio, platino, palladio o iridio che sono considerati metalli preziosi. A causa della loro scarsa disponibilità e prezzi piuttosto alti, negli ultimi decenni la ricerca si è concentrata nell'individuazione di metalli alternativi. Soffermandosi sui metalli della prima fila di transizione della tavola periodica, il ferro offre una buona alternativa essendo un metallo non tossico, abbondante, economico ed ecologico.

Numerosi gruppi di ricerca, ispirandosi alla Natura, hanno sviluppato complessi di ferro sia strutturali che funzionali in grado di mimare il sito attivo dell'enzima ferro-idrogenasi esibendo una elevata reattività nella scissione dell' H_2. Solitamente la presenza di basi "pendenti" incorporate all'interno dei complessi di Fe è fondamentale per l'ottenimento di sistemi reattivi. Alla luce di questi recenti sviluppi, nel secondo capitolo si è cercato di sintetizzare complessi di ferro (II) che presentassero come base interna un' ammina e che fornissero un sito di coordinazione vacante per l'approccio del substrato fungendo da catalizzatori per l'attivazione dell' H_2. I complessi pentacoordinati di Fe (II) a basso spin [(^{Ph}PNP)Fe(CO)(bdt)] (**1**), [(^{Ph}PNP)Fe(CO)(Nbt)] (**4**), [(^{Cy}PNP)Fe(CO)(Nbt)] (**5**), [(dppe)Fe-(CO)Nbt)] (**6**) e il complesso paramagnetico [(^{Cy}PNP)FeCl$_2$] (**10**) sono stati sintetizzati e caratterizzati. Sfortunatamente, quando testati come catalizzatori per l'idrogenazione di una vasta gamma di substrati insaturi, nessuno di questi complessi si è rivelato attivo. Lo stesso comportamento è stato osservato per i complessi [(^{Cy}PNP)Fe(CO)(Cp)] (**11**) e [(^{Cy}PNP)Fe-(CH$_3$CN)(Cp)] (**12**) in cui il legante Cp è stato aggiunto in modo da modulare sia le proprietà elettroniche che steriche del centro metallico.

Nel terzo capitolo, viene riportata una nuova classe di complessi "pincer" di ferro. Diversi complessi di Fe (II) supportati dal legante 2,6-bis(fosfino)piridina (PONOP) sono stati sintetizzati e caratterizzati. In particolare, i complessi Fe-idruro [(^{iPr}PONOP)Fe(CO)(H)Br] (**14**) e [(^{iPr}PONOP)Fe(CO)(H)(CH$_3$CN)](OTf) (**15**) si sono rilevati efficienti catalizzatori sia per l'attivazione dell'H_2 che per l'idrogenazione selettiva delle aldeidi a temperatura ambiente. In presenza di formiato di sodio come donatore di idrogeno, **14** e **15** si sono rivelati attivi nella reazione di trasferimento di idrogeno di aldeidi. I meccanismi di attivazione dell' idrogeno e della reazione di idrogenazione sono stati discussi in base alla reattività osservata

dai complessi di ferro. La caratteristica di essere chemioselettivi nei confronti delle aldeidi assieme ad un'ampia tolleranza verso diversi gruppi funzionali rendono questi sistemi ferro-idruro di notevole importanza nella famiglia di catalizzatori per la reazione di idrogenazione a base di metalli abbondanti sulla Terra.

Il quarto capitolo è dedicato alla messa a punto dei sistemi di Fe-PONOP riportati nel capitolo tre con l'obiettivo di sintetizzare complessi di ferro (II) simili ma che presentassero allo stesso tempo una migliore reattività sia nell' attivazione dell' H_2 che nella reazione di idrogenazione di substrati insaturi diversi dalle aldeidi. Come primo tentativo, il complesso [(^{Cy}PONOP)Fe(CO)Br$_2$] (**22**) e il cloruro analogo [(^{Cy}PONOP)Fe(CO)Cl$_2$] (**23**) avente il legante ^{Cy}PONOP che è un donatore piu' forte, sono stati sintetizzati e testati come catalizzatori nella reazione di idrogenazione anche se nessuno dei substrati utilizzati è stato ridotto. Come secondo tentativo, il ligante CO è stato sostituito con il ligante *tert*-butyl isocyanide che è noto esser un miglior donatore, in presenza di ^{iPr}PONOP come legante pincer. In particolare il complesso Fe-idruro [(^{iPr}PONOP)Fe(^{t}BuNC)(H)Br] (**25**) si è dimostrato reattivo nei confornti della reazione di idrogenazione delle aldeidi utilizzando le condizioni di reazione già riportate per **14**. Sfortunatamente, nessuna reattività è stata osservata in presenza di substrati quali acetofenone, cicloesene e 1-decene, dimostrando che anche se spettroscopicamente diverso, **25** non esibisce una migliore reattività rispetto a **14**.

Parole chiave: attivazione di idrogeno, reazione di idrogenazione, reazione di trasferimento di idrogeno, complessi ferro-idruro, idrogenasi, leganti "pincer", catalisi omogenea, aldeidi.

Symbols and abbrevation

δ	chemical shift
λ	wavelenght
br	broad
bdt	1,2-benzenedithiol
Cl_2bdt	3,6-dichloro-1,2-benzenedithiol
Nbt	2-aminobenzenethiol
^{Me}Nbt	2-dimethyl-aminobenzenethiol
Bn	benzyl
Bu	butyl
calcd	calculated
cat	catalyst
CH_2Cl_2	dichloromethane
cod	1,5- cyclooctadiene
Cy	cyclohexyl
Cp	Cyclopentadienil
D- or d	deuterated
d	doublet
dba	dibenzylideneacetone
dd	doublet of doublets
DBU	1,8-diazabicycloundec-7-ene
DFT	density functional theory
dq	doublet of quartets
dt	doublet of triplets
e.e	enantiomeric excess
equiv.	equivalent
ESI	electrospray ionization
Et_3N	triethylamine
Et	ethyl
fac	facial
EtOH	ethanol
FID	flame ionization detector
GC	gas chromatography

h	hour
^{i}Bu	iso-butyl
^{i}Pr	iso-propyl
Me	methyl
MeOH	methanol
MHz	mega-hertz
mer	meridional
MS	mass spectrometry
n-BuLi	normal-Butyllithium
n-pentane	normal pentane
NaOMe	sodium methoxide
HCOONa	sodium formate
NMR	nuclear magnetic resonance
O^{t}Bu	*tert*-butoxide
O^{i}Pr	*iso*-propoxide
OAc	acetate
OTf	triflate
Ph	phenyl
PPh$_3$	triphenylphosphine
dppp	1,3-bis(diphenylphosphino)propane
^{Ph}PS	2-(diphenyl-phosphino)benzenethiol
r.t.	room temperature
s	singlet
t	triplet
T	temperature
^{t}Bu	*tert*-butyl
THF	tetrahydrofuran
TMEDA	tetramethylethylenediamine
TMS	trimethylsilyl
TON	turnover number
TOF	turnover frequency
^{Cy}PONOP	2,6-bis(dicyclohexylphosphinito) pyridine
^{Et}PONOP	2,6-bis(diethylphosphinito) pyridine

^{iPr}PONOP   2,6-bis(di*iso*-propylphosphinito) pyridine

^{tBu}PONOP   2,6-bis(di*tert*-butyl phosphinito)

Units and Prefixes

Å	angstrom
º	degree
atm	atmosphere
g	gram
h	hour
J	joule
K	Kelvin
l	liter
M	molar
mol	mole
s	second
k	kilo- (10^3)
c	centi- (10^{-2})
m	mili- (10^{-3})
μ	micro- (10^{-6})

List of Complexes

1	[(^{Ph}PNP)Fe(CO)(Cl$_2$bdt)]
2	[(^{Ph}PNP)Fe(CO)(bdt)]
3	[(dppp)Fe(CO)(Cl$_2$bdt)]
4	[(^{Ph}PNP)Fe(CO)(Nbt)]
5	[(^{Cy}PNP)Fe(CO)(Nbt)]
6	[(dppe)Fe(CO)(Nbt)]
7	[Fe(^{Me}Nbt)$_2$]$_2$
8	[Fe(CO)$_2$()]
9	[Fe(^{Ph}PS)$_2$]$_3$
10	[(^{Cy}PNP)FeCl$_2$]
11	[(^{Cy}PNP)Fe(CO)(Cp)](FeCl$_4$)
12	[(^{Cy}PNP)Fe(CH$_3$CN)(Cp)](BAr$^F_4$)
13	[(^{iPr}PONOP)Fe(CO)Br$_2$]
14	[(^{iPr}PONOP)Fe(CO)(H)Br]
14-D	[(^{iPr}PONOP)Fe(CO)(D)Br]
15	[(^{iPr}PONOP)Fe(CO)(H)(CH$_3$CN)](OTf)
16	[(^{iPr}PONOP)Fe(CO)(H)(η$_2$-H$_2$)](Br)
16-D	[(^{iPr}PONOP)Fe(CO)(H)(η$_2$-D$_2$)](Br)
17	[(^{iPr}PONOP)Fe(CO)(D)(η$_2$-HD)](Br)
18	[(^{iPr}PONOP)Fe(CO)(H)(η$_2$-HD)](Br)
19	[(^{iPr}PONOP)Fe(CO)(H)$_2$]
20	[(^{iPr}PONOP)Fe(CO)(H)]$^+$
21	[(^{iPr}PONOP)Fe(H)(CO)(OOCH)]
22	[(^{Cy}PONOP)Fe(CO)Br$_2$]
23	[(^{Cy}PONOP)Fe(CO)Cl$_2$]
24	[(^{iPr}PONOP)Fe(^{t}BuNC)Br$_2$]
25	[(^{iPr}PONOP)Fe(^{t}BuNC)(H)Br]
27	[Fe(CO)$_3$(^{iPr}PON)]
29	[(^{iPr}PONOP)FeBr$_2$]
30	[(^{Cy}PONOP)FeBr$_2$]
31	[(^{iPr}PONOP)Fe(CO)(H)(PEt$_3$)]

Table of Contents

Chapter 1
Introduction

1.1 Industrial processes involving hydrogen

Hydrogen production is a large and growing industry. Globally, around 40-50 million tons of hydrogen are produced every year with an estimated consumption of about 868 billion cubic meters in 2018[1-3]. Nearly 96% of all hydrogen is derived from fossil fuels, with natural gas being by far the most frequently used with an estimated 49%, followed by liquid hydrocarbons at 29%, coal at 18%, and electrolysis and other by-product sources of hydrogen with 4% (SRI Consulting[4]).

Around half of the hydrogen produced is used for the production of ammonia via Haber process, thus in the production of fertilizers, around one fifth is used for hydrocracking in petroleum refining, with the balance used to make methanol and other industrial applications such as the cleaning of fossil fuels via hydrodesulfurization (Fig 1.1).
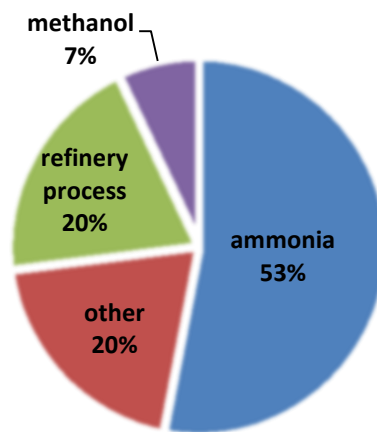
Fig 1.1: Hydrogen usage in percentage.

In the coming years, hydrogen itself is considered as a promising energy carrier. The term "hydrogen economy" refers to the vision of using hydrogen as a low-carbon energy source replacing, for example, gasoline as transport fuel. If generated from renewable sources, hydrogen can be considered a clean fuel because when burning it does not produce carbon dioxide but only water as byproduct. Yet, there are major problems to be overcome before it can be used as an alternative fuel such as its manufacture, storage and distribution.

1.1.1 Ammonia production: the Haber process

The industrial synthesis of ammonia from nitrogen and hydrogen has been considered of great importance to the modern world. Ammonia was first manufactured using the Haber process on an industrial scale in 1913 in the BASF's Oppau plant in Germany (Fig. 1.2).

The Haber process nowadays produces 450 million tonnes of nitrogen fertilizer per year, mostly in the form of ammonia, ammonium nitrate and urea[5]. Moreover, 3-5% of the world's natural gas production is consumed in the Haber process.
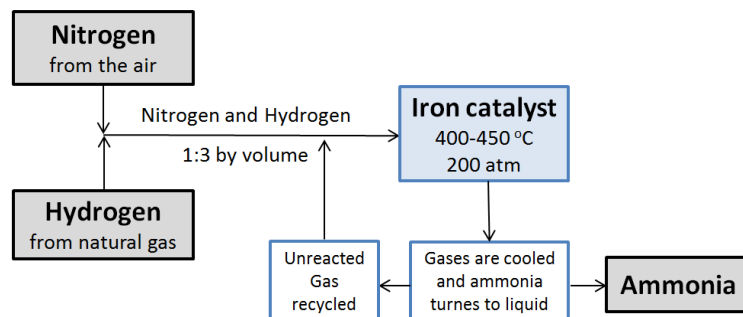
Fig 1.2: Simplified flow scheme of the Haber process.

The reaction is typically conducted at 200-250 bar and 400-500 ^{o}C, with the gases passing over four beds of catalyst and reaching 15% of conversion on each passage. The most popular catalyst used in the process is a highly porous material made of iron with a small percentage of oxides of calcium, potassium, silicon and aluminium[6].

1.1.2 Methanol production

Methanol is manufactured from synthesis gas, a mixture of carbon monoxide and hydrogen. With 65 million tonnes produced worldwide in 2013[7], about 30 % of methanol is converted to formaldehyde therefore employed in the production of a variety of plastics. Polymers such as polyesters and polymethyl methacrylate use methanol as the original feedstock. Moreover, methanol is now the principal source for the manufacture of acetic acid (Fig 1.3).
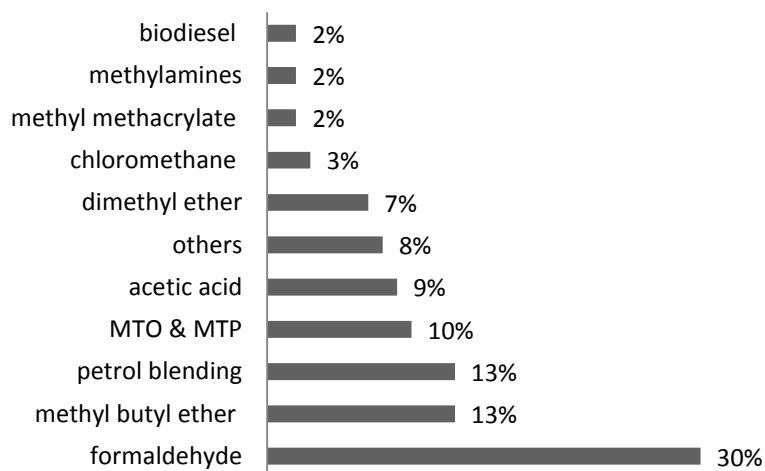
Fig 1.3: Uses of methanol (MTO "methanol to olefins", MTP "methanol to propene")

On industrial scale methanol is produced in two steps[8-10]. In the first step the feedstock natural gas is converted into a synthesis gas stream composed of CO, CO_2, H_2O and hydrogen by a catalytic reforming of feed gas and steam. In the second step, the gaseous mixture produced is converted into methanol by passing through a catalyst bed. If an external source of CO_2 is available, the hydrogen in excess is converted in additional methanol (Scheme 1.1).

$$1^{st} \text{ step:} \quad 2\,CH_4 + 3\,H_2O \longrightarrow CO + CO_2 + 7\,H_2 \text{ (Synthesis Gas)}$$

$$2^{nd} \text{ step:} \quad CO + CO_2 + 7\,H_2 \longrightarrow 2\,\mathbf{CH_3OH} + 2\,H_2 + H_2O$$
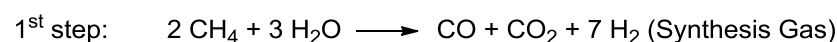
Scheme 1.1: Synthesis of methanol on industrial scale

The first industrial production of methanol employed as catalytic system a mixture of ZnO and Cr_2O_3 used at 300-450° C and 250-350 bar, highly stable to the sulphur and chlorine contaminants present in synthesis gas. However, due to the extreme conditions of pressure and temperature required, the last methanol plant based on this process closed in the mid-1980s. A low-pressure catalyst based on Cu-ZnO thermally stabilized with alumina was developed in 1966 showing high selectivity and stability[11]. Nowadays, all commercially available catalytic systems are based in Cu-ZnO-Al_2O_3 or $Cr_2O_3$with different additives such as zinc, chromium, magnesium and rare earth metals[12,13].

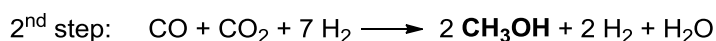Possible alternative routes for the synthesis of methanol involve the use of either methane[14-16] or CO_2[17-19] as starting material and both ways are currently active fields of research (methanol economy)[20]. In the latter case, the required hydrogen can be obtained from the electrolysis of water or, alternatively direct aqueous electrochemical or photochemical reduction of CO_2 is also feasible. However, several challenges are still present: difficult conversion of methane to methanol owing to the strong methane CH bond (105 Kcal/mol) and the ease of over-oxidation of methanol, life-time, stability, resistance to poisoning and optimization of the catalysts employed. Because of these drawbacks so far none of these synthetic routes has been scaled up in industrial size.

1.1.3 Hydrocracking

Hydrocracking is an established and reliable method for transforming heavy aromatic feedstock into high-valued saturated hydrocarbons. As of 2014, the feedstock processing capacity of the hydrocrackers in the United States was 2'208'000 barrels per day[21], with a hydrocracker consuming 140 tons of hydrogen a day[22]. In general, the hydrocracking process

depends largely on the nature of the feedstock and the relative rates of the two competing reactions involved: hydrogenation and cracking.

Heavy oil fractions recovered from the crude are mixed with hydrogen at high pressure (35-200 bar) and temperature (260-425^0 C) inside a reactor filled with the catalyst. The heavy feed is broken down or cracked to produce naphtha, kerosene ready to be used as jet fuel and crude oils blended together to make diesel (Fig. 1.4).
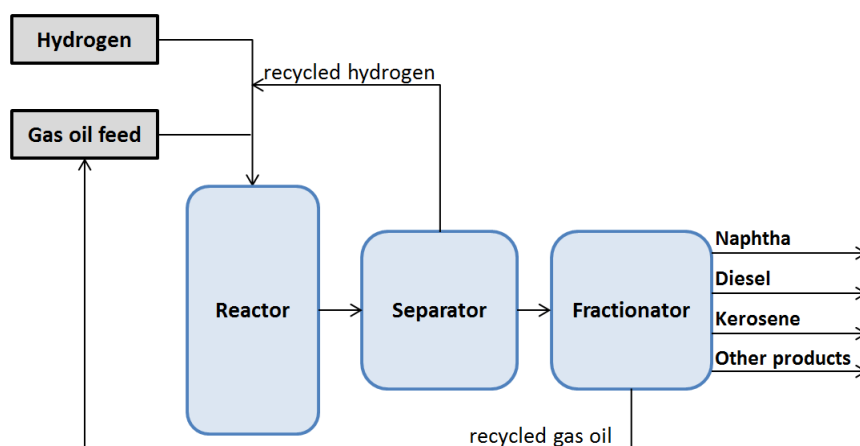
Fig 1.4: Overview of the hydrocracking process

Most of the catalytic systems used in hydrocracking are bifunctional zeolite-based catalyst comprising a hydrogenation component and an acidic support for hydrocarbon absorption[23,24]. The supports mentioned in literature are mainly made of silica with different additive such as Al_2O_3, ZrO_2, B_2O_3 or TiO_2. The hydrogenation component is a metal such as cobalt, nickel, vanadium, molybdenum or a combination of metals. An increase of the performance of the catalyst can be achieved by altering the acidic function and/or the hydrogenation function in order to improve the activity whilst maintaining selectivity or vice versa.

1.1.4 Hydrodesulfurization

Hydrodesulfurization (HDS) is a well-established industrial catalytic process used to remove sulphur-containing impurities from refined petroleum products (gasoline, jet fuel, diesel) and heavy oils[24,25] (Scheme 1.2). The sulphur-contaminants have a severe environmental impact, being the precursors of the highly toxic sulphur dioxide produced during the combustion of the petroleum-based fuels in automotive vehicles. Regulations have been introduced in many countries to reduce the sulphur content in fuels and the global trend

for sulphur content in diesel fuels is 10-15 ppm[26,27]. Moreover, in naphtha's pre-treating process the purpose of HDS is to avoid the poisoning of sulphur-sensitive metal catalysts used in reforming.

Hydrodesulfurization

$$\text{"[R-S]"} + H_2 \xrightarrow[\text{300 - 450}^{\circ}\text{ C}]{\text{catalyst}} \text{"[R-H]"} + H_2S$$
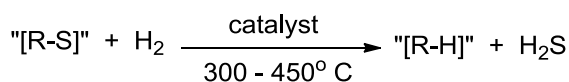
Scheme 1.2: Hydrodesulfurization reaction

In an industrial hydrodesulfurization unit called hydrotreater, the HDS reaction takes place in a fixed-bed reactor at elevated temperatures (300- 400 °C) and pressures (30-130 bar), where the H_2S produced is captured and converted into either sulphur or sulphuric acid. Typical HDS catalysts consist of CoO and MoO_3 or NiO and MoO_3 on alumina carrier[28-30].

Similarly to the HDS, the hydrodenitrogenation (HDN) process is used in industrial scale for the removal of nitrogen-containing impurities from petroleum. These impurities generate undesirable compounds upon combustion (in the specific the pollutant NO_x) and poison the catalyst used in subsequent cracking transformations. If the sulphur content of crude oils usually ranges from 0.2 to 4%, the nitrogen one is approximately 0.1-0.9%[31,32]. Catalytic systems based on $NiMoP/Al_2O_3$ are generally used in HDN processes[33] and this process is concomitant to the HDS one[34,35].

1.1.5 Pharmaceutical and fine chemical industries

The higher complexity of pharmaceuticals and fine chemicals makes catalysis more demanding and process development more expensive than the production of commodity chemicals as the catalytic processes are mainly selectivity driven[36]. In particular, catalytic hydrogenation is a key process in both pharmaceutical and fine chemicals industry replacing chemical reduction methods employing stoichiometric amounts of metal hydride reagents that generate large quantities of waste[37,38]. Usually, the hydrogenation is carried out with heterogeneous catalysts[39], but homogeneous catalysts are also applied for highly selective transformations such as enantioselective reductions[40]. For instance, the growing need for enantiopure chemical products has promoted the development of new catalytic systems and hydrogenation techniques[41], and several significant inventions have been reported in the past years.

The most common hydrogenation reaction performed in industry is probably the stereoselective hydrogenation of C-C double bonds, intensively used in the synthesis of vitamins. *Alpha*-tocopherol is the form of vitamin E that is preferentially absorbed and accumulated in humans[42] and it is the economically most important member of the group of vitamin E compounds due to its biological and antioxidant properties, produced on a scale of >30'000 tonnes per year. One of the key building blocks for the chemical production of synthetic vitamin E is trimethylhydroquinone (TMHQ), that is converted into (all-*rac*)-α-tocopherol by condensation with (all-*rac*)-isophytol[43,44](Scheme 1.3).
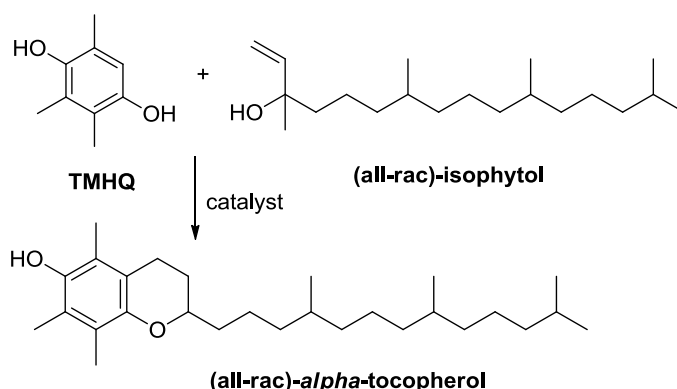
Scheme 1.3: Synthesis of (all-rac)-alpha-tocopherol (vitamin E).

TMHQ is accessible *via* either catalytic hydrogenation of trimethylbenzoquinone (TMBQ) using a palladium on carbon catalyst, or from 2,6-dimethylbenzoquinone (2,6-DMQ), which firstly undergoes hydrogenation, methylation, followed by hydrogenolysis[45] (Scheme 1.4).
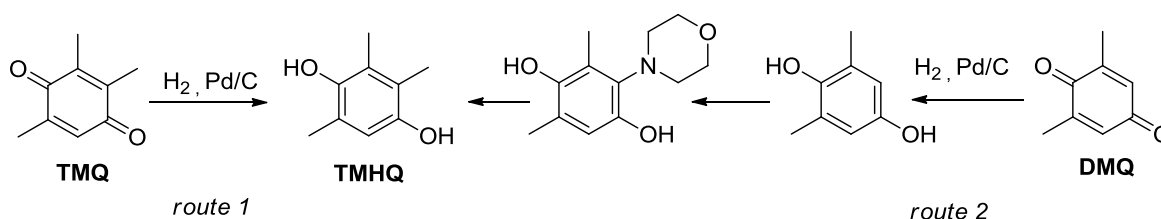
Scheme 1.4: Synthetic routes for the synthesis of TMHQ.

Differently, one of the synthetic routes for the production of isophytol starts from acetone building up the isoprenic side chain by a sequence of C_2 and C_3 elongations, or from the cheap isobutene. In both cases, the C_3-elongation can be carried out by Saucy-Marbet or Carroll reactions and the C_2 elongation by ethynylation or vinylation reactions[36,38]. In such reaction sequences several hydrogenations of C=C bonds are necessary[46,47]. In the past Pd/C

was used as catalyst (temperature of 80 °C and pressure of H_2 <10 bar)[48]; but also Pd and Rh-containing polymers on Al_2O_3 were investigated[49].

For the semi-hydrogenation of carbon-carbon triple bonds to alkenes, one of the most widely used selective catalysts is Lindlar catalyst consisting of palladium deposited on calcium carbonate[48,49]. The selectivity can be enhanced by using suitable catalyst poisons (lead acetate or sulphur) that modify the activity of the metal catalyst. Among several uses, Lindlar catalyst has been exploited by the fragrance industry for the synthesis of linalool and linalyl acetate mainly used as perfume components in soaps, shampoos and lotions due to pleasant floral and spicy odours[36,50] (Scheme 1.5).
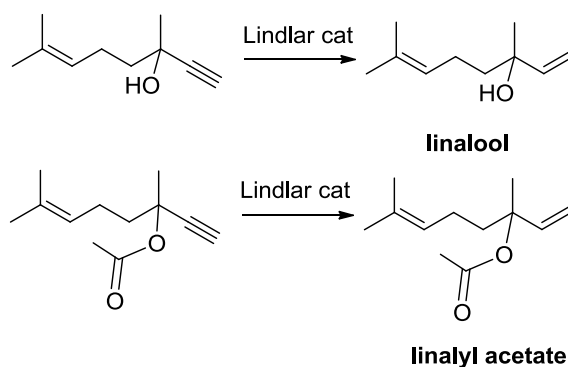
Scheme 1.5: Linalool and linalyl acetate synthesis.

Similarly to the hydrogenation of C-C multiple bonds, the hydrogenolysis of C-X bonds is another interesting reaction for the production of vitamins and fine chemicals. Approximately 100'000 tonnes of vitamin C (L-ascorbic acid) are produced worldwide every year[36]. The procedure employed for the synthesis of vitamin C is the Reichstein process in which D-glucose is firstly fully hydrogenated to D-sorbitol using a Ni-based catalyst. Successively, D-sorbitol is converted to L-ascorbic acid through a series of both chemical and microbiological steps [51-53] (Scheme 1.6).
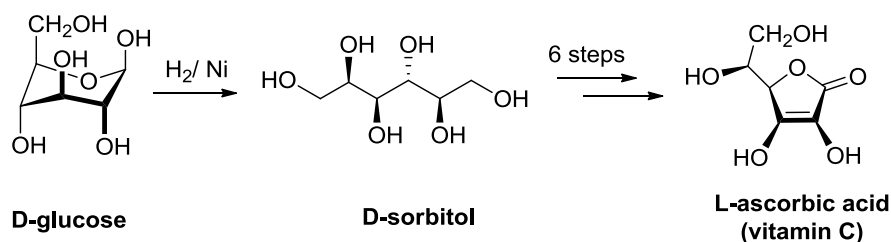
Scheme 1.6: Reduction of D-glucose to D-sorbitol in the Reichstein process for the synthesis of L-ascorbic acid.

The reaction is usually carried out at high pressure and elevated temperature in a batch-mode or continuous process. Under these conditions D-sorbitol is obtained in high selectivity and almost quantitative yield with only minor amounts of D-mannitol and L-iditol as by-products.

In the family of lactones, chiral D-lactone is a key intermediate in the commercially interesting biotin synthesis and it is produced through catalytic asymmetric reduction of the corresponding cyclic anhydride (Scheme 1.7).
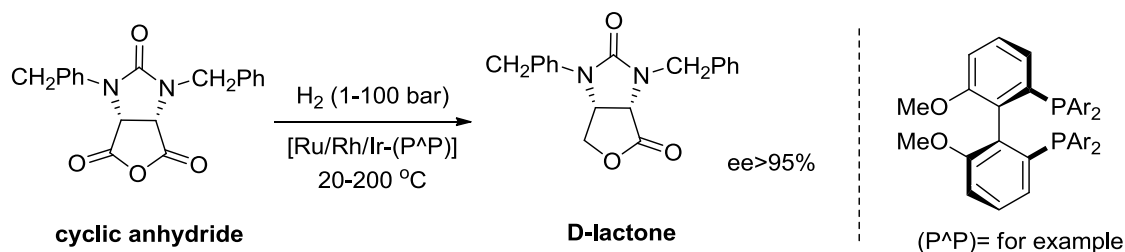
Scheme 1.7: Industrial procedure for the synthesis of D-lactone.

Until 2006, the reduction of the corresponding cyclic anhydride to D-lactone was only possible by using the chiral aluminium-based catalyst (*R*)-BINAL-H[54] in over-stoichiometric amounts. Due to its high price the process definitely was not applicable on larger scale. A successful production of D-lactone on tonne scale was possible only when Ir- and Rh-complexes with atropisomeric ligands were adopted, reaching full conversion and *ee* values of >95%[40].

1.2 Hydrogenation reaction

Catalytic hydrogenation of organic substrates using either molecular hydrogen (H_2) or a different hydride source is one of the most commonly practiced reaction types in organic synthesis. The first catalytic systems used for this purpose were heterogeneous catalysts mainly based on platinum group metals[55]. In 1863 Debus discovered that by passing cyanide vapour mixed with hydrogen over a platinum block, methylamine was produced[56].

Non precious metal catalysts have been developed in this field. Due to its great stability and high catalytic activity in hydrogenation reaction under very mild conditions, the Raney nickel catalyst is today probably the most common used catalyst not only for laboratory uses but also intensively applied in a large number of industrial processes[55]. For

instance benzene is routinely reduced to cyclohexane using Raney nickel in industrial scale for the production of nylon[57].

In the mid 1960's Sir G. Wilkinson and co-workers performed a pioneering work in the field of homogeneous catalysis by developing a new versatile catalytic system based on rhodium[58]. Although homogeneous catalysts had been reported before, the complex $RhCl(PPh_3)_3$ where PPh_3 = triphenylphosphine was the first one that compared in rates with the well-established heterogeneous counterparts showing great reactivity towards the hydrogenation of differently substituted olefines. Moreover, when the phosphine ligands were replaced by chiral ones (e.g. DIPAMP or chiraphos) the catalyst converted prochiral alkenes into alkanes with high enantiomeric excesses[59]. This catalyst is compatible with a variety of functional group such as ketones, ester, carboxylic acid, nitriles, nitro groups and ethers.

In the well-established mechanism, $RhCl(PPh_3)_3$ activates the molecular dihydrogen by oxidative addition yielding a 16-e⁻ dihydride complex. In the next step the dihydride species binds to the olefin with the concomitant loss of solvent or PPh_3 ligand. At this point, one of the hydride undergoes migratory insertion at the double bond (rate determining step) and the alkane is released rapidly by an irreversible reductive elimination step completing the catalytic cycle (Scheme 1.8).
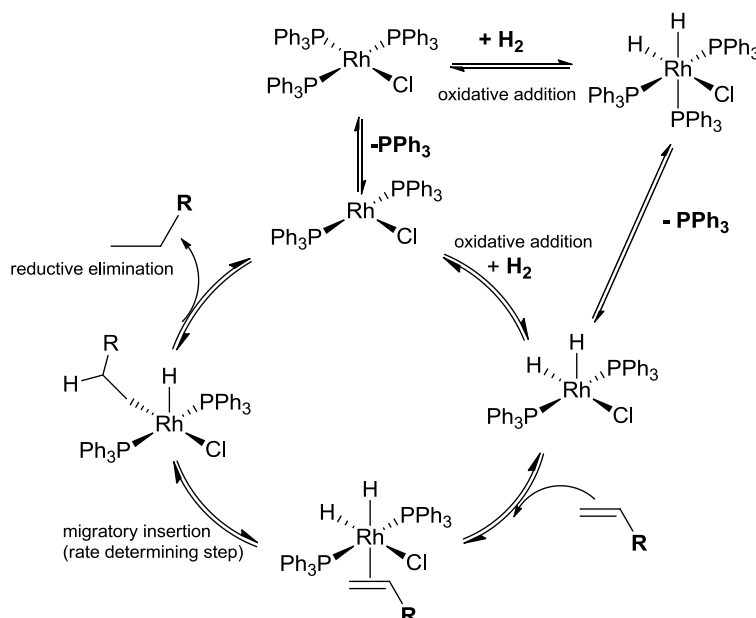
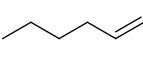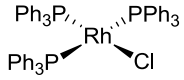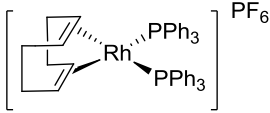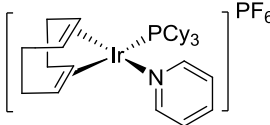**Scheme 1.8:** Mechanism of the hydrogenation of olefines catalysed by Wilkinson's catalyst.

A year later Wilkinson's discoveries, L. Vaska synthesized the well-defined $Ir(CO)(PPh_3)_3$ catalyst, a 16-e⁻ complex able to reversibly activate hydrogen through an

oxidative addition pathway[60]. Noteworthy, the hydrogen adduct [H$_2$IrCl(CO)(PPh$_3$)$_2$] was the first example of isolated and fully characterized hydride species[61].

Along the same lines, Osborn and Schrock made an important observation: cationic Rh(I) complexes of the type [Rh(cod)(PR$_3$)$_2$]$^+$ (with R= Ph, Cy, Me and cod=1,5-cyclooctadiene) were also active catalysts for hydrogenation of olefins. By exposing complex [Rh(cod)(PPh$_3$)$_2$]$^+$ to H$_2$ in polar and coordinating solvents such as THF, acetone and ethanol, the cod ligand dissociated and the corresponding solvate species [RhH$_2$(solv)$_2$(PPh$_3$)$_2$]$^+$ was isolated. In particular, these systems required dissociation of a solvent ligand rather than of a phosphine before the olefin accesses the active site like in Wilkinson's case[62].

Following the previous discoveries, particular importance received the catalytic system developed by Crabtree in the 1970s. The cationic complex [(PCy$_3$)(cod)Ir(py)]PF$_6$ (where py =pyridine) resulted 100 times more active than the previous catalytic systems in the hydrogenation of olefines[63] (Scheme 1.9). Differently from Wilkinson's system that needed to undergo dissociation before the substrate could access the active site, in Crabtree's system the principal species seems to be the complex [Ir(olefin)$_2$(py)(PCy$_3$)]$^+$ that interacts with H$_2$ yielding the corresponding dihydride complex[64].

Scheme 1.9: Rate* of hydrogenation of substituted olefins with different catalytic systems[63]. *In mol of substrate reduced (mol of catalyst)$^{-1}$ h^{-1}.

Decisive for the development of asymmetric hydrogenation of prochiral olefines was the concept of replacing the triphenylphosphine ligand of the Wilkinson's catalyst with a

chiral ligand. Aware of the developments on the synthesis of chiral phosphines[65], Knowles and co-workers focused on bidentate chiral phosphine ligands such as (*R,R*)-1,2-Bis[(2-methoxyphenyl)(phenylphosphino)]ethane (abbr. (*R,R*)-DIPAMP), whose stereogenic center lies directly on the phosphorus atom[66].

To date, this approach has been one of the most impressive achievements in asymmetric synthesis because it demonstrated that a chiral metal complex could effectively transfer chirality to a non-chiral substrate. Moreover, in the past when chiral compounds were needed chemists either adopted tedious biochemical processes or synthesized racemic mixtures that needed to be further separated with laborious techniques.

Knowles and his co-workers found that the complex [Rh(*R,R*)-DIPAMP)(cod)]PF$_6$ hydrogenated in high enantiomeric excess α-acetamidocinnamatic acid, used in the synthesis of *L*-Dopa, an important pharmaceutical for the treatment of Parkinson's disease[67] (Scheme 1.10). In this system the olefin binds to the metal center *via* either its *si*-face or *re*-face prior to the H$_2$ oxidative addition that is the rate determining step of the reaction.
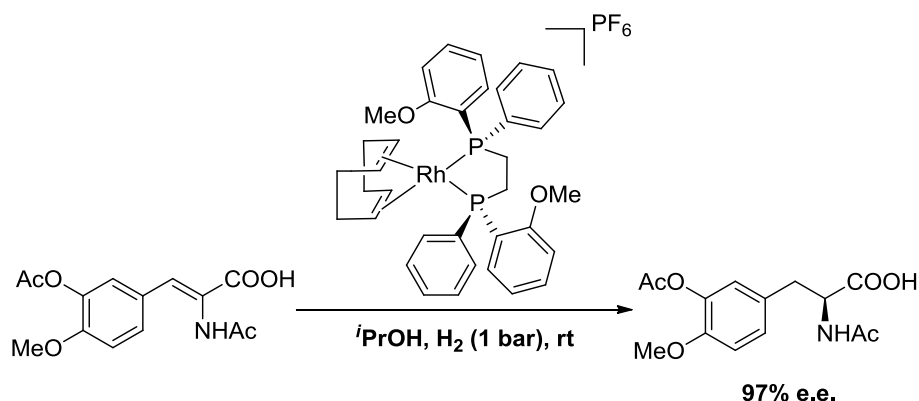
Scheme 1.10: Hydrogenation of α-acetamidocinnamatic acid by [Rh(R,R)-DIPAMP)(cod)]PF$_6$.

A broad variety of bidentate chiral diphosphines have since been synthesized and used in the production of amino acids by hydrogenation of the corresponding enamides[68] (Fig. 1.5).
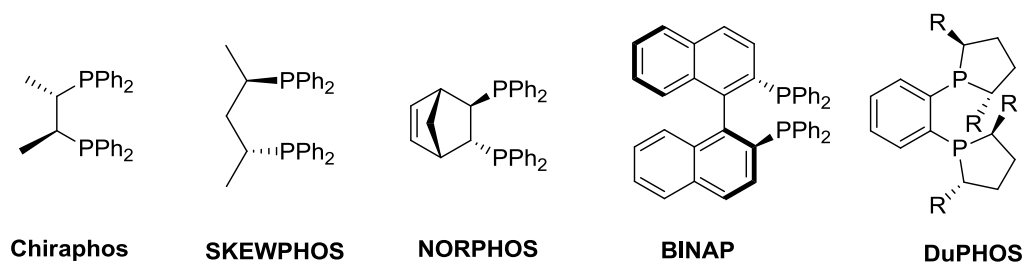
Fig. 1.5: Chiral diphosphine employed in asymmetric hydrogenation of enamides.

Among these diphosphine BINAP is of particular importance being used in the asymmetric hydrogenation of ketones, aldehydes and imines. In the late 1980s, Noyori discovered that ruthenium complexes based on the BINAP ligand were excellent catalysts for the hydrogenation of prochiral β-keto carboxylic esters into optically active β-hydroxy esters in high enantiomeric purity at room temperature (23-30 °C) and at 70-100 bar of H_2[69](Scheme 1.11).
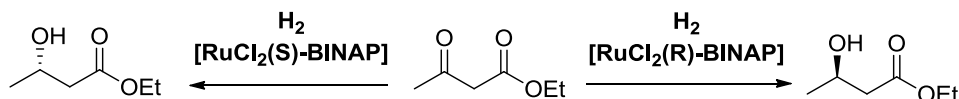
Scheme 1.11: Hydrogenation of β-keto carboxylic esters by using the Ru-BINAP system.

Nowadays, the system $[Ru((S)\text{-BINAP})X_2]_2$ is intensively used in several important industrial applications such as the synthesis of antibacterial levofloxacin from the (*R*)-1,2-propandiol precursor, the synthesis of the antibiotic carbapenem from the (*2S,3R*)-methyl 2-(benzamidomethyl)-3-hydroxybutanoate, and the synthesis of the anti-inflammatory drug naproxen obtained in 97% ee from an a-aryl-acrylic acid[70].

Few years later along the same line of reasoning, Noyori et all. found that hydrogenation in presence of $[RuCl_2(BINAP)(diamine)]$ complex plus an alkaline base provided a great solution in the challenging chemoselective reduction of C=O group in presence of C=C groups[71]. Among various complexes, the $[RuCl_2(xylbinap)(diapen)]$ system catalysed rapid and highly enantioselective hydrogenation of a range of aromatic, heteroaromatic and olefin ketones in presence of KOH as base and isopropanol (*i*PrOH) as solvent[72] (Fig. 1.6). For instance, acetophenone and its derivatives were hydrogenated quantitatively with a ratio substrate/catalyst (S:C) of up to 100000:1 and in 99% ee.

[RuCl₂(xylbinap)(diapen)]
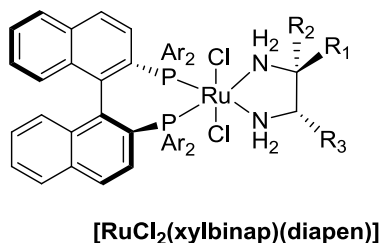
(S,S)- Ru complex Ar = 3,5- $(CH_3)_2C_6H_3$; $R_1 = R_2$= 4-$CH_3OC_6H_4$; R_3 = $(CH_3)_2CH$
(S,SS)-Ru complex Ar = 3,5- $(CH_3)_2C_6H_3$; $R_1 = R_3$= C_6H_5; R_2 = H

Fig. 1.6: Chiral [RuCl₂(xylbinap)(diapen)] systems

This discovery not only increased the substrate scope for asymmetric hydrogenations, but most importantly it was at the origin of the new concept of metal-ligand bifunctional catalysis.

In the BINAP/diamine-Ru catalytic system the hydrogenation of functionalized ketones is catalysed by a six membered cyclic transition state (TS) involving the metal center, the substrate and the ligand. The H-Ru-N-H$_{ax}$ moiety, having a small dihedral angle, forms a 1,4-dipole which fits with the C=O dipole. This TS facilitates the hydrogenation of C=O bonds with higher rate and chemoselectivity compared to the four-center transition state of the BINAP-Ru systems[73,74] (Fig. 1.7).
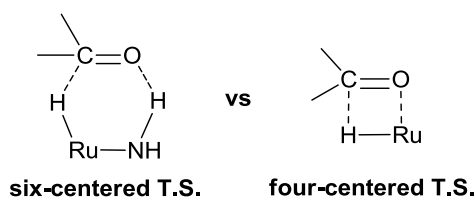
Fig. 1.7: Metal-ligand bifunctional TS (left) and conventional [2+2] TS.

In the metal-ligand bifunctional catalysis the hydridic Ru-H and the protic NH are simultaneously transferred to the C=O group via the six-membered cyclic TS, yielding directly the alcoholic product. In this way, the metal and the ligand participate cooperatively in the bond-forming and bond-breaking processes[75]. In the proposed catalytic cycle, the ketone substrate reacts in an outer sphere mechanism with the 18-e$^-$ RuH species without interacting with the metallic center, through the formation of the six-membered ring TS. Thereafter, the 16-electron Ru-amide complex reacts directly with H$_2$ in a [2+2] manner, or by a stepwise mechanism assisted by an alcohol and a base, to give back the reducing RuH complex (Scheme 1.12).
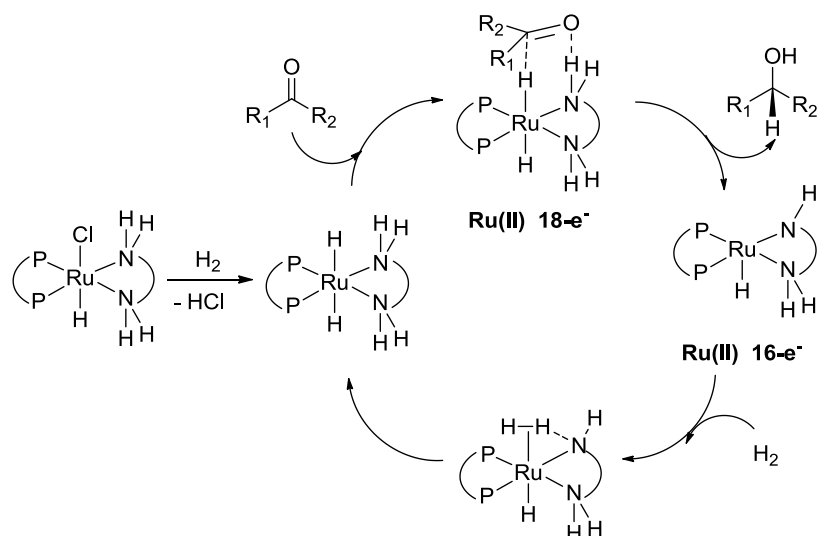
Scheme 1.12: Catalytic cycle of chiral hydrogenation of ketones involving the six-membered TS.

Moreover, both the steric hindrance between the BINAP ligand and the substituent group on the ketone and the chirality of the BINAP/diamine-Ru complex make possible a differentiation of the enantiofaces of the prochiral ketone on the molecular surface of the coordinatively saturated RuH intermediate, allowing an enantioselective reduction of the substrate. The *Si*-TS leading to a (*R*)-alcohol is more favoured over the *Re*-TS which suffers significant nonbounded repulsion between the p-tolyl ring belonging to the BINAP ligand and the phenyl substituent of the ketone[70,75](Scheme 1.13).
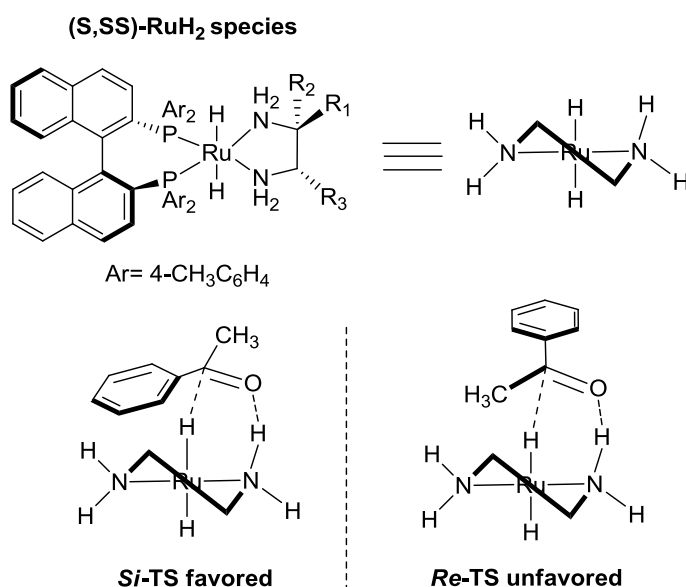
Scheme 1.13: Reducing (S,SS)-RuH$_2$ species and the two diastereomeric transition states in the metal-ligand bifunctional catalysis. Si-TS favoured on the bottom left and the Re-TS unflavoured on the right.

In the light of the previous discoveries, few years later Noyori et all. found that by replacing the diphosphine ligand with a η^6-arene ligand differently substituted, systems such as $[RuCl((R,R)\text{-}or(S,S)\text{-}YCH(C_6H_5)CH(C_6H_5)NH_2)(\eta^6\text{-}arene)]$ (Y=O or NTs) and their analogous ones catalysed asymmetric transfer hydrogenation of aromatic and acetylenic carbonyl compounds yielding the corresponding (*S*)-alcohols in high enantiomeric purity in presence of *^{i}*PrOH as solvent and an alkaline base[76-78] (Scheme 1.14).
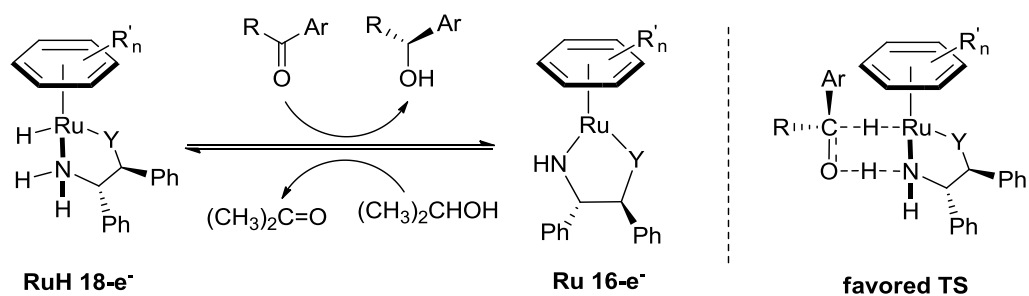
Scheme 1.14: Metal-ligand bifunctional mechanism in asymmetric transfer hydrogenation catalysed by $[RuH((S,S)\text{-}YCH(C_6H_5)CH(C_6H_5)NH_2)(\eta^6\text{-}arene)]$ (R= alkyl or D; Y=O or NTs).

Both Knowles for its pioneering work in asymmetric hydrogenation reaction of olefines, and Noyori for its discoveries in the asymmetric hydrogenation of ketones, aldehydes and imines including the brilliant work in the metal-ligand bifunctional catalysis were awarded the Nobel Prize in Chemistry 2001 together with K. Barry Sharpless for his work on chirally catalysed oxidation reactions.

1.3 Hydrogen transfer reaction

Addition of hydrogen to a molecule from a source other than gaseous H_2 is called hydrogen transfer (HT) reaction. In recent years, the HT methodology has gained increasing success in both laboratory scale and industrial applications cause of its operational simplicity and reduction of the risk associated with the use of an easily inflammable gas such as H_2. The more active hydrogen donors for homogeneous catalysis are principally alcohols, formic acid and its salts, but also ascorbic acid, cyclohexene and cyclic esters can be found[79].

Among the alcohols, secondary ones have probed to be the best hydrogen donors cause of the hydrogen on the carbon attached to the hydroxyl group (α-hydrogen) that is easily transferred in the first reductive step. In particular, *^{i}*PrOH is the conventional hydrogen source for its favourable properties being stable, easy to handle (bp 82 °C), nontoxic, environmentally friendly and inexpensive. During the process *^{i}*PrOH is oxidised to acetone

making the reduction of ketones a reversible process. Moreover, to shift the equilibrium towards the desired product ^{i}PrOH is used as solvent in the reaction since it dissolves easily many organic compounds. In order to activate the catalyst a base such as sodium or potassium carbonate, hydroxide or alkoxide is also added to the reaction mixture[80].

Another hydrogen donor used in HT reaction is the couple formic acid/triethylamine (HCOOH/Et$_3$N). Formic acid and its salts are better suited hydrogen donors than ^{i}PrOH because they are irreversibly converted to CO_2 upon reduction of the substrate, shifting the reaction towards the desired product. An azeotropic 5:2 mixture of HCOOH and Et$_3$N is most frequently employed as reducing agent, being miscible with many solvents at 20-60 ^{o}C[81]. The only drawback is that the catalyst could either undergo decomposition or react with the HCOOH losing its catalytic activity (Scheme 1.15).
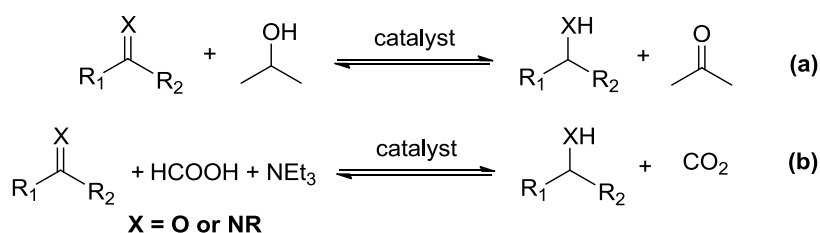
Scheme 1.15: Common sources of hydrogen in HT reaction: ^{i}PrOH (a) and formic acid (b).

At the beginning, aluminium isopropoxide was used as catalyst to promote transfer of hydrogen from ^{i}PrOH to a ketone. This reaction was called the Meerwein-Ponndorf-Verlay (MPV) reduction from the names of its discoverers[82,83]. The reaction can also be run in the opposite direction and the inverse process was studied by Oppenauer in the middle of the 1930s (Scheme 1.16).
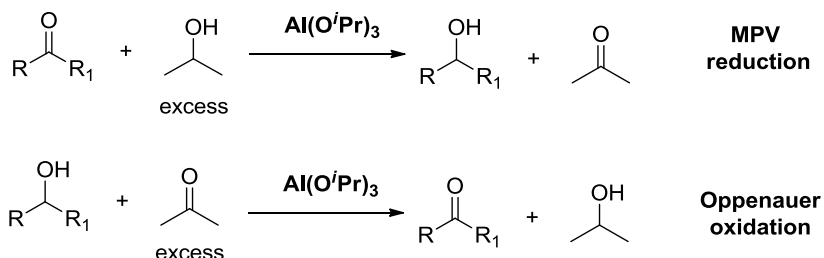
Scheme 1.16: The MPV reduction (top) and the Oppenauer oxidation (bottom).

Therefore, the two hydrogen transfer reactions (MPV and Oppenauer) are in equilibrium to each other and this equilibrium can be pushed in both directions by using an excess of either alcohol or ketone in the starting material. Thus, for the MPV reduction ^{i}PrOH is used in excess, while for the Oppenauer oxidation acetone. Concerning the mechanism, it has been recently demonstrated that a direct hydrogen transfer mechanism involving a concerted six-member ring transition state is the most favourable pathway, with the hydride transfer as the rate determining step[84]. This mechanism is more likely to take place in presence of non-transition metals such as in the aluminium-catalysed MPV, while the "hydridic route" is believed being the mechanism for transition metal-based reduction catalysts since the corresponding hydride species have been isolated in some cases[85] (Scheme 1.17).

Direct transfer (Non-transition metals)
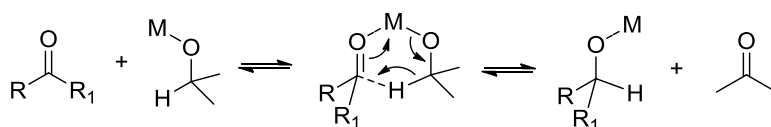
Hydridic route (Transition metals)
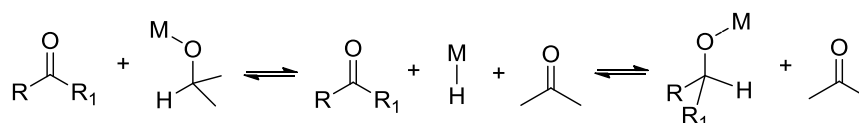
Scheme 1.17: The direct transfer mechanism occurring in the aluminium-MPV reduction (top) and the hydridic route for transition metal-based reduction catalysts (bottom).

In 2002 chiral ligands on the aluminium alkoxide were tested in order to affect the stereochemical outcome of the MPV reduction. The method employed ^{i}PrOH as hydride source and the system 2,2'-dihydroxy-1,1'-biphenyl (BINOL) with $AlMe_3$ as chiral catalyst leading to the reduction of substituted acetophenones in high ee (up to 83%)[86].

One of the main drawbacks for using aluminium alkoxides in HT reaction is that the aluminium salts are often required in stoichiometric amounts being inconvenient for scaling up and industrial applications. Moreover, the activity is relatively low by comparison with the transition metal-based systems.

In the area of organic synthesis, the first well-established HT reaction was described in 1952 when Braude, Linstead et al. found that hydrogen transfer was taking place between cyclohexene and a wide range of acceptors containing acetylenic, ethylenic, azo- and nitro-

groups such as 1-octene, cinnamic acid, benzoquinone, N-benzylideneaniline etc., in refluxing THF and in presence of palladium black as catalyst [87].

In 1971 the first ruthenium-catalysed HT reaction of practical use was reported by Sasson and Blum. The [RuCl$_2$(PPh$_3$)$_3$] complex was employed for the reduction of α,β unsaturated ketones but it required very high temperature (200 ^{o}C) and the turnover frequencies were quite low[88,89]. As a consequence, a useful family of hydrogen transfer catalysts have been developed through the years, mainly based on ruthenium and rhodium complexes employing a wide variety of ligands[80,90].

Nowadays, half-sandwich π-complexes such as Ru-arene and Rh- or Ir-cyclopentadienyl moieties are the most exploited metal fragments in the synthesis of transition metal-based reduction catalysts. Usually they are associated to protic ligands such as 1,2-amino alcohols or monotosylated diamine ligands in order to operate through a metal-ligand bifunctional mechanism (Fig 1.8).
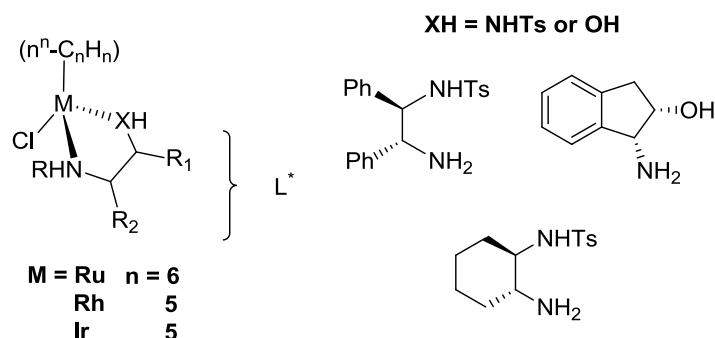
Fig. 1.8: Privileged catalytic system for HT reaction.

Very well-known catalysts belonging to this family are Noyori's complexes [RuCl((*S,S*)-Tsdpen)(p-cymene)] and [RuCl((*S,S*)-Tsdpen)(mesitylene)]. So far, both are the catalysts with the broadest substrate scope, providing significant enantiocontrol during the reaction[90,91]. These well-designed chiral Ru(II)-arene complexes catalyse the asymmetric transfer hydrogenation of ketones and imines in presence of either ^{i}PrOH or formic acid as hydrogen source (Fig 1.9).
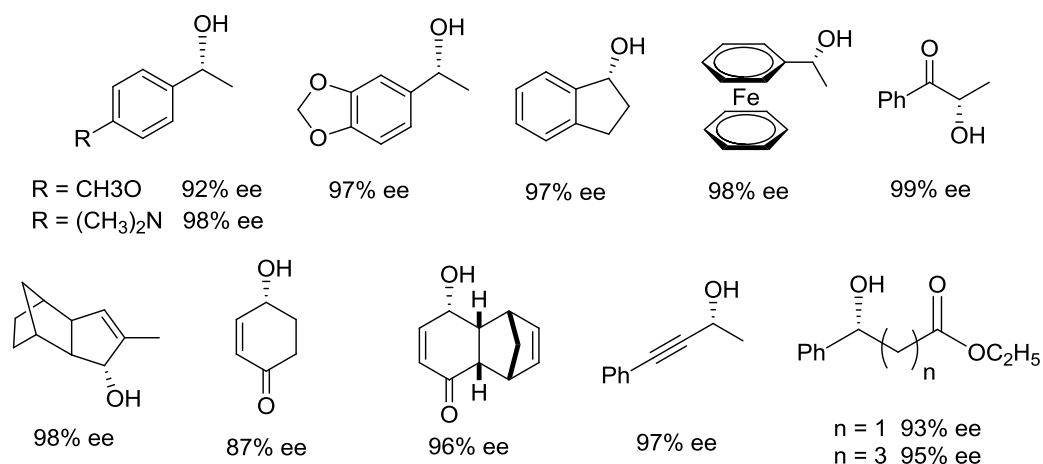
Fig. 1.9: Some of the chiral products obtained by asymmetric transfer hydrogenation using Noyori's chiral Ru catalysts.

Among the recent and successful evolutions of this structural motif there are tethered ruthenium catalysts developed by Wills and co-workers[92,93], in which the monotosylated diamine is covalently bound to the arene group. This modification has been made in order to achieve an improved enantiocontrol by locking together the chiral elements with the aryl group, therefore to reach a better conformation for the transition state (Fig. 1.10).
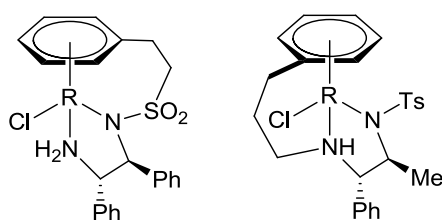
Fig. 1.10: Two examples of tethered chiral Ru(II) catalysts for asymmetric HT of ketones.

Both complexes have shown an enantioselectivity similar to the untethered counterpart, although the complex in which the tether is attached directly to the amino group has shown a higher catalytic activity compared to the one bearing the SO_2 group in the tether.

Another fascinating example of catalyst for transfer hydrogenation to alkenes, alkynes, carbonyl groups and imines from alcohols, amines and dihydrogen is the Ru-based cyclopentadienone complex $[(\eta^5-C_5Ph_4O)_2HRu_2H(CO)_4]$, discovered by Shvo et al. in the early 1980s. The compound, an air- and water-stable crystalline solid, contains a pair of equivalent Ru centres that are bridged by a strong hydrogen bond and a bridging hydride (Fig 1.11)[94].
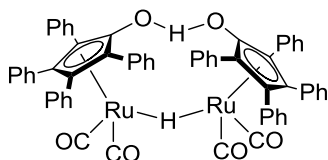
Fig. 1.11: Shvo's catalyst

The mechanism of hydrogenation and dehydrogenation reactions catalysed by Shvo's catalyst is unique among transition-metal catalysts since in solution it dissociates unsymmetrically in two moieties: $[(\eta^5\text{-}C_5Ph_4OH)RuH(CO)_2]$ (the reducing moiety) and $[(\eta^4\text{-}C_5Ph_4O)Ru(CO)_2]$ (the oxidizing moiety) involved at the same time during the hydrogen transfer reaction, but with opposite reactivity. Thus, Shvo's catalyst is an example of a ligand-metal bifunctional catalyst wherein the redox activity is distributed between the metal center and the cyclopentadienone ligand. The concentrations of these active forms are governed by equilibrium effects, since the two species are interconverted in solution through the gain or loss of "H_2" from donors and acceptors. Although there is no crystal structure for both species, solution NMR data, mechanistic probes, and trapping experiments have been utilized to establish their structures (Scheme 1.18)[95].
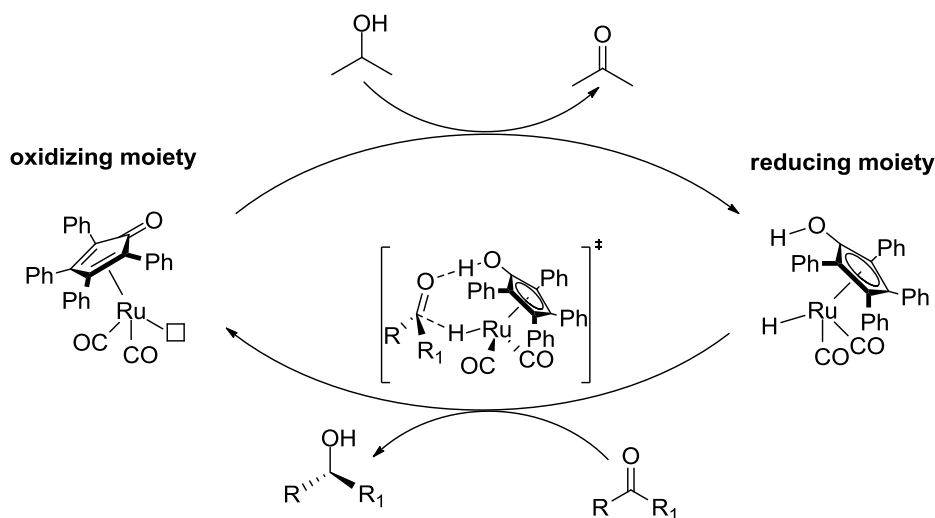
Scheme 1.18: Dissociation of Shvo's catalyst in two monomers in solution and the metal-ligand bifunctional HT mechanism.

The mechanism of hydrogenation and dehydrogenation by Shvo's catalyst has garnered intense interest. An outer-sphere mechanism in which the cyclopentadienone oxygen is involved in the transition state has been recently proven, displaying another example of ligand-metal bifunctional catalyst similar to Noyori's ones. According to recent DFT calculations of reversible formaldehyde reduction with Shvo's complex, an outer-sphere mechanism is lower in energy that the inner-sphere one involving the metal center[95].

Many applications of Shvo's catalyst have been reported since its discovery in the mid-1980s. Along the HT and hydrogenation reaction of ketones and alkenes, there is also the hydroboration of aldehydes and ketones, the alkylation of amines and the oxidation of steroidal alcohols, of amines to imines and of alcohols to form ketones[95].

1.4 Mechanistic aspects of transition metal-catalysed hydrogenation and HT reactions

Catalytic cycles of both hydrogenation and hydrogen transfer reactions can be divided into two different parts: (1) the reaction of the hydride with the unsaturated compound, (2) and the regeneration of the hydride from either H_2 or a hydrogen donor. Although mechanistic studies on transition metal-catalysed hydrogenation and HT reactions present common features, the first important question that needs to be answered is whether the hydride is transferred to the substrate coordinated to the metal (inner-sphere hydrogen transfer) or if there is a concerted transfer of hydrogen between the metal and the substrate (outer-sphere hydrogen transfer). The second question is whether the ligand assists or not the hydrogen transfer through a metal-ligand bifunctional catalysis. An explicative flowchart summarizing all these aspects has been presented by Morris and it is herein reported [96] (Scheme 1.19).
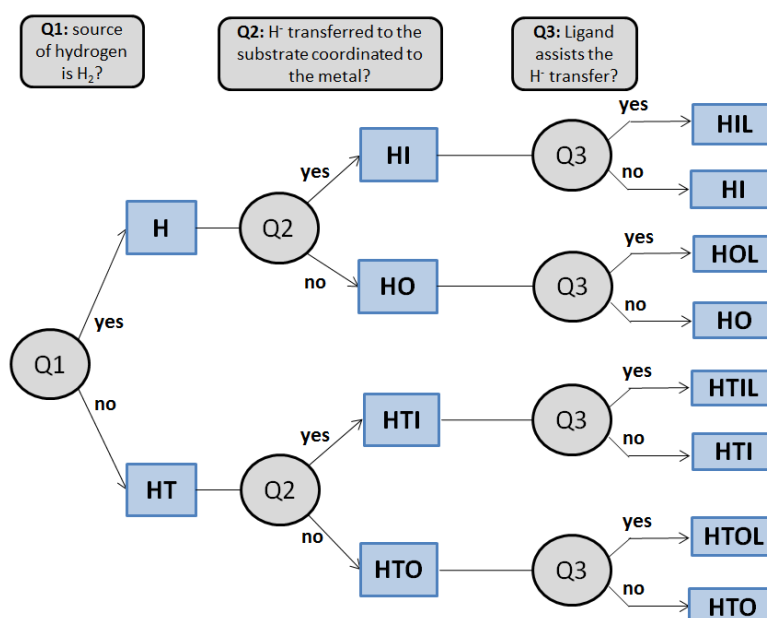
Scheme 1.19: Flowchart to classify the mechanism involved, where H is hydrogenation; HT, hydrogen transfer; I, inner-sphere; O, outer-sphere; L, ligand assisted (metal-ligand bifunctional catalysis).

Mechanisms labelled as HI or HTI (inner-sphere mechanism) usually involve dissociation of an ancillary ligand in order to provide a vacant coordination site for substrate binding. Often the catalyst has a site occupied by a weakly coordinated solvent molecule serving for this purpose. Ancillary ligands L bounded to the metal and bearing an acidic hydrogen bond donor group provide additional activation of the substrate (Fig 1.12).

Fig. 1.12: The attack of the hydride through an inner-sphere mechanism (left) and an inner-sphere ligand-assisted mechanism (right). Where Q = O/NR and E=electrophile.

A drawback on catalysts operating through an inner-sphere mechanism is the lack of selectivity for C=O bonds over C=C bonds, presumably due to the competition of C=C and C=O for the vacant site, like in the case of α,β-unsaturated ketones and aldehydes. For instance, the complex $[H_2Ru(CO)_2(PPh_3)_2]$ hydrogenates acetophenone through a proposed mechanism involving the coordination of the substrate to the metal, followed by its insertion into the ruthenium-hydride bond with formation of the corresponding alkoxide. But, when trans-4-phenylbut-3-en-2-one is used as substrate, the C=C double bond is preferentially hydrogenated with a high chemoselectivity (yield 92.4% at 100 °C)[97]. In addition, another undesired side reaction might be the isomerization of olefines and imines promoted by metal mono-hydride complexes[96].

In a different route, the hydride transfer to the substrate can take place in the second or outer coordination sphere of the metal complex. Since the carbon in a C=O or C=N bond usually has a low hydride affinity, it needs an electrophilic activation by either an external or an internal electrophile (Fig. 1.13). In the latter case the electrophile usually belongs to an ancillary ligand, like in the case of metal-ligand bifunctional catalysis proposed by Noyori in which the ancillary ligand *cis* to the hydride provides a proton that is transferred meanwhile the hydride is transferred from the metal to the substrate[74].
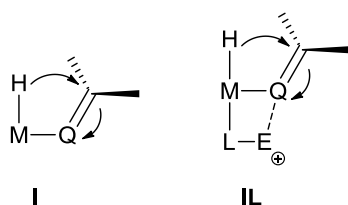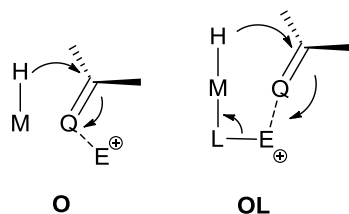
Fig. 1.13: The attack of the hydride through an outer-sphere mechanism (left) and an outer-sphere ligand-assisted mechanism (right). Where Q = O/NR and E=electrophile.

1.4.1 Hydrogen activation

In the hydrogenation catalytic cycle, hydrogen gas has to coordinate firstly to the metal at its vacant site as an η^2- dihydrogen ligand. In general, dihydrogen complexes are more than intermediates for oxidative addition of H_2. They can be generated as either stable species or elusive intermediates, in the course of both hydrogenation and dehydrogenation processes. The H-H σ orbitals donate electron density to an empty metal d orbital of σ symmetry. This interaction is augmented by back-donation from filled metal d orbitals[98] (Fig. 1.14).
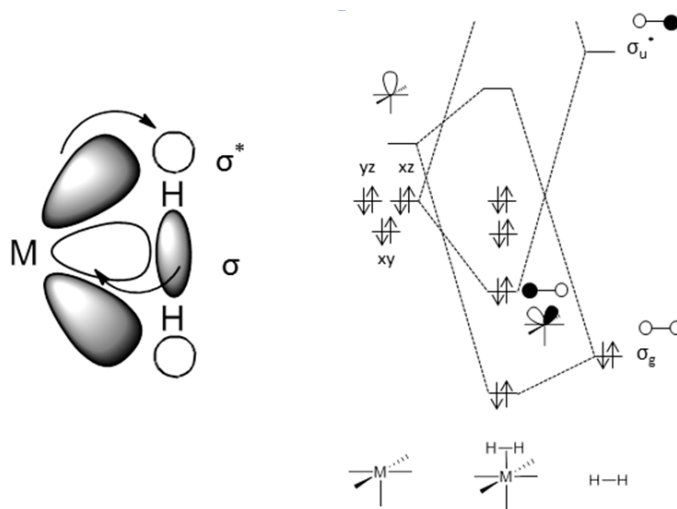
Figure 1.14: Bonding model in transition metal dihydrogen complexes illustrating the synergistic flow of electrons (left) and interaction diagram of H_2 interacting with ML_5 metal fragment (right).

Moreover, the η^2-H_2 ligand does not necessarily need the intervention of molecular hydrogen to be formed as it may also be obtained from a terminal hydride by treatment with various proton donors; including many solvents of common use in organometallic synthesis and homogeneous catalysis.

In general, once H_2 binds the metal center, the H_2 splitting might occur via either homolytic, heterolytic H_2 splitting or σ-bond metathesis[99,100] (Figure 1.15).

Homolytic splitting

$$M-\square \longrightarrow M-\underset{H}{\overset{H}{|}} \longrightarrow M\underset{H}{\overset{H}{<}}$$

Heterolytic splitting

$$\underset{M-\square}{\overset{L:}{|}} \longrightarrow \underset{M-\underset{H^-}{\overset{H^+}{|}}}{\overset{L:^-}{|}} \longrightarrow \underset{M-H}{\overset{LH}{|}}$$

Sigma-bond methathesis

$$M-E + E'-H \longrightarrow \begin{bmatrix} M----H \\ | \quad\quad | \\ E----E' \end{bmatrix}^+ \longrightarrow M-E' + E-H$$
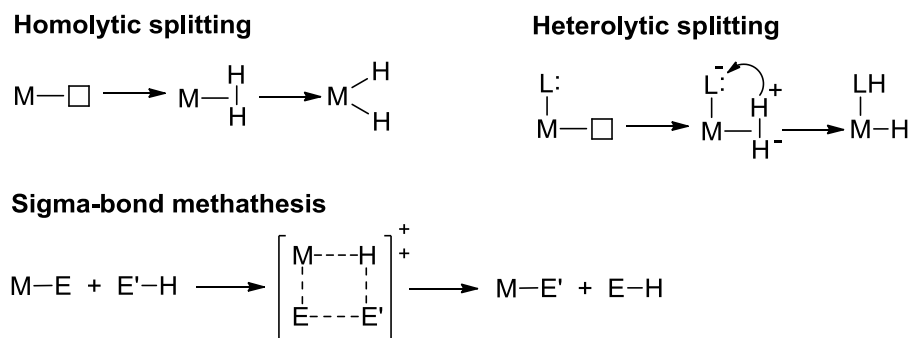
Fig 1.15: Comparison of different H_2 splitting mechanisms. Where L=ligand and E=heteroatom.

The oxidative addition or homolytic splitting of H_2 activate the dihydrogen molecule, changing the acidic or basic characteristics of the H sites. In this case, both of the H atoms possess the same reaction potential. Many homogeneous hydrogenation catalysts, including Wilkinson's catalyst, induce homolysis of H_2[101-104]. Heterolytic cleavage is also well known but it is normally achieved only by strong bases, since H_2 is a very weak acid. The reported pK_a of H_2 in THF is 35[105]. When H_2 is coordinated to a metal center, particularly to a cationic metal center, H_2 can be dramatically activated with respect to heterolysis[106]. This possibility was first realized by Crabtree and Lavin in $[Ir(PPh_3)_2(bq)(\eta^2-H_2)H]^+$[107]. The process of heterolytic splitting, which occurs with formal generation of H^+, in general generates a metal hydride complex and a corresponding protonated base.

On the other hand, σ-bond metathesis is another possible mechanism. In general, the reaction proceeds via a [2σ + 2σ] cycloaddition of a metal−ligand bond with a substrate throughout a concerted process. Therefore, the formal cycloaddition step is a transition state rather than an intermediate. Reactions proceeding via σ-bond metathesis should favor substrates that possess more favorable orbitals to engage in continuous bonding, despite the obvious geometric constraints of a four centered transition state. Historically, this transformation is typical for early-transition-metal complexes, in particular to metal compounds with a d^0 electron count, where the metal centers are in their highest possible oxidation states and are unable to change to lower states, thus excluding reductive elimination and oxidative addition mechanisms[108-110].

1.5 Iron as alternative to precious metals

Nowadays, sustainable catalysis is emerging as key point in the field of green chemistry. Catalytic chemical processes that minimize waste formation, while maximizing yield and selectivity are an important challenge, mainly due to unprecedented growth of the human population[111] along with an increase of energy consumption[112].

During the last decades, most of the work in transition metal homogeneous catalysis has been performed using noble metal catalysts based on Pd, Rh, Ir and Pt, extremely efficient for a large number of applications. However, due to their limited availability, considerable toxicity and high price, these precious metal-based catalysts are unsuitable in terms of sustainable chemistry. Therefore, attention has been driven on first-row transition metals such as iron, copper or nickel because of their advantages and unique features. Especially iron is well-suited for the economic and regulatory pressures facing modern chemistry, because it is the second most abundant metal on earth's crust (~4.7 wt %) after aluminium and it is an inexpensive and environmentally benign transition metal[113,114] (Fig. 1.16). Iron takes part of innumerable applications. From being a catalyst for a wide range of organic synthesis such as reduction, oxidation and coupling reactions to key element for the transport or metabolism of small molecules in biological systems such as metalloproteins, enzymes, nucleic acids[115].
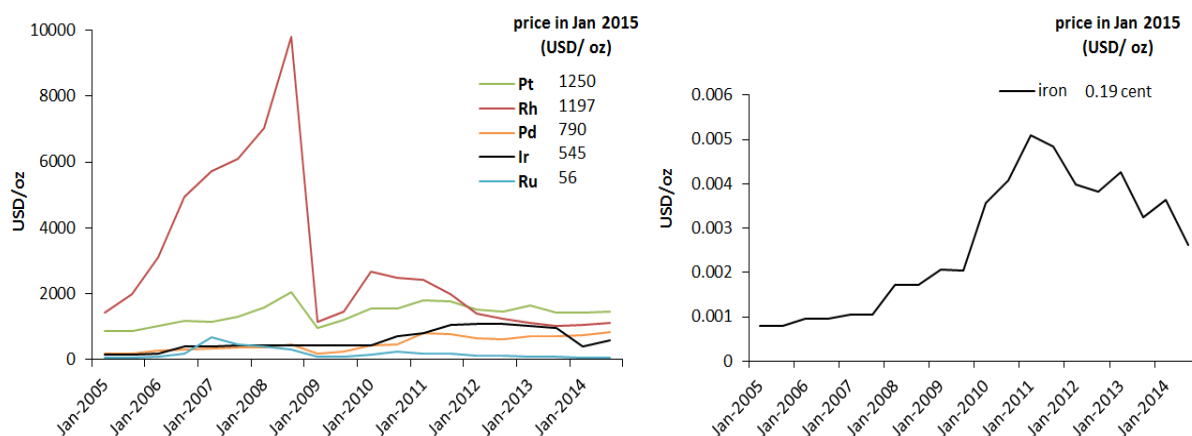
Fig 1.16: Market prices of transition metals in the time interval 2005-2014. Price fluctuation for platinum, rhodium, palladium, iridium and ruthenium metals on the left, for iron metal (iron ore) on the right[116].

Organoiron chemistry started in 1891 with the discovery of ironpentacarbonyl independently by Mond[117] and Berthelot[118]. Fifty years later, $Fe(CO)_5$ was used for the first time as catalyst in the Reppe process of hydroformylation of ethylene to produce propionaldehyde and 1-propanol in basic solutions[119]. In 1951 another important milestone in iron chemistry was the discovery of ferrocene[120], followed by $Na_2Fe(CO)_4$ in 1959[121].

Furthermore, iron is an effective catalyst at industrial level: the Haber process that utilises iron oxide as catalyst for the production of ammonia produces over 450 million tons of nitrogen fertilizer per year (section 1.1.1). Since then a number of impressive examples demonstrated the increased potential of iron as catalytic system in organic synthesis.

1.5.1 Reduction of alkenes and alkynes

The first breakthrough in the reduction of alkenes and alkynes was done by Bianchini et al. in early 90s[122]. Terminal alkynes were selectivity hydrogenated to alkenes by the iron (II) catalyst precursors $[(PP_3)FeH(N_2)]BPh_4$ and $[(PP_3)FeH(H_2)]BPh_4$ bearing aromatic tetraphosphine ligands $(PP_3 = P(CH_2CH_2PPh_2)_3)$ in THF under very mild conditions (temperature of 20-60 ^{o}C and 1 bar of H_2). In the proposed catalytic cycle the key point is the formation of the $Fe(\eta^2-H_2)$ species that undergoes reversible dissociation of one of the phosphine moieties of the PP_3 ligand in order to create a free coordination site for alkyne insertion. The coordinated alkyne inserts into the Fe-H bond in the intermediate step leading to the formation of the Fe-vinyl species. The chemoselectivity was assumed to be due to the better bonding capabilities of the triple bond of the alkynes and electronic factors associated with the nature of the Fe-olefin bond[123] (Scheme 1.20).
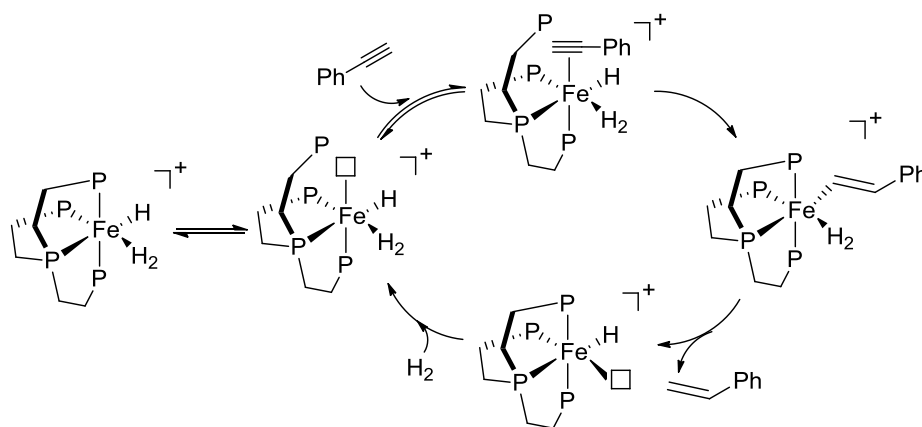
Scheme 1.20: Proposed mechanism for the hydrogenation of terminal alkynes catalysed by $[(PP_3)FeH(H_2)]BPh_4$.

In 2004, Peters and co-workers found that complexes of the type $[(PhBP^{iPr}_3)Fe-R]$ (where $PhBP^{iPr}_3 = [PhB(CH_2P^iPr_2)_3]^-$ and $R=Me, CH_2Ph, CH_2C(CH_3)_3$) served as precatalysts for the hydrogenation of non-functionalised olefines (styrene, ethylene, 1-hexene, cyclooctene) and 2-pentyne reaching TOF up to 24h^{-1} under 1-4 bar of H_2 pressure[124].

In recent years, active pincer-type iron complexes have been reported by Chirik et al for hydrogenation and hydrosilylation of alkenes with excellent group tolerance[125,126]. As example, the aryl-substituted [(^{iPr}PDI)Fe(N$_2$)$_2$] complex (where ^{iPr}PDI=2,6-(2,6-^{i}Pr$_2$-C$_6$H$_3$N=CMe)$_2$-C$_5$H$_3$N) served as effective precursor for the catalytic hydrogenation of oxygen-substituted and halogenated olefins in nearly quantitative conversion with 0.3 mol % of catalyst loading, 4 bar of H$_2$ pressure and at room temperature. The activity decreased in the following order: terminal alkenes>internal alkenes= geminal alkenes> trisubstituted alkenes[127] (Scheme 1.21).
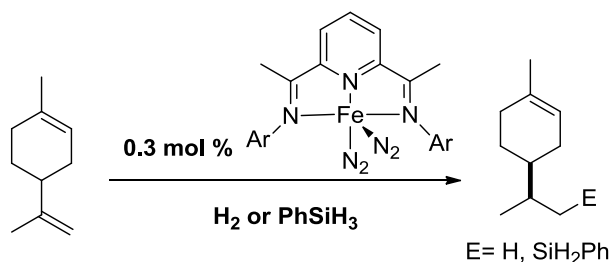
Scheme 1.21: Olefin hydrogenation catalysed by the [(^{iPr}PDI)Fe(N$_2$)$_2$] complex.

As an example of selective iron-catalysed transfer semihydrogenation of terminal alkynes, the iron-based system generated in situ by combining Fe(BF$_4$)$_2$·6H$_2$O and tetraphos ligand [P(CH$_2$CH$_2$PPh$_2$)$_3$, PP$_3$], showed high selectivity towards a broad range of aromatic and aliphatic alkynes. This system, developed by Beller and co-workers in 2012, employs formic acid as hydrogen donor in base-free and mild conditions (5h, 40 ^{o}C). Besides, internal alkynes were found to be unreactive in presence of the same catalytic system. In a plausible reaction mechanism, the iron intermediate [Fe(PP$_3$)F]$^+$ is proposed as the catalytic active species[128] (Scheme 1.22). Recently, this system has shown great reactivity in the transfer hydrogenation of aldehydes in presence of formic acid as hydrogen source (1.1 equiv.) at 60 ^{o}C in 2h. Remarkably, α,β-unsaturated aldehydes were selectively reduced under such base-free conditions[129].
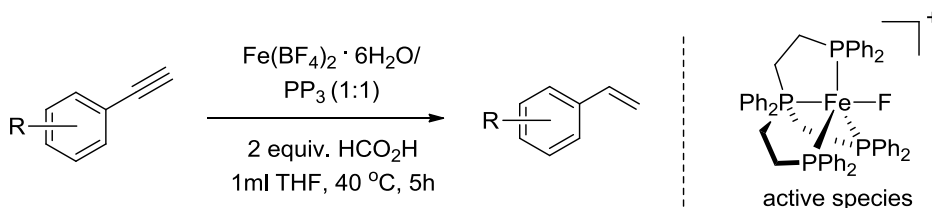
Scheme 1.22: Reduction of terminal alkynes to alkenes catalysed by Fe(BF$_4$)$_2$·6H$_2$O and tetraphos.

A new pincer-type iron system bearing 4,5-bis(diphenylphosphino)-acridine (^{HACR}PNP) ligand active towards the hydrogenation of internal alkynes to produce E-alkenes has been recently reported by Milstein et al. The complex [(^{HACR}PNP)Fe(CH$_3$CN)(η^2-CH$_3$CHCNBH$_3$)] showed great selectivity yielding E-alkenes as major products with a small amount of over-reduced alkanes as by-product tolerating functional groups such as ester, nitrile, ketone and trimethylsilyl[130] (Scheme 1.23).
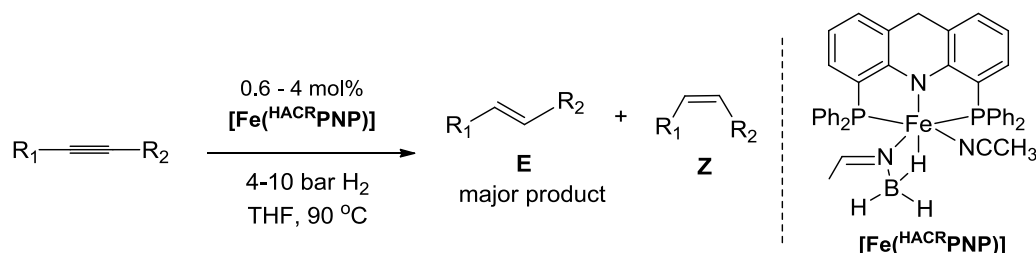
Scheme 1.23: Iron catalysed hydrogenation of alkynes to E-alkenes.

1.5.2 Reduction of carbonyl derivatives (aldehydes, ketones and imines)

The first catalytic effort on the reduction of carbonyl derivatives was presented by Marko' et al. in 1981. Reduction of acetophenone was possible in presence of Fe$_3$CO$_{12}$ and Fe$_2$CO$_9$ at 100 ^{o}C and 100 bar of H$_2$. Thus, addition of triethylamine as co-catalyst was necessary to obtain reasonable yields[131].

One of the first efficient iron-catalysed hydrogenation of ketones and imines under mild conditions was reported in 2007 by Casey and Guan with Knölker's complex [2,5-(SiMe$_3$)$_2$-3,4-(CH$_2$)$_4$(η^4-C$_4$C=O)]Fe(CO)$_2$(HOCH$_2$C$_6$H$_5$)] as catalyst. The hydrogenation reaction takes place at room temperature under low pressure of H$_2$ (3 bar) and with 2 mol% of catalyst loading, showing high chemoselectivity in presence of esters, epoxides, isolated alkenes and alkynes groups. For α,β-unsaturated ketones both the carbonyl group and the C=C group were reduced. A detailed study of the mechanism indicated that both the hydride ligand and the hydroxyl group contributed in the reduction of the substrate in an inner-sphere and ligand-assisted mechanism. Notably, this catalytic system also displayed activity in transfer hydrogenation reaction using ^{i}PrOH as hydrogen source[132,133] (Scheme 1.24).
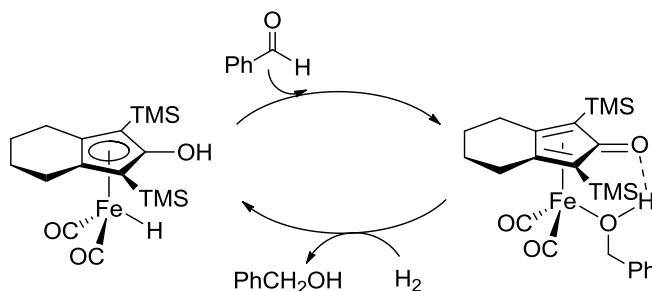
Scheme 1.24: Hydrogenation of carbonyl compounds in presence of Casey's complex. Both the hydride and the hydroxyl group contribute to the hydrogenation (TMS=trimethylsilyl).

A year later Morris developed a new class of iron (II) complexes bearing chiral tetradentate diiminophosphines, PNNP-type ligands based on his previous results in the hydrogenation reaction catalysed by ruthenium complexes[134]. These complexes were the first examples of efficient catalysts for both asymmetric hydrogenation and asymmetric transfer hydrogenation of ketones from ^{i}PrOH and without a base, under very mild conditions (25 bar of H_2 and 50 ^{o}C for the hydrogenation and room temperature for the HT reaction), exhibiting good enantiomeric excess (up to 98 %). Moreover, it is noteworthy that both the activity and the enantioselectivity of these systems depend on the substituents on the diamine in the hydrocarbon bridge of the ligand [135,136](Fig. 1.17).
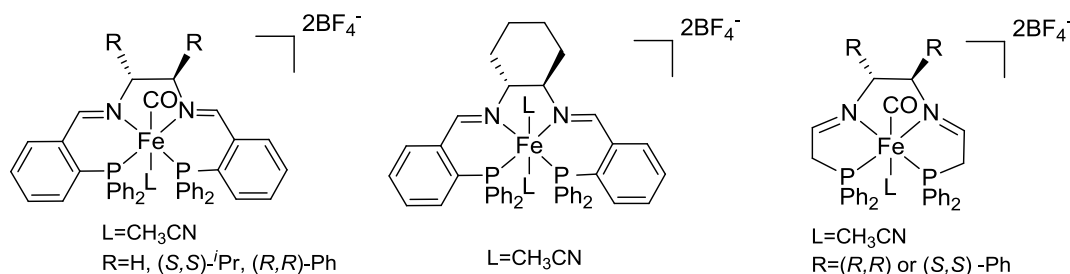
Fig 1.17: Some examples of Morris' PNNP-based iron (II) complexes active in both hydrogenation and HT reactions.

The complex [Fe(CO)(CH$_3$CN)(^{R}PNNP)]$^{2+}$ with R=(R,R)-Ph (Fig 1.15, right) reduces acetophenone in 90% conversion and with ee up to 82% in 30 min and at room temperature, exhibiting TOF of 3600 h^{-1}. With hindered ketones (e.g. ^{t}BuCOPh) the reaction time ranges from 8 to 200 min achieving 14-99% of ee. Aliphatic ketones were also reduced with excellent conversions but moderate ee (up to 50%). Notably, when the α,β-unsaturated ketone *E*-PhCH=CHCOMe was used as substrate, the corresponding allylic alcohol was obtained as only product in 82% conversion and 60% ee[137].

When the acetonitrile ligand was replaced by a bromide, the complex [Fe(CO)(Br)(^{R}PNNP)] with R=(R,R)-Ph showed similar activities in the reduction of ketones, indicating that the ligand *trans* to the CO did not effect the reaction rate. Notably, detailed kinetic and DFT studies on this catalytic species elucidated the HT mechanism. The catalytic system is activated by a base resulting in a selective reduction of one imine group of the PNNP ligand, yielding an imino/enamido intermediate that reacts slowly with KO^{i}Pr to generate the active species. The active species, *via* an outer-sphere mechanism involving ^{i}PrOH, generates the hydride species that reacts with acetophenone yielding 1-phenylethanol (Scheme 1.25)[138,139].
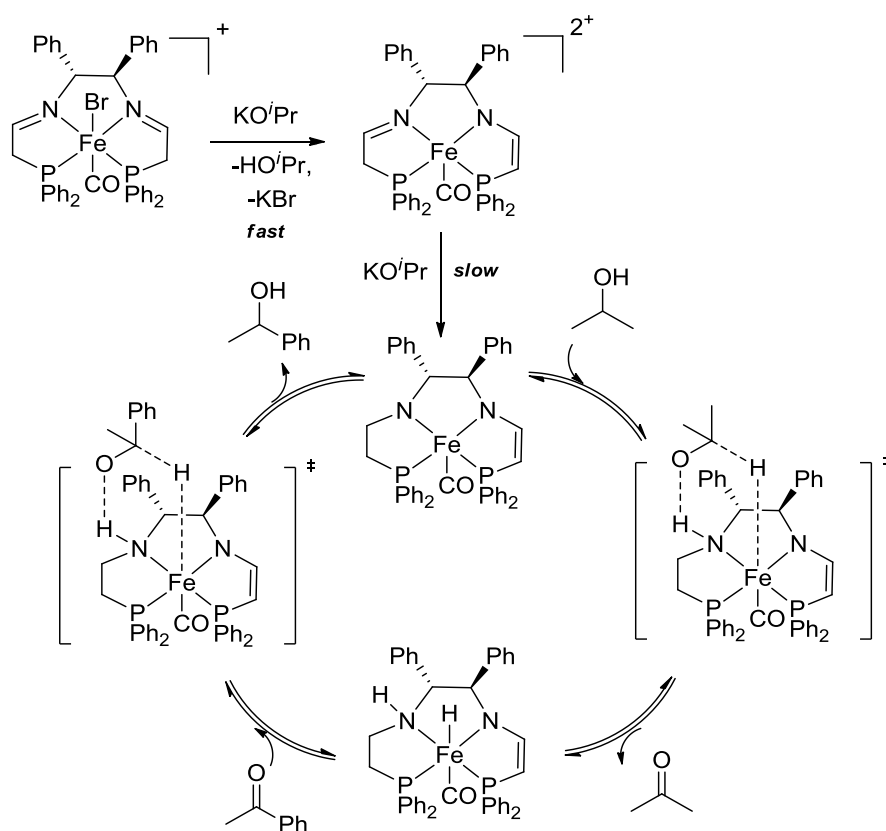
Scheme 1.25: Proposed outer-sphere mechanism for the transfer hydrogenation of acetophenone catalysed by [Fe(CO)(Br)(^{R}PNNP)], where R=(R,R)-Ph.

Similar macrocyclic iron (II) systems providing significant enantiocontrol during the asymmetric transfer hydrogenation reaction of ketones have been recently reported by Mezzetti et al[140]. The bis-isonitrile chiral complexes [Fe(CNR)$_2$(N$_2$P$_2$)](BF$_4$)$_2$ (where R= CEt$_3$ and N^{i}Pr$_2$) catalysed the reduction of several ketones, enones and imines in presence of ^{i}PrOH as hydrogen source, NaOtBu as base, with low catalyst loading (0.1 mol %), at 40°C in

1h. Interestingly when benzylideneacetone was used as substrate, the corresponding allylic alcohol was obtained as only product with enantioselectivity up to 65-70% (Scheme 1.26).
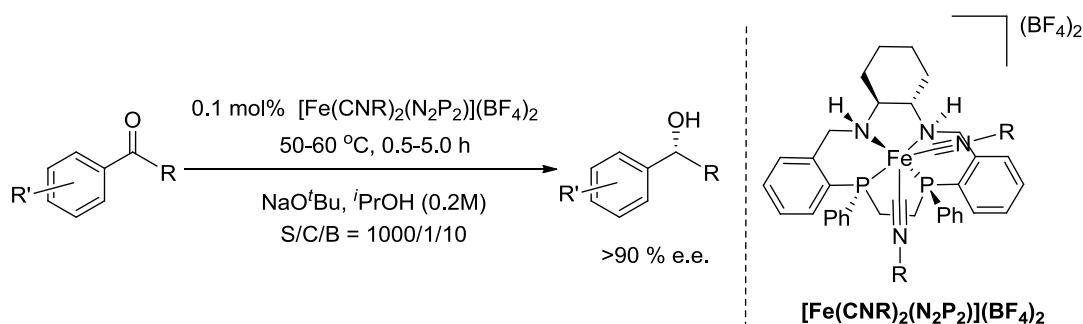
Scheme 1.26: Iron catalysed asymmetric transfer hydrogenation of ketones reported by Mezzetti.

In 2014 Morris et al. described the unsymmetrical iron dicarbonyl complexes *mer-trans*-[Fe(Br)(CO)$_2$(P-CH=N-P')][BF$_4$] (where P-CH=N-P'= R$_2$PCH$_2$CH=NCH$_2$CH$_2$PPh$_2$ or P-CH=N-P'=(S,S)-Cy$_2$PCH$_2$CH=NCH(Me)CH(Ph)-PPh$_2$) for the asymmetric hydrogenation of ketones into alcohols after treatment with LiAlH$_4$ and KO^{t}Bu as additive in THF at 50 °C and 5 bar H$_2$, reaching turnover frequency (TOF) up to 2000 h^{-1} and enantioselectivity up to 86% (Scheme 1.27)[141].
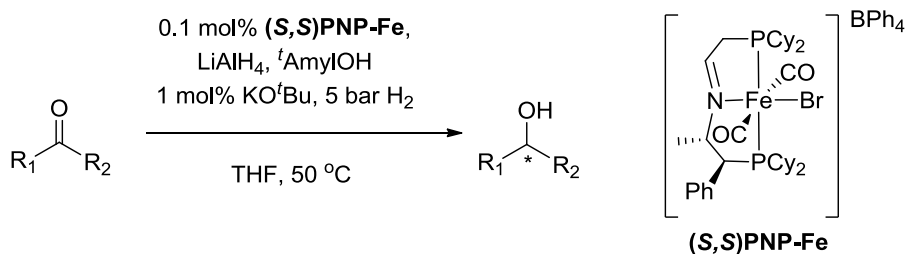
Scheme 1.27: Iron catalysed asymmetric hydrogenation of ketones recently reported by Morris.

Another important milestone in the hydrogenation of ketones and aldehydes has been recently achieved by Milstein and his group. Two new pincer iron(II) complexes bearing 2,6-bis(diisopropylphosphinomethyl)pyridine (^{iPr}PNP type-ligand) have been synthesized and fully characterized (Fig. 1.18). Both [(^{iPr}PNP)FeH(CO)Br] and [(^{iPr}PNP)FeH(CO)(HBH$_3$)] complexes exhibit great reactivity towards H$_2$ in the reduction of a broad variety of ketones in ethanol at 4.1 bar of H$_2$ (30 bar of H$_2$ are needed for the hydrogenation of aldehydes), achieving turnover numbers (TON) up to 1780 and TOF of 300 h^{-1} for acetophenone hydrogenation. Mechanistic investigations and DFT calculations on these systems have led to the conclusion of an aromatization-dearomatization of the PNP ligand occurring during the catalytic cycle[142,143] (full mechanism reported in section 3.1, scheme 3.2).
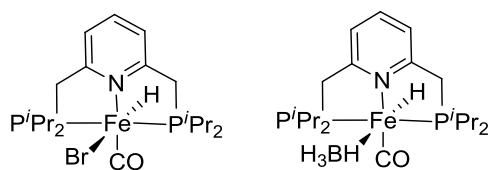
Fig 1.18: *^{iPr}*PNP- Iron (II) complexes active in the hydrogenation of ketones and aldehydes.

An improvement in the reduction of the more challenging α,β-unsaturated aldehydes was achieved by Beller and his group by using the tricarbonyl(η^4-1,3-bis(trimethylsilyl)-4,5,6,7-tetrahydro-2H-inden-2-one)iron complex (Knölkner's type) as catalyst in 0.1-0.5 mol% loading and 30 bar of H$_2$ at 100 ^{o}C. After activation with K$_2$CO$_3$ in ^{i}PrOH/water solution the hydrogenation of different α,β-unsaturated aldehydes occurred only on the carbonyl group achieving the corresponding allylic alcohols in 80-99% yields[144](Scheme 1.28, a). Similar results were also achieved by using the [FeF(tris(2-diphenylphosphino)-phenylphosphino)]BF$_4$ complex ([FeF(P(Ph$_2$)$_3$)]BF$_4$, 0.2-0.4 mol%) in presence of 1-5 mol% of trifluoroacetic acid (TFA) in ^{i}PrOH under 20 bar of H$_2$ at 120 ^{o}C. Aromatic and aliphatic aldehydes were reduced with excellent yields (95-99%) and groups such as ester, sulphide, C=C bond and ketone were tolerated[145] (Scheme 1.28, b).
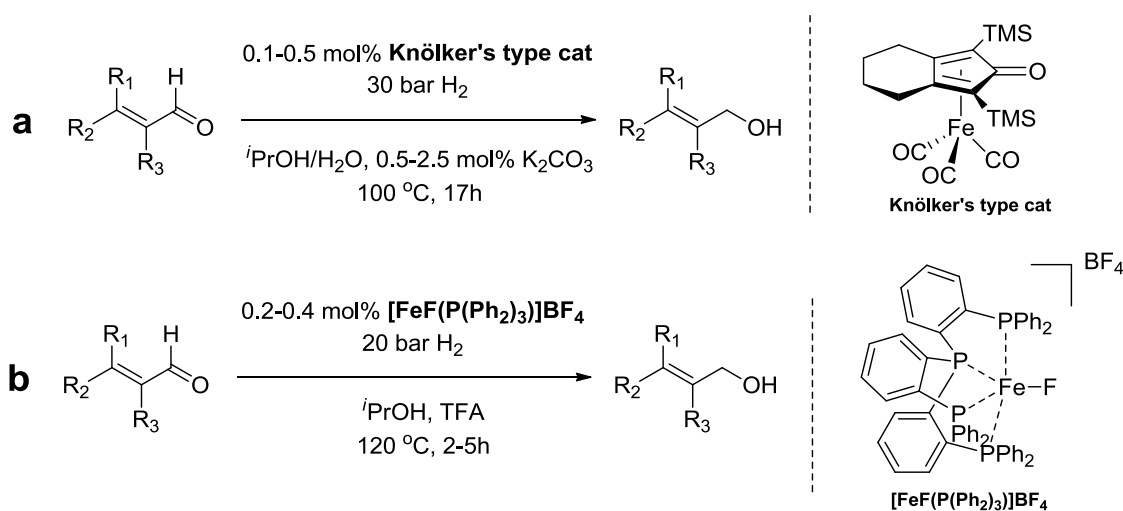
Scheme 1.28: Iron catalysed hydrogenation of α,β-unsaturated aldehydes by using a Knölker type catalyst (top. a) and [FeF(P(Ph$_2$)$_3$)]BF$_4$ (bottom, b) as catalysts.

In the proposed mechanism, when ([FeF(P(Ph$_2$)$_3$)]BF$_4$ is used as catalyst, the catalytic species is the hydride complex [FeH(P(Ph$_2$)$_3$)]BF$_4$ generated in two successive steps: the addition of H$_2$ followed by release of HF as supported by NMR and DFT investigations. By reacting with a second H$_2$ molecule the diamagnetic species [Fe(H)(H$_2$)(P(Ph$_2$)$_3$)]BF$_4$ forms, followed by dissociation of one of the phosphine moieties of the P(Ph$_2$)$_3$ ligand (*via* either an

acid catalysed or an acid-free route) in order to create a free coordination site for substrate insertion. After hydride insertion on the C=O bond the resulting allylic alcohol is produced[145] (Scheme 1.29).
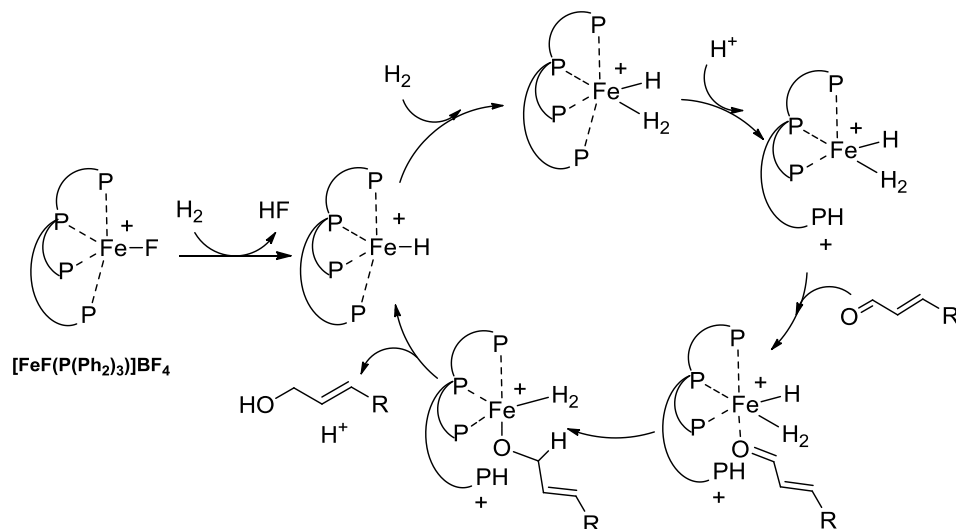
Scheme 1.29: Proposed mechanism for the chemoselective hydrogenation of α,β-unsaturated aldehydes using [FeF(P(Ph$_2$)$_3$)]BF$_4$ *via* an acid catalyzed route.

Beller's group also reported the first catalytic hydrogenation of imines to amines employing the Knölker's complex plus the chiral Brønsted acid 3,3'-bis(2,4,6-triisopropyl-phenyl)-1,1'-binaphthyl-2,2'-diyl hydrogen phosphate (TRIP) as catalytic system. The in *situ* catalyst reduced a wide range of N-arylketimines into the corresponding amines in 60-94 % of isolated yield and enantiomeric excess up to 94%, under 50 bar of H$_2$ at 65 °C[146] (Scheme 1.30).
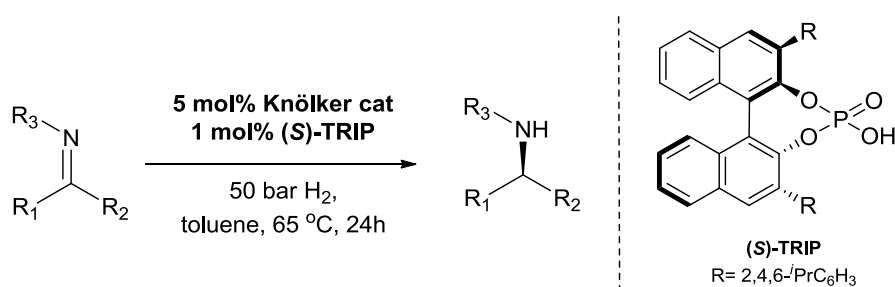
Scheme 1.30: Catalytic asymmetric hydrogenation of C=N bonds by Knölker complex and the chiral (S)-TRIP ligand.

Other recent catalysts active in hydrogenation of both ketones and aldehydes under mild conditions have been recently reported by Kirchner et al. The pincer-type iron(II) complexes [Fe(^{iPr}PNP)(H)(CO)L] (where L=Br, CH$_3$CN, BH$_4^-$) based on the 2,6-diaminopyridine scaffold bearing -NH or -NMe as spacers ([(PNP)Fe] and [(^{Me}PNP)Fe]

respectively) catalyze the reduction of ketones and aldehydes under 5 bar of H_2 at room temperature and in presence of KO^{t}Bu as base. Noteworthy, the hydrogenation of ketones proceeds with a catalyst loading of 0.5 mol%, while in the case of aldehydes 5 mol% of loading is needed[147] (Scheme 1.31). DFT calculations support a heterolytic dihydrogen cleavage occurring *via* metal oxide cooperation but without reversible aromatization-dearomatization of the PNP ligand like previously reported by Milstein (for the aromatization/dearomatization mechanism see scheme 3.2).
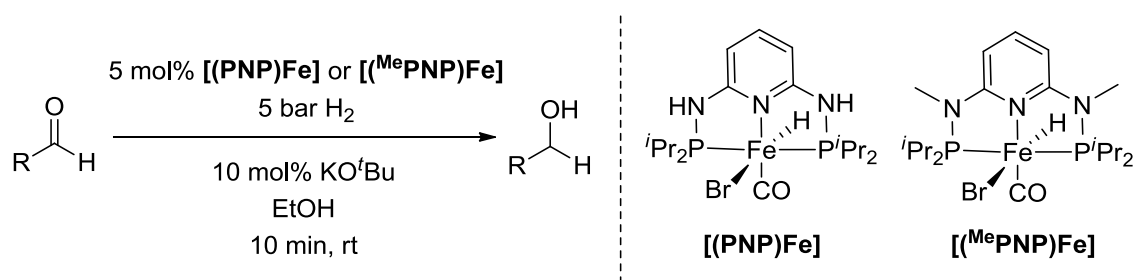
Scheme 1.31: Catalytic hydrogenation of aldehydes by [(PNP)Fe] and [^{Me}(PNP)Fe] complexes.

The Meerwein-Ponndorf-Verley-type reaction mechanism has been proposed for the iron(II) complex consisting of bis(isonitrile) ligand (BINC) and FeCl$_2$ in the ratio 2:1, described in 2010 by Reiser and co-workers. This complex catalysed the transfer hydrogenation of both aromatic and heteroaromatic ketones in presence of KO^{t}Bu as base in ^{i}PrOH with enantioselectivities up to 91%. On the basis of IR and NMR studies, the authors proposed a MPV mechanism in which the ketone binds *via* its carbonyl group (or alternatively through the respective heteroatom in the case of heteroaromatic substrates) to the iron centre of the catalyst acting as Lewis acid. Hydride transfer then occurs directly from the reduced isonitrile group that acts as the hydrogen donor[148] (Scheme 1.32).
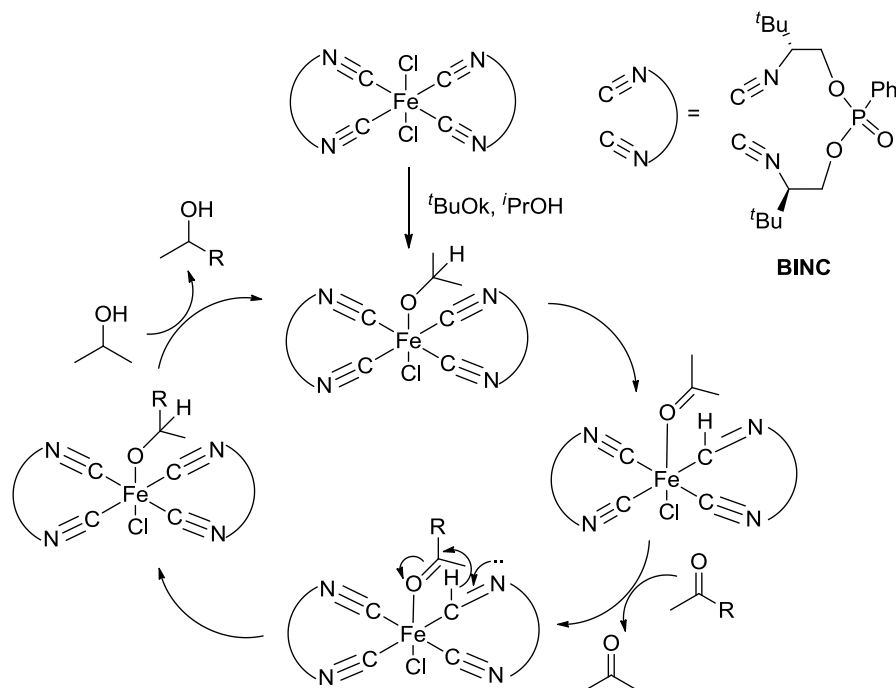
Scheme 1.32: Proposed mechanism for iron (II) –bis(isonitrile) catalysed hydrogen transfer.

1.5.3   Reduction of carboxylic acid derivatives

The reduction of carboxylic acid derivatives with respect to their reactivity at the carbonyl group is more challenging than that one of ketones and aldehydes. Usually this reaction is performed using stoichiometric amount of metal hydrides such as LiAlH$_4$ or NaBH$_4$, but some examples of iron catalysed reduction have been reported in recent years.

In early 2014, Milstein and his group reported the selective hydrogenation of activated trifluoroacetic esters by using the PNP-type iron complex [(PNP)Fe(H)$_2$(CO)]. The hydrogenation yields 2,2,2-trifluoroethanol and the corresponding alcohols derived from the ester alkoxy groups as products in 52-99% of yield, under 25 bar of H$_2$, 1 mol% catalyst loading and 5 mol% of NaOMe as base. Although the steric hindrance of the alkoxy group has an influence on the reactivity of the system, functional groups such as C=C are tolerated[149] (Scheme 1.33).
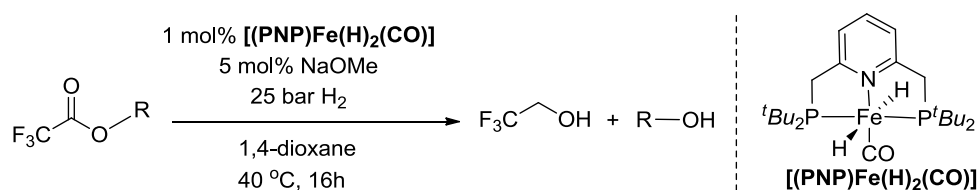
Scheme 1.33: Hydrogenation of trifluoroacetic esters catalysed by [(PNP)Fe(H)$_2$(CO)] complex.

Catalytic hydrogenation of esters was also achieved simultaneously by Beller[150] and Guan[151]. They both described the use of the bifunctional iron pincer-type complex [(PNP)Fe-(H)(HBH$_3$)] as an efficient catalyst of aromatic and aliphatic esters in base-free conditions. A wide range of esters were reduced under 30 bar of H$_2$, at 100-120 ^{o}C in 6-19h as reported by Beller, while fatty-fatty esters were reduced in Guan's work (Scheme 1.34).
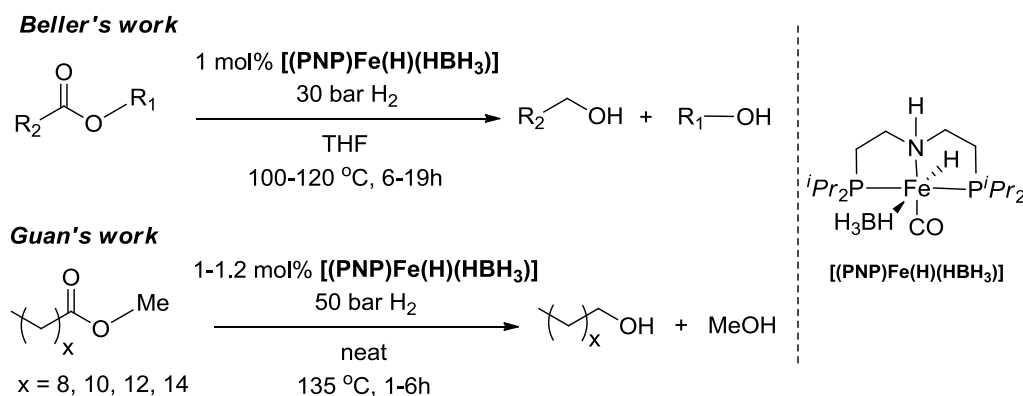
Scheme 1.34: Hydrogenation of esters catalysed by [(PNP)Fe(H)(HBH$_3$)].

1.6   The role of iron in hydrogenase enzymes

Hydrogenases are a group of metalloenzymes that catalyse the conversion of H$_2$ into two protons and two electrons and its reverse reaction. In particular, the heterogenesis of H$_2$ involves the respective coupling of H$^+$ and H$^-$. The reaction takes place at a metal center, in the core of the enzyme where the acidity of H$_2$ is increased by interaction with the metal and the heterolytic splitting occurs accelerated by a nearby base. The heterolytic mechanism has been proven by H/D isotope exchange experiments[152].

Several organisms such as bacteria, archea and some eukarya utilise H$_2$, therefore hydrogenases are widespread in nature and these enzymes are classified into three different types based on the metal included in their reactive sites: [NiFe], [FeFe] and [Fe] hydrogenases[153](Fig. 1.19).
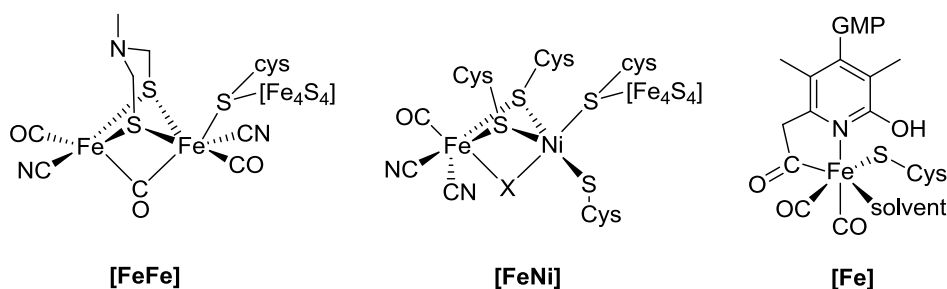
Fig 1.19: Active sites of structurally characterised representatives of the three classes of hydrogenases. GMP=guanyl nucleotide.

In terms of active site composition the common feature is the presence of Fe and/or Ni as central ions connected by sulphur-bridge and coordinated by strong-field ligands such as CO and CN leading to low-spin iron complexes and providing empty acceptor orbitals for H_2 activation and heterolytic splitting. Hydrogenases are known to be highly efficient catalysts with high turnover number (up to 10^4 s^{-1}), low overpotential and good stability working even at elevated temperature[153].

Immediately after the publication of the crystal structures of the [NiFe][154] and [FeFe][155] hydrogenases in the mid-1990s and of the [Fe] hydrogenase[156] in 2008, compounds mimicking the unusual active sites of the enzymes have been synthesized and fully characterised. This turned out to be challenging due to the complex chemistry required to correctly place the ligands around the metal core and to generate functional models with catalytic activity. It is for the capability of interacting with H_2 that the active sites of these enzymes have become particularly interesting for the design and synthesis of model catalysts (either biomimetic or bio-inspired) for large scale production of hydrogen either electrochemically or photochemically. Although an increasing number of studies in structural models of the [NiFe], [FeFe] and [Fe] active sites has been developed so far[151], in this section only some of the latest discoveries in functional models based on the active sites of the three different hydrogenases are resumed.

1.6.1 [NiFe]-Hydrogenase functional model

Among the family of functional model inspired by the [NiFe] active site, a recent breakthrough has been reported by Ogo et al. in 2013. The model complex [Ni(X)Fe-(CH$_3$CN)(P(OEt)$_3$)$_3$](BPh$_4$)$_2$ where X=N,N'-diethyl-3,7-diazanone-1,9-dithiolate bears all the characteristics present in the [NiFe] active site: a bimetallic core, a sulphur bridge and ligands capable of accepting π-back donation from the iron center. This complex (the iron center specifically) activates H_2 in a heterolytic manner in CH$_3$CN/MeOH at room temperature and

under atmospheric pressure. In presence of a strong base such as NaOMe abstraction of a proton form the bounded H_2 it's possible and this reaction yields to the corresponding hydride complex $[Ni(X)Fe(H)(P(OEt)_3)_3](BPh_4)_2$. In common with the [NiFe]-hydrogenase the hydride species is capable of reducing substrates by either hydride ion or electron transfer[157] (Scheme 1.35).
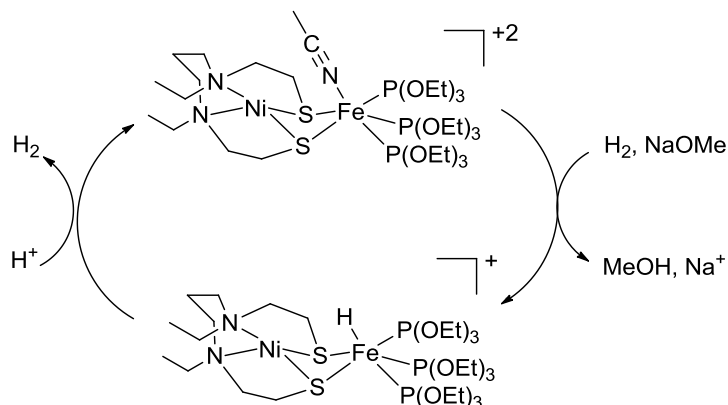
Scheme 1.35: Heterolytic activation of H_2 (0.1MPa) by $[Ni(X)Fe(CH_3CN)(P(OEt)_3)_3](BPh_4)_2$ in CH3CN/MeOH in presence of NaOMe as base.

1.6.2 [FeFe]-Hydrogenase functional model

Over the last few decades close to a hundred functional and structural [FeFe] models have been synthesized and their stable intermediates have been characterized mostly by NMR, EPR, FTIR, and UV−Vis spectroscopy[158]. One of the last examples of heterolytic cleavage of hydrogen by an [FeFe] hydrogenase-inspired complex has been published by Bullock and co-workers in 2014. DFT calculations on the [FeFe] active site have shown that the nitrogen atom is a suitable base for assisting heterolytic cleavage of hydrogen at the active site[159,160]. Therefore, they reported the synthesis and characterization of the complex $[Cp^{C5F4N}Fe(P^{tBu}_2N^{tBu}_2)Cl]$ bearing two pendant amines crucial for the hydrogen cleavage. As expected, the complex cleaved hydrogen heterolytically leading to the corresponding hydride complex $[Cp^{C5F4N}FeH(P^{tBu}_2N^{tBu}_2H)]BAr^F_4$ exhibiting a strong Fe-H···H-N dihydrogen bond (Scheme 1.36). The structure was determined by single-crystal neutron diffraction where the measured distance H-H between the protic N-H$^+$ and the hydridic Fe-H$^-$ was remarkably short (1.489(10)Å). Due to these outstanding results, an experimental support for both the previously proposed binding of H_2 to the distal Fe center of the [FeFe] hydrogenase enzyme and the participation of a pendant amine in the heterolytic cleavage have been provided[161].
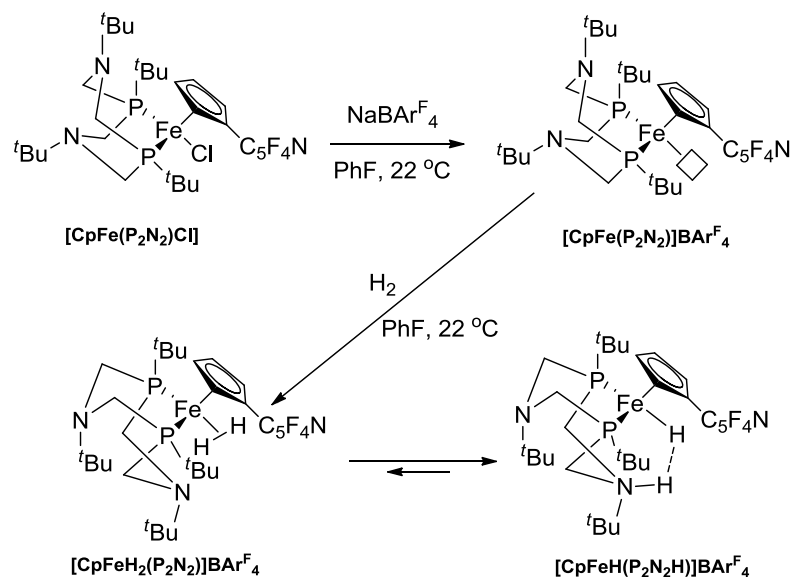
Scheme 1.36: Heterolytic H_2 splitting by the bio-inspired complex $[Cp^{C5F4N}Fe(P^{tBu}_2N^{tBu}_2)Cl]$.

Another significant discovery of synthetic models of the active site of the [FeFe] hydrogenase undergoing catalytic proton reduction while exhibiting doubly protonated intermediates was made in 2012 by Caroll et al. The complex $[Fe_2(adt^{NH})(CO)_2(dppv)_2]$ where dppv= *cis*-$C_2H_2(PPh_2)_2$ and adt^{NH}=$((SCH_2)_2NH)^{2-}$, undergoes protonation with strong acids to give a terminal hydride species $[Fe\text{-}FeH(adt^{NH})(CO)_2(dppv)_2]$. This specie can either undergo further protonation in presence of a strong acid yielding complex $[Fe\text{-}FeH(Hadt^{NH})\text{-}(CO)_2(dppv)_2]$ followed by reduction and release of H_2, or can directly give proton reduction in presence of a weak acid[162] (Scheme 1.37).
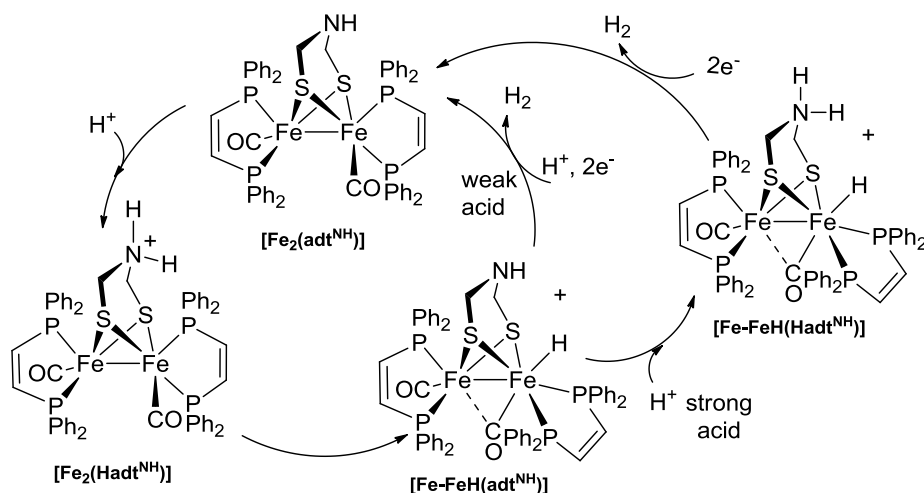
Scheme 1.37: Proposed mechanism for proton reduction catalysed by $[Fe_2(adt^{NH})(CO)_2(dppv)_2]$ complex: two cycle are shown for weak and strong acids.

1.6.3   [Fe]-Hydrogenase functional model

Despite all the structural model published so far[153], no functional synthetic analogue that mimics [Fe] hydrogenase reactivity has been yet developed. The functional model inspired by the frustrated Lewis pair concept reported by Meyer et al. in 2014 provides experimental insights into the enzyme's mechanism. Although based on ruthenium rather than iron, the complex $[RuCp(CO)_2]$ reacts in presence of H_2 emulating the heterolytic splitting of H_2 through the cooperative action of Lewis acid imidazolium salt ion serving as hydride acceptor (similar to the methenyl-H_4MPT^+ cofactor present on the [Fe] hydrogenase site), and the metal complex itself acting as Lewis base, accepting the proton and yielding the species $[HRuCp(CO)_2]$ (Fig. 1.20). In order to find a suitable hydride acceptor molecule structurally related to methenyl-H_4MPT^+, a variety of imidazolium salts was synthesized and screened with respect to their hydride accepting ability in a test reaction with $NaBH_4$. The best results were achieved by using $[^{Tol}Im^{F4}]^+Br^-$ and $[^{Mes}Im^{F4}]^+Br^-$ as hydride acceptors[163].

methenyl-H_4MPT^+ / FeGP Cofactor $[^{Tol}Im^{F4}]^+Br$ / $[RuCp(CO)_2]$
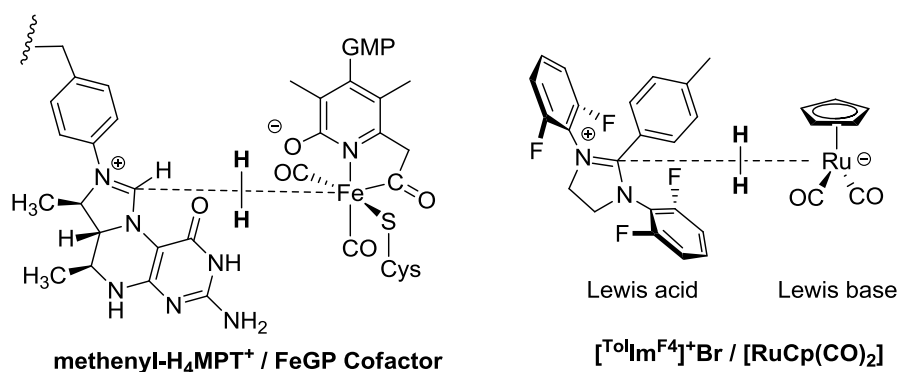
Fig. 1.20: Comparison between the active site pf the [Fe] hydrogenase and the system imidazolium salt/ruthenium complex reported by Meyer et al.

1.7 References

(1) Badwal, S. P. S.; Giddey, S.; Munnings, C. *Wiley Interdisciplinary Reviews: Energy and Environment* **2013**, *2*, 473.

(2) Andrews, J.; Shabani, B. *Wiley Interdisciplinary Reviews: Energy and Environment* **2014**, *3*, 474.

(3) *"Integrated Hydrogen Production, Purification and Compression System; DOE Hydrogen Program FY 2008 Annual Progress Report"*, United States Department of Energy.

(4) Consulting, S. *SRI Consulting is the world's leading business research service for the global chemical industry* **2008**.

(5) Erisman, J. W.; Sutton, M. A.; Galloway, J.; Klimont, Z.; Winiwarter, W. *Nature Geosci* **2008**, *1*, 636.

(6) Modak, J. *Reson* **2002**, *7*, 69.

(7) *Chinese methanol demand analysis - ICIS China Methanol Annual Study*, *2013*.

(8) Klier, K. In *Advances in Catalysis*; D.D. Eley, H. P., Paul, B. W., Eds.; Academic Press: **1982**; Vol. Volume 31, p 243.

(9) Lormand, C. *Industrial & Engineering Chemistry* **1925**, *17*, 430.

(10) Natta, G. *Catalysis* **1955**, *3*, 349.

(11) J. Gallagher, Y. H. Kiold *ICI, GB 1159035* **1965**.

(12) P. Courty, C. M. *Preparation of catalysts III*, *Elsevier*, **1983**, 485.

(13) *Crit. Report Appl. Chem.* **1985**, *13*, 102.

(14) Hammond, C.; Jenkins, R. L.; Dimitratos, N.; Lopez-Sanchez, J. A.; ab Rahim, M. H.; Forde, M. M.; Thetford, A.; Murphy, D. M.; Hagen, H.; Stangland, E. E.; Moulijn, J. M.; Taylor, S. H.; Willock, D. J.; Hutchings, G. J. *Chem. Eur. J.* **2012**, *18*, 15735.

(15) Osako, T.; Watson, E. J.; Dehestani, A.; Bales, B. C.; Mayer, J. M. *Angewandte Chemie* **2006**, *118*, 7593.

(16) Alayon, E. M. N., Maarten; Ranocchiari, Marco; van Bokhoven, Jeroen *CHIMIA* **2012**, *66*, 668.

(17) Studt, F.; Sharafutdinov, I.; Abild-Pedersen, F.; Elkjær, C. F.; Hummelshøj, J. S.; Dahl, S.; Chorkendorff, I.; Nørskov, J. K. *Nat Chem* **2014**, *6*, 320.

(18) Ménard, G.; Stephan, D. W. *J. Am. Chem. Soc.* **2010**, *132*, 1796.

(19) Riduan, S. N.; Zhang, Y.; Ying, J. Y. *Angewandte Chemie* **2009**, *121*, 3372.

(20) Olah, G. A. *Angew. Chem. Int. Ed.* **2005**, *44*, 2636.

(21) *Number and Capacity of Petroleum Refineries* **2014**, *U.S. Energy Information Administration*, retrieved from http://www.eia.gov/

(22) *The hydrocracking process rertieved* from http://www.refiningnz.com

(23) John W. Ward, S. A. Q. *ACS Symposium Series; American Chemical Society: Washington, DC* **1975**, *ISBN 0-8412-0303-2*.

(24) B. Delmon, J. Y. *Hydrotreatment and Hydrocracking of oil fractions,* **1999**, *Elsevier, ISBN: 0-444-50214-9*.

(25) Miranda-Galindo, E. Y.; Segovia-Hernández, J. G.; Hernández, S.; Bonilla-Petriciolet, A. *Industrial & Engineering Chemistry Research* **2014**, *53*, 16425.

(26)   Barrow, K. *Oil Gas Journal* **2009**, *107*, 38.

(27)   F.L. Plantenga, R. G. L. *Appl Catal A: Gen* **2003**, 1.

(28)   Churchill, D. G.; Bridgewater, B. M.; Parkin, G. *J. Am. Chem. Soc.* **2000**, *122*, 178.

(29)   Buccella, D.; Janak, K. E.; Parkin, G. *J. Am. Chem. Soc.* **2008**, *130*, 16187.

(30)   Al-Daous, M. A.; Ali, S. A. *Fuel* **2012**, *97*, 662.

(31)   W.L.Orr , C. M. White. *ACS Symposium Series 429,* **1990**, *American Chemical Society, Washington, DC*.

(32)   V.A.Aksenov, V. F. K. *Pergamon Press, New York* **1981**.

(33)   Zhu, G.; Tanski, J. M.; Churchill, D. G.; Janak, K. E.; Parkin, G. *J. Am. Chem. Soc.* **2002**, *124*, 13658.

(34)   Furimsky, E.; Massoth, F. E. *Catalysis Reviews* **2005**, *47*, 297.

(35)   Angelici, R. J. *Encyclopedia of Inorganic Chemistry John Wiley & Sons, Ltd* **2006**.

(36)   Bonrath, W.; Medlock, J.; Schütz, J.; Wüstenberg, B.; Netscher, T. *Hydrogenation in the Vitamins and Fine Chemicals Industry – An Overview*, **2012**, DOI: 10.5772/48751.

(37)   R.A.Sheldon, H. v. *Fine chemicals through heterogeneous catalysis, Wiley-VCH, Weinheim, Germany,* **2001**, chapter 1, 589.

(38)   T.Netscher, W. B. *Appl. Catal. A* **2005**, *280*, 55.

(39)   Lindlar, H. *Helvetica Chimica Acta* **1952**, *35*, 446.

(40)   Bonrath, W.; Karge, R.; Roessler, F.; Google Patents: **2006**.

(41)   Reinaldo M. Machado, K. R. H., & Robert R. Broekhuis *Current Opinion in Drug Discovery & Development* 2001, *4 (6) PharmaPress Ltd ISSN 1367-673,* retrieved from http://www.airproducts.com.

(42)   Rigotti, A. *Molecular Aspects of Medicine* **2007**, *28*, 423.

(43)   Bonrath, W.; Eggersdorfer, M.; Netscher, T. *Catalysis Today* **2007**, *121*, 45.

(44)   Netscher, T. In *Vitamins & Hormones*; Gerald, L., Ed.; Academic Press: **2007**; Vol. Volume 76, p 155.

(45)   Bonrath, W.; Netscher, T.; Schütz, J.; Wüstenberg, B.; Patent US20140323767 A1, **2012**.

(46)   Aquila, W.; Breuer, K.; Dirnsteiner, T.; Dobler, W.; Goebbel, H. G.; Hahn, T.; Kaibel, G.; Miller, C.; Patent WO2004007413, **2004**.

(47)   Bonrath, W.; Kircher, T.; Kuenzi, R.; Tschumi, J; Patent WO2006029737, **2006**.

(48)   Surmatis J.D, Weber J.; Patent US 2783257, **1957**.

(49)   Mirzoeva, E. S.; Bronstein, L. M.; Valetsky, P. M.; Sulman, E. M. *Reactive Polymers* **1995**, *24*, 243.

(50)   Kirk-Othmer, S. C. *Encyclopedia of Chemical Technology NY, John Wiley & Sons; Terpenoids* **2001**, ISBN: 978-0-471-48496-7.

(51)   Reichstein, T. u. G., A. *Helv. Chim. Acta* **1934**, 311.

(52)   Bronnimann, C.; Bodnar, Z.; Hug, P.; Mallat, T.; Baiker, A. *J. Catal.* **1994**, *150*, 199.

(53)   Hancock, R. D.; Viola, R. *Trends in Biotechnology* **2002**, *20*, 299.

(54)   Sikervar, V. In *Encyclopedia of Reagents for Organic Synthesis*; John Wiley & Sons, Ltd **2001**, ISBN: 9780470842898.

(55)   Nishimura, S. *Handbook of heterogeneous catalytic hydrogenation for organic synthesis* **2001**, ISBN: 978-0-471-39698-7.

(56)   Debus, H. J. *Liebigs Ann. Chem.* **1863**, 200.

(57)   Fouilloux, P. *Applied Catalysis* **1983**, *8*, 1.

(58)   Osborn, J. A.; Jardine, F. H.; Young, J. F.; Wilkinson, G. *J. Chem. Soc. A.* **1966**, 1711.

(59)   Knowles, W. S. *Advanced Synthesis & Catalysis* **2003**, *345*, 3.

(60)   Vaska, L.; Rhodes, R. E. *J. Am. Chem. Soc.* **1965**, *87*, 4970.

(61)   Vaska, L.; DiLuzio, J. W. *J. Am. Chem. Soc.* **1962**, *84*, 679.

(62)   Schrock, R. R.; Osborn, J. A. *J. Am. Chem. Soc.* **1976**, *98*, 2134.

(63)   Crabtree, R. *Acc. Chem. Res.* **1979**, *12*, 331.

(64)   Crabtree, R. H.; Demou, P. C.; Eden, D.; Mihelcic, J. M.; Parnell, C. A.; Quirk, J. M.; Morris, G. E. *J. Am. Chem. Soc.* **1982**, *104*, 6994.

(65)   Korpiun, O.; Mislow, K. *J. Am. Chem. Soc.* **1967**, *89*, 4784.

(66)   Knowles, W. S. *Angew. Chem. Int. Ed.* **2002**, *41*, 1998.

(67)   Halpern, J. *Science* **1982**, *217*, 401.

(68)   Burk, M. J. *Acc. Chem. Res.* **2000**, *33*, 363.

(69)   Noyori, R.; Ohkuma, T.; Kitamura, M.; Takaya, H.; Sayo, N.; Kumobayashi, H.; Akutagawa, S. *J. Am. Chem. Soc.* **1987**, *109*, 5856.

(70)   Noyori, R. *Angew. Chem. Int. Ed.* **2002**, *41*, 2008.

(71)   Ohkuma, T.; Ooka, H.; Hashiguchi, S.; Ikariya, T.; Noyori, R. *J. Am. Chem. Soc.* **1995**, *117*, 2675.

(72)   Ohkuma, T.; Koizumi, M.; Doucet, H.; Pham, T.; Kozawa, M.; Murata, K.; Katayama, E.; Yokozawa, T.; Ikariya, T.; Noyori, R. *J. Am. Chem. Soc.* **1998**, *120*, 13529.

(73)   Ohkuma, T.; Ooka, H.; Ikariya, T.; Noyori, R. *J. Am. Chem. Soc.* **1995**, *117*, 10417.

(74)   Noyori, R.; Ohkuma, T. *Angew. Chem. Int. Ed.* **2001**, *40*, 40.

(75)   Sandoval, C. A.; Ohkuma, T.; Muñiz, K.; Noyori, R. *J. Am. Chem. Soc.* **2003**, *125*, 13490.

(76)   Matsumura, K.; Hashiguchi, S.; Ikariya, T.; Noyori, R. *J. Am. Chem. Soc.* **1997**, *119*, 8738.

(77)   Yamada, I.; Noyori, R. *Organic Letters* **2000**, *2*, 3425.

(78)   Noyori, R.; Yamakawa, M.; Hashiguchi, S. *J.Org. Chem.* **2001**, *66*, 7931.

(79)   Johnstone, R. A. W.; Wilby, A. H.; Entwistle, I. D. *Chem. Rev.* **1985**, *85*, 129.

(80)   Gladiali, S.; Alberico, E. *Chem. Soc. Rev.* **2006**, *35*, 226.

(81)   Takashi, K.; Takao, I. *Advanced Synthesis & Catalysis* **2004,** *346*, 37-41.

(82)   Meerwein, H.; Schmidt, R. *Justus Liebigs Annalen der Chemie* **1925**, *444*, 221.

(83)   Ponndorf, W. *Angewandte Chemie* **1926**, *39*, 138.

(84)   Cohen, R.; Graves, C. R.; Nguyen, S. T.; Martin, J. M. L.; Ratner, M. A. *J. Am. Chem. Soc.* **2004**, *126*, 14796.

(85)   Bäckvall, J.-E. *J. Organomet. Chem.* **2002**, *652*, 105.

(86)   Campbell, E. J.; Zhou, H.; Nguyen, S. T. *Angew. Chem. Int. Ed.* **2002**, *41*, 1020.

(87)   Linstead, R. P.; Braude, F. A.; Mitchell, P. W. D.; Wooldridge, K. R. H.; Jackman, L. M. *Nature* **1952**, *169*, 100.

(88)   Sasson, Y.; Blum, J. *Tetrahedron Letters* **1971**, *12*, 2167.

(89)   Sasson, Y.; Blum, J. *J. Org. Chem.* 1975.

(90)   Ikariya, T.; Murata, K.; Noyori, R. *Org. Biomol. Chem.* **2006**, *4*, 393.

(91) Haack, K.-J.; Hashiguchi, S.; Fujii, A.; Ikariya, T.; Noyori, R. *Angew. Chem. Int. Ed.* **1997**, *36*, 285.

(92) Aidan, M. H.; David, J. M.; Guy, J. C.; Martin, W. *J. Am. Chem. Soc.* **2005**, *127*, 7318.

(93) Fung Kei, C.; Aidan, M. H.; Jerome, H.; Aveline, S. Y. Y.; Martin, W. *J. Org. Chem.* **2005**, *70*, 3188.

(94) Shvo, Y.; Czarkie, D.; Rahamim, Y.; Chodosh, D. F. *J. Am. Chem. Soc.* **1986**, *108*, 7400.

(95) Conley, B. L.; Pennington-Boggio, M. K.; Boz, E.; Williams, T. J. *Chem. Rev.* **2010**, *110*, 2294.

(96) Clapham, S. E.; Hadzovic, A.; Morris, R. H. *Coord.Chem.Rev.* **2004**, *248*, 2201.

(97) Salvini, A.; Frediani, P.; Gallerini, S. *Appl.Organometal. Chem.* **2000**, *14*, 570.

(98) Heinekey, D. M.; Oldham, W. J. *Chem. Rev.* **1993**, *93*, 913.

(99) Waterman, R. *Organometallics* **2013**, *32*, 7249.

(100) Perutz, R. N.; Sabo-Etienne, S. *Angew. Chem. Int. Ed.* **2007**, *46*, 2578.

(101) Earl, K. A.; Jia, G.; Maltby, P. A.; Morris, R. H. *J. Am. Chem. Soc.* **1991**, *113*, 3027.

(102) Rabaâ, H.; Saillard, J. Y.; Schubert, U. *J. Organomet. Chem.* **1987**, *330*, 397.

(103) Crabtree, R. H.; Quirk, J. M. *J. Organomet. Chem.* **1980**, *199*, 99.

(104) Mura, P.; Segre, A.; Sostero, S. *Inorg. Chem.* **1989**, *28*, 2853.

(105) Buncel, E.; Menon, B. *J. Am. Chem. Soc.* **1977**, *99*, 4457.

(106) Rocchini, E.; Mezzetti, A.; Rüegger, H.; Burckhardt, U.; Gramlich, V.; Del Zotto, A.; Martinuzzi, P.; Rigo, P. *Inorg.Chem.* **1997**, *36*, 711.

(107) Crabtree, R. H.; Lavin, M. *J. Chem. Soc., Chem. Commun.* **1985**, 794.

(108) Arndtsen, B. A.; Bergman, R. G.; Mobley, T. A.; Peterson, T. H. *Acc. Chem. Res.* **1995**, *28*, 154.

(109) Labinger, J. A.; Bercaw, J. E. *Nature* **2002**, *417*, 507.

(110) Brintzinger, H. H. *J. Organomet. Chem.* **1979**, *171*, 337.

(111) *U.S Census Bureau. International Data Base* Last update Dec. **2013**.

(112) In *U.S. Energy Information Administration, "International Energy Statistics",* Dept. of Energy, Washington, DC **2011**.

(113) Enthaler, S.; Junge, K.; Beller, M. *Angew. Chem. Int. Ed.* **2008**, *47*, 3317.

(114) Bernd Plietker *Iron Catalysis in Organic Chemistry: Reactions and Applications,* **2008**, , *Wiley-VCHVerlag, Weinheim.* DOI: 10.1002/9783527623273.ch5

(115) Bolm, C.; Legros, J.; Le Paih, J.; Zani, L. *Chem. Rev.* **2004**, *104*, 6217.

(116) Values based on *www.platinum.matthey.com*. For iron the price is based on iron ore, *http://www.indexmundi.com/*

(117) Mond, L. Q., F. *J. Chem. Soc.* **1891**, *59*, 604.

(118) Berthelot, M. C. R. *Hebd. Seances Acad. Sci.* **1981**, *112*, 343.

(119) Reppe, W. V., H *Liebigs Ann. Chem.* **1953**, *582*, 13.

(120) Kealy, T. J. P., P. L. *Nature* **1951**, *168*, 1039.

(121) Collman, J. P. *Acc. Chem. Res.* 1975, *8*, 342.

(122) Bianchini, C.; Meli, A.; Peruzzini, M.; Vizza, F.; Zanobini, F.; Frediani, P. *Organometallics* **1989**, *8*, 2080.

(123) Bianchini, C.; Meli, A.; Peruzzini, M.; Frediani, P.; Bohanna, C.; Esteruelas, M. A.; Oro, L. A. *Organometallics* **1992**, *11*, 138.

(124) Daida, E. J.; Peters, J. C. *Inorg. Chem.* **2004**, *43*, 7474.

(125) Bart, S. C.; Hawrelak, E. J.; Lobkovsky, E.; Chirik, P. J. *Organometallics* **2005**, *24*, 5518.

(126) Yu, R. P.; Darmon, J. M.; Hoyt, J. M.; Margulieux, G. W.; Turner, Z. R.; Chirik, P. J. *ACS Catalysis* **2012**, *2*, 1760.

(127) Bart, S. C.; Lobkovsky, E.; Chirik, P. J. *J. Am. Chem. Soc.* **2004**, *126*, 13794.

(128) Wienhofer, G.; Westerhaus, F. A.; Jagadeesh, R. V.; Junge, K.; Junge, H.; Beller, M. *Chem. Commun.* **2012**, *48*, 4827.

(129) Wienhöfer, G.; Westerhaus, F. A.; Junge, K.; Beller, M. *J. Organomet. Chem.* **2013**, *744*, 156.

(130) Srimani, D.; Diskin-Posner, Y.; Ben-David, Y.; Milstein, D. *Angew. Chem. Int. Ed* **2013**, *52*, 14131.

(131) Markó, L.; Radhi, M. A.; Ötvös, I. *J. Organomet. Chem.* **1981**, *218*, 369.

(132) Casey, C. P.; Guan, H. *J. Am. Chem. Soc.* **2007**, *129*, 5816.

(133) Casey, C. P.; Guan, H. *J. Am. Chem. Soc.* **2009**, *131*, 2499.

(134) Rautenstrauch, V.; Hoang-Cong, X.; Churlaud, R.; Abdur-Rashid, K.; Morris, R. H. *Chem. Eur.J.* **2003**, *9*, 4954.

(135) Morris, R. H. *Chem. Soc.Rev.* **2009**, 38, 2282.

(136) Zuo, W.; Lough, A. J.; Li, Y. F.; Morris, R. H. *Science* **2013**, *342*, 1080.

(137) Mikhailine, A. A.; Morris, R. H. *Inorg. Chem.* **2010**, 49, 11039.

(138) Prokopchuk, D. E.; Morris, R. H. *Organometallics* **2012**, 31, 7375.

(139) Mikhailine, A. A.; Maishan, M. I.; Lough, A. J.; Morris, R. H. *J. Am. Chem. Soc.* **2012**, 134, 12266.

(140) Bigler, R.; Huber R.; Mezzetti, A. *Angew. Chem. Int. Ed.* **2015**, 54, 5171.

(141) Lagaditis, P. O.; Sues, P. E.; Sonnenberg, J. F.; Wan, K. Y.; Lough, A. J.; Morris, R. H. *J. Am. Chem. Soc.* **2014**, 136, 1367.

(142) Langer, R.; Leitus, G.; Ben-David, Y.; Milstein, D. *Angew. Chem. Int. Ed.* **2011**, 50, 2120.

(143) Zell, T.; Ben-David, Y.; Milstein, D. *Catalysis Science & Technology* **2015**, *5*, 822.

(144) Fleischer, S.; Zhou, S.; Junge, K.; Beller, M. *Angew. Chem. Int. Ed.* **2013**, *52*, 5120.

(145) Wienhöfer, G.; Westerhaus, F. A.; Junge, K.; Ludwig, R.; Beller, M. *Chem. Eur. J.* **2013**, *19*, 7701.

(146) Zhou, S.; Fleischer, S.; Junge, K.; Beller, M. *Angew. Chem. Int. Ed.* **2011**, *50*, 5120.

(147) Gorgas, N.; Stöger, B.; Veiros, L. F.; Pittenauer, E.; Allmaier, G.; Kirchner, K. *Organometallics* **2014**, *33*, 6905.

(148) Naik, A.; Maji, T.; Reiser, O. *Chem.Commun.* **2010**, *46*, 4475.

(149) Zell, T.; Ben-David, Y.; Milstein, D. *Angew. Chem. Int. Ed.* **2014**, *53*, 4685.

(150) Werkmeister, S.; Junge, K.; Wendt, B.; Alberico, E.; Jiao, H.; Baumann, W.; Junge, H.; Gallou, F.; Beller, M. *Angew. Chem. Int. Ed.* **2014**, *53*, 8722.

(151) Chakraborty, S.; Dai, H.; Bhattacharya, P.; Fairweather, N. T.; Gibson, M. S.; Krause, J. A.; Guan, H. *J. Am. Chem. Soc.* **2014**, *136*, 7869.

(152) Alvin, I. K. *Enzyme and Microbial Technology* **1979,** *1*, 165–172.

(153) Lubitz, W.; Ogata, H.; Rüdiger, O.; Reijerse, E. *Chem. Rev.* **2014**, *114*, 4081.

(154) Volbeda, A.; Charon, M.-H.; Piras, C.; Hatchikian, E. C.; Frey, M.; Fontecilla-Camps, J. C. *Nature* **1995**, *373*, 580.

(155) Peters, J. W.; Lanzilotta, W. N.; Lemon, B. J.; Seefeldt, L. C. *Science* **1998**, *282*, 1853.

(156) Shima, S.; Pilak, O.; Vogt, S.; Schick, M.; Stagni, M. S.; Meyer-Klaucke, W.; Warkentin, E.; Thauer, R. K.; Ermler, U. *Science* **2008**, *321*, 572.

(157) Ogo, S.; Ichikawa, K.; Kishima, T.; Matsumoto, T.; Nakai, H.; Kusaka, K.; Ohhara, T. *Science* **2013**, *339*, 682.

(158) Tschierlei, S.; Ott, S.; Lomoth, R. *Energy Environ. Sci.***, 2011**, *4*, 2340.

(159) Fan, H.-J.; Hall, M. B. *J. Am. Chem. Soc.* **2001**, *123*, 3828.

(160) Niu, S.; Thomson, L. M.; Hall, M. B. *J. Am. Chem. Soc.* **1999**, *121*, 4000.

(161) Liu, T.; Wang, X.; Hoffmann, C.; DuBois, D. L.; Bullock, R. M. *Angew. Chem. Int. Ed.* **2014**, *53*, 5300.

(162) Carroll, M. E.; Barton, B. E.; Rauchfuss, T. B.; Carroll, P. *J. Am. Chem. Soc.* **2012**, *134*, 18843.

(163) Kalz, K. F.; Brinkmeier, A.; Dechert, S.; Mata, R. A.; Meyer, F. *J. Am. Chem. Soc,* **2014**, *136*, 24.

Chapter 2:

Biomimetic Iron Complexes
for Hydrogen Activation

2.1 Hydrogenases models based on earth-abundant metals

Determination of the structures of [FeFe] hydrogenases has revealed that active sites consist of bimetallic iron complexes bridged by a di(thiomethyl)amine ligand[1-6], $HN(CH_2S^-)_2$. In its reduced form, one iron is bound to two terminal CO ligands and one cyanide ligand with a vacant coordination site adjacent to the di(thiomethyl)amine ligand (Fig. 2.1).
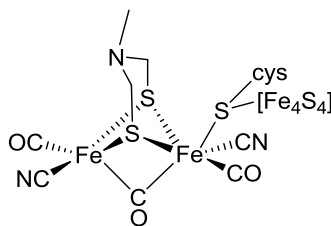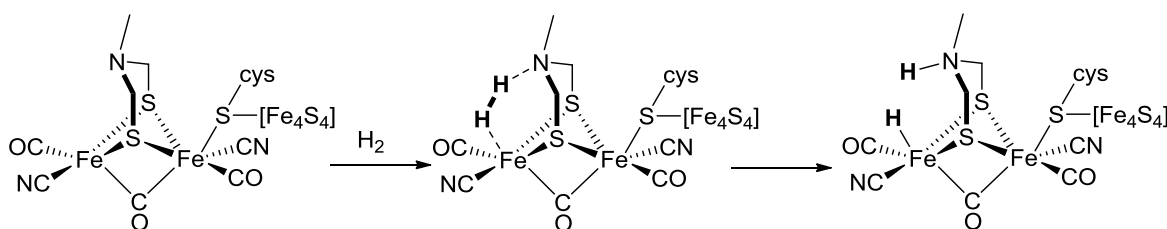

Fig. 2.1: Active site of the [FeFe] hydrogenase enzyme

DFT calculations have shown that the nitrogen atom is a suitable base for assisting heterolytic cleavage of hydrogen at the active site, providing a low energy pathway for the transfer of protons from the active site to the exterior of the enzyme via a proton-transfer pathway[7,8]. The reaction involving the N base is much more favourable than that one involving terminal CN or bridging S. A strong $Fe-H^{\delta-} \cdots H^{\delta+}-N$ "dihydrogen bond" has been found in the H_2 heterolytic cleavage product. Noteworthy, the six-membered ring structure proposed in the [FeFe] hydrogenase has a boat conformation, so that the pendant amine is properly positioned to facilitate the binding and cleavage of the H_2 ligand (Scheme 2.1).

Scheme 2.1: Active site of the [FeFe] hydrogenase enzyme and its reaction with H_2. This drawing focuses only on the active metal site and does not show the complexity of the protein surrounding the active site. Delivery of electrons occurs through an Fe_2S_4 cluster so that protons and H_2 are delivered to and from the active site by channels present in the enzyme.

Organometallic complexes mainly based on earth-abundant metals bearing pendant bases have shown great reactivity in the proton/hydride exchange reaction[9-16] or as electrocatalysts for H_2 production or oxidation[17-22] (Scheme 2.2).
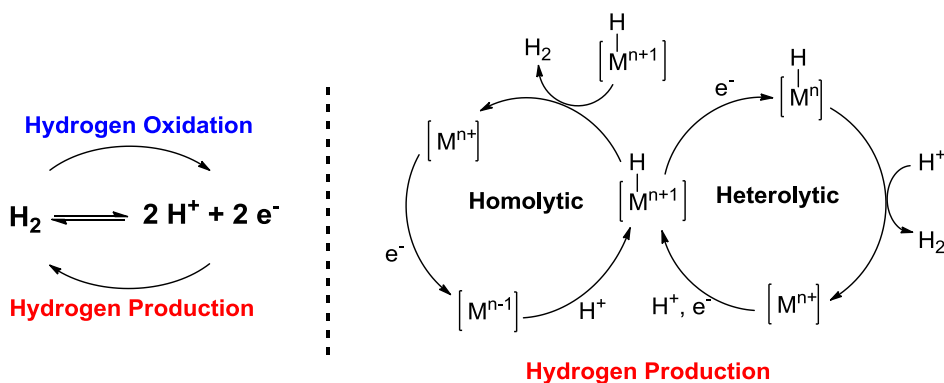
Scheme 2.2: General equation for the oxidation of H_2 and production of H_2 by reduction of protons (left). Proposed mechanism for H_2 evolution *via* the formation of metal-hydride intermediate (right).

A central concept in the design of efficient catalysts is the positioning of a pendant base in the second coordination sphere and close to a vacant coordination site on the metal, in order to lead to a bifunctional activation of H_2 during the heterolytic cleavage or formation of the H-H bond. Systematic modifications of the steric and electronic properties of the ligands change the thermodynamic driving force for either oxidation or production of H_2 (Scheme 2.3).
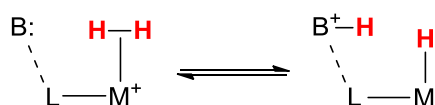
Scheme 2.3: Intramolecular deprotonation of H_2 bounded to the metal center

Useful thermodynamic measurements of H_2 addition[19] have been made on the complex $[Ni(P^R_2N^{R'}_2)_2]^{2+}$ (Scheme 2.4). Equation 1 shows the ability of the metal complex to accept the hydride, where $-\Delta G^0_{H^-}$ is the free energy associated. In equation 2 is reported the energy of protonation of a pendant amine that can vary according to the groups present on the phosphine moieties. For the heterolytic cleavage of H_2 in CH_3CN the value of 76 Kcal/mol is calculated[23,24].
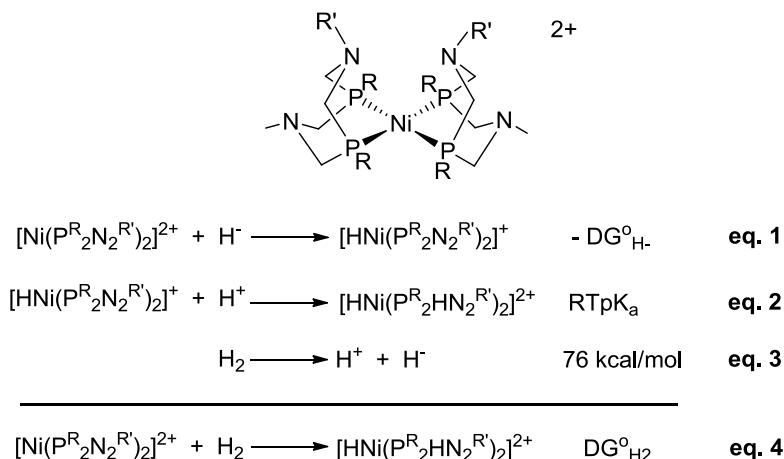
Scheme 2.4: Thermodynamics of H$_2$ addition to [Ni(P$^R_2$N$^{R'}_2$)$_2$]$^{2+}$

The final free energy for addition of H$_2$ calculated for the whole process ΔG^0_{H2} (equation 4) determines the nature of a potential catalyst. When ΔG^0_{H2} is negative, incorporation of H$_2$ into the metal complex is thermodynamically favourable, and therefore complexes would be good candidates for oxidation of H$_2$. On the other hand, with a positive ΔG^0_{H2} value the expulsion of H$_2$ is favored, leading to more suitable catalysts for H$_2$ production.

From this starting point, several research groups have focused on transition metal complexes containing pendant amines incorporated into diphosphane ligands, abbreviated P(N)P- or simply PNP-type ligands[25-31] (Scheme 2.5). These complexes have a structural motif that should permit facile tuning of the electronic and steric properties by varying substituents on the phosphine moieties, whereas the pendant amine promotes facile heterolytic cleavage or formation of H-H bond.
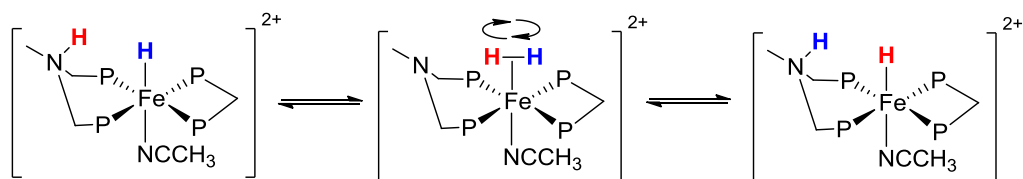
Scheme 2.5: Intramolecular proton/hydride exchange in an iron (II) complex bearing a chelating N-containing bis-phosphane ligand. The PNHP$^+$ ligand approach the hydride ligand in the boat conformation.

While the incorporation of a pendant amine into the bis-phosphane ligand leads to a significant decrease in the overpotential for the electrocatalytic oxidation of H$_2$, the six-membered ring M-P(N)P undergoes chair/boat conversions as observed for cyclohexane-type ring structures. Consequently, the pendant amine is positioned optimally for interaction with a

M–H bond only when it is in a boat conformation[10,19,27]. A crystal structure of a derivative of $[Ni(PNP)_2]^{2+}$ (Scheme 2.4, with an *n*Bu groups on each N) shows that both six-membered rings are in the chair form[28] so conversion to the boat conformation contributes to the barrier for oxidation of H_2 by $[Ni(PNP)_2]^{2+}$.

As described in literature[32-36], once H_2 binds the metal center a dihydrogen complex forms, exhibiting a characteristic dihydrogen resonance visible at negative chemical shift in the ^{1}H-NMR. Dihydrogen complexes can be generated as either stable species or intermediate. In scheme 2.6 is reported the example of an active iron complex bearing a pendant amine used as electrocatalyst for oxidation of hydrogen[20].
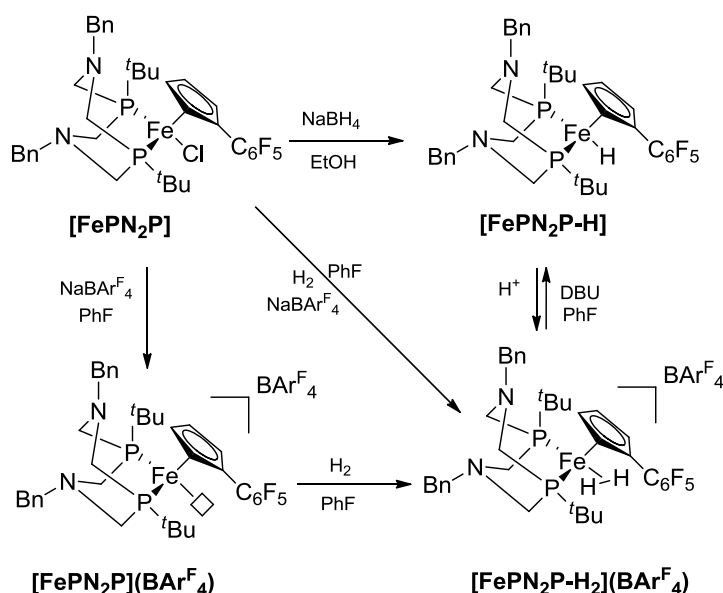
Scheme 2.6: Reactivity of [FePN$_2$P] in presence of H$_2$.

Interestingly, complex **[FePN$_2$P-H$_2$](BAr$^F_4$)** exhibited a characteristic dihydrogen resonance at -13.45 ppm in the ^{1}H-NMR, while **[FePN$_2$P-H]** showed a triplet hydride signal at -16.99 ppm (J_{PH}=60 Hz).

In the view of previous developments, we decided to investigate the coordination chemistry and reactivity of novel iron (II) complexes bearing an amine as internal base for H_2 activation.

2.2 Synthesis and characterization of novel iron (II) complexes bearing an internal base

In this section, the synthesis and characterization of several low spin iron (II) complexes bearing pendant amines incorporated into diphosphane ligands are reported. A low spin configuration on the metal center would allow both the donation of electron density from the σ orbital of H_2 to an empty d orbital of σ symmetry on the metal ($\sigma(\eta_2\text{-}H_2) \rightarrow d^{\sigma}(M)$) and the back-donation from filled d orbitals of the metal to the σ^* orbital of H_2 ($d^{\pi}(M) \rightarrow \sigma^*(\eta_2\text{-}H_2)$).

All the complexes were tested for hydrogen activation and hydrogenation reaction of a large number of synthetically useful unsaturated substrates. Ligand synthesis

2.2.1.1 PNP-type ligands

The PNP-type ligands with a pendant amine were synthesized by reaction of two equivalents of R_2PCH_2OH (readily preformed from equimolar amounts of $(CH_2O)_n$ and a secondary phosphine R_2PH) with the appropriate stoichiometry of primary amine $R'\text{-}NH_2$ in either refluxing MeOH or EtOH[37-39] (Scheme 2.7 and 2.8). High yields and clean products were obtained by working with air-free techniques.
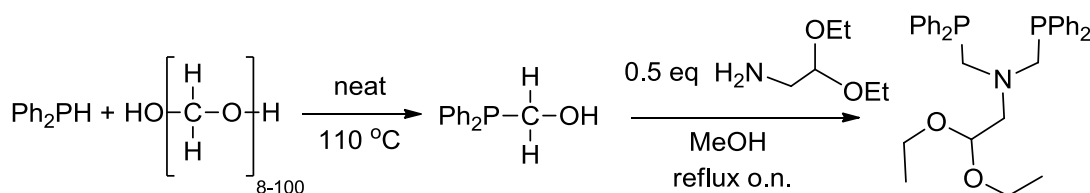
Scheme 2.7: Synthesis of the aromatic Ph_2PNPPh_2 ligand.
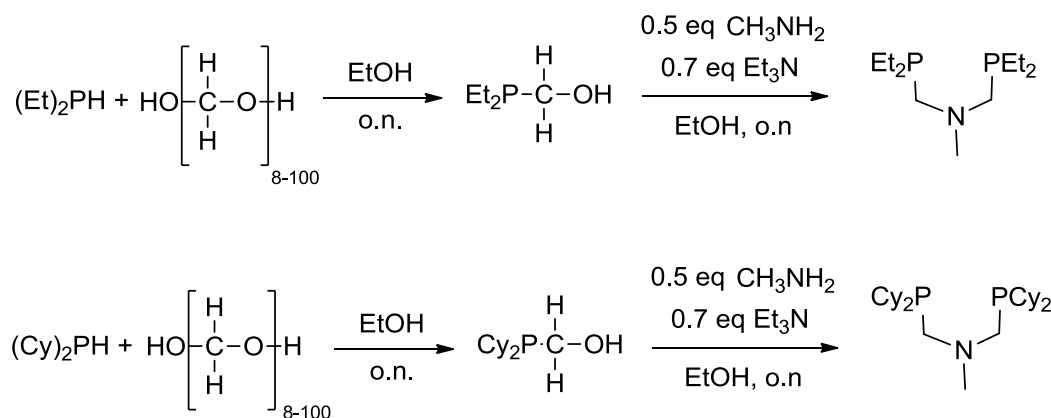
Scheme 2.8: Synthesis of the aliphatic Et_2PNPEt_2 and Cy_2PNPCy_2 ligands.

The Ph$_2$PNPPh$_2$ (^{Ph}PNP) ligand exhibited a characteristic signal at δ -27.58 ppm in the ^{31}P- NMR while the aliphatic Et$_2$PNPEt$_2$ (^{Et}PNP) at δ -32.13 ppm and Cy$_2$PNPCy$_2$ (^{Cy}PNP) at δ -16.64 ppm.

### 2.2.1.2 Amidothiophenolate ligands

Strong π-donor ligands such as the 2-amidothiophenolate dianion are well known in the synthesis of 16-electron iron carbonyl complexes[40-42]. For this purpose the sodium 2-aminobenzenethiolate was synthesized from the 2-aminobenzenethiol in presence of Na (Scheme 2.9). Differently, dithiolate ligands such as 1,2-benzenedithiol (bdt) and 3,6-dichloro-1,2-benzenedithiol (Cl$_2$bdt) were deprotonated *in situ* by addition of a slightly excess of Et$_3$N.
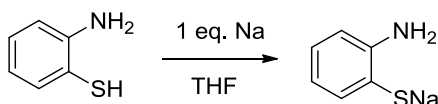
Scheme 2.9: Synthesis of sodium 2-aminobenzenethiolate.

As mono-anionic ligand, sodium 2-dimethyl-aminobenzenethiolate was synthesized in a 2-step synthesis from 2-[(2-aminophenyl)disulfanyl]phenylamine (Scheme 2.10).
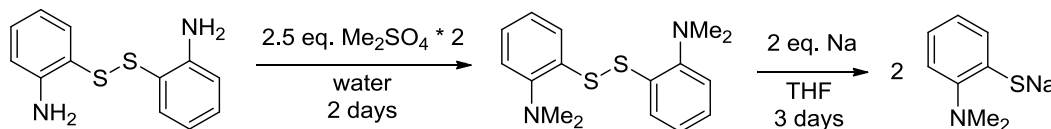
Scheme 2.10: Synthesis of sodium 2-dimethyl-aminobenzenethiolate.

2.2.2 Metallation using iron salts

Stable iron (II) low spin complexes were synthesized reacting the Ph$_2$PNPPh$_2$ ligand with FeCl$_2$ in anhydrous MeOH or THF, under CO atmosphere and in presence of an anionic ligand as reported in literature[22]. Complex [(^{Ph}PNP)Fe(CO)(Cl$_2$bdt)] (**1**) was synthesized in a one-pot reaction mixing the Ph$_2$PNPPh$_2$ ligand with FeCl$_2$ under CO (1.5 bar). After 30 min of stirring, a solution of Cl$_2$bdt and Et$_3$N was added in the reaction mixture affording **1** as dark powder in 42% yield after the work-up (Scheme 2.11).
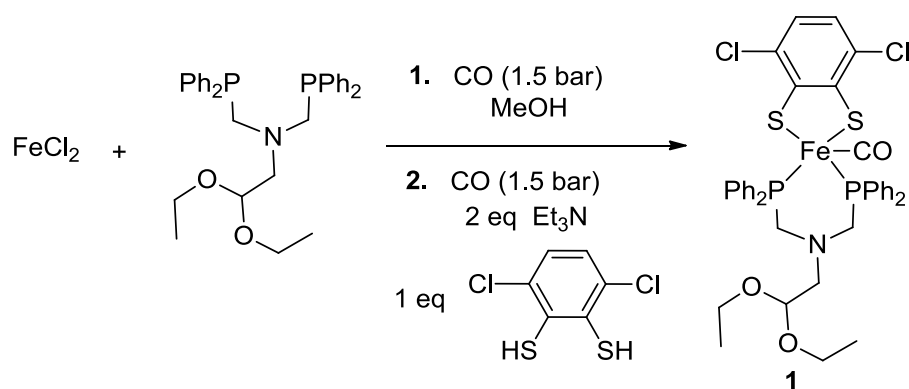
Scheme 2.11: Synthesis of complex **1**.

Complex **1** is a neutral pentacoordinated Fe(II) low spin complex providing an open site for substrate binding without the need of ligand dissociation. Moreover, it contains an amine functionality in the bis-phosphane ligand as a potential protonation site. Additional ether chains at the amine provided increased solubility in polar aprotic solvents. The ^{31}P-NMR spectrum exhibited a characteristic singlet at δ 48.95 ppm and the CO vibrational frequency measured was 1907 cm^{-1}.

Similar complexes have been recently reported as active catalysts for H$_2$ formation from weak acid at low overpotential showing good stability[22,43] (Fig. 2.2, complex **2** and **3**). The presence of the two chlorine atoms on the dithiolate ligand should lead to a higher acidity of **1** with respect to **2** thus, to a different electronic environment on the metal center as confirmed by FT-IR analysis. The reported X-Ray structure of **2** showed a square pyramidal geometry with the carbonyl group on the apical position. Unfortunately, no suitable crystals of **1** were obtained for X-Ray analysis due to its high solubility.
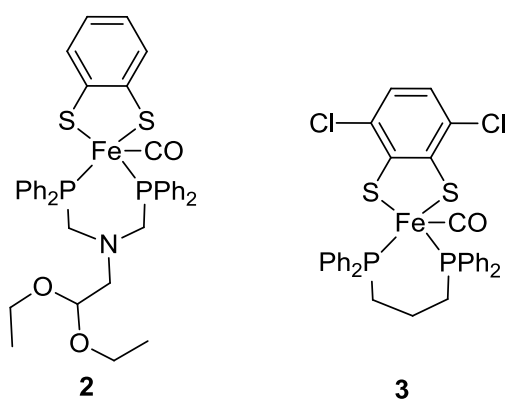

Fig 2.2: Complexes **2** and **3** active catalysts for H$_2$ formation from weak acids.

In order to tune the electronic properties on the iron center the Cl_2bdt ligand was substituted with the 2-aminobenzenethiol. When the synthesis was conducted as reported for **1** (Scheme 2.9) only a mixture of products formed as demonstrated by the ^{31}P-NMR spectrum. Therefore, a different synthetic procedure was adopted (Scheme 2.12).
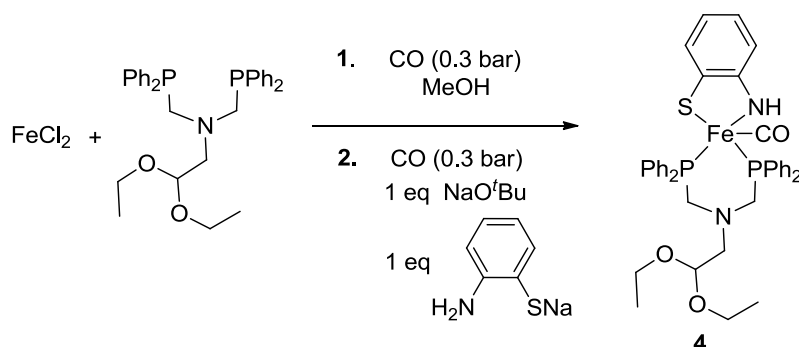
Scheme 2.12: Synthesis of complex **4**.

The 2-aminobenzenethiol was substituted with sodium 2-aminobenzenethiolate (Nbt), the Et_3N with a stronger base such as NaO^{t}Bu and the CO pressure lowered at 0.3 bar. Complex [(^{Ph}PNP)Fe(CO)(Nbt)] (**4**) was obtained in 78% yield and it exhibits a CO vibrational frequency of 1950 cm^{-1} and a characteristic signal at δ 56.75 ppm in the ^{31}P-NMR. Suitable crystals of **4** for X-Ray analysis were obtained from THF.

When the 2-aminobenzenethiolate was replaced by different ligands such as 1,2-Diaminobenzene, 1,2-Diaminocyclohexane, the neutral 1,2-Bis(diphenylphosphino)-ethane (dppe) and the chiral (1*R*,2*R*)-2-(Diphenylphosphino)cyclohexylamine no reaction occurred.

Likewise, when the Ph_2PNPPh_2 ligand was replaced by the aliphatic Et_2PNPEt_2 phosphine a mixture of products was observed in the ^{31}P-NMR. Differently, when Cy_2PNPCy_2 was used, complex [(^{Cy}PNP)Fe(CO)(Nbt)] (**5**) was synthesized as dark powder in 60% yield (Scheme 2.13).
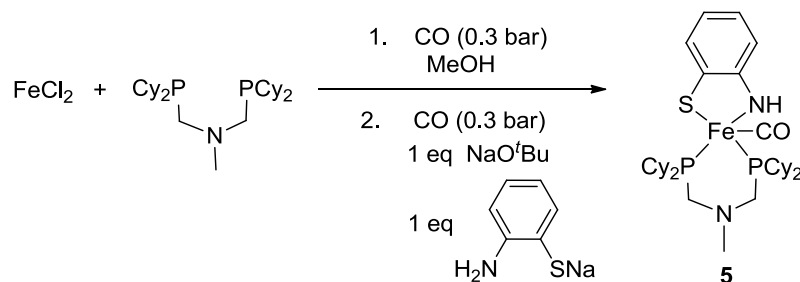
Scheme 2.13: Synthesis of complex **5**.

Complex **5** exhibited a characteristic signal at δ 60.35 ppm in the ^{31}P-NMR with a CO vibrational frequency lowered at 1890 cm^{-1} due to the cyclohexyl groups on the phosphine ligand. Suitable crystals for X-Ray analysis were obtained by diffusion of n-pentane in a saturated solution of **5** in THF.

A different low spin iron (II) complex [(dppe)Fe(CO)(Nbt)] (**6**) with a free coordination site was obtained by replacing the Ph$_2$PNPPh$_2$ ligand with the commercially available 1,2-Bis(diphenylphosphino)ethane (dppe). The synthetic procedure adopted was different than those reported above. The intermediate [FeCl$_2$(CO)$_2$(dppe)], was synthesized as reported in literature[44], and it was reacted with sodium 2-aminobenzenethiolate in presence of NaO^{t}Bu as base affording **6** as dark green powder in 75% yield (Scheme 2.14).
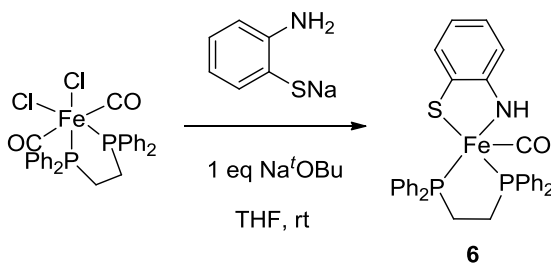
Scheme 2.14: Synthesis of complex **6**.

The CO vibrational frequency was observed at 1902 cm^{-1}, while a characteristic singlet was measured at δ 94.84 ppm in the ^{31}P-NMR, chemical shift slightly higher compared to the previous complexes.

In order to synthesize a cationic complex similar to **6** that might allow the iron center to become more electrophilic, sodium 2-aminobenzenethiolate ligand was replaced by sodium 2-dimethyl-aminobenzenethiolate. When the reaction was conducted as reported for **6,** starting material was still observed after either prolonged stirring or refluxing. Thus, the

reaction mixture was refluxed overnight in THF with 2 equiv. of sodium 2-aminobenzenethiolate ligand. Unfortunately, it was not possible to synthesize the desired product, but the dimeric iron complex [Fe(^{Me}Nbt)$_2$]$_2$ (**7**) with sulphur atoms bridging the two metal centres formed, as confirmed by the X-Ray analysis (Fig. 2.3).

7
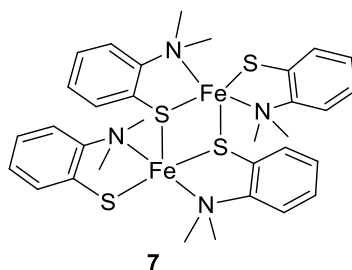
Fig. 2.3: Complex **7**.

Likewise, by changing the 2-aminobenzenethiolate ligand with the 2-(diphenyl-phosphino)benzenethiol (^{Ph}PS) it was not possible to synthesize a cationic iron (II) 16-e$^-$ low spin complex because the stable 18-e$^-$ complex [Fe(CO)$_2$(^{Ph}PS)] (**8**) formed as major product (Scheme 2.15).
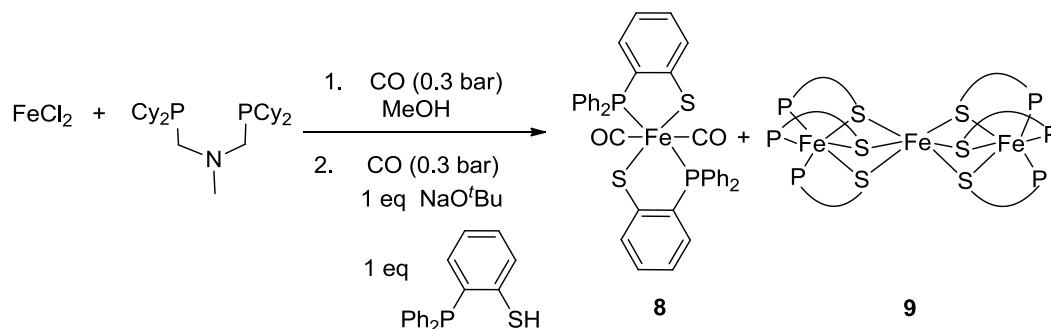
Scheme 2.15: Synthesis of complexes **8** and **9**

In **8** two 2-(Diphenyl-phosphino)benzenethiol ligands reacted with FeCl$_2$ and CO yielding a neutral complex that exhibited a CO vibration frequency at 1900 cm^{-1} and a singlet at δ 74.00 ppm in the ^{31}P-NMR. The structure was confirmed by X-Ray analysis on orange crystals obtained by diffusion of n-pentane in a saturated solution of **8** in THF. As minor product, complex [Fe(^{Ph}PS)$_2$]$_3$ (**9**) crystallized as black crystals showing a trimeric iron complex with sulphur atoms bridging the metal centres. Selective synthesis of **8** was achieved by reacting FeCl$_2$ with 2 equivalents of 2-(Diphenyl-phosphino)benzenethiol and NaO^{t}Bu under CO (0.4 bar).

A 14-e$^-$ paramagnetic Fe(II) complex [(^{Cy}PNP)FeCl$_2$] (**10**) bearing a pendant nitrogen base in the bis-phosphane ligand as a potential protonation site was synthesized by addition of Cy$_2$PNPCy$_2$ to FeCl$_2$· 1.8 THF precursor in THF as solvent (Scheme 2.16).
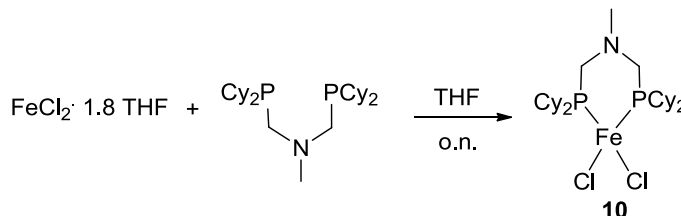
Scheme 2.16: Synthesis of complex **10**.

Complex **10** was obtained in 80% yield and its structure confirmed by X-Ray analysis and Mass Spectrometry. No reaction occurred when **10** was pressurized with CO (2 bar).

A different approach on the synthesis of stable iron (II) low spin complexes was possible by replacing the 2-aminobenzenethiolate ligand with the Cyclopentadienyl (Cp) one. The use of Cp ring substituents is an established and effective strategy for modulating the physical properties and chemical reactivity of Cp complexes[45,46]. In particular, in the field of heterolytic cleavage of H$_2$ efficient iron complexes bearing a Cp ligand and a pendant amine in the bis-phosphane ligand as a potential protonation site have been reported[10,20].

Direct reaction of **10** with NaCp ligand did not lead to a stable complex. Thus, the FeCp(CO)$_2$Cl precursor was synthesized[47] and reacted with Cy$_2$PNPCy$_2$ under UV light[10] affording complex [(^{Cy}PNP)Fe(CO)(Cp)]$^+$ (**11**) as a yellow powder in a 63 % yield (Scheme 2.17).
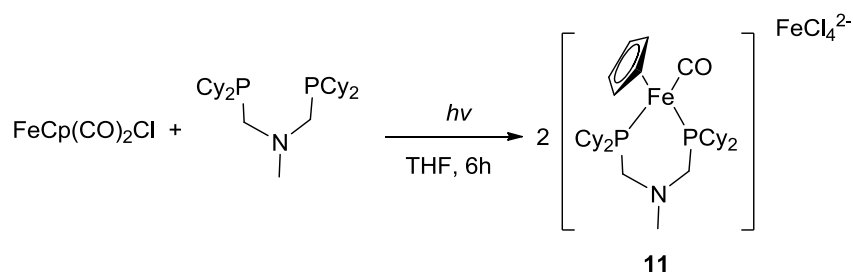
Scheme 2.17: Synthesis of complex **11.**

The X-Ray structure of **11** showed [FeCl$_4$]$^{2-}$ as counter ion. Infrared spectroscopy of **11** exhibited a CO vibration frequency at 1910 cm^{-1} , and a singlet at δ 53.00 ppm in the ^{31}P-NMR was observed.

Because **11** is an 18-e$^-$ complex with no free site for substrate binding, a second photolysis reaction was carried out with the intent of removing the CO ligand. Moreover, the counter ion [FeCl$_4$]$^{2-}$ was easily replaced by BAr$^F_4$ anion (Scheme 2.18).
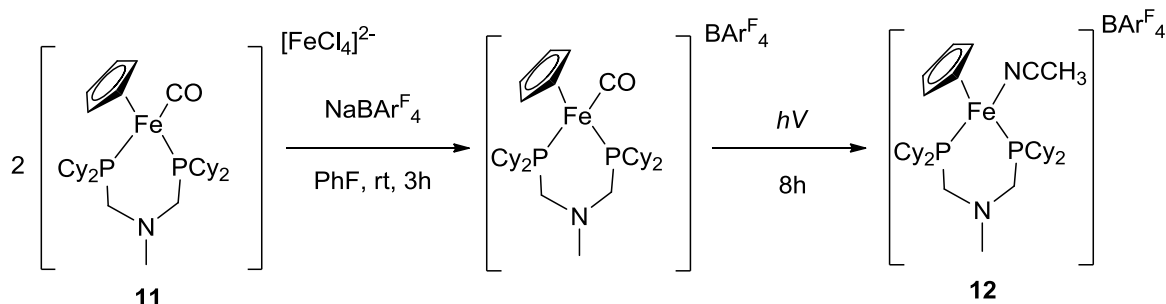
Scheme 2.18: Synthesis of complex **12.**

The stable cationic complex [(^{Cy}PNP)Fe(CH$_3$CN)(Cp)] (**12**) was synthesized and isolated only when CH$_3$CN was used as solvent in the reaction. Suitable crystals for X-Ray analysis were obtained by diffusion of n-pentane in a saturated solution of **12** in THF.

Unfortunately, when Cy$_2$PNPCy$_2$ ligand was replaced by Et$_2$PNPEt$_2$ only a mixture of products was observed in the ^{31}P-NMR spectrum.

2.2.3 Structures of Fe complexes

The solid state structures of complexes **4**, **5, 6, 7, 8, 9, 10, 11** and **12** were determined by X-Ray crystallography. The thermal ellipsoids are drawn at 30% probability and the hydrogen atoms are omitted for clarity in all the structure reported in this section.

The crystal structure of **4** showed a distorted square pyramidal geometry at the Fe center with the bidentate bis-phosphane and the 2-aminobenzenethiol ligand *trans* to one another. The apical CO ligand resulted *trans* to the free coordination center (Fig. 2.4). The six-member ring formed by the bis-phosphane ligand binding the metal center adopted a chair conformation with an angle Fe-P(1)-C(2) of 114.38(12) and P(1)-C(2)-N(2) of 116.39(6). The bite angle P(1)-Fe-P(2) was 93.13(2)^o. The distance calculated between the pendant amine and the iron center was 3.676 Å.

Fig. 2.4: X-Ray structure of **4**. The nitrogen atoms are coloured in blue, the phosphorous atoms in yellow, the sulphur atom in green and the oxygen ones in red. Selected bond lengths [Å] and angles [°]: Fe(1)-C(1) 1.7371(19), Fe(1)-N(1) 1.8678(15), Fe(1)-P(1) 2.2098(6), Fe(1)-P(2) 2.1955(5), Fe(1)S(1) 2.2476(6), P(1)-Fe(1)-P(2) 93.13(2), N(1)-Fe(1)-S(1) 85.04(5).

Similarly, complex **5** showed a pentacoordinated iron complex with the CO ligand *trans* to the free coordination site (Fig. 2.5). The distance calculated between the iron center and the pendant base was 3.733 Å. The six-member ring formed by the bis-phosphane ligand binding the metal center adopted a chair conformation with an angle Fe-P(1)-C(2) of 116.47(4), Fe-P(2)-C(3) of 111.89(4), P(1)-C(2)-N(2) of 116.08(8)^{o} and P(2)-C(3)-N(2) of 111.91(7)^{o}. The bite angle measured for the bis-phosphane ligand was 96.057(13) ^{o}.
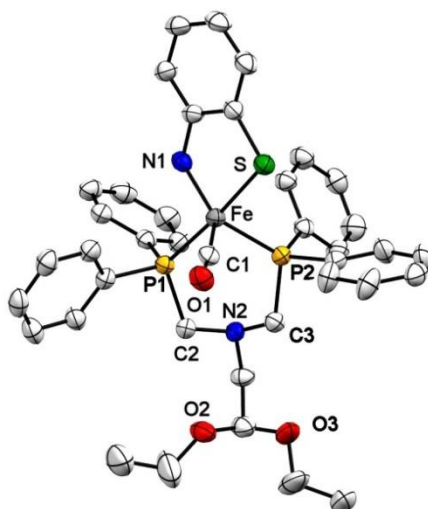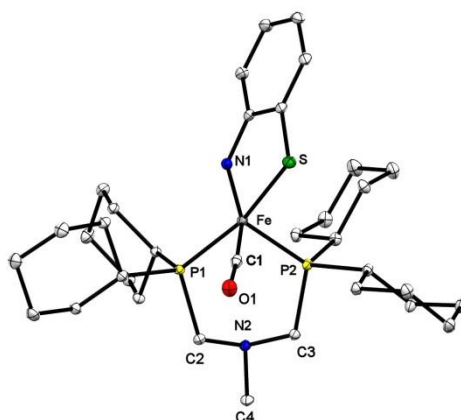

Fig. 2.5: X-Ray structure of **5**. The nitrogen atoms are coloured in blue, the phosphorous atoms in yellow, the sulphur atom in green and the oxygen one in red. Selected bond lengths [Å] and angles [°]: Fe(1)-C(1) 1.7563(12), Fe(1)-N(1) 1.8837(10), Fe(1)-P(1) 2.1752(4), Fe(1)-P(2) 2.2274(4), Fe(1)S(1) 2.2382(4), P(1)-Fe(1)-P(2) 96.057(13) ^{o} , N(1)-Fe(1)-S(1) 84.96(3).

The crystal structure of complex **6** exhibited a distorted square planar geometry with the CO ligand in the apical position (Fig. 2.6). The bite angle of the dppe ligand was 86.04(3)$^{\circ}$.
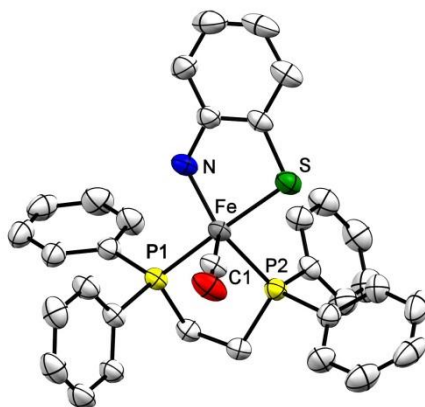
Fig. 2.6: X-Ray structure of **6**. The nitrogen atom is painted in blue, the phosphorous atoms in yellow, the sulphur atom in green and the oxygen in red. Selected bond lengths [Å] and angles [°]: Fe(1)-C(1) 1.719(3), Fe(1)-N(1) 1.893(3), Fe(1)-P(1) 2.2268(8), Fe(1)-P(2) 2.1868(9), Fe(1)-S(1) 2.2232(9), P(1)-Fe(1)-P(2) 86.04(3), N(1)-Fe(1)-S(1) 86.35(9).

The structure of the dimeric iron complex **7** showed two sulphur atoms belonging to two different 2-dimethyl-aminobenzenethiol ligands, bridging the metal centres (Fig. 2.7).
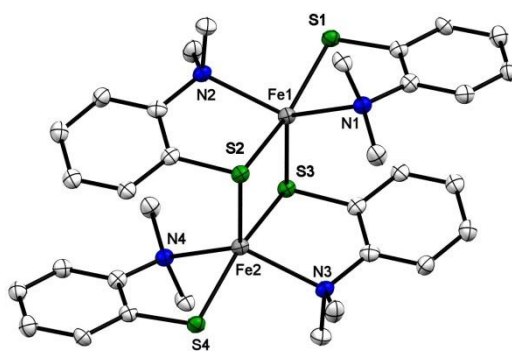
Fig. 2.7: X-Ray structure of **7**. The nitrogen atoms are painted in blue and the sulphur atoms in green.

The crystal structures of **8** and **9** (products of the reaction illustrated in scheme 2.15) are reported in Fig. 2.8 and 2.9. Complex **8** exhibited an octahedral geometry with the two 2-(Diphenyl-phosphino)benzenethiol ligands *trans* one to another and the CO ligands in the apical positions. The bite angle of both 2-(Diphenyl-phosphino)benzenethiol ligands resulted 86.26(4)$^{\circ}$, comparable with the dppe ligand in **6**.

The structure of **9** resulted more complex, as it showed a trimeric iron complex with six sulphur atoms belonging to different 2-(Diphenyl-phosphino)benzenethiol ligands, bridging the metal centres.
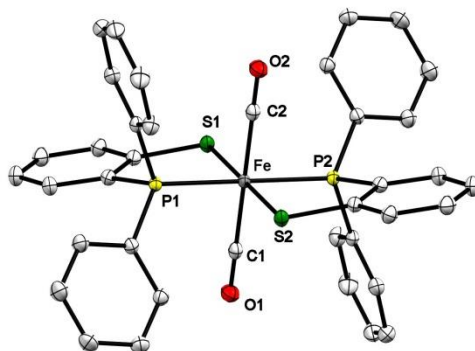
Fig. 2.8: X-Ray structure of **8**. The sulphur atoms are coloured in green, the phosphorous atoms are reported in yellow and the oxygen ones in red.
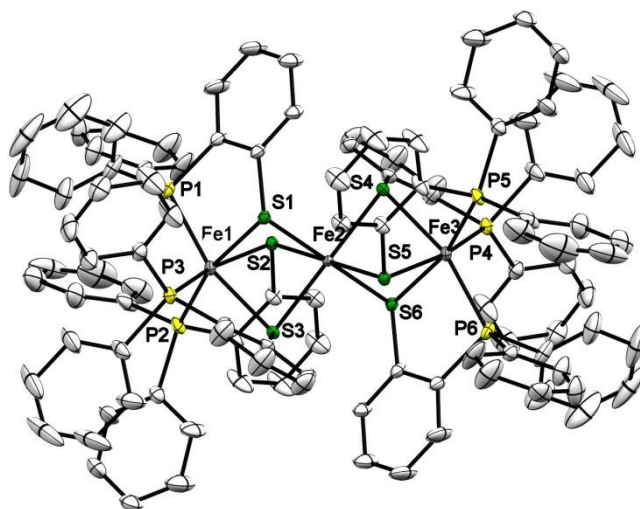
Fig. 2.9: X-Ray structure of **9**. The sulphur atoms are coloured in green and the phosphorous atoms are reported in yellow.

Complex **10** is a tetrahedral iron complex (Fig 2.10). The distance calculated between the iron center and the pendant base was 3.743 Å. The bite angle measured for the bis-phosphane ligand was $92.67(7)^{o}$.
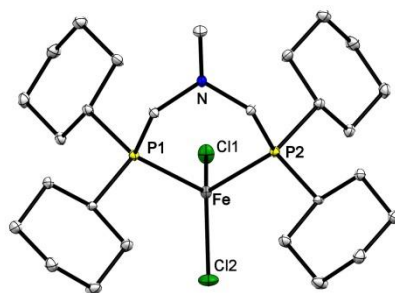
Fig. 2.10: X-Ray structure of **10**. The chloride atoms are reported in green, the nitrogen atom in blue and the phosphorous atoms are reported in yellow. Selected bond lengths [Å] and angles [°]: Fe(1)-Cl(1) 2.245(2), Fe(1)-Cl(2) 2.218(2), Fe(1)-P(1) 2.4498(15), Fe(1)-P(2) 2.4498(15), P(2)-Fe(1)-P(1) 92.67(7).

Complex **11** adopted a typical three-legged piano stool geometry, where the Fe-C(6) bond length resulted shorter than the Fe-P bond (Fig. 2.11). The bite angle of the PNP ligand resulted 90.70(6)° comparable with the other complexes reported above, and the calculated distance Fe-N was 3.775 Å. The six-member ring formed by the bis-phosphane ligand binding the metal center adopted a chair conformation with an angle Fe-P(1)-C(2) of 114.8(2)°, Fe-P(2)-C(3) of 110.2(2)°, P(1)-C(2)-N of 114.1(4)° and P(2)-C(3)-N of 110.0(4)°.
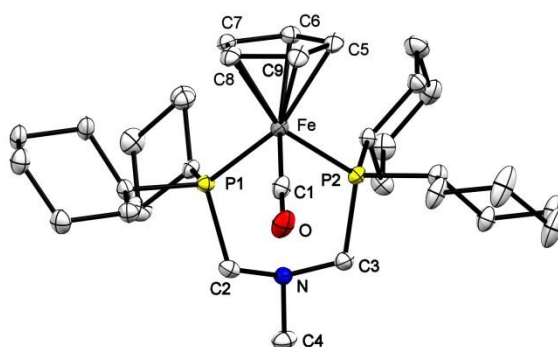
Fig. 2.11: X-Ray structure of **11**. The nitrogen atom is reported in blue, the phosphorous atoms are reported in yellow and the oxygen in red. The counter ion is omitted for clarity. Selected bond lengths [Å] and angles [°]: Fe(1)-C(1) 1.755(7), Fe(1)-P(1) 2.2266(17), Fe(1)-P(2) 2.252(17).

Similarly, complex **12** exhibited a three-legged piano stool geometry, where the Fe-N(1) bond length resulted shorter than the Fe-P bond (Fig. 2.12). The bite angle of the PNP ligand was 90.30° and the calculated distance Fe-N(2) resulted 3.759 Å. The six-member ring formed by the bis-phosphane ligand binding the metal center adopted a chair conformation with an angle Fe-P(1)-C(1) of 112.81(10)°, Fe-P(2)-C(2) of 111.65(10)°, P(1)-C(1)-N(2) of 112.16(19)° and P(2)-C(2)-N(2) of 112.27(19)°.
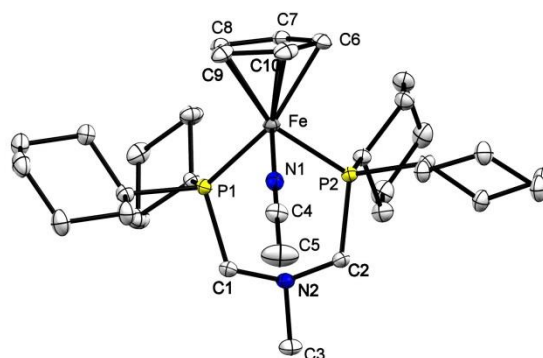
Fig. 2.12: X-Ray structure of **12**. The nitrogen atoms are reported in blue and the phosphorous atoms in yellow. The counter ion is omitted for clarity. Selected bond lengths [Å] and angles [°]: Fe(1)-N(1) 1.901(3), Fe(1)-P(1) 2.2314(8), Fe(1)-P(2) 2.2138(8).

2.3   Hydrogenation activation and Hydrogenation reaction using Fe complexes as catalyst

Complexes **1**, **2** and **4** bearing the Ph_2PNPPh_2 ligand; **5**, **11** and **12** bearing Cy_2PNPCy_2 and complexes **6** and **10** were tested as potential catalyst for both H_2 activation and hydrogenation reaction of different unsaturated substrates.

2.3.1   Hydrogen activation

In a typical experiment for hydrogen activation, the iron complex was dissolved in a deuterated solvent and loaded into a high pressure sapphire NMR tube. Upon pressurization with H_2 (typical pressure 80 bar) ^{1}H-NMR experiments were performed in order to detect either the formation of an hydride ligand as subsequence of heterolytic cleavage of H_2 upon interaction with the complex, or a η^2-H_2 ligand appearing at negative chemical shifts. The results are summarized in table 2.1.

Table 2.1: Hydrogen activation experiments

Entry	Complex	Solvent	Observations
		MeOD-*d4*	
1	**1**	THF-*d8*	No reaction
		CD_2Cl_2	
		MeOD-*d4*	
2	**2**	THF-*d8*	No reaction
		CD_2Cl_2	
		MeOD-*d4*	
3	**4**	THF-*d8*	No reaction

		CD$_2$Cl$_2$	
		MeOD-*d4*	
4	**5**	THF-*d8*	No reaction
		CD$_2$Cl$_2$	
		MeOD-*d4*	
5	**6**	THF-*d8*	No reaction
		CD$_2$Cl$_2$	
		MeOD-*d4*	
6	**10**	THF-*d8*	No reaction
		CD$_2$Cl$_2$	
		MeOD-*d4*	
7	**11**	THF-*d8*	No reaction
		CD$_2$Cl$_2$	
		MeOD-*d4*	
8	**12**	THF-*d8*	No reaction
		CD$_2$Cl$_2$	

Reaction conditions: complex (10 mg), H$_2$ (80 bar), deuterated solvent (0.6 ml). ^{1}H-NMR spectra were recorder every 2h for the first 8h and after 24h.

Unfortunately, as depicted in the table above, no reaction occurred when the complexes were reacted in presence of H$_2$.

2.3.2 Hydrogenation reaction

Screenings of the complexes as potential catalysts for hydrogenation reaction were performed. As standard condition, substrates such as benzaldehyde and acetophenone were tested in either MeOH, EtOH, ^{i}PrOH, CH$_2$Cl$_2$ or THF as solvent. As bases NaO^{t}Bu, NaO^{i}Pr, KO^{t}Bu, HCOONa and NaOMe were employed in slightly excess regarding the catalyst loading (10 or 20 mol%) and the reaction vessels were pressurized at 4 bar of H$_2$ (Scheme 2.19).
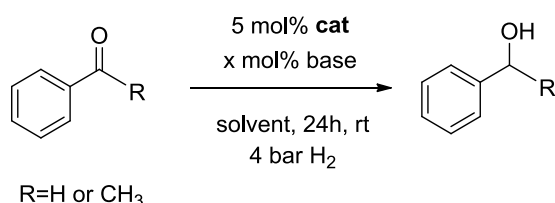
Scheme 2.19: Reaction conditions used for the hydrogenation reaction. Substrate (0.3 mmol), base (10/20 mol %), catalyst (0.015 mmol, 5 mol %), H$_2$ (4 bar), solvent (3 ml).

The reactions were performed also in absence of base and with a higher pressure of H$_2$ (8 bar), but no products were detected by GC-MS analysis. As for the hydrogen activation reaction, no substrate was hydrogenated to the corresponding alcohol by using the iron complexes reported as catalysts.

2.4 Conclusions

Concluding, new iron (II) low and high spin complexes bearing a pendant nitrogen base in the bis-phosphane ligand as a potential protonation site were synthesized (complex **1**, **2**, **4**, **5**, **11** and **12**). These complexes were tested as potential catalysts for hydrogenation reaction in presence of benzaldehyde and acetophenone as substrate and for hydrogen activation. Unfortunately, none of them served as catalyst for the reduction of these substrates and no reactivity was observed when treated with high pressure of H_2.

2.5 Experimental

Materials and methods:

All experiments were carried out under an inert N_2 (g) atmosphere using standard Schlenk or glovebox techniques. Solvents were purified using a two-column solid-state purification system (Innovative Technology, NJ, USA) and transferred to the glove box without exposure to air. Methanol (99.8%, extra dry, over molecular sieve) was purchased from AcroSeal®. Deuterated solvents were purchased from Cambridge Isotope Laboratories, Inc., and were degassed and stored over activated 3 Å molecular sieves. All other reagents were purchased from commercial sources and were degassed by standard freeze-pump-thaw procedures prior to use. ^{1}H and ^{31}P spectra were recorded at ambient temperature on a Bruker Avance 400 spectrometer. ^{1}H NMR chemical shifts were referenced to residual solvent as determined relative to TMS (δ 0.00ppm). GC-MS measurements were conducted on a Perkin-Elmer Clarus 600 GC equipped with Clarus 600T MS and Agilent J&W GC column, DB-5MS UI 25m, 0.250mm, 0.25 μm. IR measurements were recorded on powder samples at ambient temperature on a Varian 800 FT-IT Scimitar Series spectrometer. Elemental analyses were performed on a Carlo Erba EA 1110 CHN Instrument. HRESI-MS measurements were conducted at EPFL ISIC Mass Spectrometry Service with a Micro Mass QTOF Ultima Spectrometer.

Ph$_2$PNPPh$_2$ synthesis

For the synthesis of Ph$_2$PNPPh$_2$, the procedure reported in the literature was followed[37,38].

Et$_2$PNPEt$_2$ and Cy$_2$PNPCy$_2$ synthesis

For Et$_2$PNPEt$_2$ and Cy$_2$PNPCy$_2$ a slightly modified procedure[39] was followed.

The phosphinoalcohol HOCH$_2$PEt$_2$ was obtained by dropwise addition of 1 g of Et$_2$PH (0.011 mol) in 0.34 g of p-formaldehyde suspended in 30 ml of EtOH dry. The solution was stirred overnight upon complete dissolution of the p-formaldehyde. The day after 2.8 ml (0.0056 mol) of a 2M solution of NH$_2$CH$_3$ in MeOH were added to the reaction mixture, followed by addition of 1 ml of Et$_3$N (0.0072 mol) freshly distilled. The clear solution was stirred at room temperature overnight. The next day all the volatiles and the solvent were evaporated affording a clear oil in a 72% yield.

^{1}H NMR (400MHz, CD$_3$CN, 20°C): δ 2.66 (s, 4H, PC*H*$_2$N), δ 2.40 (s, 3H, NC*H$_3$*), δ 1.40 ppm (quadruplet, 8H, ^{3}J$_{HH}$ = 8.0 Hz, PC*H*$_2$CH$_3$), δ 1.06 (quintuplet, 12H, ^{3}J$_{HH}$ = 4.2Hz) ppm. ^{31}P-NMR (162MHz, CD$_3$CN, 20°C): δ -32.49 (s) ppm

The same procedure was followed for the synthesis of Cy$_2$PNPCy$_2$. The final product resulted in a white powder obtained in 83 % yield.

^{1}H NMR (400MHz, CDCl$_3$, 20°C): δ 2.65 (s, 4H, PC*H*$_2$N), δ 2.38 (s, 3H, NC*H$_3$*), δ 1.77 ppm (m, 24H, cyclohexyl), δ 1.22 (m, 30H, cyclohexyl) ppm. ^{31}P-NMR (162MHz, CD$_3$CN, 20°C): δ -16.74 (s) ppm

Synthesis of sodium 2-aminobenzenethiolate

2 g of 2-aminothiophenol (0.01195 mol) and 0.275 g of sodium (0.01195 mol) were mixed in 50 mL of dry THF in a round-bottom flask in the glovebox and the reaction mixture was stirred for 3 days (until complete dissolution of Na). A fine white powder precipitated during the reaction and it was filtered off, washed with excess of n-pentane and dried under vacuum (yield 92 %).

Anal. calcd. for C$_6$H$_6$NNaS: C 48.97%, H 4.11%, N 9.52%. Found: C 48.65%, H 4.02 %, N 9.47%.

Synthesis of sodium 2-dimethyl-aminobenzenethiolate

2 g of bis-(2-aminophenyl)-disulphide (0.0081 mol) were suspended in 50 ml of degassed water and 1.83 ml of (CH$_3$)$_2$SO$_4$ (0.0193 mol) were added. The solution turned

yellow and it was stirred for 2 h. The reaction mixture was then neutralized with 20% m/V KOH solution. A second aliquot of $(CH_3)_2SO_4$ (1.8 ml) was added, and the mixture stirred overnight. The next day upon basification of the solution with 20% m/V KOH solution, the product was extracted with CH_2Cl_2 affording a yellow oil as crude of the reaction in 87 % yield. In the second step of the synthesis, the crude oil was dissolved in 50 ml of THF and 0.32 g of sodium (0.014 mol) were added. A fine yellow powder precipitated during the reaction and it was filtered off, washed with excess of n-pentane and dried under vacuum (yield 75 %).

Anal. calcd. for $C_8H_{10}NNaS$: C 54.84%, H 5.75%, N 7.99%. Found: C 54.55%, H 5.68 %, N 7.85%. ESI-MS (*m/z, pos*) 154.00 (100%, $C_8H_{11}NS$).

Synthesis of complex 1

0.26 g of $FeCl_2$ (0.002 mol) and 1.087 g of Ph_2PNPPh_2 (0.002 mol) were mixed in 60 ml of MeOH dry in an ACE round-bottom pressure flask in the glovebox and the reaction mixture was pressurized with 1.5 bar of CO and stirred for 30 min. The color turned immediately orange. Successively, a solution of 0.433g of Cl_2bdt (0.002 mol) and 0.55 ml of Et_3N (0.004 mol) in 20 ml of dry MeOH previously prepared, was added dropwise to the reaction mixture and the flask pressurized back at 1.5 bar and stirred for additional 2h. The final dark solution was filtered through a PTFE filter and concentrated. n-Pentane was then added to promote the precipitation of the product as dark powder that was filtered and washed with additional n-pentane (yield: 42 %). The crude product obtained was purified by column chromatography on silica with CH_2Cl_2/hexane (7:3) as eluent. A dark grey powder was obtained in low yield (30 %).

^{1}H NMR (400MHz, C_6D_6, 20°C): δ 8.06-6.80 (m, 22H, aryl-*H*), δ 4.60 (t, 1H, $^3J_{HH}$ = 4.1Hz, C*H*O$_2$), δ 4.11 (quint, 2H, C*H*CH$_3$), δ 3.56 (m, 2H, PC*H*N), δ 3.50 (m, 2H, PC*H*N) PC*H*N), δ 3.38 (m, 2H, C*H*CH$_3$), δ 2.70 (d, 2H, NC*H*, $^3J_{HH}$ = 3.8 Hz), δ 1.23 (t, 6H, C*H*$_3$ $^3J_{HH}$ = 3.8 Hz). ^{31}P-NMR (162MHz, C_6D_6, 20°C): δ 50.20 (s) ppm. FT-IR: ν[cm^{-1}] 1907 (s, ν$_{CO}$).
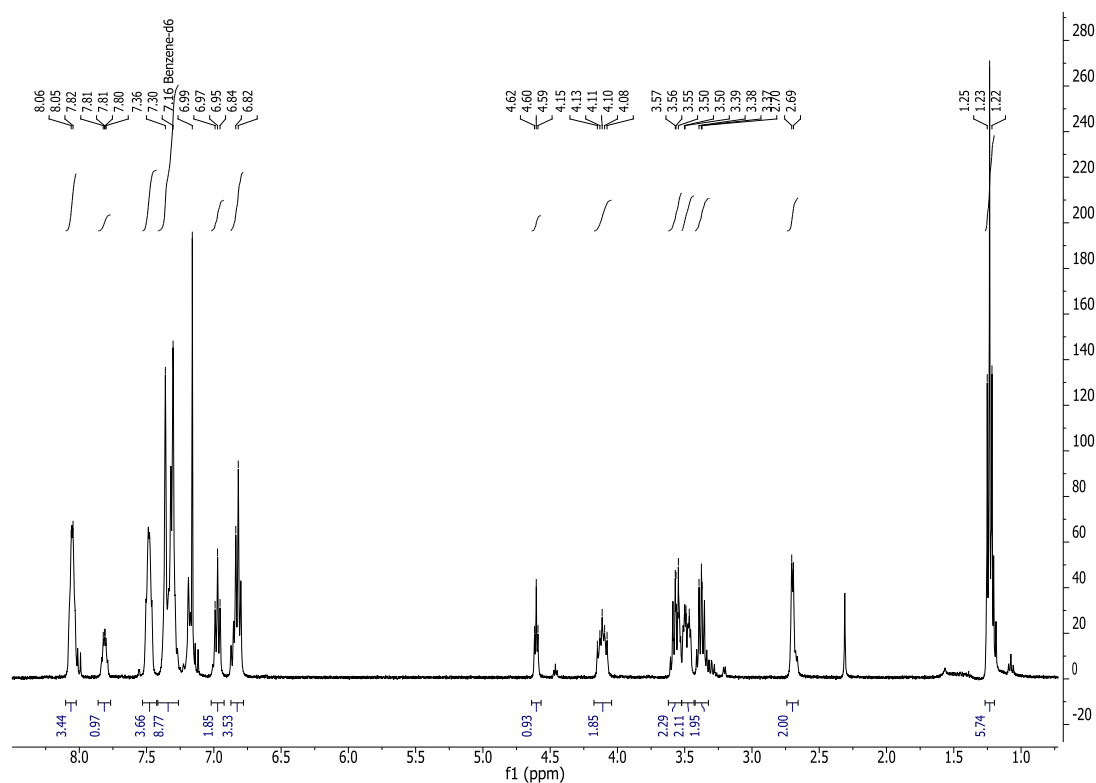
Fig. 2.13: ^{1}H NMR of **1** (400 MHz, C_6D_6, 20°C)

Synthesis of complex 2

For the synthesis of **2** the procedure reported in the literature was followed[22].

Synthesis of complex 4

0.3 g of $FeCl_2$ (0.0024 mol) and 1.25 g of Ph_2PNPPh_2 (0.0024 mol) were mixed in 60 ml of MeOH dry in an ACE round-bottom pressure flask in the glovebox and the reaction mixture was pressurized with 0.3 bar of CO and stirred for 30 min. The color turned immediately orange. Successively, 0.348 g of sodium 2-aminobenzenethiolate (0.0024 mol) and 0.227 g of NaO^tBu (0.0024 mol) in 20 ml of dry MeOH were added dropwise to the reaction mixture. The solution turned dark green and the flask was pressurized again at 0.3 bar and stirred for additional 2h. At the end, the dark solution was filtered through a PTFE filter and concentrated. n-pentane was then added and the product precipitated as dark green powder that was filtered off, washed with additional n-pentane and dried under vacuum (yield: 78%).

^{1}H NMR (400MHz, CD_2Cl_2, 20°C): δ 8.33 (s, 1H, N*H*), δ 7.63-6.88 (m, 24H, aryl-*H*), δ 4.60 (t, 1H, $^3J_{HH}$ = 4.1Hz, C*H*O$_2$), δ 4.12 (quint, 2H, PC*H*N), δ 3.60 (m, 2H, C*H*CH$_3$), δ

3.41 (m, 2H, C*H*CH$_3$), δ 3.19 (m, 5H, PC*H*N), δ 2.85 (d, 2H, NC*H*CH, ^{3}J$_{HH}$ = 3.8 Hz), δ 1.13 (t, 6H, C*H$_3$* ^{3}J$_{HH}$ = 3.8 Hz). ^{31}P-NMR (162MHz, C$_6$D$_6$, 20°C): δ 56.74 (s) ppm. FT-IR: ν [cm$^-$^{1}] 1950 (s, ν$_{CO}$). ESI-MS (*m/z, pos*) 737.23 (100%, C$_{39}$H$_{43}$FeN$_2$O$_3$P$_2$S).

Synthesis of complex 5

The complex was synthesized following the same procedure used for **4** but with Cy$_2$PNPCy$_2$ as bis-phosphane ligand. The dark product precipitated upon concentration of the reaction mixture, by addition of excess of n-pentane (yield: 75 %).

^{1}H NMR (400MHz, CD$_3$Cl, 20°C): δ 8.76 (s, 1H, N*H*), δ 7.86-6.95 (m, 4H, aryl-*H*), δ 3.13 (m, 2H, PC*H*N), δ 2.39 (m, 5H, PC*H*N and NC*H$_3$*), δ 2.05-1.11 (m, 44H, cyclohexyl). ^{31}P-NMR (162MHz, CD$_3$Cl, 20°C): δ 60.35(s) ppm. FT-IR: ν [cm^{-1}] 1890 (s, ν$_{CO}$). ESI-MS (*m/z, pos*) 737.23 (100%, C$_{39}$H$_{43}$FeN$_2$O$_3$P$_2$S).

Synthesis of complex 6

0.646g of Fe(CO)$_2$dppeCl$_2$ (0.0011 mol), previously synthesized[44] were mixed with 0.1635g of sodium 2-aminobenzenethiolate (0.0011 mol) and 0.1068g of NaO^{t}Bu (0.0011 mol) in 50 ml of THF dry. The reaction mixture was stirred overnight, during this time the color turned from orange to dark green. The final dark solution was filtered through a PTFE filter and concentrated. n-Pentane was then added to promote the precipitation of the product as dark green powder that was filtered, washed with additional n-pentane and dried under vacuum (yield: 75%). Suitable crystals for X-Ray analysis formed by diffusion of n-pentane in a saturated solution of **6** in THF.

^{1}H NMR (400MHz, CD$_2$Cl$_2$, 20°C): δ 8.73 (s, 1H, N*H*), δ 7.75-6.93 (m, 24H, aryl-*H*), δ 2.67 (m, 2H, PC*H*), δ 2.46 (m, 2H, PC*H*). ^{31}P-NMR (162MHz, CD$_2$Cl$_2$, 20°C): δ 94.84 (s) ppm. FT-IR: ν [cm^{-1}] 1902 (s, ν$_{CO}$). ESI-MS (*m/z, pos*) 737.23 (100%, C$_{39}$H$_{43}$FeN$_2$O$_3$P$_2$S).

Synthesis of complex 8

0.7g of 2-(Diphenyl-phosphino)benzenethiol (0.0024 mol) and 0.227g of NaO^{t}Bu (0.0024 mol) were dissolved in 20 ml of dry MeOH. This solution was added dropwise to 0.15g of FeCl$_2$ (0.0012 mol) suspended in 30 ml of dry MeOH in an ACE round-bottom pressure flask. The color of the reaction mixture turned immediately brown and a fine powder precipitated. The flask was pressurized with 0.4 bar of CO and the solution stirred for 2h. The

powder formed during the reaction, was filtered off, washed with excess of n-pentane and dried under vacuum. The product resulted in an orange powder obtained in a 65% yield. Crystals formed by diffusion of n-pentane in a saturated solution of **8** in THF, or using the combination CH_2Cl_2 to dissolve the product and diethyl ether.

^{1}H NMR (400MHz, CDCl$_3$, 20°C): δ 7.65 (m, 5H, P-aryl-*H*), δ 7.42 (m, 5H, P-aryl-*H*), δ 7.17-6.93 (m, 4H, aryl-*H*) ppm. FT-IR: ν [cm^{-1}] 1900 (s, ν$_{CO}$).

Synthesis of complex 10

0.5 g of FeCl$_2$·1.8 THF (0.0019 mol) and 0.873 g of Cy$_2$PNPCy$_2$ (0.0019 mol) were mixed in 40 ml of THF dry. In order to help the solubilisation ca. 10 ml of MeOH dry were added. The reaction mixture was stirred overnight. A white powder precipitated (1st aliquot of product) and it was filtered off, washed with excess of n-pentane and dried under vacuum. The 2nd aliquot precipitated from the reaction mixture after concentration of the solvent and addition of an excess of n-pentane. Overall yield 80% (combination of the two aliquots). Complex **10** is a paramagnetic species; therefore NMR analysis was not possible. The structure was confirmed by ESI-MS(*m/z, pos*): 578.23 (100%, C$_{27}$H$_{51}$FeCl$_2$P$_2$N). Suitable crystals for X-Ray analysis formed by diffusion of n-pentane in a saturated solution of **10** in THF.

Synthesis of complex 11

0.188 g of FeCp(CO)$_2$Cl (0.00089mol) previously synthesized according to literature[47], and 0.4 g of Cy$_2$PNPCy$_2$ (0.00089 mol) were mixed in 25 ml of dry THF. The reaction mixture turned immediately red and it was irradiated with an UV lamp for 2 h. The solution gradually changed from red to brown with concomitant formation of a yellow precipitate. The precipitate was filter off, washed with an excess of n-pentane and dried under vacuum (Yield 63%). Suitable crystals for X-Ray analysis formed by diffusion of diethyl ether in a saturated solution of **11** in either CH$_3$CN or CH$_2$Cl$_2$.

^{1}H NMR (400MHz, CD$_2$Cl$_2$, 20°C): δ 4.98 (s, 5H, Cp-*H*), δ 3.20 (m, 2H, PC*H*), δ 2.39 (s, 3H, NC*H*), δ 2.28 (m, 2H, PC*H*), δ 2.08-1.76 (m, 22H, cyclohexyl), δ 1.53-1.21 (m, 22H, cyclohexyl) ppm. ^{31}P-NMR (162MHz, CD$_2$Cl$_2$, 20°C): δ 54.09 (s) ppm. FT-IR: ν [cm^{-1}] 1910 (s, ν$_{CO}$). ESI-MS (*m/z, pos*) 600.32 (100%, C$_{33}$H$_{56}$FeNOP$_2$).

Synthesis of complex 12

0.15 g of **11** (0.0024 mol) and 0.21 g of NaBAr$^F_4$ were dissolved in 20 ml of PhF. The reaction mixture was stirred for 1h. The yellow solution gradually turned darker and a fine white powder precipitated. The reaction mixture was filtered through a PTFE filter and the solvent evaporated until dryness yielding a yellow product. The product was dissolved in 20ml of CH_3CN and irradiated with an UV lamp for 8h. The solution gradually changed from yellow to red. The solvent was evaporated affording an orange product that was washed with n-pentane and died under vacuum (Yield 68%). Suitable crystals for X-Ray analysis formed by diffusion of pentane in a saturated solution of **12** in THF. FT-IR analysis did not show the typical CO signal, confirming the ligand exchange.

^{1}H NMR (400MHz, CD_2Cl_2, 20°C): δ 7.72-7.56 (m, 12H, BAr$^F_4$), δ 4.41 (s, 5H, Cp-*H*), δ 2.96 (m, 2H, PC*H*), δ 2.30 (s, 3H, C*H$_3$*CN) δ 2.19 (s, 3H, NC*H*), δ 2.13 (m, 2H, PC*H*), δ 1.99-1.81 (m, 22H, cyclohexyl), δ 1.51-1.27 (m, 22H, cyclohexyl) ppm. ^{31}P-NMR (162MHz, CD_2Cl_2, 20°C): δ 51.08 (s) ppm.

General procedure for catalytic hydrogenation

A 35 mL ACE pressure tube was charged with catalyst (0.03 mmol), substrate (0.3 mmol), base (10/20 mol %, 0.3-0.6 mmol), dodecane (30μL, 0.133 mmol), 3 mL of dry solvent and 8 bar of hydrogen. The solution was stirred at ambient temperature (20-22 °C) for 24h. The reaction was quenched by exposure to air and by addition of diethyl ether. The alcohol products were identified and quantified by GC-MS with dodecane as an internal standard. External calibration curves were made using the commercial available products (purity >98%) or the isolated ones with dodecane as an internal standard.

X-ray Crystallography

The diffraction data were measured using Mo Kα radiation on a Bruker APEX II CCD diffractometer equipped with a kappa geometry goniometer. The datasets were reduced by EvalCCD[48] and then corrected for absorption[49]. The data were measured using Cu Kα radiation on an Agilent Technologies SuperNova dual system in combination with an Atlas CCD detector. The data reduction was carried out by Crysalis PRO[50]. The solutions and refinements were performed by SHELX[51] .The crystal structures were refined using full-

matrix least-squares based on F^2 with all non hydrogen atoms anisotropically defined. Hydrogen atoms were placed in calculated positions by means of the "riding" model.

X-ray Structural Analysis of 4:

Crystal Data: $C_{39}H_{42}FeN_2O_3P_2S$, 0.33 x 0.19 x 0.17 mm^3, Triclinic, *P*-1, a = 9.8062(5) Å, b= 11.0654(19) Å, c = 18.183(2) Å, α= 90.908(11)°, β= 97.312(8)°, γ= 112.193(7)°. T= 100(2) K, V= 1807.6(4) Å^3, Z= 2, ρ_c= 1.353 Mg/m^3, μ= 0.603 mm^{-1}.

Data Collection and Processing: 20494 reflections collected, -13 ≤ h ≤ 13, -15 ≤ k ≤ 15, -25 ≤ l ≤ 25, 30234 [R(int) = 0. 0287].

Solution and refinement: Refinement method used Full-matrix least-squares on F^2. 10300 data with 0 restraints and 435 parameters. Goodness-of-fit on F^2=1.069, largest diff. peak= 0.904 e.Å^{-3} and hole= -0.857 e.Å^{-3}.Final R indices [I>2σ(I)]: R1 = 0.0408, wR2 = 0.0910. R indices (all data): R1=0.0566, wR2 = 0.1015.

Table 2.2. Selected bond lengths and angles for **4.**

	Bond length [Å]		Bond angles [°]
Fe(1)-C(1)	1.7371(19)	N(1)-Fe(1)-P(2)	132.45(5)
Fe(1)-N(1)	1.8678(15)	P(1)-C(2)-N(2)	116.39(6)
Fe(1)-P(2)	2.1955(5)	Fe-P(1)-C(2)	114.38(12)
Fe(1)-S(1)	2.2476(6)	N(1)-Fe(1)-S(1)	85.04(5)
Fe(1)-P(1)	2.2098(6)	P(2)-Fe(1)-P(1)	93.13(2)

X-ray Structural Analysis of 5:

Crystal Data: $C_{34}H_{56}FeN_2OP_2S$, 0.44 x 0.34 x 0.14 mm^3, Triclinic, *P*-1, a = 9.9760(10) Å, b=10.8164(8) Å, c = 16.3672(14) Å, α= 89.602(8)°, β= 84.432(7)°, γ= 77.570(7)°. T= 100(2) K, V= 1716.4(3) Å^3, Z= 2, ρ_c= 1.274 Mg/m^3, μ= 0.622 mm^{-1}.

Data Collection and Processing: 38792 reflections collected, -15 ≤ h ≤ 14, -16 ≤ k ≤ 16, -22 ≤ l ≤ 25, 12989 [R(int) = 0.0267].

Solution and refinement: Refinement method used Full-matrix least-squares on F^2. 12989 data with 0 restraints and 375 parameters. Goodness-of-fit on F^2=1.117, largest diff. peak= 0.526 e.Å^{-3} and hole= -0.424 e.Å^{-3}. Final R indices [I>2σ(I)]: R1 = 0.0327, wR2 = 0.0709. R indices (all data): R1 = 0.0499, wR2 = 0.0805.

Table 2.3. Selected bond lengths and angles for **5.**

	Bond length [Å]		Bond angles [°]
Fe(1)-C(1)	1.7563(12)	P(2)-C(3)-N(2)	111.91(7)
Fe(1)-N(1)	1.8837(10)	P(1)-C(2)-N(2)	116.08(8)
Fe(1)-P(2)	2.2274(4)	Fe-P(1)-C(2)	116.47(4)
Fe(1)-S(1)	2.2382(4)	N(1)-Fe(1)-S(1)	84.96(3)
Fe(1)-P(1)	2.1752(4)	P(2)-Fe(1)-P(1)	96.057(13)

X-ray Structural Analysis of 6:

Crystal Data: $C_{33}H_{29}FeNOP_2S$, 0.45 x 0.31 x 0.28 mm^3, Monoclinic, $P2_1/c$, a = 11.2243(4) Å, 13.4464(4) Å, c = 19.5307(7) Å, α= 90°, β= 94.783(3)°, γ= 90°. T= 293(2) K, V= 2937.44(17) $Å^3$, Z= 4, ρ_c= 1.369 Mg/m^3, μ= 6.018 mm^{-1}.

Data Collection and Processing: 20494 reflections collected, -13 ≤ h ≤ 13, -16 ≤ k ≤ 11, -23 ≤ l ≤ 23, 5825 [R(int) = 0.0564].

Solution and refinement: Refinement method used Full-matrix least-squares on F^2. 5825 data with 0 restraints and 352 parameters. Goodness-of-fit on F^2=1.034, largest diff. peak= 0.693 e.$Å^{-3}$and hole= -0.475 e.$Å^{-3}$.Final R indices [I>2σ(I)]: R1 = 0. 0583, wR2 = 0.1584. R indices (all data): R1 = 0. 0646, wR2 = 0. 1693.

Table 2.4. Selected bond lengths and angles for **6.**

	Bond length [Å]		Bond angles [°]
Fe(1)-C(1)	1.719(3)	C(1)-Fe(1)-S(1)	93.33(11)
Fe(1)-N(1)	1.893(3)	N(1)-Fe(1)-S(1)	86.35(9)
Fe(1)-P(2)	2.1868(9)	P(2)-Fe(1)-S(1)	89.23(3)
Fe(1)-S(1)	2.2232(9)	N(1)-Fe(1)-P(1)	94.22(8)
Fe(1)-P(1)	2.2268(8)	P(2)-Fe(1)-P(1)	86.04(3)

X-ray Structural Analysis of 10:

Crystal Data: $C_{27}H_{51}Cl_2FeNP_2$, 0.30 x 0.26 x 0.18 mm^3, Orthorhombic, $Pmn2_1$, a = 21.2113(8) Å , b=8.0064(3) Å, c = 8.7683(4) Å, α= 90°, β= 90°, γ= 90°. T= 100(2) K, V= 1489.09(10) $Å^3$, Z= 2, ρ_c= 1.290 Mg/m^3, μ= 6.833 mm^{-1}.

Data Collection and Processing: 9720 reflections collected, -22 ≤ h ≤ 26, -7 ≤ k ≤ 9, -10 ≤ l ≤ 9,

5825 2952 [R(int) = 0.0540].

Solution and refinement: Refinement method used Full-matrix least-squares on F^2. 2952 data with 7 restraints and 158 parameters. Goodness-of-fit on F^2=1.179, largest diff. peak= 1.681 e.$\text{Å}^{-3}$and hole= -0.805 e.Å^{-3}. Final R indices [I>2σ(I)]: R1 = 0.0602, wR2 = 0.1590. R indices (all data): R1 = 0.0609, wR2 = 0.1593.

Table 2.5. Selected bond lengths and angles for **10.**

	Bond length [Å]		Bond angles [°]
Fe(1)-Cl(1)	2.245(2)	C(13)-P(1)-Fe(1)	116.39(17)
Fe(1)-Cl(2)	2.218(2)	P(2)-Fe(1)-P(1)	92.67(7)
Fe(1)-P(2)	2.4498(15)	Cl(2)-Fe(1)-Cl(1)	113.56(10)
Fe(1)-P(1)	2.4498(15)	N(1)-C(13)-P(1)	111.2(4)

X-ray Structural Analysis of 11:

Crystal Data: $C_{66}H_{112}Cl_4Fe_3N_2O_2P_4$, 0.371 x 0.281 x 0.212 mm^3, Monoclinic, $P2_1/n$, a = 13.5395(4) Å, b=15.8700(4) Å , c = 18.5093(5) Å, α= 90°, β= 108.032(3)°, γ= 90°. T= 140(2) K, V= 3781.77(19) Å^3, Z= 2, ρ_c= 1.228 Mg/m^3, μ= 6.951 mm^{-1}.

Data Collection and Processing: 27635 reflections collected, -16 ≤ h ≤ 16, -18 ≤ k ≤ 19, -20 ≤ l ≤ 22, 7461 [R(int) = 0.0386].

Solution and refinement: Refinement method used Full-matrix least-squares on F^2. 7461 data with 0 restraints and 390 parameters. Goodness-of-fit on F^2=1.170, largest diff. peak= 1.524 e.$\text{Å}^{-3}$and hole= -0.628 e.Å^{-3}. Final R indices [I>2σ(I)]: R1 = 0.0913, wR2 = 0.2023 R indices (all data): R1 = 0. 0933, wR2 = 0. 2312.

Table 2.6. Selected bond lengths and angles for **11.**

	Bond length [Å]		Bond angles [°]
Fe(1)-C(1)	1.755(7)	Fe-P(1)-C(2)	114.8(2)
P(1)-C(2)	2. 837(6)	Fe-P(2)-C(3)	110.2(2)
Fe(1)-P(2)	2.2252(17)	P(1)-C(2)-N	114.1(4)
P(2)-C(3)	2.2232(9)	P(2)-C(3)-N	110.0(4)
Fe(1)-P(1)	2.2266(17)	P(2)-Fe(1)-P(1)	90.70(6)

X-ray Structural Analysis of 12:

Crystal Data: $C_{70}H_{79}BF_{24}FeN_2OP_2$, 0.40 x 0.35 x 0.28 mm^3, Monoclinic, *I 2/a*, a = 28.5446(11) Å, b=12.9931(4) Å, c=39.5486(12)Å, α= 90°, β= 99.980(3)°, γ= 90°. T= 140(2) K, V= 14445.9 Å^3, Z= 8, ρ_c= 1.424 Mg/m^3, μ= 3.032 mm^{-1}.

Data Collection and Processing: 50530 reflections collected, -35 ≤ h ≤ 29, -16 ≤ k ≤ 12, -45 ≤ l ≤ 48, 14274 [R(int) = 0.0356].

Solution and refinement: Refinement method used Full-matrix least-squares on F^2. 14274 data with 0 restraints and 913 parameters. Goodness-of-fit on F^2=1. 080, largest diff. peak= 1.614 e.Å^{-3}and hole= -1.109 e.Å^{-3}. Final R indices [I>2σ(I)]: R1 = 0.0683, wR2 = 0. 1863 R indices (all data): R1 = 0. 0713, wR2 = 0. 1896.

Table 2.7. Selected bond lengths and angles for **12.**

	Bond length [Å]		Bond angles [°]
Fe(1)-N(1)	1. 901(3)	Fe-P(1)-C(1)	112.81(10)
P(1)-C(2)	1.847(3)	P(1)-C(1)-N(2)	112.16(19)
Fe(1)-P(2)	2. 2138(8)	P(2)-Fe(1)-P(1)	90.30(3)
P(2)-C(3)	1.850(3)	Fe-P(2)-C(2)	111.65(10)
Fe(1)-P(1)	2. 2314(8)	P(2)-C(2)-N(2)	112.27(19)

2.6 References

(1)   Nicolet, Y.; de Lacey, A. L.; Vernède, X.; Fernandez, V. M.; Hatchikian, E. C.; Fontecilla-Camps, J. C. *J. Am. Chem. Soc.* **2001**, *123*, 1596.

(2)   Peters, J. W.; Lanzilotta, W. N.; Lemon, B. J.; Seefeldt, L. C. *Science* **1998**, *282*, 1853.

(3)   Pereira, A. S.; Tavares, P.; Moura, I.; Moura, J. J. G.; Huynh, B. H. *J. Am. Chem. Soc.* **2001**, *123*, 2771.

(4)   Garcin, E.; Vernede, X.; Hatchikian, E. C.; Volbeda, A.; Frey, M.; Fontecilla-Camps, J. C. *Structure* **1999**, *7*, 557.

(5)   Higuchi, Y.; Ogata, H.; Miki, K.; Yasuoka, N.; Yagi, T. *Structure* **1999**, *7*, 549.

(6)   Volbeda, A.; Garcin, E.; Piras, C.; de Lacey, A. L.; Fernandez, V. M.; Hatchikian, E. C.; Frey, M.; Fontecilla-Camps, J. C. *J. Am. Chem. Soc. y* **1996**, *118*, 12989.

(7)   Niu, S.; Thomson, L. M.; Hall, M. B. *J. Am. Chem. Soc.* **1999**, *121*, 4000.

(8)   Fan, H.-J.; Hall, M. B. *J. Am. Chem. Soc.* **2001**, *123*, 3828.

(9)   Lee, D.-H.; P. Patel, B.; H. Crabtree, R.; Clot, E.; Eisenstein, O. *Chem. Commun.* **1999**, 297.

(10)   Liu, T.; Chen, S.; O'Hagan, M. J.; Rakowski DuBois, M.; Bullock, R. M.; DuBois, D. L. *J. Am. Chem. Soc.* **2012**, *134*, 6257.

(11)   Jessop, P. G.; Morris, R. H. *Inorg. Chem.* **1993**, *32*, 2236.

(12)   Chu, H. S.; Lau, C. P.; Wong, K. Y.; Wong, W. T. *Organometallics* **1998**, *17*, 2768.

(13)   Lough, A. J.; Park, S.; Ramachandran, R.; Morris, R. H. *J. Am. Chem. Soc.* **1994**, *116*, 8356.

(14)   Park, S.; Lough, A. J.; Morris, R. H. *Inorg.Chem.* **1996**, *35*, 3001.

(15)   Ayllon, J. A.; Sayers, S. F.; Sabo-Etienne, S.; Donnadieu, B.; Chaudret, B.; Clot, E. *Organometallics* **1999**, *18*, 3981.

(16)   Custelcean, R.; Jackson, J. E. *Chem. Rev.* **2001**, *101*, 1963.

(17)   Fang, M.; Wiedner, E. S.; Dougherty, W. G.; Kassel, W. S.; Liu, T.; DuBois, D. L.; Bullock, R. M. *Organometallics* **2014**, *33*, 5820.

(18)   Thoi, V. S.; Sun, Y.; Long, J. R.; Chang, C. J. *Chem.Soc.Rev.* **2013**, *42*, 2388.

(19)   DuBois, D. L.; Bullock, R. M. *Eur. J. Inorg. Chem.* **2011**, *2011*, 1017.

(20)   Liu, T.; DuBois, D. L.; Bullock, R. M. *Nat Chem* **2013**, *5*, 228.

(21)   Karunadasa, H. I.; Montalvo, E.; Sun, Y.; Majda, M.; Long, J. R.; Chang, C. J. *Science* **2012**, *335*, 698.

(22)   Beyler, M.; Ezzaher, S.; Karnahl, M.; Santoni, M.-P.; Lomoth, R.; Ott, S. *Chem. Commun.* **2011**, *47*, 11662.

(23)   Curtis, C. J.; Miedaner, A.; Ellis, W. W.; DuBois, D. L. *J. Am. Chem. Soc.* **2002**, *124*, 1918.

(24)   Wayner, D. D. M.; Parker, V. D. *Acc.Chem. Res.* **1993**, *26*, 287.

(25)   Hulley, E. B.; Welch, K. D.; Appel, A. M.; DuBois, D. L.; Bullock, R. M. *J. Am. Chem. Soc.* **2013**, *135*, 11736.

(26)   Doud, M. D.; Grice, K. A.; Lilio, A. M.; Seu, C. S.; Kubiak, C. P. *Organometallics* **2012**, *31*, 779.

(27) Henry, R. M.; Shoemaker, R. K.; DuBois, D. L.; DuBois, M. R. *J. Am. Chem. Soc.* **2006**, *128*, 3002.

(28) Curtis, C. J.; Miedaner, A.; Ciancanelli, R.; Ellis, W. W.; Noll, B. C.; Rakowski DuBois, M.; DuBois, D. L. *Inorg. Chem.* **2003**, *42*, 216.

(29) Wilson, A. D.; Newell, R. H.; McNevin, M. J.; Muckerman, J. T.; Rakowski DuBois, M.; DuBois, D. L. *J. Am. Chem. Soc.* **2006**, *128*, 358.

(30) Jacobsen, G. M.; Yang, J. Y.; Twamley, B.; Wilson, A. D.; Bullock, R. M.; Rakowski DuBois, M.; DuBois, D. L. *Energy Environ. Sci.* **2008**, *1*, 167.

(31) Wiedner, E. S.; Yang, J. Y.; Dougherty, W. G.; Kassel, W. S.; Bullock, R. M.; DuBois, M. R.; DuBois, D. L. *Organometallics* **2010**, *29*, 5390.

(32) Jessop, P. G.; Morris, R. H. *Coord. Chem. Rev.* **1992**, *121*, 155.

(33) Albeniz, A. C.; Heinekey, D. M.; Crabtree, R. H. *Inorg.Chem.* **1991**, *30*, 3632.

(34) Heinekey, D. M.; Oldham, W. J. *Chem. Rev.* **1993**, *93*, 913.

(35) Sabo-Etienne, S.; Chaudret, B. *Chem. Rev.* **1998**, *98*, 2077.

(36) Waterman, R. *Organometallics* **2013**, *32*, 7249.

(37) Kühl, O.; Blaurock, S.; Sieler, J.; Hey-Hawkins, E. *Polyhedron* **2001**, *20*, 2171.

(38) Durran, S. E.; Elsegood, M. R. J.; Hawkins, N.; Smith, M. B.; Talib, S. *Tetrahedron Letters* **2003**, *44*, 5255.

(39) Weiss, C. J.; Groves, A. N.; Mock, M. T.; Dougherty, W. G.; Kassel, W. S.; Helm, M. L.; DuBois, D. L.; Bullock, R. M. *Dalton Trans.* **2012**, *41*, 4517.

(40) Liaw, W.-F.; Lee, N.-H.; Chen, C.-H.; Lee, C.-M.; Lee, G.-H.; Peng, S.-M. *Journal of the American Chemical Society* **2000**, *122*, 488.

(41) Hsu, H.-F.; Koch, S. A.; Popescu, C. V.; Münck, E. *J. Am. Chem. Soc.* **1997**, *119*, 8371.

(42) Liu, T.; Li, B.; Popescu, C. V.; Bilko, A.; Pérez, L. M.; Hall, M. B.; Darensbourg, M. Y. *Chem. Eur. J.* **2010**, *16*, 3083.

(43) Orthaber, A.; Karnahl, M.; Tschierlei, S.; Streich, D.; Stein, M.; Ott, S. *Dalton Transactions* **2014**, *43*, 4537.

(44) Manuel, T. A. *Inorg. Chem.* **1963**, *2*, 854.

(45) Deck, P. A. *Coord. Chem. Rev.* **2006**, *250*, 1032.

(46) Wilkinson, G.; Cotton, F. A. In *Progress in Inorganic Chemistry*; John Wiley & Sons, Inc.: **2007**, p 1. ISBN: 978-0-471-19957-1

(47) Teixeira, Z.; Vasconcellos, S. P.; Koike, L.; Dias, G. H. M. *Química Nova* **2007**, *30*, 494.

(48) Duisenberg, A. J. M.; Kroon-Batenburg, L. M. J.; Schreurs, A. M. M. *Journal of Applied Crystallography* **2003**, *36*, 220.

(49) Blessing, R. H. *Acta Crystallographica Section A* **1995**, *51*, 33.

(50) Crysalis PRO, A. T., release 1.171.36.28, 2013.

(51) Sheldrick, G. M. *Acta Crystallographica Section A* **2008**, *64*, 112.

Chapter 3

Iron Complexes bearing a PONOP Pincer Ligand for Hydrogen Activation and Catalytic Hydrogenation

3.1 Tridentate Pincer Ligands

The concept of "Pincer Chemistry" was born in 1976 with the synthesis of the first pincer type ligand by Moulton and Shaw[1]. At that time the ligand 1,3-bis[(di-tert-butylphosphino) methyl] benzene was considered as a new chelating diphosphine, and only in the late 80's the concept of pincer ligand was reconsidered a cause of the extraordinary stability of the corresponding metal complexes.

D, D' = P, S, N, O
Y= CH_2, NH, O
X= C, N
M= metal center
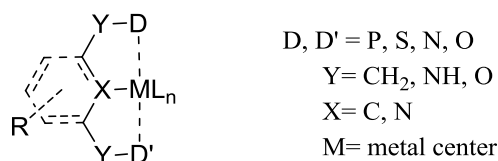
Fig. 3.1: Pincer-ligand type moiety and possible modifications

Although the pincer-transition metal chemistry concentrated firstly on PCP[1] and SCS[2] ligands (where P- and S- are "soft" donor sites), variations have been developed by introducing "hard" tertiary amine donor groups[3,4] (NCN pincer type ligand).

Regarding the central coordinating group position X (Fig. 3.1) many complexes feature a metal-carbon bond responsible of their stability, but nitrogenous donors, such as pyridines[5-7] or amines[8,9], can also be introduced. Therefore, the pincer type ligand can act as 2e (via X), 4e (via X and D) or 6e (X, D, D') donor ligand (Fig. 3.1).

Pincer complexes are generally viewed as stable compounds in which the pincer ligand framework remains unchanged during catalytic reactions. However, several cases of bifunctional catalysis involving the pincer ligand have been investigated during the last decades[10-14]. In particular, it has been found that PNP type ligands while binding metal centers, easily undergo deprotonation on the -CH_2- spacer with concomitant dearomatization of the pyridine[15-18] resulting in cooperative catalysts. As reported by Milstein et al.[16] the PNP iron based system [(^{iPr}PNP)Fe(H)(CO)Br] is an efficient catalyst for hydrogenation of ketones under mild conditions (Scheme 3.1).
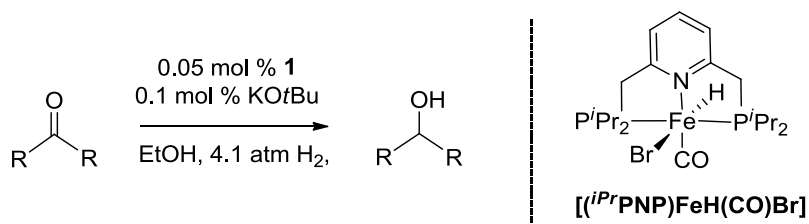
Scheme 3.1: Hydrogenation of ketones catalysed by [(^{iPr}PNP)FeH(CO)Br]**.**

Based on NMR studies, the reaction might involve the formation of a reactive dearomatized species **A** as intermediate making the insertion of the ketone into the Fe-H bond possible. The proposed catalytic cycle is depicted in scheme 3.2.
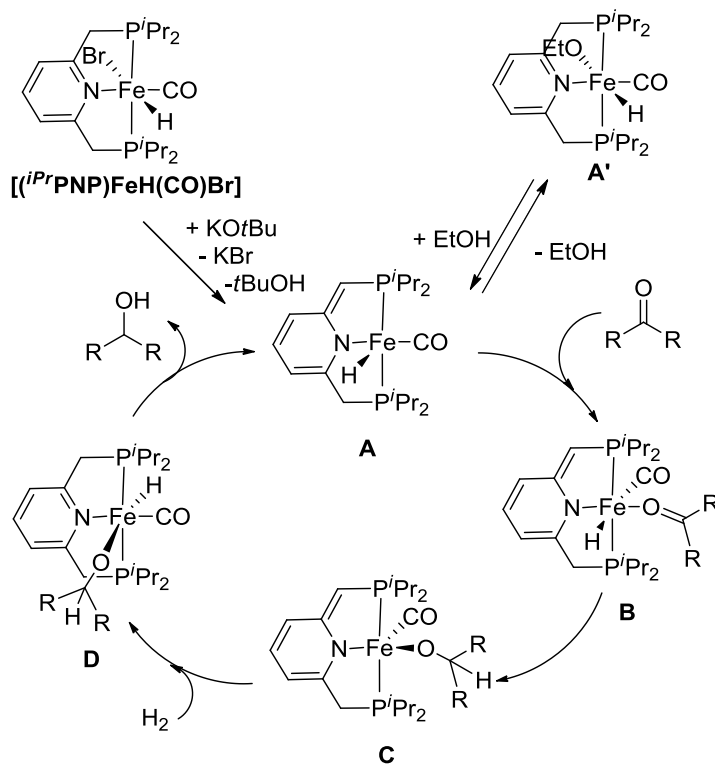
Scheme 3.2: Proposed catalytic cycle for the hydrogenation of ketones utilizing the dearomatization-reprotonation chemistry displayed by complex [(^{iPr}PNP)FeH(CO)Br]**.**

A similar inner-sphere mechanism involving the reversible aromatization/ dearomatization of the pyridine moiety has been described by Kirchner et al. for the pincer-type iron(II) complex [(^{iPr}PN^{NH}P)Fe(H)(CO)Br] based on the 2,6-diaminopyridine scaffold bearing -NH as spacer[19].

Therefore, the non-innocent behaviour of the PNP scaffold is a key feature for the reactivity of the corresponding metal complexes. Similar chemistry is not available for PCP ligands due to the higher resonance energy of the benzene[20].

Thus, intrigued by the increasing attention on pincer type ligands as powerful tool to achieve stable and reactive transition metal complexes, we considered the possibility of synthesize new iron complexes bearing the phosphinite *iPr*PONOP type ligand (*iPr*PONOP =2,6-bis(di-iso-propylphosphinito)pyridine). The PONOP ligand has the feature of an -O-bridging unit in both side arms which precludes the ligand deprotonation in the presence of a strong base followed by dearomatization of the pyridine as observed in Milstein's systems.

The first tridentate PONOP type ligand (*tBu*PONOP=2,6-bis(di-*tert*-butylphosphinito) pyridine) was synthesized by Brookhart et al.[21] in 2009, and used to stabilize reactive iridium (I) and Ir (III) complexes active for C-H bond cleavage. In the same year, Milstein et al.[22] described the first 18-electron Ru (0) complex based on the phosphinite PONOP type ligand, reactive towards water and different electrophiles. In 2011 new nickel, platinum and palladium PONOP pincer complexes, in which the pyridine was reduced in presence of 1 equiv. of superhydride, were reported by Jones et al.[23,24] Moreover, due to the stability of the PONOP ligand, iridium-hydride[25], iridium-methylene[26-28] and dihydrogen rhodium[29] complexes have been recently synthesized and fully characterized. To the best of our knowledge, to date only few iron complexes bearing the PONOP type ligand have been described[29], but none of them showed a catalytic activity.

In the light of the previous developments, we become interested in exploring the coordination chemistry and reactivity of iron (II) complexes stabilized by the phosphinite *iPr*PONOP type ligand.

3.2 Synthesis and characterization of iron (II) complexes bearing the *iPr*PONOP pincer ligand

In this section, the synthesis and characterization of three well-defined low spin iron (II) complexes bearing the tridentate ligand 2,6-bis(di-iso-propylphosphinito) pyridine (*iPr*PONOP) are reported. The novelty is that these complexes showed high catalytic activity for both hydrogenation and hydrogen transfer reactions of unsaturated substrates such as aldehydes.
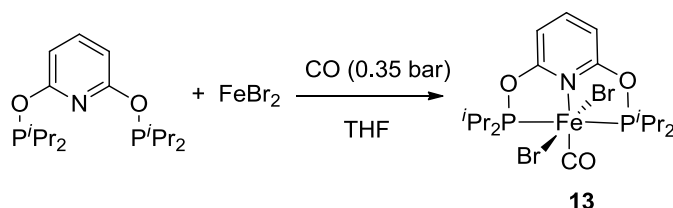
3.2.1 Ligand Synthesis

The ligand ^{iPr}PONOP has been synthesized as reported in literature[22] (Scheme 3.3). High yield and a clean product can be obtained by working with air-free techniques.
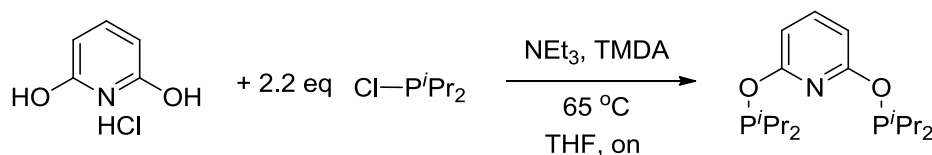
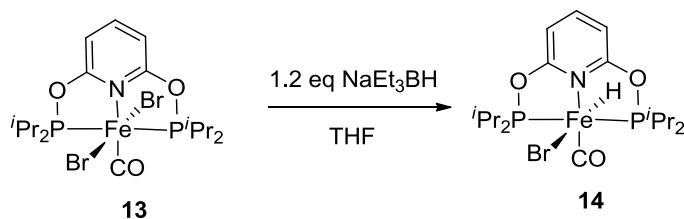**Scheme 3.3**: Synthesis of the ^{iPr}PONOP type ligand

3.2.2 Metallation using iron salts

The new Fe-PONOP complexes were prepared following standard procedures in Fe-pincer chemistry[16] (Scheme 3.4). Reaction of ^{iPr}PONOP with FeBr$_2$ in THF under pressure of CO gave [(^{iPr}PONOP)Fe(CO)Br$_2$] (**13**) as blue powder in very high yield. Complex **13** is diamagnetic and exhibited a characteristic singlet at δ 215 ppm in the ^{31}P{^{1}H} NMR spectrum. The Fe-bound CO ligand gives a strong IR band at 1961 cm^{-1}.

Scheme 3.4: Synthesis of the iron pincer complex **13**.

When complex **13** was reacted with a slightly excess of NaEt$_3$BH in THF, the bromide was replaced by the hydride ligand affording complex [(^{iPr}PONOP)Fe(CO)(H)Br] (**14**) as yellow powder (Scheme 3.5). The CO vibrational frequency lowered to 1928 cm^{-1} in the IR spectrum. In the ^{31}P{^{1}H} NMR spectrum of **14** one singlet was observed at δ 239 ppm while in the ^{1}H NMR spectrum the hydride ligand showed a characteristic triplet at δ -20.74 ppm ($^2J_{PH}$ = 56.6 Hz).

Scheme 3.5: Synthesis of the iron-hydride pincer complex **14.**

By adding an excess of TMSOTf to a solution of complex **14** in acetonitrile, the bromide ligand was replaced by a neutral acetonitrile molecule affording the cationic complex [(^{iPr}PONOP)Fe(CO)(H)(CH$_3$CN)](OTf) (**15**) as yellow powder (Scheme 3.6). The ^{31}P{^{1}H} NMR spectrum of the cationic Fe-hydride complex was nearly identical to that of **14**, while the ^{1}H NMR signal of the hydride ligand was shifted to δ -18.48 ppm ($^2J_{PH}$ = 53.7 Hz). The CO IR frequency was observed at 1951 cm^{-1}, consistent with a lower electronic density at the iron center.
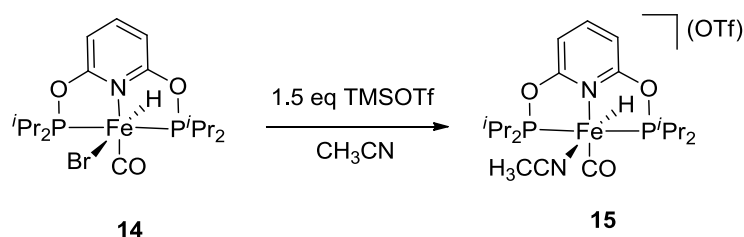
Scheme 3.6: Synthesis of the iron-hydride cationic pincer complex **15.**

3.2.3   Structure of Fe-PONOP complexes

The solid state structures of complexes **13**, **14** and **15** were determined by X-Ray crystallography. The crystal structure of **13** showed a distorted octahedral geometry at the Fe center with the two bromine ligands *trans* to one another, and the CO ligand *trans* to the nitrogen of the pyridine (Fig. 3.2).
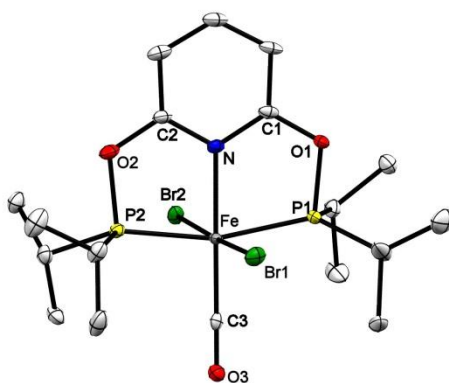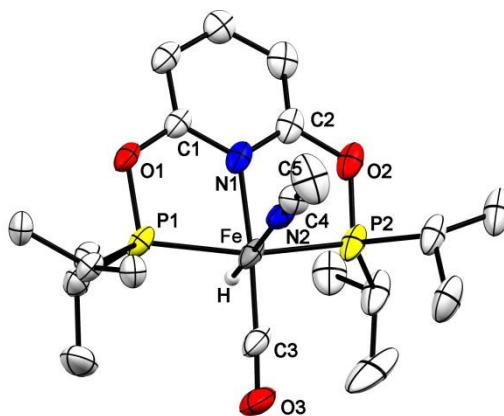

Fig. 3.2: X-Ray structure of **13**; the thermal ellipsoids are drawn at 30% probability. The hydrogen atoms are omitted for clarity. Selected bond lengths [Å] and angles [°]: Fe-C(3) 1.820(12), Fe-N 1.996(8), Fe-P(1) 2.251(3), Fe-P(2) 2.257(3),), Fe-Br(2) 2.4730(16), Fe-Br(1) 2.4724(16), N-Fe-P(1) 81.7(2), N-Fe-P(2) 80.7(2), N-Fe-C(3) 177.0(4), P(1)-Fe-P(2) 162.23(10).

The solid-state structure of complex **14** (Fig. 3.3) reveals a distorted octahedral geometry. The Fe-H bond is 1.38(3) Å. The hydride is *trans* to the bromide ligand while the CO is trans to the nitrogen of the pyridine.
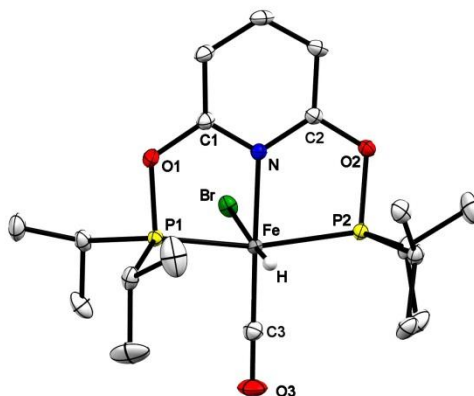
Fig. 3.3: X-Ray structure of **14**; the thermal ellipsoids are drawn at 30% probability. The hydrogen atoms are omitted for clarity. Selected bond lengths [Å] and angles [°]: Fe-N 1.9839(16), Fe-Br 2.5156(4), Fe-P(2) 2.1574(6), Fe-P(1) 2.1702(5), Fe-H 1.38(3), Fe-C(3) 1.736(2), P(2)-Fe-P(1) 160.89(2).

The crystal structure of **15** indicates again a distorted octahedral geometry (Fig. 3.4). The hydride ligand is *trans* to the acetonitrile molecule and the Fe-H distance is 1.43(4) Å. The other bond distances are comparable for complexes **14** and **15**.

Fig. 3.4: X-Ray structure of **15**; the thermal ellipsoids are drawn at 30% probability. The hydrogen atoms and the counter ion are omitted for clarity. Selected bond lengths [Å] and angles [°]: Fe-C(3) 1.734(5), Fe-N(2) 1.972(3), Fe-N(1) 1.995(3), Fe-P(1) 2.1771(10), Fe-P(2) 2.1815(12), Fe-H 1.43(4), N(2)-Fe-P(2) 95.62(9), N(1)-Fe-P(2) 81.94(9), P(1)-Fe-P(2) 161.23(5).

3.3 Hydrogenation and HT reactions catalysed by Fe-PONOP hydride complexes

Surprisingly, the Fe-PONOP hydride complexes [(^{iPr}PONOP)Fe(CO)(H)Br] (**14**) and [(^{iPr}PONOP)Fe(CO)(H)(CH$_3$CN)](OTf) (**15**) were found of being excellent catalysts for

hydrogenation and HT reactions of a wide range of aldehydes under very mild conditions. In this section test reactions, catalytic protocols and the substrate scopes are reported.

3.3.1 Insertion reaction

Firstly, the insertion reactions of iron hydride complexes **14** and **15** with a large number of unsaturated substrates including ketones, aldehydes, nitrobenzene, alkynes, and alkenes were tested. It's quite common for transition metal hydride complexes to have the hydride ligand acting as either hydride or proton source[31]. This strongly depends on the acidic or basic properties of the complex and on the influence of solvent effects. Unfortunately, in our case, no hydride insertion reaction took place in solvents such as MeOH, THF, CH_3CN indicating a low hydridicity of the Fe-H bonds in both **14** and **15**.

However, stoichiometric hydrogenation of benzaldehyde was observed under pressure of H_2. When a high pressure sapphire NMR tube charged with **14** and 1 equiv. of benzaldehyde in MeOD-*d4* was pressurized with 80 bar of H_2, in the ^{1}H-NMR spectrum the characteristic signal of the aldehyde group at 9.97 ppm disappeared with concomitant decrease of the hydride signal at -20.74 ppm within 2 hours (Scheme 3.7, Fig. 3.5). Unfortunately, it was not possible to detect the -CH_2- signal of the related benzyl alcohol since, in the region between 4.5 and 5.0 ppm, there were both the signal of H_2 and H_2O present in MeOD-d_4 overlapping it.
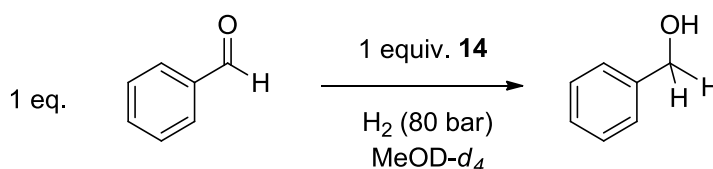
Scheme 3.7: Insertion reaction of benzaldehyde with **14** under H_2 (80 bar) in MeOD-d_4.

To overcome this problem a similar experiment was run but in presence of D_2 (30bar) and using MeOH as solvent. After 2 h under pressure of D_2, the solution contained in the high pressure sapphire NMR tube was dried and the powder dissolved in $CDCl_3$. At this point, by switching to a ^{2}H-NMR, it was possible to detect at 4.65 ppm the characteristic signal of the -CHD- group belonging to the benzyl alcohol formed in solution.
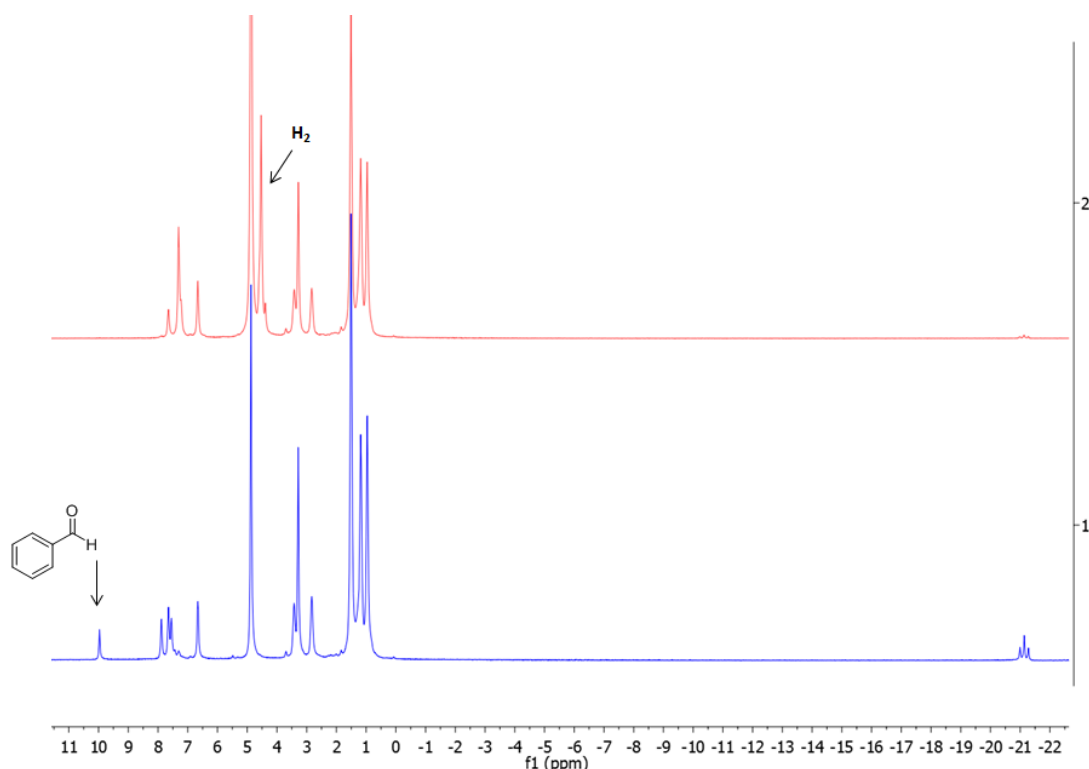
Fig. 3.5: ^{1}H-NMR spectrum of **14** and 1 equiv. of benzaldehyde in MeOD-d_4 before (in blue) and after (in red) addition of H$_2$ (80 bar).

No stoichiometric hydrogenation of benzaldehyde was observed under pressure of H$_2$ using **15** as catalyst. Moreover, with **14** as catalyst other unsaturated substrates such as ketones, alkynes, or alkenes were tested under the same conditions, but no insertion reaction took place.

3.3.2   Hydrogenation reaction

The results obtained from the insertion reaction of benzaldehyde in presence of H$_2$ suggested that complex **14** could serve as chemoselective hydrogenation catalyst of aldehydes.

A screening of conditions indeed led to a catalytic protocol using **14** as catalyst (Table 3.1). The best performance could be achieved in MeOH using 10 mol% of catalyst loading, at room temperature, under 8 bar of H$_2$, and within 24 h. Significantly, no reaction occurred in presence of other protic solvents such as EtOH, ^{i}PrOH, EtOH/H$_2$O, and in THF. The catalysis was slower with either a lower loading of catalyst or a lower pressure of H$_2$. Without **14** no hydrogenation reaction occurred.

Table 3.1: Screening of the conditions of the hydrogenation reaction using benzaldehyde as substrate and 3 as catalyst[a].
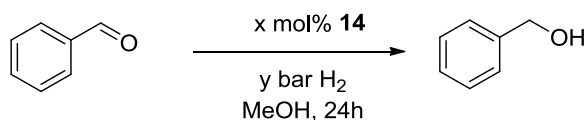
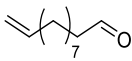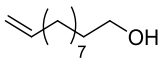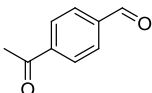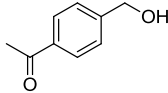|	**4 bar H$_2$**	**8 bar H$_2$**
5 mol% 14	No product	25 %
10 mol% 14	5 %	90 %
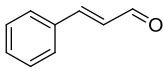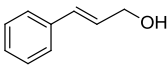
[a]Reaction conditions: substrate (0.3 mmol), catalyst (0.015-0.03 mmol, 5-10mol%), in MeOH (3 mL), at room temperature in 24h. [b]Yield of alcohol determined by calibrated GC analysis.

When **14** was replaced by **15**, under the same conditions, none of the aldehydes tested was hydrogenated. Although full conversion was observed, the only products detected were acetals from the nucleophilic addition of MeOH to the aldehyde.

The optimized conditions using **14** as catalyst were applied for the hydrogenation of a wide range of aldehydes. The substrate scope and the reaction conditions are summarized in table 3.2.

Table 3.2: Catalytic and chemoselective hydrogenation of aldehydes[a]

Entry	Aldehyde	Product	Yield[%][b]
1			90 (82)
2			88 (65)
3			94 (90)
4			96 (85)

5			65 (60)
6			74
7			60
8			55
9			80 (74)

[a]Reaction conditions: substrate (0.3 mmol), catalyst (0.03 mmol, 10 mol%), H_2 (8 bar) in MeOH (3 mL), 24h.
[b]Yield of alcohol determined by calibrated GC analysis ; the isolated yields are in parenthesis.

As already reported for the insertion reaction, benzaldehyde was hydrogenated in high yield (Table 3.2, entry 1). Both the electron-withdrawing Br substituent and electron donating OMe and Me groups on the aromatic system were tolerated with yields of 88-96% (Table 3.2, entries 2-4). Switching to aliphatic aldehydes the cyclic cyclohexanecarboxaldehyde, the 3-cyclohexene-1-carboxaldehyde and the linear undecylenic aldehyde were hydrogenated in good yields (Table 3.2, entries 6-8).

The chemoselectivity of hydrogenation is an important issue and a good test for chemoselectivity is the hydrogenation of α,β-unsaturated aldehydes. The Fe-PNP complex of Milstein was highly efficient for ketone hydrogenation, but was unselective for the hydrogenation of α,β-unsaturated ketones due to competitive reduction of C-C double bonds[16]. As reported in section 1.5, so far only two Fe catalysts could selective hydrogenate α,β-unsaturated aldehydes to the corresponding allylic alcohols, but they required elevated temperature and pressure[32,33]. To our delight, the hydrogenation reduced *trans*-cinnamaldehyde yielding the corresponding allylic alcohol as the only product in a good yield (Table 3.2, entry 5). Moreover, the hydrogenation readily tolerates alkene groups (Table 3.2, entries 7 and 8). Most impressively, the hydrogenation is selective toward aldehyde even in the presence of a ketone group. Thus, hydrogenation of 4-acetylbenzaldehyde gave exclusively 1-[4-(Hydroxymethyl)phenyl]ethanone in a high yield (Table 3.2, entry 9).

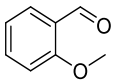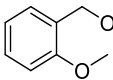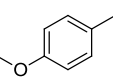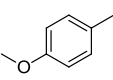### 3.3.3 Hydrogenation reaction promoted by HCOONa
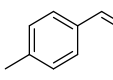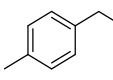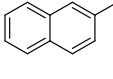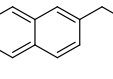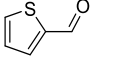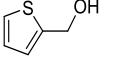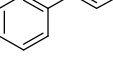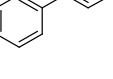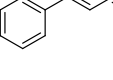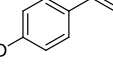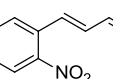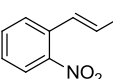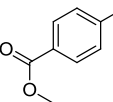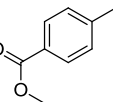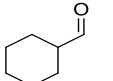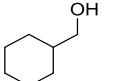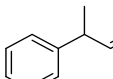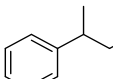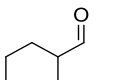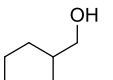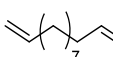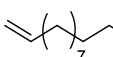
Interestingly, during the screening process it was found that hydrogenation of ortho-methylbenzaldehyde was accelerated by a catalytic amount of HCOONa. For example, with 5 mol% **14**, 4 bar of H_2, and at room temperature, the yield of this reaction was only 18 % after 24 h. But in the presence of 10 mol% HCOONa, the reaction was much faster and nearly quantitative yield was obtained after 24 h. Without H_2 the yields were below 8%, indicating the hydrogenation rather than transfer hydrogenation nature of the catalysis. The hydrogenation was carried out in the presence of excess of Hg, but no poisoning of the reaction was observed indicating a homogeneous process.

However, when HCOONa was replaced by other bases such as NaO^iPr, KO^tBu, CH_3COONa, $Na_2C_2O_4$ and NaOMe in the same conditions, the hydrogenation was ineffective. Same results were obtained when MeOH was replaced by EtOH, ^iPrOH, THF and CH_3CN.

The optimized conditions for HCOONa co-catalyzed reactions were then applied for the hydrogenation of functionalized aldehydes (Table 3.3). Interestingly, both complexes **14** and **15** could serve as catalysts showing similar efficiency for most substrates.

Table 3.3: Catalytic and chemoselective hydrogenation of aldehydes using HCOONa co-catalyst[a]

Entry	Aldehyde	Product	Yield[%][b] (cat = 14)	Yield[%][b] (cat = 15)
1			80 (75)	75
2			83 (80)	94
3			86 (81)	76

4			92 (88)	72
5			56 (50)	53
6			95 (87)	76
7			66 (62)	76
8			71	57
9			65 (60)	78
10			(64)	(67)
11			70 (63)	64
12			87 (83)	92
13			84	90
14			60	68
15			58	65
16			75	83

96

| 17 | | | 84 (76) | 82 |
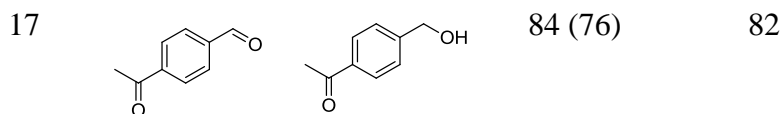
^aReaction conditions: substrate (0.3 mmol), HCOONa (0.03 mmol, 10 mol%), catalyst (0.015mmol, 5mol%), H$_2$ (4 bar) in MeOH (3 mL), 24h. ^bYield of alcohol determined by calibrated GC analysis ; the isolated yields are in parenthesis.

Benzaldehyde was hydrogenated in over 80% yield (Table 3.3, entry 1). The presence of electron withdrawing substituents such as halogens on the aromatic system enhanced the activity of both complex **14** and **15** with yields up to 94% (Table 3.3, entries 2 and 3). Similarly, in presence of a strong electron donating group such as –OMe yields up to 92% were observed for the *orto*-anysaldehyde (Table 3.3, entry 4) while the *para*-anysaldehyde was reduced only in moderate yields (53-56%, Table 3.3, entry 5). P*ara*-tolualdehyde and 2-naphthaldehyde were also hydrogenated in good yields (Table 3.3, entries 6-7). Interestingly also the sulfur- containing substrate 2-thiophenecarbaldehyde, which can potentially coordinate the iron center, was reduced in good yield (Table 3, entry 6).

Gratifyingly, selective hydrogenation of the aldehyde group of α,β-unsaturated aldehydes was again possible (Table 3.3, entries 9-10). Furthermore, other potentially reducible groups such as ester and nitro were tolerated (Table 3.3, entries 11-12). Both α branched and linear aliphatic aldehydes could be hydrogenated (Table 3.3, entries 13-16) achieving good chemoselectivity, as either internal or terminal C-C double bond were tolerated (Table 3.3, entries 15-16). Significantly, 4-acetylbenzaldehyde was hydrogenated only at the aldehyde group with a yield of 84% (Table 3.3, entry 17).

Hydrogenation of benzaldehyde was also conducted in the presence of acetophenone under the same conditions (Scheme 3.8). In this case only the aldehyde but not the ketone was reduced highlighting the chemoselectivity of the hydrogenation method.
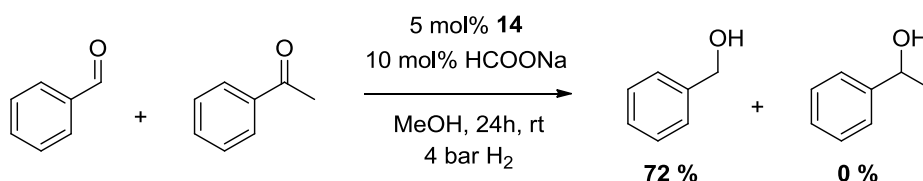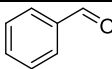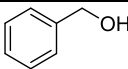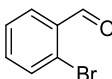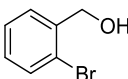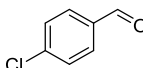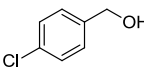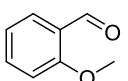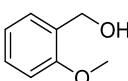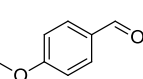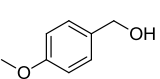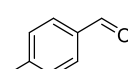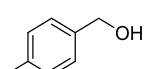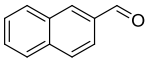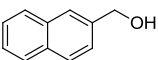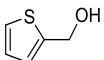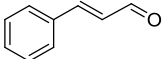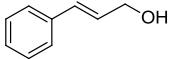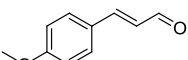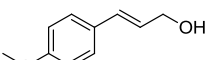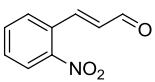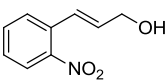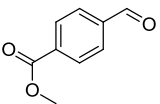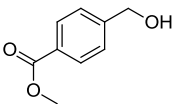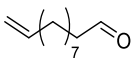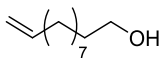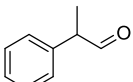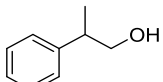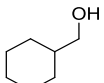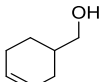
Scheme 3.8: Hydrogenation of 1:1 mixture of acetophenone and benzaldehyde. Yield of the benzyl alcohol determined by calibrated GC analysis.

3.3.4   Hydrogen Transfer reaction promoted by HCOONa

The promotion of catalytic hydrogenation by HCOONa described above suggested that complexes **14** and **15** might be used as transfer hydrogenation catalysts in presence of HCOONa as hydride source[34-37]. Transfer hydrogenation is convenient when handling of H_2 is undesirable[38]. While a number of precious metal complexes have been reported as selective catalysts for transfer hydrogenation of aldehydes[39,40], there is only one precedent for an iron catalyst, generated in situ by reaction of $Fe(BF)_4 \cdot 6H_2O$ and $P(CH_2CH_2PPh_2)_3$ and exhibiting very high yields (up to 99%) and excellent chemoselectivity[41]. In our case both complexes **14** and **15** catalysed transfer hydrogenation of aldehydes with HCOONa in MeOH. The optimized conditions are 5 mol% of catalyst, 5 equiv. of HCOONa, at 40 ^{o}C and in 6 hours. Table 3.4 shows the selectivity and tolerance of the catalysis.

Table 3.4: Catalytic and chemoselective transfer hydrogenation of aldehydes using HCOONa as hydrogen donor[a]

Entry	Aldehyde	Product	Yield[%][b] (cat = 14)	Yield[%][b] (cat = 15)
1			98 (91)	95
2			98 (93)	94
3			98 (91)	95
4			97 (92)	85
5			93 (89)	86
6			99 (92)	96

7			99 (93)	98
8			82	79
9			85 (76)	72
10			(72)	(68)
11			78 (65)	69
12			97 (87)	95
13			95	75
14			95	90
15			97	84
16			98	94

[a]Reaction conditions: substrate (0.3 mmol), HCOONa (0.0015 mol, 5 equiv.), catalyst (0.015 mmol, 5 mol%), in MeOH (3 mL), at 40^0C, 6h. [b]Yield of alcohol determined by calibrated GC analysis ; the isolated yields are in parenthesis.

To our delight, most of the substrates were converted to the corresponding alcohols in very high yields. Benzaldehyde was fully converted to benzyl alcohol (Table 3.4, entry 1). Halogen, methoxy, and methyl substitution at the aromatic rings were tolerated with yields up to 99 % (Table 3.4, entries 2-6). Similarly, naphthalene and thiophene groups were tolerated (Table 3.4, entries 7-8).

Once again various α,β-unsaturated aldehydes bearing different functional groups were selectively reduced on the formyl group (Table 3.4, entries 9-11). According to the literature, only few catalysts are capable of chemoselective transfer hydrogenation of α,β-unsaturated aldehydes[37,39,42,43]. Aldehydes with sensitive and reducible functional groups such as methyl 4-formylbenzoate (Table 3.4, entry 12) and undecylenic aldehyde were selectively reduced (Table 3.4, entry 13). Aliphatic aldehydes were also reduced in high yields (Table 3.4, entries 14-16).

3.4   Mechanistic investigations

Intrigued by the reactivity showed by **14** and **15,** we decided to investigate possible mechanistic pathways for the H_2 activation, hydrogenation and HT reactions.

3.4.1   H/D scrambling reaction

Both complexes **14** and **15** are capable of activating H_2 as confirmed by H/D exchange experiments. When a solution of **14** in MeOD-d_4 was pressurized with D_2 (30 bar), the formation of H_2 (δ 4.58, singlet) and HD (δ 4.54 ppm, 1:1:1 triplet, J_{H-D}= 42 Hz) was observed within minutes in the ^{1}H-NMR spectra. Meanwhile the hydride signal at δ -20.74 ppm decreased in intensity and completely disappeared after 45 minutes (Fig. 3.6).
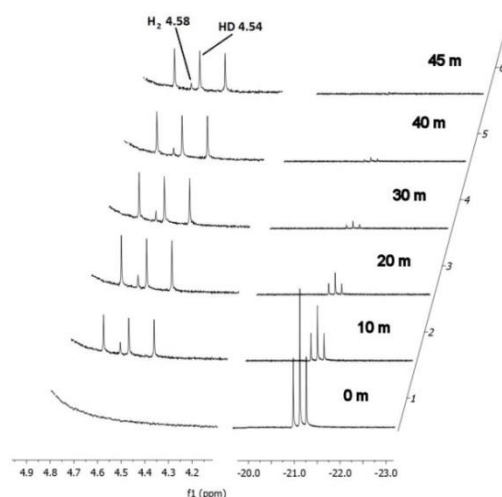
Figure 3.6: The time-dependent ^{1}H-NMR spectral change of the reaction of **14** with D_2 (30 bar) in MeOD-d_4 at ambient temperature.

This indicates that the Fe-H moiety was converted into Fe-D during the process. The same behaviour was observed when the pressure of D_2 was reduced at 1 bar, although the

100

hydride signal completely disappeared only after 32h. The H/D exchange on **14** also occurred in THF, but much slower. In CH$_3$CN no exchange was observed but, interestingly, it was found that **14** slowly converted to **15** according to the ^{1}H-NMR, due to the replacement of Br$^-$ by CH$_3$CN which is in large excess (Table 3.5, Fig 3.7 and 3.8).

Differently, complex **15** showed great stability in both THF and methanol where the CH$_3$CN ligand was not replaced by the solvent molecule. The H/D exchange reaction mediated by **15** had a similar rate in methanol and in THF.

Overall, in methanol the H/D exchange mediated by **15** is slower than the exchange mediated by **14**, but in THF the opposite order was observed. Neither **14** nor **15** mediated H/D exchange with D$_2$ in CH$_3$CN.

Table 3.5: Comparison of the rates of H/D exchange

Entry	Complex	Solvent	Time for 50% exchange(h)
1	**14**	MeOD-d4	0.18
2	**14**	THF-d8	> 150[a]
3	**14**	CD$_3$CN	no H/D exchange
4	**15**	MeOD-d4	18
5	**15**	THF-d8	20
6	**15**	CD$_3$CN	no H/D exchange

The rates of H/D exchange were calculated based on the decrease of the area of the hydride signals in the ^{1}H-NMR spectra. [a]After 150 h the conversion was 35%.
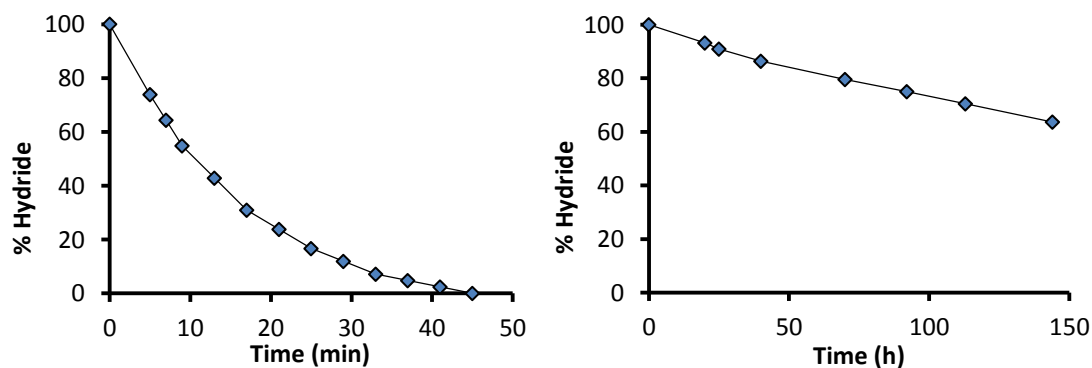
Figure 3.7: Time-dependent H/D scrambling of complex **14** in MeOD-*d4* (**left**) and THF-*d8* (**right**) under 30 bar of D$_2$
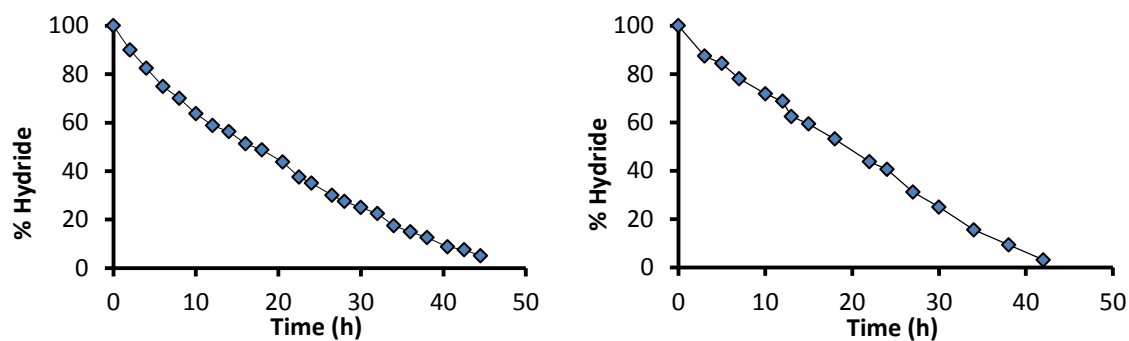
Figure 3.8: Time-dependent H/D scrambling of complex **15** in MeOD-*d4* (**left**) and THF-*d8* (**right**) under 30 bar of D_2

The H/D exchange by complex **14** in THF might be rationalized by the following reaction sequence (Scheme 3.9): the complex first binds to D_2 to form a dideuterium hydride complex **16-D,** likely preceded by dissociation of Br⁻. Reversible splitting of D_2 in **16-D** followed by H/D scrambling gives complex **17**. Release of HD then generates the iron deuterated complex **14-D**. Repetition of this process produces also H_2.
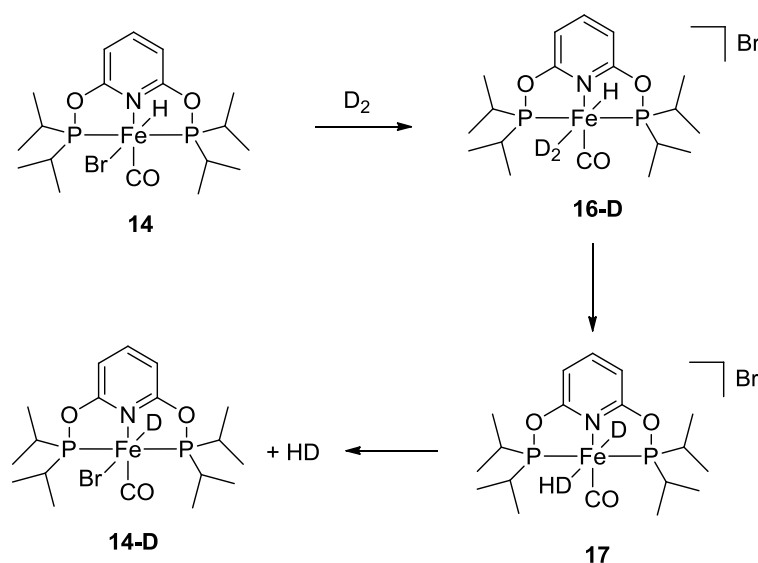
Scheme 3.9: H/D exchange in THF mediated by complex **14**.

As reported in section 1.4.1 dihydrogen complexes are more than intermediates for oxidative addition of H_2. They can be generated as either stable species or elusive intermediates, where the H-H σ orbitals donate electron density to an empty metal d orbital of σ symmetry. This interaction is augmented by back-donation from filled metal d orbitals[48].

The η^2-H_2 ligand does not necessarily need the intervention of molecular hydrogen to be formed as it may also be obtained from a terminal hydride by treatment with various proton donors; including many solvents of common use in organometallic synthesis and homogeneous catalysis. In our case no H_2 evolution was observed in the ^{1}H-NMR spectra when complex **14** was treated with different acids in both MeOD and THF-d8 solvents although the hydride signal disappeared within few minutes.

In general, once H_2 binds the metal center, the H_2 splitting might occur via homolytic, heterolytic H_2 splitting or σ-bond metathesis[50,51] (section 1.4.1, Fig. 1.15).

In our case, homolytic H_2 splitting requires a very electron-rich Fe center and yields formally to a Fe(IV) species. The electron-poor phosphinide in **14** seems incompatible to such homolytic splitting mechanism. Heterolytic cleavage is also well known but it is normally achieved only by strong bases, since H_2 is a very weak acid. The process of heterolytic splitting, which occurs with formal generation of H^+, in general generates a metal hydride complex and a corresponding protonated base. In our case, heterolytic H_2 splitting is possible, as Br^- might serve as a base to deprotonate coordinated H_2. Alternatively, the solvent might act as a proton acceptor.

On the other hand, σ-bond metathesis between coordinated H^- and H_2 ligands can lead to the same H/D exchange. For σ-bond metathesis to occur, isomerization of **16-D** so that the H^- and H_2 ligands are *cis* to one another is required[51]. In general, the reaction proceeds via a [2σ + 2σ] cycloaddition of a metal−ligand bond with that of a substrate throughout a concerted process. Therefore, the formal cycloaddition step is a transition state rather than an intermediate. For our system the distinction between heterolytic H_2 splitting and σ-bond metathesis is difficult with the available data, and it is perhaps best probed by future DFT calculations.

The mechanism of H/D exchange in THF by complexes **14** and **15** should be similar. The faster exchange rate by **15** is possibly due to a more rapid substitution of CH_3CN by H_2 in **15** than the substitution of Br^- by H_2 in **14**.

Two observations indicate that the H/D exchange in MeOH by complexes **14** and **15** is more complex: (1) In MeOD-d_4 and under H_2, H/D exchange occurred in presence of either **14** or **15**. (2) No H/D exchange was observed in absence of H_2 under otherwise same conditions. Thus, MeOH is involved in the H/D exchange, which favours a heterolytic H_2 splitting over σ-bond metathesis for reactions in methanol. We tentatively propose that MeOH acts as shuttle accepting the proton from **16** and becoming involved in the H_2 splitting (Scheme 3.10).
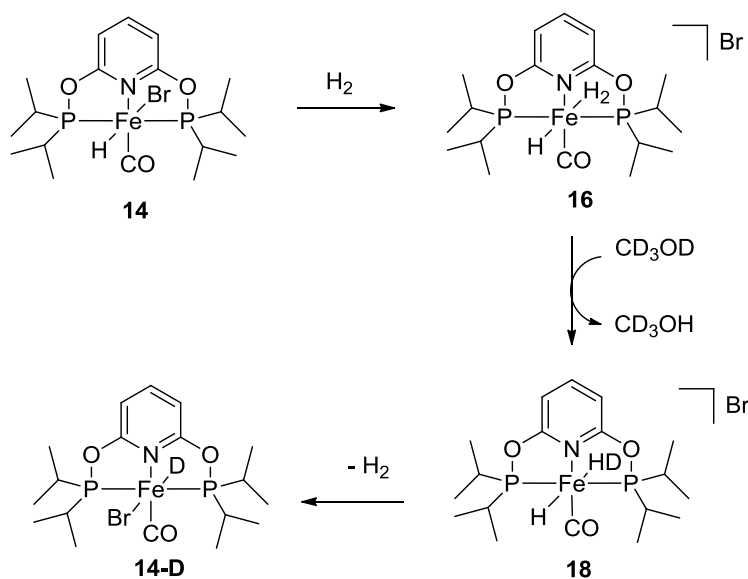
Scheme 3.10: Methanol-assisted H/D exchange by complex **14**.

It is well known in literature that dihydrogen complex intermediates may play a role in intermolecular proton exchange between hydrides and alcohols[47,62]. The first intermolecular dynamic proton transfer equilibrium between an hydride and coordinated H_2 mediated by ROH was observed in a Ru-hydride complex[63]. Moreover, also hydrogenases carry out this H^+/D_2 exchange efficiently, although this is not the physiological role of these enzymes[63,64]. In particular, two different mechanisms for the H^+/D_2 exchange have been described in the case of the $[Ir(PPh_3)_2(bq)(H_2O)H]$[62] (Scheme 3.11). In mechanism A, H_2 and ROH compete for the same coordination site and for efficient catalysis their binding ability should be comparable. Differently, mechanism B requires an alcohol basic enough to deprotonate the H_2 ligand.

Mechanism A
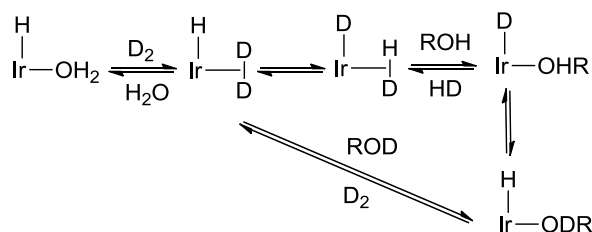
Mechanism B
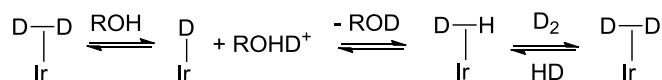
Scheme 3.11: General Mechanism A (top) and B (bottom) proposed for the H^+/D_2 exchange on Ir-hydride complex.

For our systems the H/D exchange rates for **15** are similar in methanol and in THF (Table 3.5). This suggests that the rate-determining step of H/D exchange does not involve methanol. Instead H_2 binding is the rate determining for **15**, and the binding appears to have a similar rate in methanol and in THF. In contrary, for **14** H/D exchange is significantly faster in methanol than in THF. This might be due to a more facile replacement of Br^- by H_2 in methanol thanks to a better solvation of Br^- by methanol than by THF, or to a faster H/D exchange due to the involvement of MeOH.

3.4.2 Mechanism of hydrogenation reaction

The mechanism of hydrogenation reaction is unclear for the moment, and only a hypothesis is outlined here (Scheme 3.12).
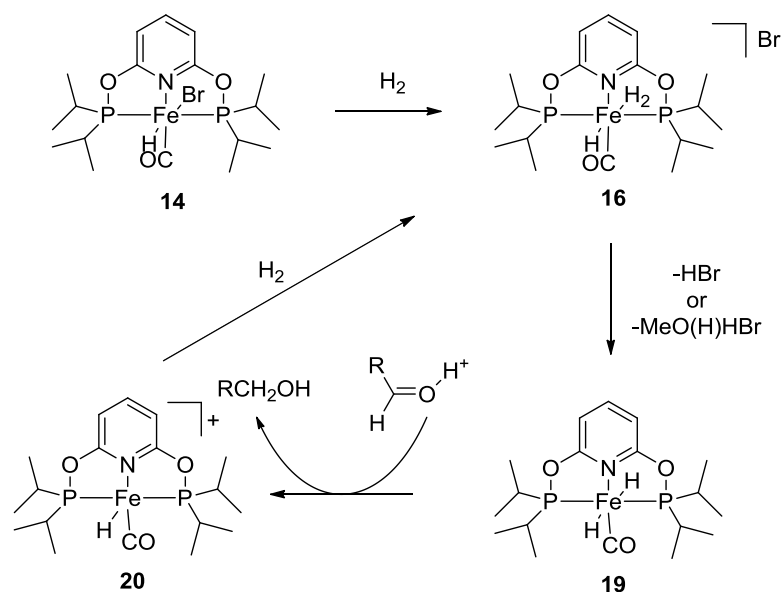
Scheme 3.12: Proposed mechanism for hydrogenation of aldehydes in methanol by complex **14**.

Because complexes **14** and **15** do not react with aldehyde in absence of H_2, they may be considered as precatalysts. Taking **14** as an example, it might be activated by H_2 to give the dihydrogen complex **16.** Interestingly, if poisoning agents such as PEt_3, CH_3CN, pyridine, 2,6-lutidine (0.3 equiv. regarding the substrate) were added in the reaction mixture, no hydrogenation occurred, underlying that the free coordination site for H_2 binding is indispensable for the reaction to take place.

In the next step, it is proposed that **16** undergoes heterolytic H_2 splitting assisted by MeOH to give a dihydride complex $[(^{iPr}PONOP)Fe(H)_2(CO)]$ (**19**). *Trans*-dihydride iron PNP complexes have been reported to be important active species in hydrogenation reactions of unsaturated substrates[66-69]. Unfortunately, in our case it was not possible to isolate independently this species from either **14** or **15**.

At this point, the proton generated in the process protonates the aldehyde and alcohol is formed following an outer-sphere hydride transfer from **19**. The resulting monohydride complex **20** binds H_2 to regenerate **16** and complete the catalytic cycle. Several penta-coordinated PNP iron monohydride complexes, active intermediate in dehydrogenation reactions, have been recently synthesized and fully characterized[70,71]. Our findings are consistent with Guan's computational studies based on the iron catalysed reduction of acetophenone[72]. In his calculated mechanism, the reduction of the substrate proceeds via a *trans*-$[Fe(PNP^{iPr})(CO)(H)_2]$ species and involves an outer-sphere hydrogen transfer from the dihydride complex to the carbonyl carbon atom of acetophenone in EtOH as solvent (Scheme 3.13). Noteworthy, the alcoholic solvent shows an essential role in the whole hydrogenation reaction, not only as stabilizer of the dearomatized intermediate but also more importantly, as assistant catalyst for the formation of the dihydride species.
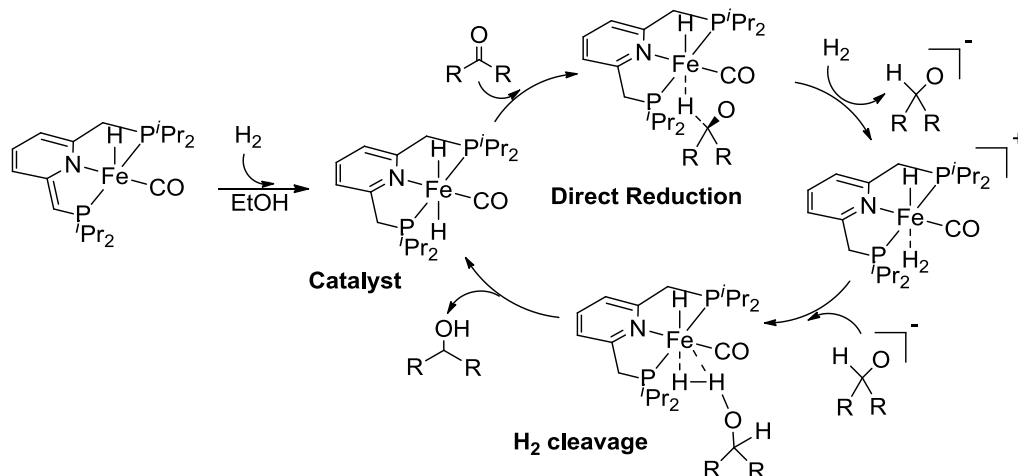
Scheme 3.13: Proposed catalytic mechanism by Guan for hydrogenation of acetophenone

An alternative mechanism involving the migratory insertion of a hydride ligand in **19** to aldehyde is possible, (inner-sphere hydrogenation mechanism) but, in our case it would require prior decoordination of a ligand to create an open coordination site for aldehyde binding. Given that the Fe center is coordinatively saturated in **19**, this mechanism is less likely.

3.4.3 Mechanism of hydrogenation and HT reaction assisted by HCOONa

For hydrogenation in presence of HCOONa, a formate complex [(^{iPr}PONOP)Fe(H)-(CO)(OOCH)] (**21**) might be formed. When an excess of HCOONa was added to a solution of complex **14** in MeOD-d_4 a new species was detected by ^{1}H-NMR spectroscopy (Fig. 3.9). This species gave a triplet hydride signal at δ -23.67 ppm ($^2J_{PH}$ = 56.6 Hz) and a pattern of signals that could be assigned to the ^{iPr}PONOP ligand belonging to the new species. Furthermore, two singlets at δ 8.19 ppm and at δ 8.62 ppm were observed. These two signals might be assigned to a HCOO$^-$ ligand on Fe and excess of HCOONa in solution, respectively. The new species exhibited a ^{31}P{^{1}H} NMR signal at δ 237.5 ppm. Concentration of the solution containing **21** led to its decomposition which precluded the isolation of this species. It is proposed that **21** undergoes β-H elimination to give a Fe dihydride complex **19** which then catalyses hydrogenation. The dihydride complex **19** is also proposed as the active species for the transfer hydrogenation.

Moreover, in presence of HCOONa both **14** and **15** serve as catalyst for both hydrogenation and HT reactions. The generation of **19,** occurring at a similar rate in the presence of HCOONa for both complexes, might be considered the rate limiting step.
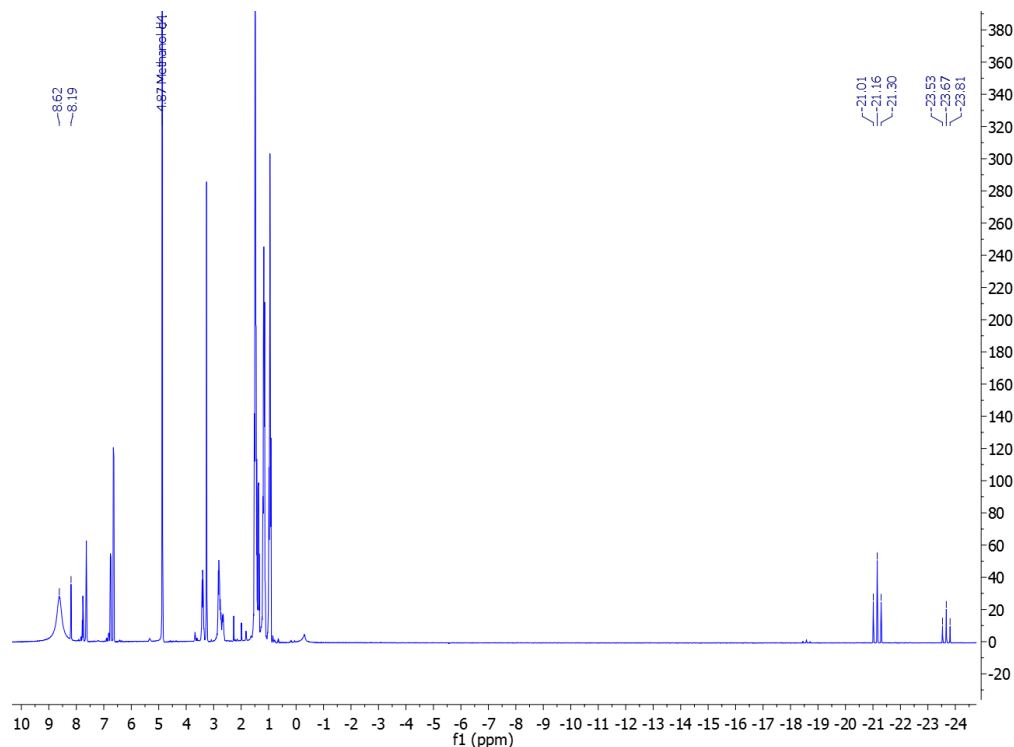
Fig. 3.9: ^{1}H-NMR of the reaction of **14** with HCOONa (1 equiv.) in MeOD-d_4 at ambient temperature

The establishment of mechanism, however, requires further experimental and computational work.

3.5 Conclusions

In summary, new Fe pincer complexes based on the PONOP ligand have been synthesized and fully characterized. The PONOP ligand is easy to prepare and modify. These complexes not only activate H$_2$, but also catalyse hydrogenation of aldehydes under mild conditions and with high functional group tolerance. The chemoselectivy towards aldehyde versus alkene and especially ketone groups is remarkable and synthetically useful. The complexes also catalyse chemoselective transfer hydrogenation of aldehydes using HCOONa as the hydride source. The mechanisms of H$_2$ activation, hydrogenation, and transfer hydrogenation are subject to future studies.

3.6 Experimental

Materials and methods:

All experiments were carried out under an inert N_2 (g) atmosphere using standard Schlenk or glovebox techniques. Solvents were purified using a two-column solid-state purification system (Innovative Technology, NJ, USA) and transferred to the glove box without exposure to air. Methanol (99.8%, extra dry, over molecular sieve) was purchased from AcroSeal®. Deuterated solvents were purchased from Cambridge Isotope Laboratories, Inc., and were degassed and stored over activated 3 Å molecular sieves. All other reagents were purchased from commercial sources and were degassed by standard freeze-pump-thaw procedures prior to use. ^{1}H and ^{31}P spectra were recorded at ambient temperature on a Bruker Avance 400 spectrometer. ^{1}H NMR chemical shifts were referenced to residual solvent as determined relative to TMS (δ 0.00ppm). GC-MS measurements were conducted on a Perkin-Elmer Clarus 600 GC equipped with Clarus 600T MS and Agilent J&W GC column, DB-5MS UI 25m, 0.250mm, 0.25 μm. IR measurements were recorded on powder samples at ambient temperature on a Varian 800 FT-IT Scimitar Series spectrometer. Elemental analyses were performed on a Carlo Erba EA 1110 CHN Instrument. HRESI-MS measurements were conducted at EPFL ISIC Mass Spectrometry Service with a Micro Mass QTOF Ultima Spectrometer.

Ligand synthesis: For the ligand synthesis the procedure reported in the literature was followed[21].

Synthesis of complex [($^{i\mathbf{Pr}}$PONOP)Fe(CO)Br$_2$] (13):

0.625 g of FeBr$_2$ (0.0029 mol) and 1 g of $^{i\text{Pr}}$PONOP (0.0029 mol) were mixed in 50 mL of dry THF in an ACE round-bottom pressure flask in the glovebox and the reaction mixture was stirred for 1 h. Afterward the flask was pressurized with 0.35 bar of CO and stirred for additional 2 h. The color turned immediately from dark yellow/brown to deep blue. The solution was filtered through a PTFE filter and concentrated. n-Pentane was then added to promote the precipitation of the product as a fine blue powder that was filtered and washed with additional n-pentane (yield: 85%). Single crystals suitable for X-ray analysis were grown by diffusion of n-pentane in a concentrated solution of complex **13** in THF. Anal. calcd. for $C_{18}H_{32}Br_2FeNO_3P_2$: C 36.76%, H 5.48%, N 2.38%. Found: C 36.46%, H 5.35%, N 2.40%.
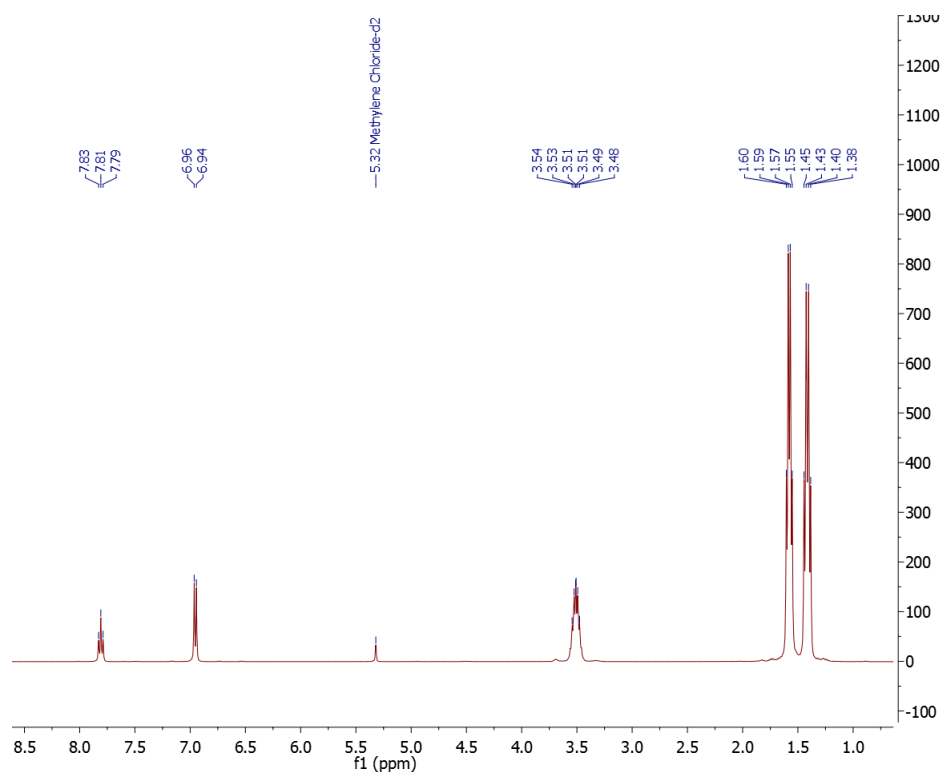
Fig. 3.10: ^{1}H NMR of **13** (400 MHz, CD$_2$Cl$_2$, 20°C)

^{1}H NMR (400MHz, CD$_2$Cl$_2$, 20°C): δ 7.81 (t, 1H, $^3J_{HH}$ = 8.1Hz, aryl-H$_4$), δ 6.95 (d, 2H, $^3J_{HH}$ = 8.1Hz, aryl-H$_{3,5}$), δ 3.51 (sept, 4H, $^3J_{HH}$ = 6.9Hz, , $^3J_{HP}$ = 13.4 Hz PCH(CH$_3$)$_2$), δ 1.50 (dq, 24H, $^3J_{HH}$ = 7.5Hz, $^3J_{HP}$ = 67.1 Hz PCH(CH_3)$_2$) ppm.
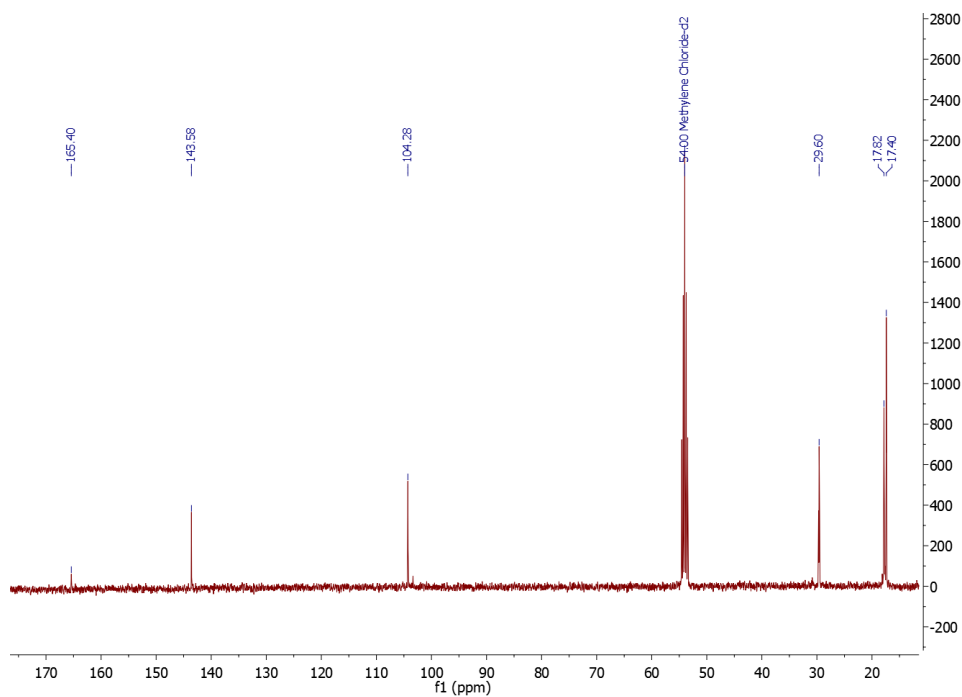
Fig. 3.11: ^{13}C NMR of **13** (400 MHz, CD$_2$Cl$_2$, 20°C)

^{13}C{^{1}H} NMR (101MHz, CD$_2$Cl$_2$, 20°C): δ 165.40 (t, Fe-CO ^{2}J$_{C-P}$ = 6.3Hz), δ 143.59 (s, aryl-C$_4$), δ 104.28 (s, aryl-H$_{3,5}$), δ 29.60 (t, ^{1}J$_{C-P}$ = 9.1 Hz, PCH(CH$_3$)$_2$), δ 17.82 (s, PCH(CH_3)$_2$), δ 17.39 (s, PCH(CH_3)$_2$) ppm. FT-IR: ν[cm^{-1}] 1961 (s, ν$_{CO}$). ESI-MS (*m/z, pos*) 508.05 (100%, [(^{iPr}PONOP)Fe(CO)Br]$^+$)

^{31}P{^{1}H} NMR (162MHz, CD$_2$Cl$_2$, 20°C): δ 215.25 (s) ppm.

Synthesis of complex [(^{iPr}PONOP)FeH(CO)Br] (14):

0.5 g of [(^{iPr}PONOP)Fe(CO)Br$_2$] (1 mmol) was dissolved in 25mL of dry THF and 1.2 mL of NaHBEt$_3$ (1M in Toluene, 1.2 mmol) was added. The color turned immediately from blue to green within a few minutes. The reaction mixture was stirred for 3h, filtered with a PTFE filter and concentrated. Addition of n-pentane promoted the precipitation of the product as a fine yellow powder that was filtered and washed with additional n-pentane (yield: 70%). Single crystals suitable for X-ray analysis were grown by diffusion of n-pentane in a concentrated solution of complex **14** in THF.

Anal. calcd. for C$_{18}$H$_{33}$BrFeNO$_3$P$_2$: C 42.46%, H 6.53%, N 2.75%. Found: C 42.60%, H 6.52%, N 2.66%. FT-IR: ν[cm^{-1}] 1928 (s, ν$_{CO}$). ESI-MS (*m/z, pos*) 428.08 ([(^{iPr}PONOP)FeH-(CO)]$^+$), 400.25 ([(^{iPr}PONOP)FeH]$^+$).
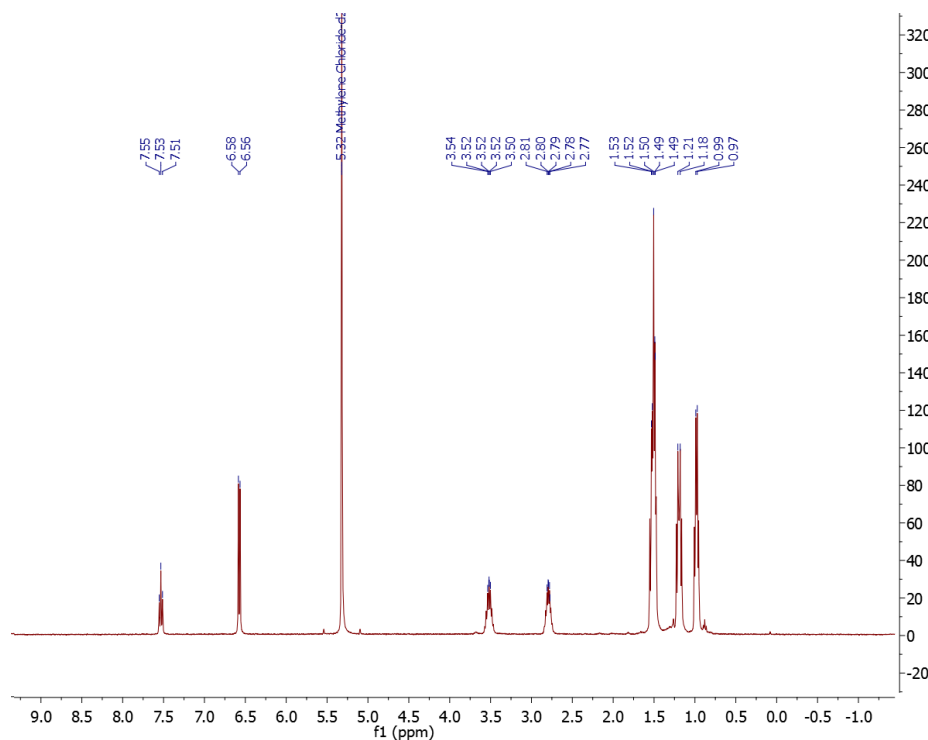
Fig. 3.12: ^{1}H NMR of **14** (400 MHz, CD$_2$Cl$_2$, 20°C)

^{1}H NMR (400MHz, CD$_2$Cl$_2$, 20°C): δ 7.53 (t, 1H, $^3J_{HH}$ = 8.0 Hz, aryl-H$_4$), δ 6.58 (d, 2H, $^3J_{HH}$ = 8.0 Hz, aryl-H$_{3,5}$), δ 3.52 (sept, 2H, $^3J_{HH}$ = 7.1 Hz, , $^3J_{HP}$ = 14.4 Hz PCH(CH$_3$)$_2$), δ 2.80 (sept, 2H, $^3J_{HH}$ = 6.6 Hz, , $^3J_{HP}$ = 13.3 Hz PCH(CH$_3$)$_2$, δ 1.51 (m, 12H, $^3J_{HH}$ = 6.8 Hz, $^3J_{HP}$ = 12.6 Hz PCH(CH_3)$_2$), δ 1.19 (q, 6H, $^3J_{HH}$ = 7.9 Hz PCH(CH_3)$_2$) δ 0.97 (m, 6H, $^3J_{HH}$ = 7.2 Hz PCH(CH_3)$_2$) δ -20.74 (t, 1H, $^2J_{HP}$ = 56.6 Hz Fe-H) ppm.
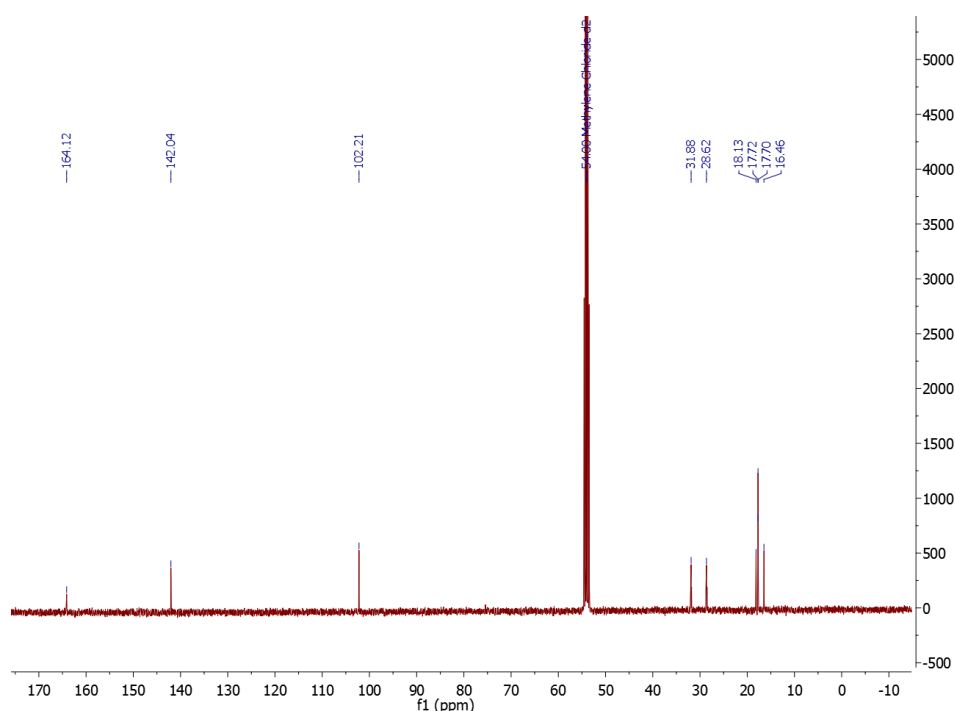
Fig. 3.13: ^{13}C NMR of **14** (400 MHz, CD$_2$Cl$_2$, 20°C)

^{13}C{^{1}H} NMR (101MHz, CD$_2$Cl$_2$, 20°C): δ 164.12 (t, Fe-CO $^2J_{C-P}$ = 6.3Hz), δ 142.04 (s, aryl-C$_4$), δ 102.21 (s, aryl-C$_{3,5}$), δ 31.88 (t, $^1J_{C-P}$ = 8.2 Hz, PCH(CH$_3$)$_2$), δ 28.62 (t, $^1J_{C-P}$ = 11.5 Hz, PCH(CH$_3$)$_2$), δ 18.14 (t, $^2J_{C-P}$ = 4.7 Hz, PCH(CH$_3$)$_2$), δ 17.86-17.38 (m, PCH(CH$_3$)$_2$), δ 16.46 (t, J_{C-P} = 2.2 Hz PCH(CH$_3$)$_2$) ppm.

^{31}P{^{1}H} NMR (162MHz, CD$_2$Cl$_2$, 20°C): δ 239.00 ($^3J_{HP}$ = 35.8 Hz) ppm.

Synthesis of complex [(^{iPr}PONOP)Fe(H)(CO)(CH$_3$CN)]OTf (15):

0.150 g of [(^{iPr}PONOP)FeH(CO)Br] (0.295 mmol) was dissolved in 25mL of dry CH$_3$CN and 80 μL of TMSOTf (1.5 equiv., 0.442 mmol) was added. The yellow solution was stirred for 7 h. The solvent was then evaporated and the resulting yellow sticky oil was dissolved in 2 mL of THF. The addition of n-pentane led the precipitation of the product as a fine yellow powder that was filtered and washed with additional n-pentane (yield: 80%).

Single crystals suitable for X-ray analysis were grown by diffusion of n-pentane in a concentrated solution of complex **15** in THF.

Anal. calcd. for $C_{21}H_{35}F_3FeN_2O_6P_2S$: C 40.72%, H 5.86%, N 4.52%. Found: C 39.7%, H 4.72%, N 4.47%. FT-IR: $\nu[cm^{-1}]$ 1951 (s, ν_{CO}). ESI-MS (*m/z, pos*) 469.15 ([(^{iPr}PONOP)Fe(CO)(CH$_3$CN)]$^+$), 428.12 ([(^{iPr}PONOP)Fe (CO)]$^+$).
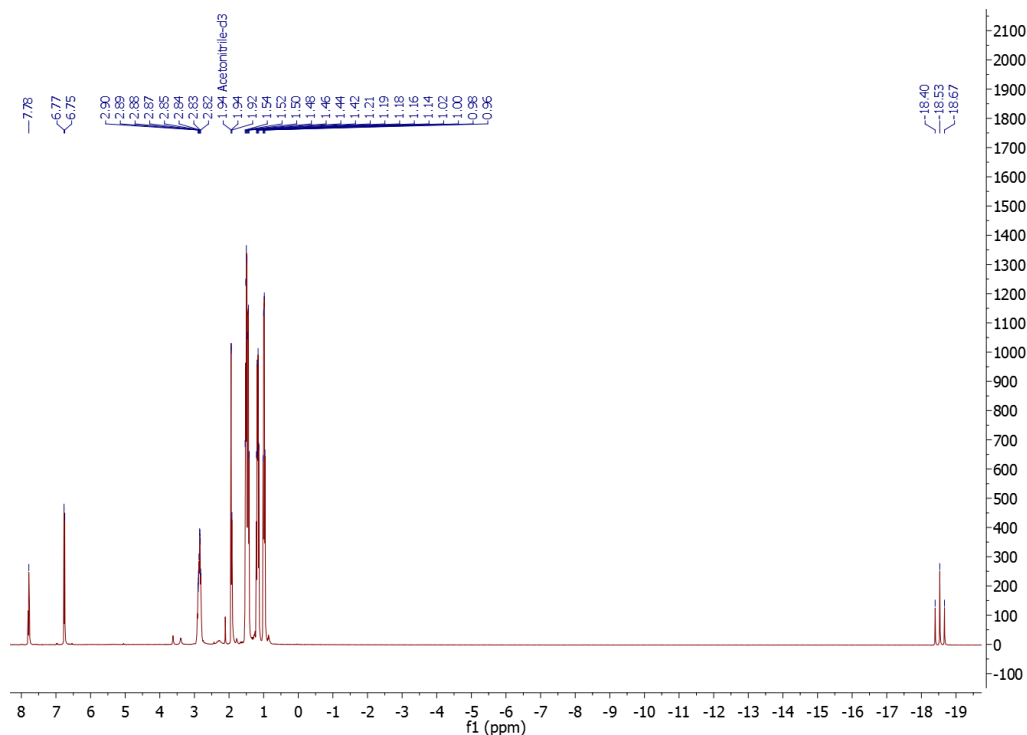
Fig. 3.14: ^{1}H NMR of **15** (400 MHz, Acetonitrile-d3, 20°C)

^{1}H NMR (400 MHz, Acetonitrile-d3, 20°C): δ 7.78 (t,1H, $^3J_{HH}$ = 8.1 Hz, aryl-H$_4$), δ 6.76 (d, 2H, $^3J_{HH}$ = 8.2 Hz, aryl-H$_{3,5}$), δ 2.92 (m, 4H, $^3J_{HP}$ = 18.6 Hz, $^3J_{HH}$ = 9.4 Hz, PC*H*(CH$_3$)$_2$), δ 1.99 (m, 3H, C*H$_3$*CN), δ 1.52 (dp, 12H , $^3J_{HP}$ = 27.0 Hz, $^3J_{HH}$ = 9.8 Hz, PCH(C*H$_3$*)$_2$), δ 1.28-1.18 (m, 6H, PCH(C*H$_3$*)$_2$), δ 1.02 (q, 6H, *J* = 7.2 Hz, PCH(C*H$_3$*)$_2$), δ -18.53 (s, 1H, $^2J_{HP}$ = 53.7 Hz Fe-*H*) ppm.
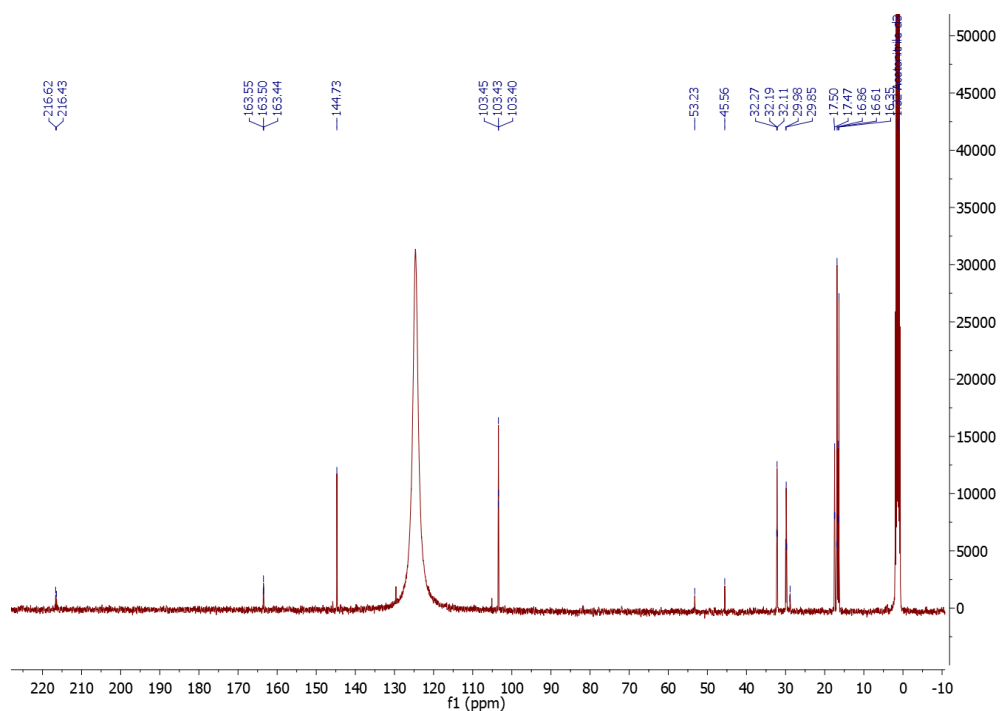
Fig. 3.15: ^{13}C NMR of **15** (101 MHz, Acetonitrile-d3)

^{13}C NMR (101 MHz, Acetonitrile-d3) δ 216.52 (t, ^{2}J$_{CP}$ = 19.8 Hz, Fe-*C*O), 163.50 (t, ^{2}J$_{PC}$ = 5.7 Hz, aryl-C$_{2,6}$), 144.73 (s, Ar-C$_4$) , 103.41 (s, Ar-C$_{3,5}$), 32.19 (t, ^{1}J$_{PC}$ = 7.8 Hz, P*C*H(CH$_3$)$_2$), 29.85 (t, ^{1}J$_{PC}$ = 13.2 Hz, P*C*H(CH$_3$)$_2$), 17.47 (t, ^{2}J$_{PC}$ = 4.04 Hz, PCH(*C*H$_3$)$_2$), 16.86 (s, PCH(*C*H$_3$)$_2$), 16.61 (t, ^{2}J$_{PC}$ = 4.04 Hz, PCH(*C*H$_3$)$_2$), 16.35 (s, PCH(*C*H$_3$)$_2$).

^{31}P{^{1}H} NMR (162 MHz, Acetonitrile-d3, 20°C): δ 237.83 (d, ^{3}J$_{HP}$ = 49.2 Hz) ppm.

General procedure for catalytic hydrogenation

A 35 mL ACE pressure tube was charged with catalyst **14** (0.03 mmol), the aldehyde (0.3 mmol), dodecane (30μL, 0.133 mmol), 3 mL of dry MeOH and 8 bar of hydrogen. The solution was stirred at ambient temperature (20-22 °C) for 24h. The reaction was quenched by exposure to air and by addition of diethyl ether.The alcohol products were identified and quantified by GC-MS with dodecane as an internal standard. External calibration curves were made using the commercial available products (purity >98%) or the isolated ones with dodecane as an internal standard..

General procedure for catalytic hydrogenation assisted by HCOONa

A 35 mL ACE pressure tube was charged with catalyst **14** or **15** (0.015 mmol), 300 μL (0.03 mmol) of a freshly prepared 0.1 M solution of HCOONa in MeOH, the aldehyde (0.3

mmol), dodecane (30μL, 0.133 mmol), 3 mL of dry MeOH and 4 bar of hydrogen. The solution was stirred at ambient temperature (20-22 °C) for 24h. The reaction was quenched by exposure to air and by addition of diethyl ether. The alcohol products were identified and quantified by GC-MS with dodecane as an internal standard. External calibration curves were made using the commercial available products (purity >98%) or the isolated ones with dodecane as an internal standard.

General procedure for transfer hydrogenation

In a vial were placed the catalyst (0.015 mmol), the aldehyde (0.3 mmol), dodecane (30μL, 0.133 mmol), HCOONa (0.0015 mol, 5 equiv.) and 3 mL of dry MeOH. The solution was stirred at 40 °C for 6h. The reaction was quenched by exposure to air and by addition of diethyl ether. The alcohol products were identified and quantified by GC-MS with dodecane as an internal standard. External calibration curves were made using the commercial available products (purity >98%) or the isolated ones with dodecane as an internal standard

Reaction of 14 and 15 with H_2 or D_2

In a typical experiment (NMR scale) a high pressure sapphire 5 mm NMR tube with a home-made titanium cap was charged with 10 mg of complex and 0.7 mL of deuterated solvent. H_2 or D_2 was added to the tube under a certain pressure.

Time-dependent H/D scrambling of complexes 14 and 15 in MeOD-d4 and THF-d^8 under D_2

0.5 mL of a 0.023 M solution of the complex in a deuterated solvent was introduced into a sapphire NMR tube which was then pressurized with 30 bar of D_2. The rates of H/D exchange were calculated based on the decrease of the area of the hydride signals in the ^{1}H-NMR spectra.
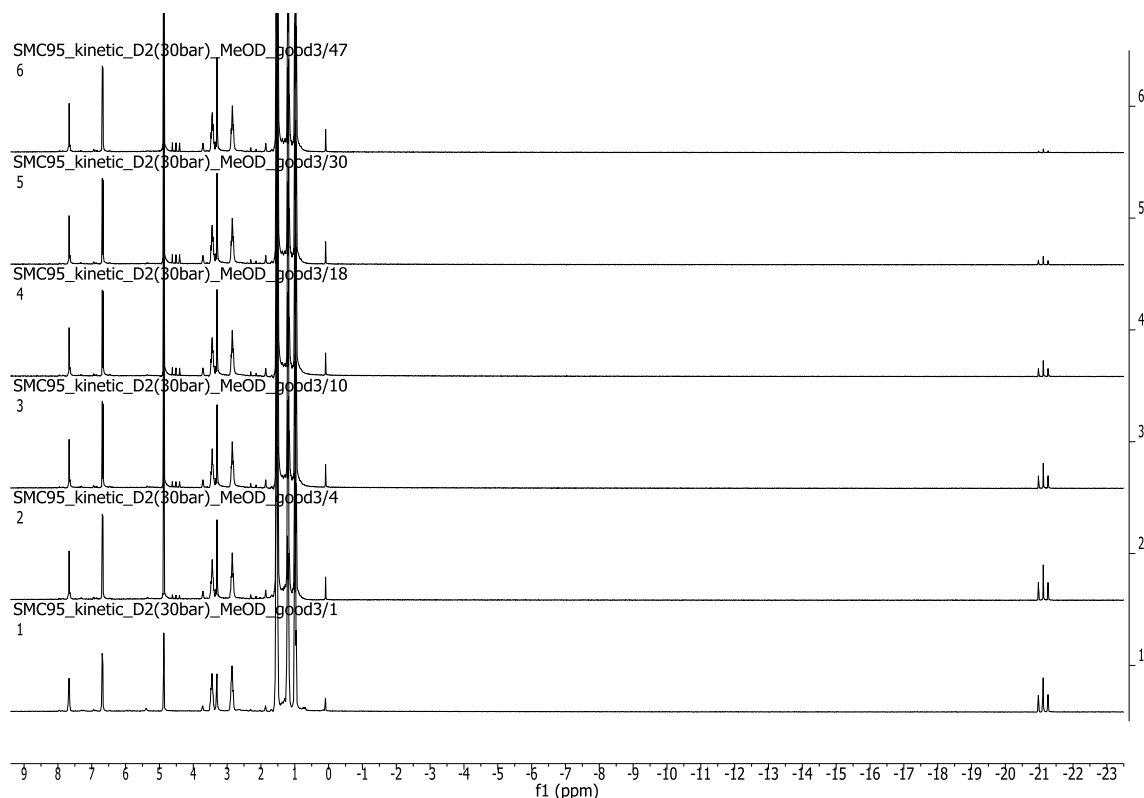
Fig. 3.16: Full spectra of the time-dependent ^{1}H-NMR spectral change of the reaction of **14** with D$_2$ (30 bar) in MeOD-d_4 at ambient temperature.

Hydrogenation of benzaldehyde using different bases and solvents

In preliminary studies different solvents like EtOH, iPrOH, THF and CH$_3$CN were investigated using 5 mol % of catalyst loading and 10 mol% of different bases such as NaOiPr, KOtBu, CH$_3$COONa, sodium oxalate and NaOMe. In all the cases benzaldehyde was only reduced in very poor yields (below 3 %).

Hydrogenation of 1:1 mixture of acetophenone and benzaldehyde

The catalytic hydrogenation of benzaldehyde under standard conditions (see General Procedure for catalytic hydrogenation) was selective in the presence of 1 equiv of acetophenone, yielding benzyl alcohol as the only product (72 % GC yield).

Characterization of the isolated products

All the products were purified thought silica column using a mixture of ethyl acetate and n-hexene as eluent. ^{1}H NMR and ^{13}C NMR spectra were collected in order to check the purity and compared with those of the commercial products. Herein we report the ^{1}H NMR and ^{13}C NMR spectra of the non-commercial alcohols.

(E)-3-(4-methoxyphenyl)prop-2-en-1-ol:

^{1}H NMR (400 MHz, CDCl$_3$, 20°C): δ 7.34 (d, 2H, ^{3}J$_{HH}$ = 8 Hz, Aryl-H$_{3,5}$), δ 6.88 (d, 2H, ^{3}J$_{HH}$ = 8 Hz, Aryl-H$_{2,6}$), δ 6.57 (d, 1H, ^{3}J$_{HH}$ = 16 Hz, C*H*=CH-CH$_2$), δ 6.25 (dt, 1H, ^{3}J$_{HH}$ = 15.8 Hz, ^{3}J$_{HH}$ = 5.9 Hz, CH=C*H*-CH$_2$), δ 4.32 (d, 2H, ^{2}J$_{HH}$ = 8 Hz CH=CH-C*H$_2$*), δ 3.81 (s, 3H, C*H$_3$*O-), δ 1.68 (bs, 1H, O*H*) ppm. ^{13}C{^{1}H} NMR (101MHz, CDCl$_3$, 20°C):) δ 159.38 (s, Aryl-C$_1$), δ 131.03 (s, *C*H=CH-CH$_2$), 129.78 (s, Aryl-C$_{3,5}$), 127.78 (s, Aryl-C$_4$), 126.35 (s, CH=*C*H-CH$_2$), 114.11 (s, Aryl-C$_{2,6}$), 64.02 (s, CH=CH-*C*H$_2$), 55.40 (*C*H$_3$O-) ppm.

(E)-3-(2-nitrophenyl)prop-2-en-1-ol:

^{1}H NMR (400 MHz, CDCl$_3$, 20°C): δ 7.89 (dd, 1H, ^{3}J$_{HH}$ = 8 Hz, Aryl-H$_6$), δ 7.63-7.47 (m, 2H, Aryl-H$_{3,5}$), δ 7.37 (d, 1H, Aryl-H$_4$), δ 7.06 (d, 1H, ^{3}J$_{HH}$ = 15.8 Hz, C*H*=CH-CH$_2$), δ 6.33 (dt, 1H, ^{2}J$_{HH}$ = 5.3 Hz ^{3}J$_{HH}$ = 15.7 Hz CH=C*H*-CH$_2$), δ 4.36 (dd, 2H, ^{2}J$_{HH}$ = 5.4 Hz CH=CH-C*H$_2$*), δ 2.26 (bs, 1H, O*H*) ppm. ^{13}C{^{1}H} NMR (101MHz, CDCl$_3$, 20°C):) δ 147.86 (s, Aryl-C$_1$), δ 134.3 (s, Aryl-C$_4$), δ 133.2 (s, *C*H=CH-CH$_2$) δ 128,83 (s, Aryl-C$_5$) δ 128.19 (s, CH=*C*H-CH$_2$), δ 125.78 (s, Aryl-C$_{2,3}$), δ 124.57 (s, Aryl-C$_6$), δ 63.27 (s, CH=CH-*C*H$_2$) ppm.

Methyl 4-(hydroxymethyl)benzoate:

^{1}H NMR (400 MHz, CDCl$_3$, 20°C): δ 7.99 (d, 2H, ^{3}J$_{HH}$ = 8.1 Hz, Aryl-H$_{2,6}$), δ 7.40 (d, 2H, ^{3}J$_{HH}$ = 8.1 Hz Aryl-H$_{3,5}$), δ 4.73 (s, 2H, C*H$_2$*), δ 3.89 (s, 3H, -OC*H$_3$*), δ 2.38 (bs, 1H, O*H*) ppm. ^{13}C{^{1}H} NMR (101MHz, CDCl$_3$, 20°C): δ 167.10 (s, CH$_3$O*C*O), δ 146.10 (s, Aryl-C$_4$), δ 129.98 10 (s, Aryl-C$_{2,6}$), δ 129.44 (s, Aryl-C$_1$), δ 126.59 (s, Aryl-C$_{3,5}$), δ 64.83 (s, *C*H$_2$), δ 52.26 (s, -OC*H$_3$*) ppm.

1-(4-(hydroxymethyl)phenyl)ethanone:

^{1}H NMR (400 MHz, CDCl$_3$, 20°C): δ 7.79 (d, 2H, ^{3}J$_{HH}$ = 8.0 Hz, Aryl-H$_{3,5}$), δ 7.32 (d, 2H, ^{3}J$_{HH}$ = 7.9 Hz Aryl-H$_{2,6}$), δ 4.63 (s, 2H, C*H$_2$*), δ 3.99 (s, 1H, O*H*), δ 2.47 (s, 3H, C*H$_3$*) ppm. ^{13}C{^{1}H} NMR (101MHz, CDCl$_3$, 20°C): δ 198.51 (s, *C*O), δ 146.75 (s, Aryl-C$_4$), δ 135.80 (s, Aryl-C$_1$), δ 128.41(s, Aryl-C$_{2,6}$), δ 126.45 (s, Aryl-C$_{3,5}$), δ 63.99 (s, *C*H$_2$), δ 26.46 (s, *C*H$_3$) ppm.

X-ray Crystallography

The diffraction data were measured using Mo Kα radiation on a Bruker APEX II CCD diffractometer equipped with a kappa geometry goniometer. The datasets were reduced by EvalCCD[73] and then corrected for absorption[74]. The data of compounds **14** and **15** were

measured using Cu Kα radiation on an Agilent Technologies SuperNova dual system in combination with an Atlas CCD detector. The data reduction was carried out by Crysalis PRO[75]. The solutions and refinements were performed by SHELX[76] .The crystal structures were refined using full-matrix least-squares based on F^2 with all non hydrogen atoms anisotropically defined. Hydrogen atoms were placed in calculated positions by means of the "riding" model.

Pseudo merohedral twinning was found for compound **13** and treated by the TWINROTMAT algorithm of PLATON[77] obtaining four BASF values: 0.112(2), 0.170(5), 0.021(2), 0.028(2). In the case of compound **15**, extensive disorder was found in an isopropyl moiety of the main complex and in the CF_3SO_3 anion. The split model with reasonable restraints (SADI, SIMU cards) was used to correctly treat it.

X-ray Structural Analysis of 13. Crystal Data: $C_{18}H_{32}Br_2FeNO_3P_2$, 0.43 x 0.39 x 0.32 mm^3, Triclinic, *P*-1, a = 10.4094(16) Å, b=14.9612(17) Å, c = 15.071(2) Å, α= 84.994(12)°, β= 89.915(15)°, γ= 87.592(8)°. T= 100(2) K, V= 2336.2(6) Å^3, Z= 4, ρ_c= 1.669 Mg/m^3, μ= 4.221 mm^{-1}. CCDC number 1006505.

Data Collection and Processing: 13285 reflections collected, $-14 \le h \le 14$, $-21 \le k \le 21$, $-21 \le l \le 21$, 13285 independent reflections [R(int) = 0.0000]

Solution and refinement: Refinement method used Full-matrix least-squares on F^2. 13285 data with 0 restraints and 491 parameters. Goodness-of-fit on F^2=1.149, largest diff. peak= 2.388 e.Å^{-3} and hole= -2.572 e.Å^{-3}.Final R indices [I>2σ(I)]: R1 = 0.0846, wR2 = 0.2150. R indices (all data): R1 = 0.1161, wR2 = 0.2304.

Table 3.6. Selected bond lengths and angles for **13**

	Bond length [Å]		Bond angles [°]
Br(1)-Fe(1)	2.4730(16)	C(1)-Fe(1)-N(1)	177.0(4)
Br(2)-Fe(1)	2.4724(16)	C(1)-Fe(1)-P(1)	97.2(3)
Fe(1)-C(1)	1.820(12)	N(1)-Fe(1)-P(1)	81.7(2)
Fe(1)-N(1)	1.996(8)	C(1)-Fe(1)-P(2)	100.5(3)
Fe(1)-P(1)	2.251(3)	N(1)-Fe(1)-P(2)	80.7(2)
Fe(1)-P(2)	2.257(3)	P(1)-Fe(1)-P(2)	162.23(10)
P(1)-O(1)	1.683(7)	P(1)-Fe(1)-Br(2)	94.32(8)
P(2)-O(2)	1.694(7)	P(2)-Fe(1)-Br(2)	87.37(8)

X-ray Structural Analysis of 14. Crystal Data: $C_{18}H_{32}BrFeNO_3P_2$, 0.45 x 0.18 x 0.15 mm^3, Monoclinic, *P2$_1$/c*, a = 16.7127(4) Å, b = 8.45507(19) Å, c = 16.6370(4) Å, α = 90°, β = 102.458(2)°, γ = 90°. T= 140(2) K, V= 2295.58(9)Å^3, Z= 4, ρ_c= 1.470 Mg/m^3, μ= 8.762 mm^{-1}. CCDC number 1006506.

Data Collection and Processing: 15102 reflections collected, -20<=h<=20, -7<=k<=10, -19<=l<=20, independent reflections 4540 [R(int) = 0.0389].

Solution and refinement: Refinement method used Full-matrix least-squares on F^2. 4540 data with 0 restraints and 240 parameters. Goodness-of-fit on F^2=1.048, largest diff. peak=0.739 e.Å^{-3}and hole= -0.442 e.Å^{-3}.Final R indices [I>2σ(I)]: R1 = 0.0314, wR2 =0.0846. R indices (all data): R1 = 0.0322, wR2 = 0.0854. The hydride was located on the difference Fourier density map and refined as isotropic with free coordinates.

Table 3.7. Selected bond lengths and angles for **14**

	Bond length [Å]		Bond angles [°]
Br(1)-Fe(1)	2.5156(4)	C(18)-Fe(1)-N(1)	176.12(9)
Fe(1)-C(18)	1.736(2)	C(18)-Fe(1)-P(2)	97.48(8)
Fe(1)-N(1)	1.9839(16)	N(1)-Fe(1)-P(2)	82.16(5)
Fe(1)-P(1)	2.1702(5)	C(18)-Fe(1)-P(1)	96.39(15)
Fe(1)-P(2)	2.1574(6)	N(1)-Fe(1)-P(1)	81.79(5)
Fe(1)-H(1)	1.38(3)	P(2)-Fe(1)-P(1)	160.89(2)
P(1)-O(1)	1.6835(15)	P(1)-Fe(1)-Br(1)	94.063(17)
P(2)-O(2)	1.6830(15)	P(2)-Fe(1)-Br(1)	95.300(18)

X-ray Structural Analysis of 15. Crystal Data: $C_{21}H_{35}F_3FeN_2O_6P_2S$, 0.49 x 0.37 x 0.29 mm^3, Monoclinic, *P2$_1$/n*, a = 12.5538(5) Å, b = 9.1895(3) Å, c = 25.0608(11) Å, α = 90°, β = 98.165(4)°, γ = 90°. T= 140(2) K, V=2861.8(2) Å^3, Z= 4, ρ_c= 1.435 Mg/m^3, μ= 6.472 mm^{-1}. CCDC number 1006507.

Data Collection and Processing: 19034 reflections collected, -15<=h<=14, -11<=k<=7, -30<=l<=31, Theta range for data collection 3.56 to 73.44°, independent reflections 5634 [R(int) = 0.0361]

Solution and refinement: Refinement method used Full-matrix least-squares on F^2. 5634 data with 261 restraints and 431 parameters. Goodness-of-fit on F^2=1.051, largest diff. peak=0.845 e.Å^{-3}and hole= -0.926 e.Å^{-3}.Final R indices [I>2σ(I)]: R1 = 0.0573, wR2 = 0.1463. R indices (all data): R1 = 0.0614, wR2 = 0.1507. The hydride was located on the difference Fourier density map and refined as isotropic with free coordinates.

Table 3.8. Selected bond lengths and angles for **15**

	Bond length [Å]		Bond angles [°]
Fe(1)-C(18)	1.734(5)	C(18)-Fe(1)-N(2)	97.38(18)
Fe(1)-N(2)	1.972(3)	C(18)-Fe(1)-N(1)	171.39(17)
Fe(1)-N(1)	1.995(3)	N(1)-Fe(1)-P(2)	82.16(5)
Fe(1)-P(1)	2.1771(10)	N(2)-Fe(1)-N(1)	91.15(11)
Fe(1)-P(2)	2.1815(12)	N(2)-Fe(1)-P(1)	94.03(9)
Fe(1)-H(1)	1.43(4)	N(1)-Fe(1)-P(1)	81.80(9)
P(1)-O(1)	1.682(3)	P(1)-Fe(1)-P(2)	161.23(5)
P(2)-O(2)	1.679(3)	C(18)-Fe(1)-H(1)	85.2(18)

3.7 References

(1)   Moulton, C. J.; Shaw, B. L. *J. Chem. Soc., Dalton Trans.***, 1976**, 1020.

(2)   Errington, J.; McDonald, W. S.; Shaw, B. L. *J. Chem. Soc., Dalton Trans.* **1980**, 2312.

(3)   Van Koten, G.; Jastrzebski, J. T. B. H.; Noltes, J. G.; Spek, A. L.; Schoone, J. C. *J. Organomet. Chem.* **1978**, 148, 233.

(4)   Van Koten, G.; Timmer, K.; Noltes, J. G.; Spek, A. L. ***J. Chem. Soc., Chem. Commun.***, **1978**, 250.

(5)   Tanaka, R.; Yamashita, M.; Nozaki, K. *J. Am. Chem. Soc.* **2009**, 131, 14168.

(6)   Hermann, D.; Gandelman, M.; Rozenberg, H.; Shimon, L. J. W.; Milstein, D. *Organometallics* **2002**, 21, 812.

(7)   Benito-Garagorri, D.; Becker, E.; Wiedermann, J.; Lackner, W.; Pollak, M.; Mereiter, K.; Kisala, J.; Kirchner, K. *Organometallics* **2006**, 25, 1900.

(8)   Chakraborty, S.; Lagaditis, P. O.; Förster, M.; Bielinski, E. A.; Hazari, N.; Holthausen, M. C.; Jones, W. D.; Schneider, S. ACS *Catalysis* **2014**, 4, 3994.

(9)   Zhang, G.; Scott, B. L.; Hanson, S. K. *Angew. Chem. Int. Ed.* **2012**, 51, 12102.

(10)   van der Vlugt, J. I.; Reek, J. N. H. *Angew. Chem. Int. Ed.* **2009**, 48, 8832.

(11)   Gunanathan, C.; Ben-David, Y.; Milstein, D. *Science* **2007**, 317, 790.

(12)   Käß, M.; Friedrich, A.; Drees, M.; Schneider, S. *Angew. Chem. Int. Ed.* **2009**, 48, 905.

(13)   Trovitch, R. J.; Lobkovsky, E.; Chirik, P. J. *Inorg. Chem.* **2006**, 45, 7252.

(14)   Vuzman, D.; Poverenov, E.; Shimon, L. J. W.; Diskin-Posner, Y.; Milstein, D. *Organometallics* **2008**, 27, 2627.

(15)   Ben-Ari, E.; Leitus, G.; Shimon, L. J. W.; Milstein, D. J. *Am. Chem. Soc.* **2006**, 128, 15390.

(16)   Langer, R.; Leitus, G.; Ben-David, Y.; Milstein, D. *Angew. Chem. Int. Ed*. **2011**, 50, 2120.

(17)   van der Vlugt, J. I.; Lutz, M.; Pidko, E. A.; Vogt, D.; Spek, A. L. *Dalton Trans.* **2009**, 1016.

(18)   van der Vlugt, J. I.; Pidko, E. A.; Vogt, D.; Lutz, M.; Spek, A. L. *Inorg. Chem.* **2009**, 48, 7513.

(19)   Gorgas, N.; Stöger, B.; Veiros, L. F.; Pittenauer, E.; Allmaier, G.; Kirchner, K. *Organometallics* **2014**, *33*, 6905.

(20)   Eicher, T.; Hauptmann, S.; Speicher, A. In The Chemistry of Heterocycles; Wiley-VCH Verlag GmbH & Co. KGaA: 2004, p 222.

(21)   Bernskoetter, W. H.; Hanson, S. K.; Buzak, S. K.; Davis, Z.; White, P. S.; Swartz, R.; Goldberg, K. I.; Brookhart, M. *J. Am. Chem. Soc.* **2009**, 131, 8603.

(22)   Salem, H.; Shimon, L. J. W.; Diskin-Posner, Y.; Leitus, G.; Ben-David, Y.; Milstein, D. *Organometallics* **2009**, 28, 4791.

(23)   Kundu, S.; Brennessel, W. W.; Jones, W. D. *Inorg. Chem.* **2011**, 50, 9443.

(24)   Kundu, S.; Brennessel, W. W.; Jones, W. D. *Inorganica Chimica Acta* **2011**, 379, 109.

(25)   Findlater, M.; Bernskoetter, W. H.; Brookhart, M. *J. Am. Chem. Soc.* **2010**, 132, 4534.

(26)   Walter, M. D.; White, P. S.; Schauer, C. K.; Brookhart, M. *J. Am. Chem. Soc.* **2013**, 135, 15933.

(27) Campos, J.; Peloso, R.; Brookhart, M.; Carmona, E. *Organometallics* **2013**, 32, 3423.

(28) Campos, J.; Kundu, S.; Pahls, D. R.; Brookhart, M.; Carmona, E.; Cundari, T. R. *J. Am. Chem. Soc.* **2013**, 135, 1217.

(29) Findlater, M.; Schultz, K. M.; Bernskoetter, W. H.; Cartwright-Sykes, A.; Heinekey, D. M.; Brookhart, M. *Inorg. Chem.* **2012**, 51, 4672.

(30) DeRieux, W.-S. W.; Wong, A.; Schrodi, Y. *J. Organomet. Chem.* **2014**, 772–773, 60.

(31) Jacobsen, H.; Berke, H. In Recent Advances in Hydride Chemistry; Poli, M. P., Ed.; *Elsevier*: Amsterdam, 2001, p 89.

(32) Fleischer, S.; Zhou, S.; Junge, K.; Beller, M. *Angew. Chem. Int. Ed.* **2013**, 52, 5120.

(33) Wienhöfer, G.; Westerhaus, F. A.; Junge, K.; Ludwig, R.; Beller, M. *Chem. Eur. J.* **2013**, 19, 7701.

(34) Rajagopal, S.; Spatola, A. F. *J. Org. Chem.* **1995**, 60, 1347.

(35) Bar, R.; Sasson, Y.; Blum, J. *Journal of Molecular Catalysis* **1984**, 26, 327.

(36) Hauwert, P.; Boerleider, R.; Warsink, S.; Weigand, J. J.; Elsevier, C. J. *J. Am. Chem. Soc.* **2010**, 132, 16900.

(37) Wu, X.; Liu, J.; Li, X.; Zanotti-Gerosa, A.; Hancock, F.; Vinci, D.; Ruan, J.; Xiao, J. *Angew. Chem. Int. Ed.* **2006**, 45, 6718.

(38) Brieger, G.; Nestrick, T. J. Chem. Rev. **1974**, 74, 567.

(39) Mizugaki, T.; Kanayama, Y.; Ebitani, K.; Kaneda, K. *J. Org. Chem.* **1998**, 63, 2378.

(40) Miecznikowski, J. R.; Crabtree, R. H. *Organometallics* **2004**, 23, 629.

(41) Wienhöfer, G.; Westerhaus, F. A.; Junge, K.; Beller, M. *J. Organomet. Chem.* **2013**, 744, 156.

(42) Selvam, P.; Sonavane, S. U.; Mohapatra, S. K.; Jayaram, R. V. *Adv. Synth. Catal.* **2004**, 542.

(43) Kidwai, M.; Bansal, V.; Saxena, A.; Shankar, R.; Mozumdar, S. *Tetrahedron Letters* **2006**, 47, 4161.

(44) Kubas, G. J.; Ryan, R. R.; Swanson, B. I.; Vergamini, P. J.; Wasserman, H. J. *J. Am. Chem. Soc.* **1984**, 106, 451.

(45) Kubas Gregory, *J. Acc. Chem. Res.* **1988**, 21, 120.

(46) Jessop, P. G.; Morris, R. H. *Coord. Chem. Rev.* **1992**, 121, 155.

(47) Albeniz, A. C.; Heinekey, D. M.; Crabtree, R. H. *Inorg. Chem.* **1991**, 30, 3632.

(48) Heinekey, D. M.; Oldham, W. *J. Chem. Rev.* **1993**, 93, 913.

(49) Sabo-Etienne, S.; Chaudret, B. *Chem. Rev.* **1998**, 98, 2077.

(50) Waterman, R. *Organometallics* **2013**, 32, 7249.

(51) Perutz, R. N.; Sabo-Etienne, S. *Angew. Chem. Int. Ed.A* **2007**, 46, 2578.

(52) Earl, K. A.; Jia, G.; Maltby, P. A.; Morris, R. H. *J. Am. Chem. Soc.* **1991**, 113, 3027.

(53) Rabaâ, H.; Saillard, J. Y.; Schubert, U. *J. Organomet. Chem.* **1987**, 330, 397.

(54) Crabtree, R. H.; Quirk, J. M. *J. Organomet. Chem.* **1980**, 199, 99.

(55) Mura, P.; Segre, A.; Sostero, S. *Inorg. Chem.* **1989**, 28, 2853.

(56) Buncel, E.; Menon, B. *J. Am. Chem. Soc.* **1977**, 99, 4457.

(57) Rocchini, E.; Mezzetti, A.; Rüegger, H.; Burckhardt, U.; Gramlich, V.; Del Zotto, A.; Martinuzzi, P.; Rigo, P. *Inorg. Chem.* **1997**, 36, 711.

(58)   Crabtree, R. H.; Lavin, M. *Journal of the Chemical Society, Chem. Commun.* **1985**, 794.

(59)   Arndtsen, B. A.; Bergman, R. G.; Mobley, T; Peterson, T. H. *Acc. Chem. Res.* **1995**, 28, 154.

(60)   Labinger, J. A.; Bercaw, J. E. *Nature* **2002**, 417, 507.

(61)   Brintzinger, H. H. *J. Organomet. Chem.* **1979**, 171, 337.

(62)   Collman, J. P.; Wagenknecht, P. S.; Hembre, R. T.; Lewis, N. S. *J. Am. Chem. Soc.* **1990**, 112, 1294.

(63)   Ayllón, J. A.; Gervaux, C.; Sabo-Etienne, S.; Chaudret, B. *Organometallics* **1997**, 16, 2000.

(64)   Lespinat, P. A.; Berlier, Y.; Fauque, G.; Czechowski, M.; Dimon, B.; Le Gall, J. *Biochimie* **1986**, 68, 55.

(65)   van der Zwaan, J. W.; Albracht, S. P. J.; Fontijn, R. D.; Slater, E. C. FEBS Letters **1985**, 179, 271.

(66)   Chakraborty, S.; Dai, H.; Bhattacharya, P.; Fairweather, N. T.; Gibson, M. S.; Krause, J. A.; Guan, H. *J. Am. Chem. Soc.* **2014**, 136, 7869.

(67)   Zell, T.; Butschke, B.; Ben-David, Y.; Milstein, D. *Chem. Eur. J.* **2013**, 19, 8068.

(68)   Zell, T.; Ben-David, Y.; Milstein, D. *Angew. Chem. Int. Ed.* **2014**, 53, 4685.

(69)   Langer, R.; Iron, M. A.; Konstantinovski, L.; Diskin-Posner, Y.; Leitus, G.; Ben-David, Y.; Milstein, D. *Chem. Eur. J.* **2012**, 18, 7196.

(70)   Chakraborty, S.; Brennessel, W. W.; Jones, W. D. *J. Am. Chem. Soc.* **2014**, 136, 8564.

(71)   Bielinski, E. A.; Lagaditis, P. O.; Zhang, Y.; Mercado, B. Q.; Würtele, C.; Bernskoetter, W. H.; Hazari, N.; Schneider, S. *J. Am. Chem. Soc.* **2014**, 136, 10234.

(72)   Yang, X. *Inorg. Chem.* **2011**, 50, 12836.

(73)   Duisenberg, A. J. M.; Kroon-Batenburg, L. M. J.; Schreurs, A. M. M. *Journal of Applied Crystallography* **2003**, 36, 220.

(74)   Blessing, R. H. *Acta Crystallographica Section A* **1995**, 51, 33.

(75)   Crysalis PRO, A. T., release 1.171.36.28, 2013.

(76)   Sheldrick, G. M. *Acta Crystallographica Section A* **2008**, 64, 112.

(77)   Spek, A. L. *Acta Crystallographica Section D* **2009**, 65, 148.

Chapter 4

Modification of the Iron PONOP Complexes:
from a Tridentate to a Bidentate Ligand

4.1   From the tridentate PONOP to the bidentate PON ligand

The development of well-defined ligand systems enabling the tuning of the properties of the metal centres in a controlled manner is one of the most important goals in modern inorganic and organometallic chemistry[1].

As described in chapter three, among the several ligand systems that can be found in the chemical literature, pincer ligands[2,3] and their complexes have attracted increasing interest mainly due to their stability, variety and tunability. Although the first pincer ligands were synthesized in the late 1970s[4], wide applications using pincer complexes were explored only starting from the late 1990s, switching this area into an intensively investigated subject in organometallic chemistry (Fig. 4.1).
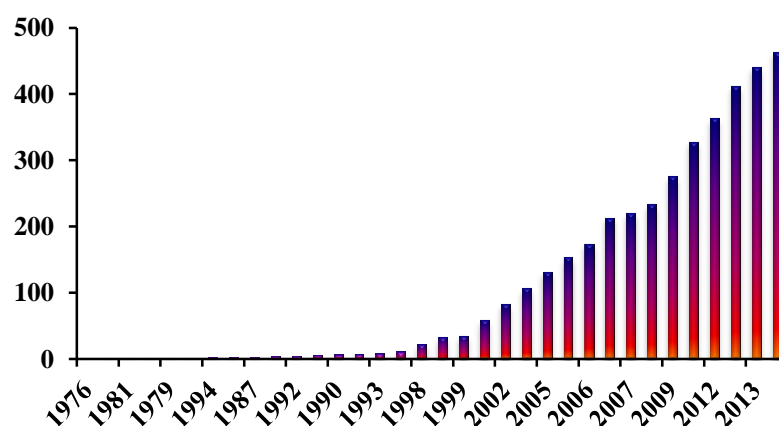
Fig. 4.1: Number of publications containing the word "pincer complex" [source: SciFinder].

In this chapter, the tuning of the Fe-PONOP system previously described (chapter three) has been taken into consideration in order to enhance its reactivity in the hydrogenation and hydrogen transfer reactions of unsaturated substrates. Precisely, the PONOP ligand is a very versatile system, whose phosphorus donor atoms can be easily modified in order to influence the electronic properties and the steric hindrance of the metal center.

Moreover, the CO ligand present in the Fe-PONOP system could be replaced by the isoelectronic tert-butyl isocyanide (^{t}BuNC). Isocyanides R^1NC are capable of displaying great π-acceptor capacity as the CO one when linked to a metal center capable of strong π-donation[5-9]. In particular tert-butyl isocyanide forms complexes that are stoichiometrically analogous to certain binary metal carbonyl complexes[10-12], such as $Fe_2(CO)_9$ and $Fe(^tBuNC)_5$. Although structurally similar, the analogous carbonyls differ in several ways mainly because the ^{t}BuNC is a better donor ligand. Thus, $Fe(^tBuNC)_5$ is easily protonated by $HBF_4 \cdot 2Et_2O$ in

anhydrous conditions[10] yielding the complex $[Fe(H)(^tBuNC)_5][BF_4]$, whereas $Fe(CO)_5$ is attacked by hydroxide[13] giving $[HFe(CO)_4]^-$, intermediate in the preparation of $[(H)_2Fe(CO)_4]$.

In the family of polydentate ligands, heterodifunctional ligands have been intensively investigated and used in coordination and organometallic chemistry[14-20]. In particularly, phosphanyl-pyridines have emerged as power tool, allowing for higher structural versatility and steric accessibility of the (first row) transition metal[21-24]. Thus, there is general interest in transition- metal complexes containing such hybrid ligands. Moreover, these soft/hard PN assemblies could coordinate reversibly to a metal center providing or protecting temporarily a vacant coordination site[25,26].

Stable and versatile iron low-spin carbonyl complexes of the type $[Fe(PN-^iPr)_2(CO)X]$ and $[Fe(PN-^iPr)(CO)_2X_2]$ (where X=Cl, Br) have been recently synthesized[24] by reacting *cis*-$Fe(CO)_4X_2$ with a strong PN donor ligand (Scheme 4.1). Noteworthy, by switching from one to two equivalents of PN ligand, iron complexes with different electronic and steric properties were synthesized.
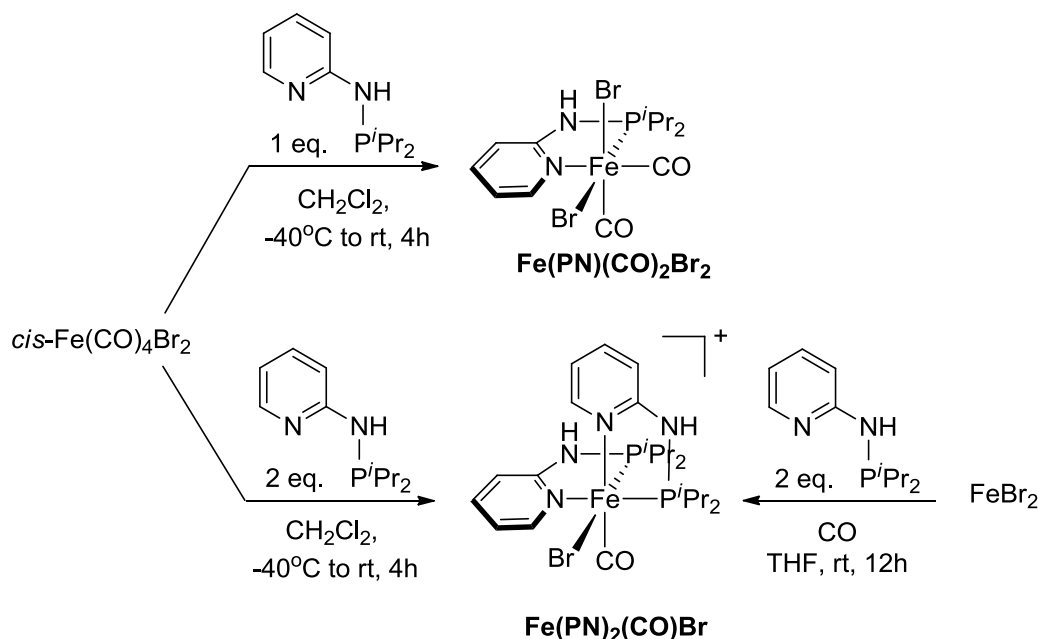
Scheme 4.1: Versatile Fe-PN complexes

In this context, the bidentate hybrid PON-^iPr ligand based on 2-aminopyridine in which the pyridine ring is separated from the phosphine moiety by an -O- bridging unit was synthesized and employed as ligand for the preparation of new stable iron complexes.

4.2 Modification of the PONOP ligand

As first attempt to synthesize new Fe-PONOP complexes with an enhanced reactivity in hydrogenation and hydrogen transfer reactions of substrates such as ketones and unsaturated C-C bond, the modification of the ^{iPr}PONOP ligand was taken into consideration.

4.2.1 Ligand Synthesis

An easy approach was to modify the phosphorus donor atoms by replacing the *iso*-propyl groups with the stronger donor cyclohexyl, the bulkier *tert*-butyl or ethyl groups.

The ligands ^{Cy}PONOP, ^{tBu}PONOP ^{Et}PONOP have been synthesized using the same procedure employed for ^{iPr}PONOP (Scheme 4.2). High yields and clean products could be obtained by working with air-free techniques.
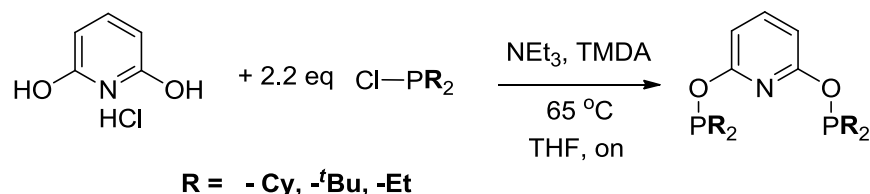
Scheme 4.2: Synthesis of the ^{Cy}PONOP, ^{tBu}PONOP and ^{Et}PONOP type ligands.

The syntheses were straightforward for ^{Cy}PONOP and ^{tBu}PONOP, while for ^{Et}PONOP only a mixture of products was obtained. The ^{Cy}PONOP ligand exhibited a characteristic signal at δ 143.96 ppm in the ^{31}P- NMR few ppm lower than ^{iPr}PONOP (δ 146.80), while ^{tBu}PONOP at δ 155.27 ppm.

4.2.2 Metallation using iron salts

Attempts to synthesize stable iron (II) complex using ^{Cy}PONOP or ^{tBu}PONOP ligands were made by following standard procedures in Fe-pincer chemistry[27]. Reaction of ^{Cy}PONOP with FeBr$_2$ in THF under pressure of CO gave [(^{Cy}PONOP)Fe(CO)Br$_2$] (**22**) as blue powder in very high yield (Scheme 4.3). Complex **22** is diamagnetic and exhibited a characteristic singlet at δ 207.58 ppm in the ^{31}P-NMR spectrum. The Fe-bound CO ligand gives a strong IR band at 1976 cm^{-1}. Suitable crystals for X-Ray analysis were obtained by diffusion of n-pentane in a saturated solution of **22** in THF.
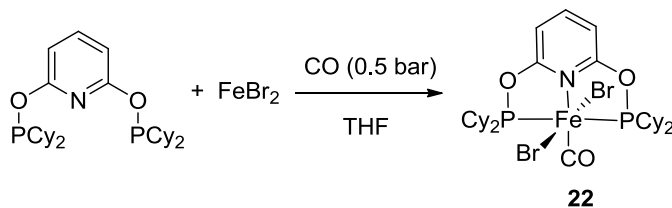
Scheme 4.3: Synthesis of the iron-^{Cy}PONOP complex **22**.

By switching to $FeCl_2$ as metal precursor, the stable $[(^{Cy}PONOP)Fe(CO)Cl_2]$ (**23**) as purple powder was synthesized in high yield (Scheme 4.4). Similarly, complex **23** is a diamagnetic complex exhibiting a characteristic singlet at δ 207.77 ppm in the ^{31}P-NMR spectrum. The Fe-bound CO ligand gives a strong IR band at 1977 cm^{-1} similar to complex **22**. Suitable crystals for X-Ray analysis were obtained by diffusion of n-pentane in a saturated solution of **23** in THF.
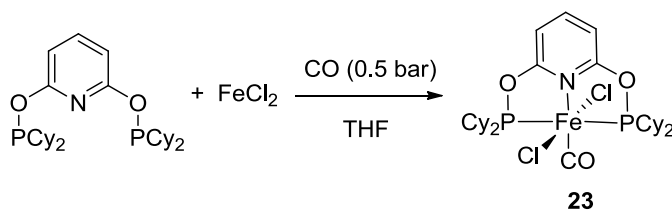
Scheme 4.4: Synthesis of the iron-^{Cy}PONOP complex **23**

In order to synthesize an iron-hydride complex bearing the ^{Cy}PONOP ligand, both complex **22** and **23** were reacted in presence of different borohydride salts in the same fashion used for the synthesis of complex **13** reported in chapter 3 (Scheme 3.4). Unfortunately, reaction with $NaEt_3BH$, $LiEt_3BH$ or $NaBH_4$ (different equivalent) as hydride sources led to the formation of several species in solution, included the iron-hydride one that was difficult to isolate.

As proof of the formation of the Fe-hydride species, a triplet at δ -20.64 ppm ($^2J_{PH} = $ 56.0 Hz) appeared in the ^{1}H-NMR spectra of the crude product. This signal had been tentatively assigned to the complex $[(^{Cy}PONOP)Fe(CO)(H)Br]$ due to the similarity with the hydride signal of complex **14** and the characteristic phosphorus-hydrogen J coupling constant measured.

When ^{tBu}PONOP was reacted with $FeBr_2$ in THF under pressure of CO a pale orange powder was obtained, differently from the intense blue color observed for both **22** and **13**. Moreover, no characteristic CO band was detected in the FT-IR spectrum of the powder. The ^{1}H-NMR spectrum exhibited broad signals typical of a paramagnetic compound, while the ^{31}P-NMR showed two broad signals at δ 153.10 ppm and δ 132.27 ppm.

Analysis of the crystals obtained by dissolution of the powder in THF revealed the decomposition of the ^{tBu}PONOP ligand.

As recently reported in literature[28], when $FeCl_2$ was used as metal precursor and mixed in presence of the ^{tBu}PONOP ligand in THF, [(^{tBu}PONOP)FeCl$_2$] formed as paramagnetic yellow product. Noteworthy, this species did not react in presence of CO to form a stable low spin iron-^{tBu}PONOP species.

4.2.3 Structure of Fe complexes

The solid state structures of complexes **22** and **23** were determined by X-Ray crystallography. The thermal ellipsoids are drawn at 30% probability and the hydrogen atoms are omitted for clarity in all the structure reported in this section.

The crystal structure of **22** showed a distorted octahedral geometry at the Fe center with the two bromine ligands *trans* to one another, and the CO ligand *trans* to the nitrogen of the pyridine (Fig. 4.2).

Fig. 4.2: X-Ray structure of **22**. The nitrogen atom is depicted in blue, phosphorous atoms in yellow, the bromine in green and the oxygen ones in red. Selected bond lengths [Å] and angles [°]:Fe(1)-C(3) 1.7830, Fe(1)-N(1) 1.9968, Fe(1)-P(1) 2.25871, Fe(1)-P(2) 2.2503, Fe(1)-Br(1) 2.4690, Fe(1)-Br(2) 2.4511, P(1)-Fe(1)-P(2)163.42.

In the same fashion, complex **23** showed a distorted a distorted octahedral geometry at the Fe center. The two Fe-halogen bonds are shorter than in **22** and the CO ligand is *trans* to the nitrogen of the pyridine (Fig. 4.3).

Fig. 4.3: X-Ray structure of **23**. The nitrogen atoms are depicted in blue, phosphorous atoms in yellow, the bromines in green and the oxygen ones in red. Selected bond lengths [Å] and angles [°]: Fe(1)-C(3) 1.7823, Fe(1)-N(1) 2.0043, Fe(1)-P(1) 2.2582, Fe(1)-P(2) 2.2465, Fe(1)-Cl(1) 2.3368, Fe(1)-Cl(2) 2.2986.

4.2.4 Hydrogenation reaction

Although it was not possible to synthesize and isolate an iron-hydride complex bearing the ^{Cy}PONOP ligand, complex **22** and **23** were tested as catalyst for the hydrogenation of unsaturated substrate.

As standard condition, substrates such as benzaldehyde and acetophenone were tested in either MeOH, EtOH, ^{i}PrOH, CH_2Cl_2 or THF as solvent. As bases NaO^{t}Bu, NaO^{i}Pr, KO^{t}Bu, HCOONa and NaOMe were employed in slightly excess regarding the catalyst loading (10 or 20 mol %) and the reaction vessels ware pressurized at 4 bar (Scheme 4.5).
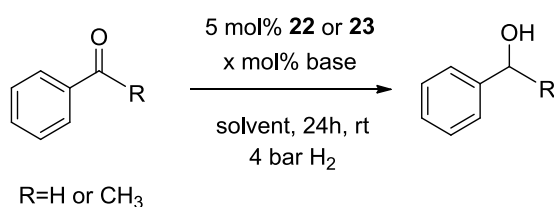
Scheme 4.5: Reaction conditions used for the hydrogenation reaction. Substrate (0.3 mmol), base (10/20 mol %), catalyst (0.015 mmol, 5 mol %), H_2 (4 bar), solvent (3 ml).

The reaction was performed also in absence of base and with a higher pressure of H_2 (8 bar). Unfortunately, no substrate was hydrogenated to the corresponding alcohol by using either **22** or **23**, as confirmed by GC-MS analysis.

4.3   Replacement of CO with the isoelectronic ^{tBu}isocyanide

As second attempt to synthesize new Fe-PONOP complexes with an enhanced reactivity, the CO ligand was replaced by the better donor ligand *tert*-butyl isocyanide in presence of ^{iPr}PONOP as pincer ligand.

4.3.1   Synthesis of Fe complexes

By reacting ^{iPr}PONOP with FeBr$_2$ in THF and 1 equiv. of ^{t}BuNC the complex [(^{iPr}PONOP)Fe(^{t}BuNC)Br$_2$] (**24**) was obtained as an apple green powder in very high yield (Scheme 4.6). Complex **24** is a diamagnetic complex exhibiting a characteristic singlet at δ 216.75 ppm in the ^{31}P-NMR spectrum. The Fe-bound CN ligand gives a strong IR band at 2121 cm^{-1}. Suitable crystals for X-Ray analysis were obtained by diffusion of n-pentane in a saturated solution of **24** in THF.
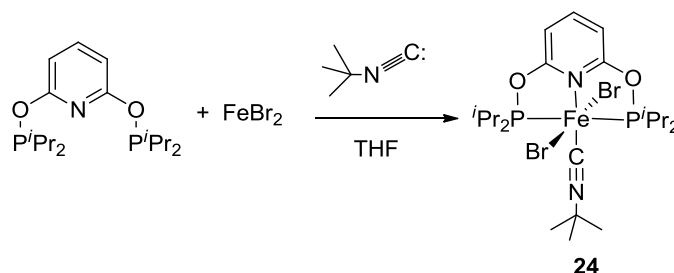
Scheme 4.6: Synthesis of complex **24.**

Complex **24** was reacted in presence of NaEt$_3$BH and NaBH$_4$ as hydride sources in order to synthesize the analogous iron-hydride species.

When NaEt$_3$BH was used (different equivalent), only a mixture of several species was detected in solution by ^{1}H-NMR, included the iron-hydride species [(^{iPr}PONOP)Fe-(^{t}BuNC)(H)Br] (**25**) that showed a characteristic triplet at δ -20.07 ppm. Unfortunately, it was not possible to isolate complex **25** since an oil appeared after evaporation of the solvent from the reaction mixture. When the oil was dissolved in CH$_2$Cl$_2$ few yellow crystals formed by addition of an excess of pentane. The X-Ray analysis confirmed the formation of **25** (Fig. 4.5 in section 4.3.2).

Differently, when NaBH$_4$ was used as hydride source the iron-hydride species **25** formed as only product (Scheme 4.7).
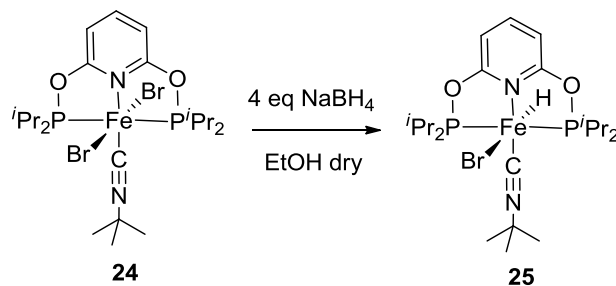
Scheme 4.7: Synthesis of complex **25**

Complex **25** is a low spin diamagnetic yellow powder exhibiting a characteristic singlet at δ 244.06 ppm in the ^{31}P-NMR spectrum. The Fe-bound ^{t}BuNC ligand gives a strong IR band at 1977 cm^{-1} and the structure was confirmed by ESI-Mass analysis.

4.3.2   Structure of Fe complexes

The solid state structures of complexes **24** and **25** were determined by X-Ray crystallography. The thermal ellipsoids are drawn at 30% probability and the hydrogen atoms are omitted for clarity.

The crystal structure of **24** showed a distorted octahedral geometry at the Fe center with the two bromine ligands *trans* to one another, and the ^{t}BuNC ligand *trans* to the nitrogen of the pyridine (Fig. 4.4).
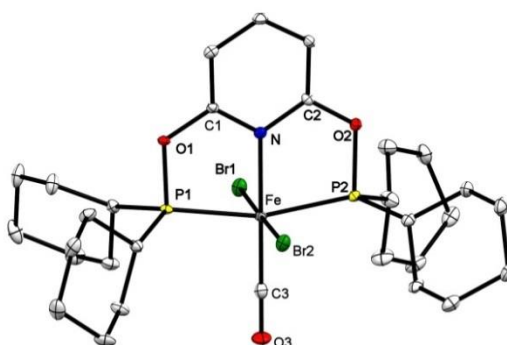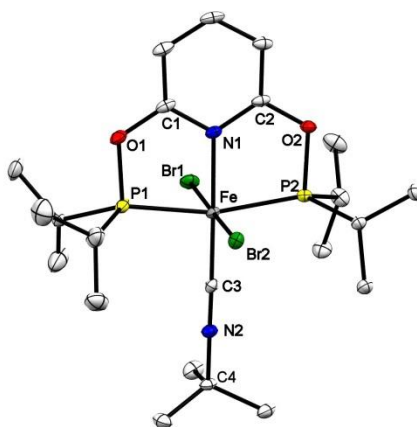

Fig. 4.4: X-Ray structure of **24**. The nitrogen atoms are depicted in blue, phosphorous atoms in yellow, the bromines in green and the oxygen ones in red. Selected bond lengths [Å] and angles [°]: Fe(1)-C(3) 1.8428, Fe(1)-N(1) 1.9878, Fe(1)-P(1) 2.2464, Fe(1)-P(2) 2.2422, Fe(1)-Br(1) 2.4809, Fe(1)-Br(2) 2.4773.

Similarly, complex **25** showed a distorted octahedral geometry at the Fe center. The bromine atoms are *trans* to the hydride ligand while the ^{t}BuNC ligand is *trans* to the nitrogen of the pyridine (Fig. 4.5).
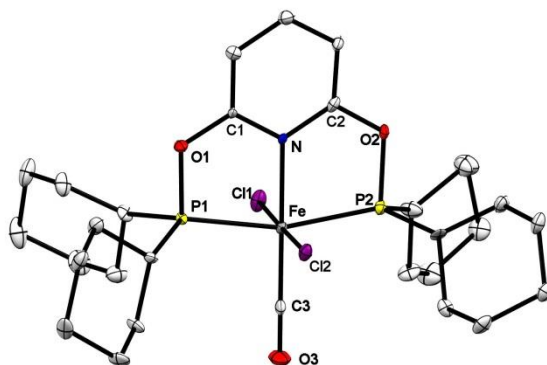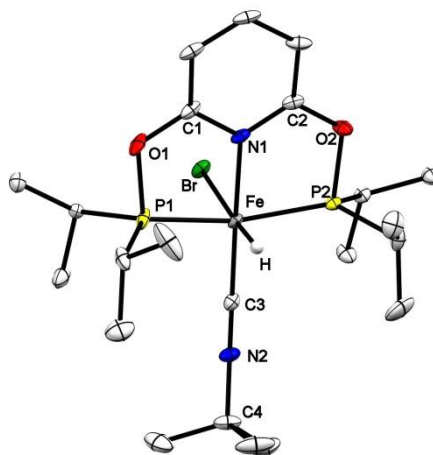
Fig. 4.5: X-Ray structure of **25**. The nitrogen atoms are depicted in blue, phosphorous atoms in yellow, the bromines in green and the oxygen ones in red. Selected bond lengths [Å] and angles [°]: Fe(1)-C(3) 1.8207, Fe(1)-N(1) 1.9857, Fe(1)-P(1) 2.1757, Fe(1)-P(2) 2.1679, Fe(1)-Br(1) 2.5625, Fe(1)-H(1) 1.434.

4.3.3   Hydrogenation and HT reactions

Complex **24** and the corresponding iron-hydride **25** were tested as potential catalysts for both hydrogenation and HT reactions.

As standard condition for the hydrogenation reaction, substrates with a carbonyl group such as benzaldehyde, acetophenone and with a C-C double bond such as cyclohexene and 1-decene were tested in either MeOH, EtOH, ^{i}PrOH, CH_2Cl_2 or THF as solvent. As bases NaO^{t}Bu, NaO^{i}Pr, KO^{t}Bu, HCOONa and NaOMe were employed in slightly excess regarding the catalyst loading (10 or 20 mol %). The reaction vessels were pressurized at 4 bar (Scheme 4.8).
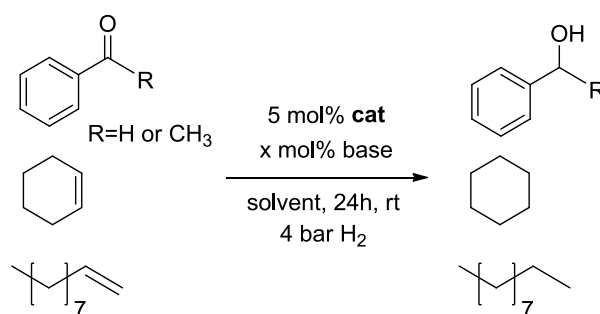
Scheme 4.8: Reaction conditions used for the hydrogenation reaction. Substrate (0.3 mmol), base (10/20 mol %), catalyst (0.015 mmol, 5 mol %), H_2 (4 bar), solvent (3 ml).

Complex **24** did not show any reactivity for the hydrogenation of unsaturated substrate also when the reaction was performed in absence of a base and with a higher pressure of H_2 (8 bar).

Differently, **25** served as catalyst for the hydrogenation of benzaldehyde. As reported for the analogous iron pincer complex [(^{iPr}PONOP)Fe(CO)(H)Br$_2$] (**14**), the best performance could be achieved in MeOH using 5 mol% of catalyst loading, 10 mol% of HCOONa as base, at room temperature, under 4 bar of H$_2$, and within 24 h reaching 90 % yield (Scheme 4.9). No reaction was observed in presence of acetophenone, cyclohexene and 1-decene. Full conversion of benzaldehyde was observed in absence of base and with a higher pressure of H$_2$ (8 bar).
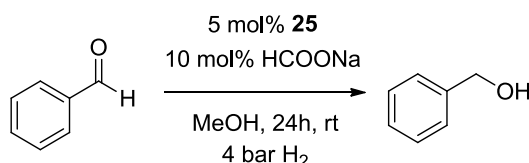
Scheme 4.9: Reaction conditions for the hydrogenation reaction of benzaldehyde using **25** as catalyst. Substrate (0.3 mmol), base (10/20 mol %), catalyst (0.015 mmol, 5 mol %), H$_2$ (4 bar), solvent (3 ml). Yield of alcohol determined by calibrated GC analysis.

The promotion of catalytic hydrogenation by HCOONa described above suggested that complex **25** might be used as transfer hydrogenation catalysts in presence of HCOONa as hydride source. As expected complex **25** catalysed the reduction of benzaldehyde in presence of 5 equiv. of HCOONa, at 40 ^{o}C, in 6 hours and in 95% yield (Scheme 4.10) as reported for the analogous iron pincer complex **14**. Unfortunately, no reaction was observed when acetophenone, cyclohexene and 1-decene were used as substrates.
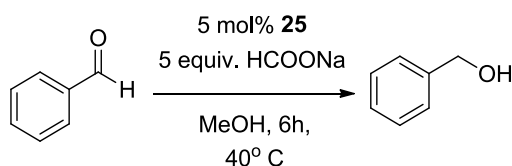
Scheme 4.10: Reaction conditions for the HT reaction of benzaldehyde using **25** as catalyst. Substrate (0.3 mmol), HCOONa (0.0015 mol, 5 equiv.), catalyst (0.015 mmol, 5 mol%), in MeOH (3 mL), at 40^{0}C, 6h. Yield of alcohol determined by calibrated GC analysis.

4.4 PON bidentate ligand

In this section, the attempts to synthesise low spin iron (II) complexes bearing the ^{iPr}PON bidentate ligand are reported. The iron complexes synthesized were further investigated as catalyst for hydrogenation reaction of unsaturated substrates.

4.4.1 Ligand Synthesis

The two ^{iPr}PON bidentate ligands were synthesized starting respectively from the 2-hydroxypyridine and the 2-hydroxy-6-methylpyridine by following the already reported procedure used for the analogous tridentate ^{iPr}PONOP (Scheme 4.11). High yields and a clean products were obtained by working with air-free techniques.
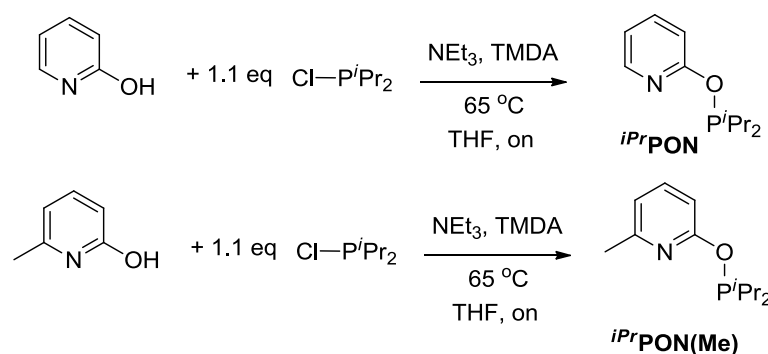
Scheme 4.11: Synthesis of the ^{iPr}PON and ^{iPr}PON(Me) bidentate ligands.

The ^{iPr}PON ligand exhibited a characteristic signal at δ 144.38 ppm in the ^{31}P- NMR few ppm lower than ^{iPr}PONOP (δ 146.80) while the ^{iPr}PON(Me) at δ 143.41 ppm.

4.4.2 Metallation using iron salts

Although the preparation of the ^{iPr}PON and ^{iPr}PON(Me) bidentate ligands was straightforward, the metalation using different iron precursors resulted more complicated.

When ^{iPr}PON was stirred in presence of FeBr$_2$ a red oil formed. ^{1}H-NMR analysis of the oil showed a paramagnetic species present in solution while in the ^{31}P-NMR no signals were detected. The red oil was reacted with CO (0.5 bar) but no carbonyl bands were observed in the FT-IR spectrum of the final product.

The reaction of 2 equiv. of ^{iPr}PON with FeBr$_2$ led to the formation of a whitish powder. Neither ^{1}H-NMR nor ^{31}P-NMR analysis on the powder was possible due to the paramagnetic nature of the product, but the X-Ray analysis on the crystals showed the

decomposition of the ligand with the concomitant formation of a cationic *exa*-coordinated iron species, complex **26** (Scheme 4.12).
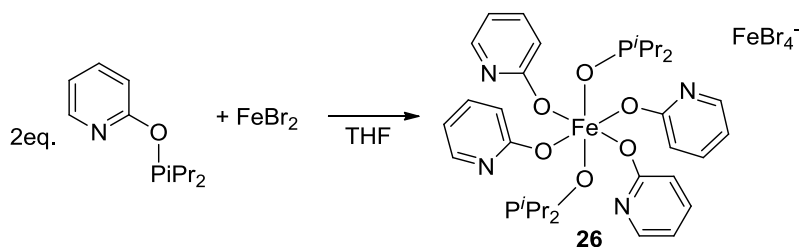
Scheme 4.12: Decomposition of the ^{iPr}PON ligand and formation of complex **26**.

When $Fe(CO)_5$ was used as iron precursor, the ^{iPr}PON did not metalate the iron center as evidenced by both the ^{1}H-NMR and ^{31}P-NMR spectra.

In order to obtain stable Fe-^{iPr}PON complexes a different iron precursor was synthesized: the complex (benzylideneacetone)iron tricarbonyl.

This red coloured compound abbreviated $[Fe(CO)_3(bda)]$ is a reagent very well known in organometallic chemistry, principally used for transferring the $Fe(CO)_3$ unit to other organic molecules[29-31]. $[Fe(CO)_3(bda)]$ was reacted with 1 equiv. of ^{iPr}PON and the expected $[Fe(CO)_3(^{iPr}PON)]$ (**27**) formed as clean orange product in 42 % yield (Scheme 4.13).
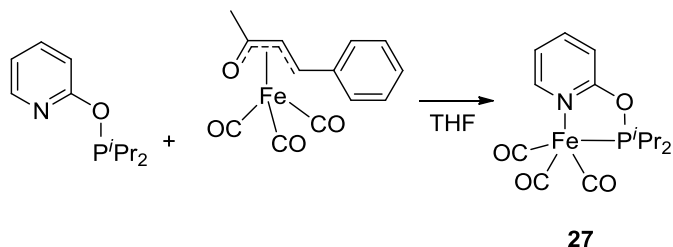
Scheme 4.13: Synthesis of complex **27**.

Complex **27** is a pentacoordinated diamagnetic iron (0) compound, exhibiting a characteristic signal at δ 237.63 ppm in the ^{31}P-NMR spectrum. The Fe-bound CO ligands give strong IR bands at 1976 and 1884 cm^{-1}. Unfortunately, no suitable crystals for X-Ray analysis were obtained, but the structure was confirmed by ESI- Mass analysis.

In order to synthesize a stable iron (II) species bearing the ^{iPr}PON ligand, complex 27 was oxidised in presence of either iodine (I_2) or N-Bromosuccinimide (NBS), but in both cases only a mixture of different species was detected in the ^{1}H-NMR and ^{31}P-NMR spectra.

4.4.3 Hydrogenation and HT reactions

Complex **27** was tested as catalyst for both hydrogenation and hydrogen transfer reaction.

As standard condition, substrates such as benzaldehyde and acetophenone were tested in either MeOH, EtOH, ^{i}PrOH, CH_2Cl_2 or THF as solvent. As bases NaO^{t}Bu, NaO^{i}Pr, KO^{t}Bu, HCOONa and NaOMe were employed in slightly excess regarding the catalyst loading (10 or 20 mol %) and the reaction vessels were pressurized at 4 bar (Scheme 4.14).

R=H or CH$_3$
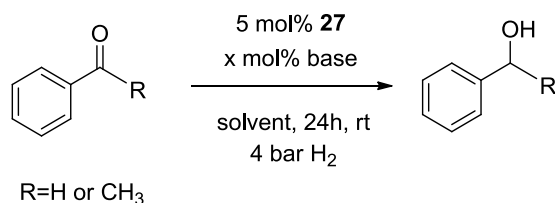
Scheme 4.14: Reaction conditions used for the hydrogenation reaction. Substrate (0.3 mmol), base (10/20 mol %), catalyst (0.015 mmol, 5 mol %), H$_2$ (4 bar), solvent (3 ml).

The reaction was performed in absence of base and with a higher pressure of H$_2$ (8 bar), but in all the cases no product was detected by GC-MS analysis. Similarly, for the HT reaction after screening different conditions, neither benzaldehyde nor acetophenone were reduced to the corresponding alcohols by using complex **27** as catalyst.

4.5 Biomimetic approach

A different approach was used with the bidentate ligand ^{iPr}PON(Me). Bearing in mind the recent results and developments in the synthesis of model iron complexes miming the active site of the iron-only hydrogenase[32-35] (scheme 4.15) a similar biomimetic approach was used to synthesize a stable iron (II) low spin complex starting from ^{iPr}PON(Me) as precursor.

R= Me, OMe
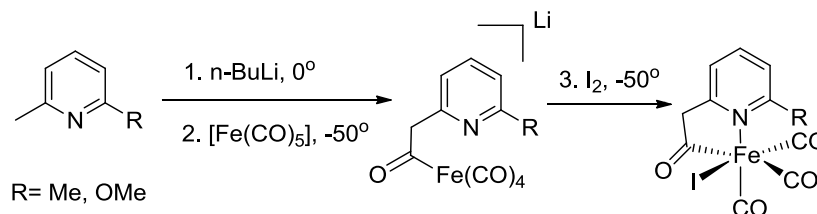
Scheme 4.15: Synthesis of the biomimetic complex [(2-CH$_2$CO-6-MeOC$_2$H$_3$N)Fe(CO)$_2$I] reported in literature[32].

As illustrated in scheme 4.15, the acylmethylpyridinyl bidentate unit was linked to the iron center by treatment of the in-situ generated methylpyridinyl anion with Fe(CO)$_5$. Successive addition of I$_2$ led to the oxidation of the iron center and the formation of a stable iron (II) low spin complex.

In the same fashion, when using the bidentate ligand ^{iPr}PON(Me), the methyl group could undergo activation in presence of n-BuLi and bind the Fe(CO)$_5$ by forming the acyl group. This procedure should lead to the formation of a new type of pincer complex with two different side arms on the tridentate ligand (Scheme 4.16).
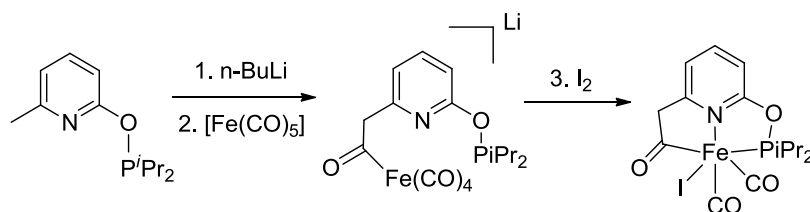
Scheme 4.16: Attempt to synthesize a stable iron pincer complex bearing the ^{iPr}PON moiety.

Different attempts were made to synthesize the asymmetric iron pincer complex showed above by following the biomimetic synthetic route, but in all the cases a mixture of products, included the unreacted ^{iPr}PON(Me), was detected in the ^{31}P-NMR spectrum.

When ^{iPr}PON(Me) was reacted in presence of [Fe(CO)$_3$(bda)] in the same fashion used for ^{iPr}PON and reported in scheme 4.14, the iron(0) complex [Fe^{iPr}PON(Me)(CO)$_3$(bda)] (**29**) formed as major species (scheme 4.17). Crystals of **28** were obtained by diffusion of n-pentane in a saturated solution of the powder in dry THF.
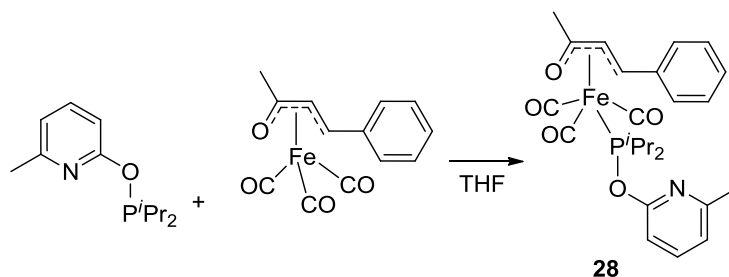
Scheme 4.17: Synthesis of complex **28**.

4.6 Conclusions

As attempt to synthesize new Fe-PONOP complexes with an enhanced reactivity, modification of the PONOP ligand resulted in the synthesis of two PONOP-type ligands: ^{Cy}PONOP and ^{tBu}PONOP. Although no metalation with iron salts was possible by using ^{tBu}PONOP as ligand, stable iron (II) low spin complexes [(^{Cy}PONOP)Fe(CO)Br$_2$] (**22**) and

[(^{Cy}PONOP)Fe(CO)Cl$_2$] (**23**) were obtained in presence of ^{Cy}PONOP, which are newly reported compounds.

The crystal structure of complexes **22** and **23** showed a distorted octahedral geometry at the Fe center for both complexes. When these compounds were used as catalysts in hydrogenation reaction, none of the substrates employed was reduced. Differently than the similar Fe-^{iPr}PONOP complex [(^{iPr}PONOP)Fe(CO)Br$_2$] (**13**), it was not possible to isolate the analogous iron-hydride species starting from either **22** or **23**.

As second attempt to synthesize new Fe-PONOP complexes, the CO ligand was replaced by the better donor ligand *tert*-butyl isocyanide in presence of ^{iPr}PONOP as pincer ligand. Complexes [(^{iPr}PONOP)Fe(^{t}BuNC)Br$_2$] (**24**) and the analogous iron-hydride [(^{iPr}PONOP)Fe(^{t}BuNC)(H)Br] (**25**) were synthesized and fully characterized. When tested as catalysts for hydrogenation and HT reactions **24** did not exhibit any reactivity, on the contrary **25** served as catalysts for hydrogenation and HT reactions of benzaldehyde. As reported for the analogous iron-hydride pincer complex [(^{iPr}PONOP)Fe(CO)(H)Br] (**14**), the best performance could be achieved in MeOH using 5 mol% of catalyst loading, 10 mol% of HCOONa as base, room temperature, under 4 bar of H$_2$, and within 24 h. No reaction was observed in presence of acetophenone, cyclohexene and 1-decene. Although spectroscopically different, **26** did not exhibit enhanced reactivity compared to **14**.

A different approach on the synthesis of stable iron (II) complexes was used by synthesizing bidentate ^{iPr}PON-type ligands: ^{iPr}PON and ^{iPr}PON(Me). The metalation using iron salts gave very complicated mixtures and only the iron (0) complex [Fe(CO)$_3$(^{iPr}PON)] (**27**) was isolated and fully characterized. No further oxidation of **27** was possible and it did not exhibit any catalytic behaviour for hydrogenation reaction of unsaturated substrates. Also the biomimetic approach used with ^{iPr}PON(Me) did not lead to the formation of a stable iron complex.

4.7   Experimental

Materials and methods:

All experiments were carried out under an inert N_2 (g) atmosphere using standard Schlenk or glovebox techniques. Solvents were purified using a two-column solid-state purification system (Innovative Technology, NJ, USA) and transferred to the glove box without exposure to air. Methanol (99.8%, extra dry, over molecular sieve) was purchased from AcroSeal®. Deuterated solvents were purchased from Cambridge Isotope Laboratories, Inc., and were degassed and stored over activated 3 Å molecular sieves. All other reagents were purchased from commercial sources and were degassed by standard freeze-pump-thaw procedures prior to use. ^{1}H and ^{31}P spectra were recorded at ambient temperature on a Bruker Avance 400 spectrometer. ^{1}H NMR chemical shifts were referenced to residual solvent as determined relative to TMS (δ 0.00ppm). GC-MS measurements were conducted on a Perkin-Elmer Clarus 600 GC equipped with Clarus 600T MS and Agilent J&W GC column, DB-5MS UI 25m, 0.250mm, 0.25 µm. IR measurements were recorded on powder samples at ambient temperature on a Varian 800 FT-IT Scimitar Series spectrometer. Elemental analyses were performed on a Carlo Erba EA 1110 CHN Instrument. HRESI-MS measurements were conducted at EPFL ISIC Mass Spectrometry Service with a Micro Mass QTOF Ultima Spectrometer.

Synthesis of ^{Cy}PONOP tridentate ligand

In a 100 ml Schlenk round bottom flask 0.381 g of 2,6-dihydroxypyridine (0.0026 mol) were suspended in 30 ml of dry THF, followed by 0.8 ml of N,N,N',N'-tetramethylethylendiamine (0.0052 mol) and 2.3 ml of Et$_3$N (0.016 mol). The reaction mixture was cooled down at 0 ^{o}C. 1.33g of (Cy)$_2$PCl (0.0057 mol) were dissolved in 20ml of dry THF and slowly added to the reaction mixture. After the mixture reached room temperature, it was refluxed at 60 ^{o}C for 20h. A fine with powder precipitated during the reaction. The reaction mixture was cooled, filtered through a fritted glass filter and dried affording a clear oil as pure product in 72 % yield.

^{1}H NMR (400MHz, CD$_2$Cl$_2$, 20°C): δ 7.46 (t, 1H, aryl-*H*), δ 6.43 (d, 2H, aryl-*H*), δ 1.91-1.67 (m, 22H, cyclohexyl-*H*), δ 1.41-1.21 ppm (m, 22H, cyclohexyl-*H*) ppm. ^{31}P-NMR (162MHz, CD$_2$Cl$_2$, 20°C): δ 142.02(s) ppm.

Synthesis of ^{tBu}PONOP ligand

The procedure reported in literature[36] was followed for the synthesis of ^{tBu}PONOP. The final product resulted in a clear oil obtained in 86 % yield. ^{1}H NMR (400MHz, CD$_2$Cl$_2$, 20°C): δ 7.51 (t, 1H, aryl-*H*), δ 6.57 (d, 2H, aryl-*H*), δ 1.18 (bs, 18H, C*H*), δ 1.15 (bs, 18H, C*H*) ppm. ^{31}P-NMR (162MHz, CD$_2$Cl$_2$, 20°C): δ 155.27 (m) ppm.

Synthesis of complex [(^{Cy}PONOP)Fe(CO)Br$_2$] (22):

0.128 g of FeBr$_2$ (0.0006 mol) and 0.3 g of ^{Cy}PONOP (0.0006 mol) were mixed in 50 mL of dry THF in an ACE round-bottom pressure flask in the glovebox and the reaction mixture was stirred for 1 h. Afterward the flask was pressurized with 0.5 bar of CO and stirred for additional 3 h. The color turned immediately from dark yellow/brown to deep blue. The solution was filtered through a PTFE filter and concentrated. n-Pentane was then added to promote the precipitation of the product as a fine blue powder that was filtered out and washed with additional n-pentane (yield: 65%). Single crystals suitable for X-ray analysis were grown by diffusion of n-pentane in a concentrated solution of complex **22** in THF.

FT-IR: ν[cm^{-1}] 1976 (s, ν$_{CO}$). ESI-MS (*m/z, pos*): 746.08 [(^{Cy}PONOP)Fe(CO)Br$_2$], 667.16 [(^{Cy}PONOP)Fe(CO)Br]$^+$.
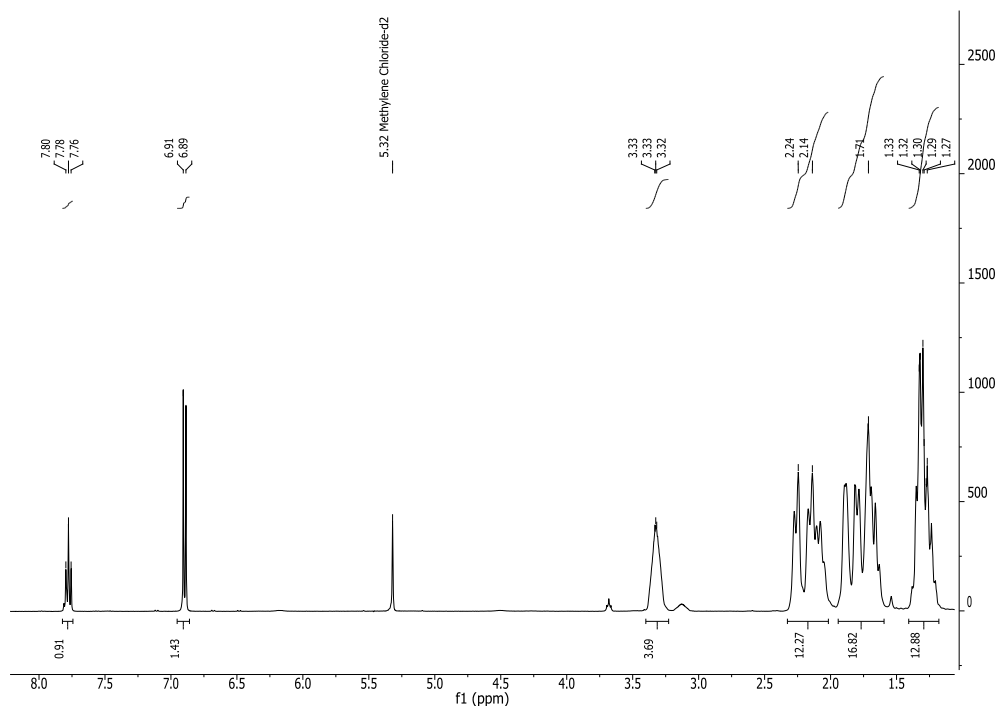
Fig. 4.6: ^{1}H NMR of **22** (400 MHz, CD$_2$Cl$_2$, 20°C)

^{1}H NMR (400MHz, CD$_2$Cl$_2$, 20°C): δ 7.78 (t, 1H, aryl-H$_4$), δ 6.90 (d, 2H, aryl-H$_{3,5}$), δ 3.33 (sept, 4H, PC*H*), δ 2.20 (m, 12H, C*H*-cyclohexyl), δ 1.90-1.71 (m, 16H, C*H*-cyclohexyl), δ 1.31 (m, 12H, C*H*-cyclohexyl) ppm. ^{31}P-NMR (162MHz, CD$_2$Cl$_2$, 20°C): δ 207.77(s) ppm. ^{31}P-NMR (162MHz, CD$_2$Cl$_2$, 20°C): δ 207.58(s) ppm. ^{13}C-NMR (101MHz, CD$_2$Cl$_2$, 20°C): δ 165.44 (t, Fe-*C*O ^{2}J$_{C-P}$ = 6.3Hz), δ 143.43 (s, aryl-C$_4$), δ 104.27 (s, aryl-H$_{3,5}$), δ 40.74 (s, PC*H*), δ 26.72-26.81 (m, C*H$_2$-*cyclohexyl) ppm.

Synthesis of complex [(^{Cy}PONOP)Fe(CO)Cl$_2$] (23)

0.115 g of FeCl$_2$·2THF (0.00043 mol) and 1 g of ^{Cy}PONOP (0. 00043 mol) were mixed in 50 mL of dry THF in an ACE round-bottom pressure flask in the glovebox and the reaction mixture was stirred for 2 h. Afterward the flask was pressurized with 0.5 bar of CO and stirred for additional 2 h. The color turned immediately from yellow to purple. The solution was filtered through a PTFE filter and concentrated. n-Pentane was added and the product precipitated as a fine purple powder. It was filtered off and washed with additional n-pentane (yield: 65%). Single crystals suitable for X-ray analysis were grown by diffusion of n-pentane in a concentrated solution of complex **23** in THF.

^{1}H NMR (400MHz, CD$_2$Cl$_2$, 20°C): δ 7.80 (t, 1H, aryl-H$_4$), δ 6.89 (d, 2H, aryl-H$_{3,5}$), δ 3.09 (m, 4H, PC*H*), δ 2.27-2.03 (m, 12H, C*H*-cyclohexyl), δ 1.89-1.67 (m, 16H, C*H*-cyclohexyl), δ 1.5-1.28 (m, 12H, C*H*-cyclohexyl) ppm. ^{31}P-NMR (162MHz, CD$_2$Cl$_2$, 20°C): δ 207.77(s) ppm. ^{13}C-NMR (101MHz, CD$_2$Cl$_2$, 20°C): δ 165.31 (t, Fe-*C*O ^{2}J$_{C-P}$ = 6.3Hz), δ 143.60 (s, aryl-C$_4$), δ 104.09 (s, aryl-H$_{3,5}$), δ 35.38 (s, PC*H*), δ 27.51-26.77 (m, C*H$_2$-*cyclohexyl) ppm. FT-IR: ν [cm^{-1}] 1977 (s, ν$_{CO}$).

Synthesis of complex [(^{iPr}PONOP)Fe(^{t}BuNC)Br$_2$] (24):

0.2 g of FeBr$_2$ (0.00093 mol) and 0.32 g of ^{iPr}PONOP (0. 00093 mol) were mixed in 30 mL of dry THF in an ACE round-bottom pressure flask in the glovebox and the reaction mixture was stirred for 2 h. 106 μl of ^{t}BuNC (0. 00093 mol) were added to the reaction mixture and stirred for additional 4 h. The color turned immediately from dark yellow/brown to apple green. The solution was filtered through a PTFE filter and concentrated. n-Pentane was then added to promote the precipitation of the product as a fine apple green powder that was filtered out and washed with additional n-pentane (yield: 71%). Single crystals suitable for X-ray analysis were grown by diffusion of n-pentane in a concentrated solution of complex **24** in THF.

FT-IR: ν[cm^{-1}] 2121 (s, ν$_{CN}$). ESI-MS (*m/z, pos*): 642.04 [(^{iPr}PONOP)Fe(^{t}BuNC)Br$_2$], 667.16 [(^{iPr}PONOP)Fe(CO)Br]$^{+}$.

^{1}H NMR (400MHz, CD$_2$Cl$_2$, 20°C): δ 7.63 (t, 1H, aryl-H$_4$), δ 6.85 (d, 2H, aryl-H$_{3,5}$), δ 3.63 (m, 4H, PC*H*), δ 1.63 (q, 12H, PCH(C*H*$_3$)$_2$), δ 1.55 (s, 9H, C*H*- ^{t}BuNC), δ 1.46 (q, 12H, PCH(C*H*$_3$)$_2$), ppm. ^{31}P-NMR (162MHz, CD$_2$Cl$_2$, 20°C): δ 216.78(s) ppm.

Synthesis of complex [(^{iPr}PONOP)Fe(^{t}BuNC)(H)Br] (25):

To a suspension of 0.232 g of **24** (0.00036 mol) in 30 ml of EtOH dry, 40 mg of NaBH$_4$ (4 equiv., 0.00144 mol) dissolved in 10 ml of dry EtOH were added. The color turned immediately from green to orange. The reaction mixture was stirred for 3 h and the solvent removed under vacuum affording a yellow/brownish powder. The powder was dissolved in a minimum amount of toluene and filtered firstly through celite and afterwards through neutral alumina. A yellow solution was collected and dried under vacuum affording **25** as yellow powder in 42 % yield.

FT-IR: ν[cm^{-1}] 1977 (s, ν$_{CN}$). ESI-MS (*m/z, pos*): 563.13 [(^{iPr}PONOP)Fe(^{t}BuNC)HBr], 483.2 [(^{iPr}PONOP)Fe(^{t}BuNC)(H)]$^{+}$.

^{1}H NMR (400MHz, CD$_2$Cl$_2$, 20°C): δ 7.32 (t, 1H, ^{3}J$_{HH}$ = 8.0 Hz, aryl-H$_4$), δ 6.41 (d, 2H, ^{3}J$_{HH}$ = 8.0 Hz, aryl-H$_{3,5}$), δ 3.29 (m, 2H, PC*H*(CH$_3$)$_2$), δ 2.78 (sept, 2H, PC*H*(CH$_3$)$_2$), δ 1.48 (m, 12H,PCH(C*H*$_3$)$_2$), δ 1.27 (s, 9H, C*H*- ^{t}BuNC), δ 1.19 (m, 6H, PCH(C*H*$_3$)$_2$), δ 0.98 (m, 6H, PCH(C*H*$_3$)$_2$), δ -19.99 (t, 1H, ^{2}J$_{HP}$ = 56.6 Hz, Fe-*H*) ppm. ^{31}P-NMR (162MHz, CD$_2$Cl$_2$, 20°C): δ 244.06(s) ppm.

Synthesis of ^{iPr}PON bidentate ligand

In a 100 ml Schlenk round bottom flask 1g of 2-hydroxypyridine (0.0105 mol) were suspended in 30 ml of dry THF, followed by 1.6 ml of N,N,N',N'-tetramethylethylendiamine (0.0105 mol) and 3.5 ml of Et$_3$N (0.0264 mol). The reaction mixture was cooled down at 0 °C. 1.93 g of (^{i}Pr)$_2$PCl (0.0126 mol) were dissolved in 20ml of dry THF and slowly added to the reaction mixture. After the mixture reached room temperature, it was refluxed at 60 °C for 20 h. A fine with powder precipitated during the reaction. The reaction mixture was cooled, passed through a fritted glass filter and dried, affording a clear oil as pure product in 95 % yield.

^{1}H NMR (400MHz, CD$_2$Cl$_2$, 20°C): δ 8.15 (m, 1H, aryl-*H*), δ 7.58 (t, 1H, aryl-*H*), δ 6.89 (t, 1H, aryl-*H*), δ 6.82 (d, 1H, aryl-*H*), δ 1.97 (m, 2H, PC*H*), δ 1.17-1.08 ppm (m, 12H, PCH(C*H$_3$*)$_2$) ppm. ^{31}P-NMR (162MHz, CD$_2$Cl$_2$, 20°C): δ 144.38(m) ppm.

Synthesis of ^{iPr}PON(Me) bidentate ligand

1.09 g of 2-hydroxy-6-metylpyridine (0.01 mol) were suspended in 30 ml of dry THF, followed by 1.6 ml of N,N,N',N'-tetramethylethylendiamine (0.0105 mol) and 4.3 ml of Et$_3$N (0.0324 mol) in a 100 ml Schlenk round bottom flask. The reaction mixture was cooled down at 0 °C and 1.675g of (^{i}*Pr*)$_2$PCl (0.011 mol) dissolved in 20 ml of dry THF were slowly added to the reaction mixture. After the mixture reached room temperature, it was refluxed at 60 °C for 20 h. A fine with powder precipitated during the reaction. The reaction mixture was cooled, passed through a fritted glass filter and dried, affording a clear oil as pure product in 78 % yield.

^{1}H NMR (400MHz, CD$_2$Cl$_2$, 20°C): δ 8.49 (m, 1H, aryl-*H*), δ 7.51 (t, 1H, aryl-*H*), δ 6.83 (m, 2H, aryl-*H*), δ 2.50 (m, 2H, PC*H*), δ 1.27-1.17 ppm (m, 12H, PCH(C*H$_3$*)$_2$) ppm. ^{31}P-NMR (162MHz, CD$_2$Cl$_2$, 20°C): δ 237.64(m) ppm.

Synthesis of the precursor [Fe(CO)$_3$(bda)]:

For the synthesis of the iron(0) precursor [Fe(CO)$_3$(bda)] the procedure reported in literature was followed[29].

Synthesis of complex [(^{iPr}PON)Fe(CO)$_3$] (27):

0.4g of [Fe(CO)$_3$(bda)] were dissolved in 30ml of dry THF. To this solution 0.3g of ^{iPr}PON (0.00142mol) dissolved in 20ml of THF were added. The color turned from orange to intense red within 1h and the reaction mixture was stirred overnight. The day after the solution was filtered and dried affording a red oil. By addition of an excess of n-pentane and by cooling down the reaction mixture an orange powder precipitated, and it was filter off, washed with additional n-pentane and dried under vacuum. The orange product was obtained in 42% yield.

FT-IR: ν[cm^{-1}] 1976 (s, ν$_{CO}$), 1884 (sb, ν$_{CO}$). ^{1}H NMR (400MHz, CD$_2$Cl$_2$, 20°C): δ 7.46 (t, 1H, aryl-*H*), δ 6.75 (t, 1H, aryl-*H*), δ 6.64 (d, 1H, aryl-*H*), δ 2.42 (s, 3H, CC*H$_3$*), δ 1.96 (m, 2H, PC*H*), δ 1.21-1.11 ppm (m, 12H, PCH(C*H$_3$*)$_2$) ppm. ^{31}P-NMR (162MHz, CD$_2$Cl$_2$, 20°C): δ 237.64(m) ppm.

Biomimetic Attempts by using ^{iPr}PON(Me) moiety.

For the biomimetic attempts to synthesize iron pincer complex bearing the ^{iPr}PON moiety, the procedure reported for the [Fe]-Hydrogenases models in literature was used[33]. Further modifications (amounts and temperature) were also tested.

General procedure for catalytic hydrogenation

A 35 mL ACE pressure tube was charged with catalyst (0.03 mmol), substrate (0.3 mmol), base (10/20 mol %, 0.3-0.6 mmol), dodecane (30μL, 0.133 mmol), 3 mL of dry solvent and 8 bar of hydrogen. The solution was stirred at ambient temperature (20-22 °C) for 24 h. The reaction was quenched by exposure to air and by addition of diethyl ether. The alcohol products were identified and quantified by GC-MS with dodecane as an internal standard. External calibration curves were made using the commercial available products (purity >98%) or the isolated ones with dodecane as an internal standard.

General procedure for transfer hydrogenation

In a vial were placed the catalyst (0.015 mmol), the substrate (0.3 mmol), dodecane (30μL, 0.133 mmol), base (0.0015 mol, 5 equiv.) and 3 mL of dry solvent. The solution was stirred at 40 °C for 6h. The reaction was quenched by exposure to air and by addition of diethyl ether. The alcohol products were identified and quantified by GC-MS with dodecane as an internal standard. External calibration curves were made using the commercial available products (purity >98%) or the isolated ones with dodecane as an internal standard.

X-ray Crystallography

The diffraction data were measured using Mo Kα radiation on a Bruker APEX II CCD diffractometer equipped with a kappa geometry goniometer. The datasets were reduced by EvalCCD[37] and then corrected for absorption[38]. The data were measured using Cu Kα radiation on an Agilent Technologies SuperNova dual system in combination with an Atlas CCD detector. The data reduction was carried out by Crysalis PRO[39]. The solutions and refinements were performed by SHELX[40] .The crystal structures were refined using full-matrix least-squares based on F^2 with all non hydrogen atoms anisotropically defined. Hydrogen atoms were placed in calculated positions by means of the "riding" model.

X-ray Structural Analysis of 22:

Crystal Data: $C_{30}H_{47}Br_2FeNO_3P_2$, 0.34 x 0.29 x 0.11mm^3, Monoclinic, P 2_1/c, a=16.3743(17) Å, b=8.4836(11) Å, c=23.797(3)Å, α= 90°, β= 101.499(7)°, γ= 90°. T= 293(2) K, V= 3239.4(7) Å^3, Z= 4, ρ_c= 1.532 Mg/m^3, μ= 3.063 mm^{-1}.

Data Collection and Processing: 40750 reflections collected, -21 ≤ h ≤ 21, -10 ≤ k ≤ 11, -27 ≤ l ≤ 30, 7426 [R(int) = 0.0680].

Solution and refinement: Refinement method used Full-matrix least-squares on F^2. 7426 data with 138 restraints and 398 parameters. Goodness-of-fit on F^2=1.116, largest diff. peak= 0.720 e.Å^{-3} and hole= -0.810 e.Å^{-3}. Final R indices [I>2σ(I)]: R1 = 0.0492, wR2 = 0.0884. R indices (all data): R1 0.0830, wR2 = 0.1020.

Table 4.1. Selected bond lengths and angles for **22.**

	Bond length [Å]		Bond angles [°]
Br(1)-Fe(1)	2.4690(7)	Br(1)-Fe(1)-Br(2)	178.83(3)
Br(2)-Fe(1)	2.4512(7)	C(3)-Fe(1)-N(1)	179.73(17)
Fe(1)-C(3)	1.781(4)	N(1)-Fe(1)-P(1)	81.66(10)
Fe(1)-N(1)	1.996(3)	C(3)-Fe(1)-P(1)	98.20(13)
Fe(1)-P(1)	2.2570(12)	N(1)-Fe(1)-Br(1)	89.13(9)
Fe(1)-P(2)	2.2501(12)	P(1)-Fe(1)-P(2)	163.43(5)

X-ray Structural Analysis of 23:

Crystal Data: $C_{30}H_{48}Cl_2FeNO_3P_2$, 0.45 x 0.31 x 0.28 mm^3, Monoclinic, P 2_1/n, a= 18.937(3) Å, b=8.6178(12) Å, c=20.528(3)Å, α= 90°, β= 106.349(11)°, γ= 90°. T= 293(2) K, V= 3214.62 Å^3, Z= 4, ρ_c= 1.369 Mg/m^3, μ= 6.018 mm^{-1}.

Data Collection and Processing: 20494 reflections collected, -13 ≤ h ≤ 13, -16 ≤ k ≤ 11, -23 ≤ l ≤ 23, 5825 [R(int) = 0.0564].

Solution and refinement: Refinement method used Full-matrix least-squares on F^2. 5825 data with 0 restraints and 352 parameters. Goodness-of-fit on F^2=1.034, largest diff. peak= 0.693 e.Å^{-3} and hole= -0.475 e.Å^{-3}. Final R indices [I>2σ(I)]: R1 = 0. 0583, wR2 = 0.1584. R indices (all data): R1 = 0. 0646, wR2 = 0. 1693.

Table 4.2. Selected bond lengths and angles for **23.**

	Bond length [Å]		Bond angles [°]
Cl(1)-Fe(1)	2.3368	Cl(1)-Fe(1)-Cl(2)	178.54
Cl(2)-Fe(1)	2.2986	C(3)-Fe(1)-N(1)	179.42
Fe(1)-C(3)	1.7823	N(1)-Fe(1)-P(1)	81.80
Fe(1)-N(1)	2.0043	C(3)-Fe(1)-P(1)	97.90
Fe(1)-P(1)	2.2582	N(1)-Fe(1)-Cl(2)	89.86
Fe(1)-P(2)	2.2465	P(1)-Fe(1)-P(2)	163.43

X-ray Structural Analysis of 25:

Crystal Data: $C_{22}H_{40}Br_2FeN_2O_2P_2$, 0.35 x 0.33 x 0.25 mm^3, Triclinic, P-1, a = 9.3732(14) Å, b = 10.0051(3) Å, c = 16.7941(17) Å, α= 106.814(6)°, β=90.067(10)°, γ= 106.957(5)°. T= 100(2) K, V= 1435.8(3) Å^3, Z= 2, ρ_c= 1.485 Mg/m^3, μ= 3.440 mm^{-1}.

Data Collection and Processing: 20860 reflections collected, -12 ≤ h ≤ 12, -12 ≤ k ≤ 12, -21 ≤ l ≤ 21, 6473 [R(int) = 0.0222].

Solution and refinement: Refinement method used Full-matrix least-squares on F^2. 6473 data with 141 restraints and 351 parameters. Goodness-of-fit on F^2=1.129, largest diff. peak= 0.505 e.Å^{-3} and hole= -0.461 e.Å^{-3}. Final R indices [I>2σ(I)]: R1 = 0.0261, wR2 = 0.0483, R indices (all data): R1 = 0.0413, wR2 = 0.0541.

Table 4.3. Selected bond lengths and angles for **25.**

	Bond length [Å]		Bond angles [°]
Br(1)-Fe(1)	2.4808(4)	Br(1)-Fe(1)-Br(2)	178.228(15)
Br(2)-Fe(1)	2.4777(4)	C(3)-Fe(1)-N(1)	176.43(8)
Fe(1)-C(3)	1.842(2)	N(1)-Fe(1)-P(1)	82.22(5)
Fe(1)-N(1)	1.9890(17)	C(3)-Fe(1)-P(1)	97.82(6)
Fe(1)-P(1)	2.2458(6)	N(1)-Fe(1)-P(2)	82.49(5)
Fe(1)-P(2)	2.2409(7)	P(1)-Fe(1)-P(2)	164.67(2)

X-ray Structural Analysis of 26:

Crystal Data: $C_{22}H_{41}BrFeN_2O_2P_2$, 0.44 x 0.24 x 0.20 mm^3, Monoclinic, P2$_1$/n, a= 10.5486(10) Å, b=15.8895(17) Å, c=16.3846(8) Å, α= 90.0°, β=94.448(7)°, γ=90.0°. T=

100(2) K, V= 2738.0(4) Å^3, Z= 4, ρ_c= 1.366 Mg/m^3, μ= 2.147 mm^{-1}.

Data Collection and Processing: 38684 reflections collected, -14 ≤ h ≤ 14, -22 ≤ k ≤ 22, -23 ≤ l ≤ 22, 7962 [R(int) = 0.0496].

Solution and refinement: Refinement method used Full-matrix least-squares on F^2. 7962 data with 8 restraints and 316 parameters. Goodness-of-fit on F^2=1.162, largest diff. peak= 0.518 e.Å^{-3}and hole= -0.666 e.Å^{-3}. Final R indices [I>2σ(I)]: R1 = 0.0393, wR2 = 0.0587, R indices (all data): R1 = 0.0841, wR2 = 0.0736.

Table 4.4. Selected bond lengths and angles for **26.**

	Bond length [Å]		Bond angles [°]
Br(1)-Fe(1)	2.5625(4)	Br(1)-Fe(1)-H(1)	176.7(11)
H(1)-Fe(1)	1.41(3)	C(3)-Fe(1)-N(1)	173.83(10)
Fe(1)-C(3)	1.819(3)	N(1)-Fe(1)-P(1)	82.41(7)
Fe(1)-N(1)	1.986(2)	C(3)-Fe(1)-P(1)	98.42(8)
Fe(1)-P(1)	2.1724(8)	N(1)-Fe(1)-P(2)	82.47(7)
Fe(1)-P(2)	2.1675(8)	P(1)-Fe(1)-P(2)	163.35(3)

4.8 References

(1) Benito-Garagorri, D.; Kirchner, K. *Acc. Chem. Res.* **2008**, *41*, 201.

(2) van Koten, G.; Gebbink, R. J. M. K. *Dalton Trans.* **2011**, *40*, 8731.

(3) Koten, G. v. *Pure & Appl. Chem.* **1989**, *61*, 1681.

(4) Moulton, C. J.; Shaw, B. L. *J. Chem. Soc., Dalton Trans.***, 1976**, 1020.

(5) Ramozzi, R.; Cheron, N.; Braida, B.; Hiberty, P. C.; Fleurat-Lessard, P. *New J. Chem.* **2012**, *36*, 1137.

(6) Stephany, R. W.; de Bie, M. J. A.; Drenth, W. *Organic Magnetic Resonance* **1974**, *6*, 45.

(7) Ugi, I.; Fetzer, U.; Eholzer, U.; Knupfer, H.; Offermann, K. *Angew.Chem. Int. Ed.* **1965**, *4*, 472.

(8) Hahn, F. E. *Angew.Chem. Int. Ed.***1993**, *32*, 650.

(9) Dart, J. W.; Lloyd, M. K.; Mason, R.; McCleverty, J. A.; Williams, *J. Chem. Soc., Dalton Trans* **1973**, 1747.

(10) Bassett, J.-M.; Farrugia, L. J.; Stone, F. G. A. *J. Chem. Soc., Dalton Trans* **1980**, 1789.

(11) Bassett, J.-M.; Barker, G. K.; Green, M.; Howard, J. A. K.; Stone, F. G. A.; Wolsey, W. C. *J. Chem. Soc., Dalton Trans* **1981**, 219.

(12) La Pierre, H. S.; Arnold, J.; Bergman, R. G.; Toste, F. D. *Inorg. Chem.* **2012**, *51*, 13334.

(13) Hieber, W.; Leutert, F. *Naturwissenschaften* **1931**, *19*, 360.

(14) Thomas, C. M.; Süss-Fink, G. *Coord. Chem. Rev.* **2003**, *243*, 125.

(15) Drozdzak, R.; Allaert, B.; Ledoux, N.; Dragutan, I.; Dragutan, V.; Verpoort, F. *Coord. Chem. Rev.* **2005**, *249*, 3055.

(16) Canovese, L.; Visentin, F.; Santo, C.; Chessa, G.; Bertolasi, V. *Organometallics* **2010**, *29*, 3027.

(17) Liu, F.; Pullarkat, S. A.; Li, Y.; Chen, S.; Yuan, M.; Lee, Z. Y.; Leung, P.-H. *Organometallics* **2009**, *28*, 3941.

(18) Grice, K. A.; Goldberg, K. I. *Organometallics* **2009**, *28*, 953.

(19) Murso, A.; Stalke, D. *Dalton Trans.* **2004**, 2563.

(20) Murso, A.; Stalke, D. *Eur.J. Inorg. Chem.* **2004**, 4272.

(21) de Boer, S. Y.; Gloaguen, Y.; Reek, J. N. H.; Lutz, M.; van der Vlugt, J. I. *Dalton Trans.***2012**, *41*, 11276.

(22) Macías-Arce, I.; Puerta, M. C.; Valerga, P. *Eur.J. Inorg. Chem.* **2010**, *2010*, 1767.

(23) Holzhacker, C.; Calhorda, M. J.; Gil, A.; Carvalho, M. D.; Ferreira, L. P.; Stoger, B.; Mereiter, K.; Weil, M.; Muller, D.; Weinberger, P.; Pittenauer, E.; Allmaier, G.; Kirchner, K. *Dalton Trans.* **2014**, *43*, 11152.

(24) Holzhacker, C.; Standfest-Hauser, C. M.; Puchberger, M.; Mereiter, K.; Veiros, L. F.; Calhorda, M. J.; Carvalho, M. D.; Ferreira, L. P.; Godinho, M.; Hartl, F.; Kirchner, K. *Organometallics* **2011**, *30*, 6587.

(25) Jiménez-Tenorio, M.; Puerta, M. C.; Valerga, P.; Moncho, S.; Ujaque, G.; Lledós, A. *Inorg. Chem.* **2010**, *49*, 6035.

(26) Kling, C.; Ott, H.; Schwab, G.; Stalke, D. *Organometallics* **2008**, *27*, 5038.

(27)   Langer, R.; Leitus, G.; Ben-David, Y.; Milstein, D. *Angew.Chem. Int. Ed.* **2011**, *50*, 2120.

(28)   DeRieux, W.-S. W.; Wong, A.; Schrodi, Y. *J. Organomet. Chem.* **2014**, *772–773*, 60.

(29)   Alcock, N. W.; Richards, C. J.; Thomas, S. E. *Organometallics* **1991**, *10*, 231.

(30)   A.S. Howell, J.; Kola, J. C.; Dixon, D. T.; Burkinshaw, P. M.; Thomas, M. J. *J. Organomet. Chem.* **1984**, *266*, 83.

(31)   Hans-Joachim Knölker, A. B., Dirk J. Bröcher, Simon Cämmerer, Wolfgang Fröhner, Peter Gonser, Holger Hermann, Daniela Herzberg, Kethiri R. Reddy and Guy Rohde *Pure Appl. Chem.* **2001**, *73*.

(32)   Chen, D.; Scopelliti, R.; Hu, X. *Angew.Chem. Int. Ed.***2011**, *50*, 5671.

(33)   Chen, D.; Scopelliti, R.; Hu, X. *Angew.Chem. Int. Ed.***2010**, *49*, 7512.

(34)   Hu, B.; Chen, D.; Hu, X. *Chem. Eur. J.* **2012**, *18*, 11528.

(35)   Hu, B.; Chen, D.; Hu, X. *Chem. Eur. J.* **2014**, *20*, 1677.

(36)   Salem, H.; Shimon, L. J. W.; Diskin-Posner, Y.; Leitus, G.; Ben-David, Y.; Milstein, D. *Organometallics* **2009**, *28*, 4791.

(37)   Duisenberg, A. J. M.; Kroon-Batenburg, L. M. J.; Schreurs, A. M. M. *Journal of Applied Crystallography* **2003**, *36*, 220.

(38)   Blessing, R. H. *Acta Crystallographica Section A* **1995**, *51*, 33.

(39)   Crysalis PRO, A. T., release 1.171.36.28, 2013.

(40)   Sheldrick, G. M. *Acta Crystallographica Section A* **2008**, *64*.

Appendix I

Metal-PONOP Complexes:
## *Synthesis and Characterization*

I.1 Novel iron(II)-PONOP complexes

In this appendix the synthesis and characterization of several new iron (II)-PONOP complexes such as [(^{iPr}PONOP)FeBr$_2$] (**29**), [(^{Cy}PONOP)FeBr$_2$] (**30**) and [(^{iPr}PONOP)-Fe(CO)(H)(PEt$_3$)] (**31**) and a different synthetic route for the synthesis of complexes **13** and **22** is described.

Complex **30** is involved in the synthesis of [(^{iPr}PONOP)Fe(CO)Br$_2$] (**13**), while **30** is involved for the synthesis of [(^{Cy}PONOP)Fe(CO)Br$_2$](**22**). Complex **31** has been synthesized to understand the mechanism of hydrogenation of aldehydes catalysed by **14** and **15**, which are reported in chapter 3.

I.1.1 Complex [(^{iPr}PONOP)FeBr$_2$]

[(^{iPr}PONOP)FeBr$_2$] (**29**) was prepared by mixing ^{iPr}PONOP with FeBr$_2$ in THF (Scheme I.1). The reaction gave **29** as a pale yellow powder in a very high yield (75 %). Due to the absence of either CO or ^{t}BuNC as 6th coordinated ligand, complex **29** is a paramagnetic, 16e$^-$ species exhibiting distorted trigonal bipyramidal geometry in the solid state (Fig. I1)
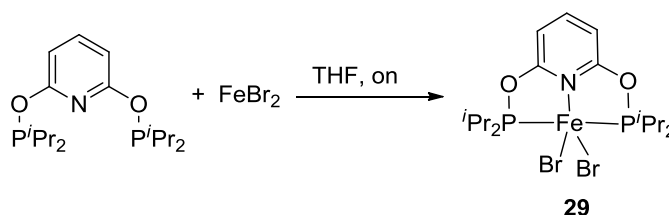
Scheme I.1: Synthesis of **29**.

Fig. I1: X-Ray structure of **29**. The thermal ellipsoids are drawn at 30% probability. The hydrogen atoms and the counter ion are omitted for clarity.

When complex **29** was solubilized in dry THF and exposed to a CO atmosphere (0.5 bar), the color turned immediately from yellow to deep blue yielding complex [(^{iPr}PONOP)Fe(CO)Br$_2$] (**13**). When ^{t}BuNC was added the color turned green yielding

[(^{iPr}PONOP)Fe(^{t}BuNC)Br$_2$](**25**). Interestingly, when solid **29** was exposed to medium pressure of CO (2 bar) it rapidly converted into solid **13** in quantitative yield.

I.1.2 Complex [(^{Cy}PONOP)FeBr$_2$]

Similarly, [(^{Cy}PONOP)FeBr$_2$] (**30**) was synthesized by reacting of ^{Cy}PONOP with FeBr$_2$ in THF (Scheme I.2). Complex **30** resulted in a paramagnetic pale yellow powder obtained in a 72% yield.
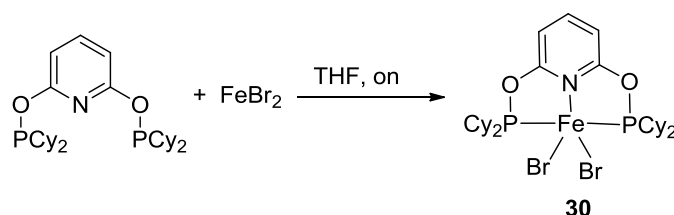
Scheme I.2: Synthesis of **30.**

When **30** was solubilized in dry THF and exposed to a CO atmosphere (0.5 bar), the color turned immediately from yellow to deep blue giving complex [(^{Cy}PONOP)Fe(CO)Br$_2$] (**22**). When ^{t}BuNC was added, the color turned green yielding complex [(^{iPr}PONOP)Fe(^{t}BuNC)Br$_2$] (**24**). As reported for **29**, exposure of **30** to CO (2 bar) gave **22** as only product in quantitative yield.

I.1.3 Complex [(^{iPr}PONOP)Fe(CO)(H)(PEt$_3$)]

Complex [(^{iPr}PONOP)Fe(CO)(H)(PEt$_3$)] (**31**) was synthesized by reacting [(^{iPr}PONOP)Fe(CO)(H)(CH$_3$CN)] (**15**) in presence of a slightly excess of triethylphosphine (PEt$_3$) (Scheme I.3). The main purpose of this synthesis was to prove that no catalytic behaviour would be observed by **31** in the hydrogenation reaction of aldehydes if the labile bromide ligand was replaced by a strong σ-donor ligand such as PEt$_3$.
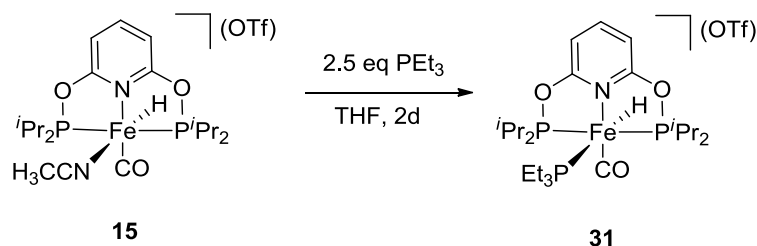
Scheme I.3: Synthesis of **31.**

As for the analogous iron complexes, the crystal structure of **31** indicated a distorted octahedral geometry. The hydride ligand is *trans* to the phosphine PEt_3, while the CO is trans to the nitrogen of the pyridine (Fig. I2).
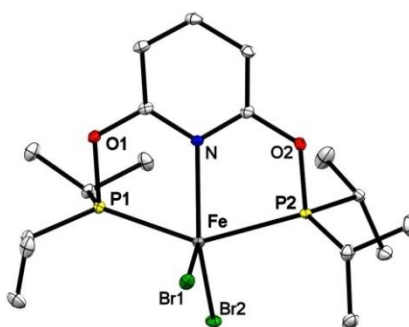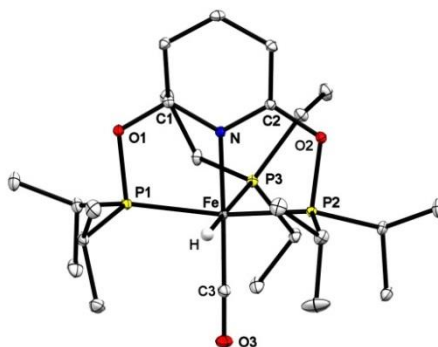

Fig. I.2: X-Ray structure of **31**; the thermal ellipsoids are drawn at 30% probability. The hydrogen atoms and the counter ion are omitted for clarity.

Complex **31** was tested as catalyst for hydrogenation reaction of benzaldehyde following the catalytic conditions reported for **14** (Scheme I.4).
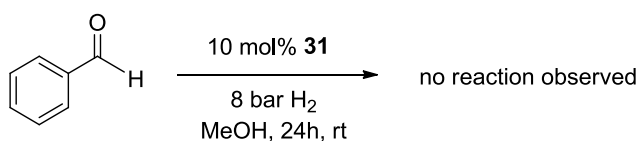
Scheme I.4: Reaction conditions used for the hydrogenation reaction. Benzaldehyde (0.3 mmol), catalyst (0.015 mmol, 5 mol %), H_2 (8 bar), solvent (3 ml).

Complex **31** did not show any catalytic activity for the hydrogenation of benzaldehyde, suggesting that the bromine dissociation in Scheme 3.9 and 3.10 (see chapter 3) is a key step for the reaction to occur.

I.1.4 Color of the Fe-PONOP complexes

The PONOP-type complexes synthesised have different colours depending on the ligands coordinated to the iron center (Fig. I3). For the bis-bromide compounds of the type [(^{X}PONOP)Fe(CO)Br$_2$] where X = ^{i}Pr or Cy, the color is blue (complexes **13** and **22**), for the analogous bis-chloride [(^{Cy}PONOP)Fe(CO)Cl$_2$] (**23**) the color is purple. When the CO was replaced by ^{t}BuNC in complex [(^{iPr}PONOP)Fe(^{t}BuNC)Br$_2$] (**24**) the color is apple green. All the remaining complexes bearing the hydride ligand show a bright yellow color (complexes **14**, **15**, **25**, and **31**).

Fig. I3: blue color (vial 1) for **13** and **22**; purple color (vial 2) for **23;** yellow color (vial 3) for **14**, **15**, **25** and **31**; apple green color (vial 4) for **24**. All complexes were dissolved in THF.

Fig. I4: UV-Vis spectra of complexes **13**, **14, 22, 23, 24** and **25.** All complexes were dissolved in dichloromethane.
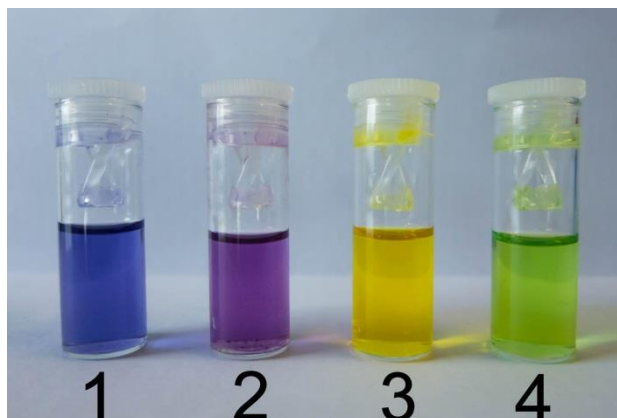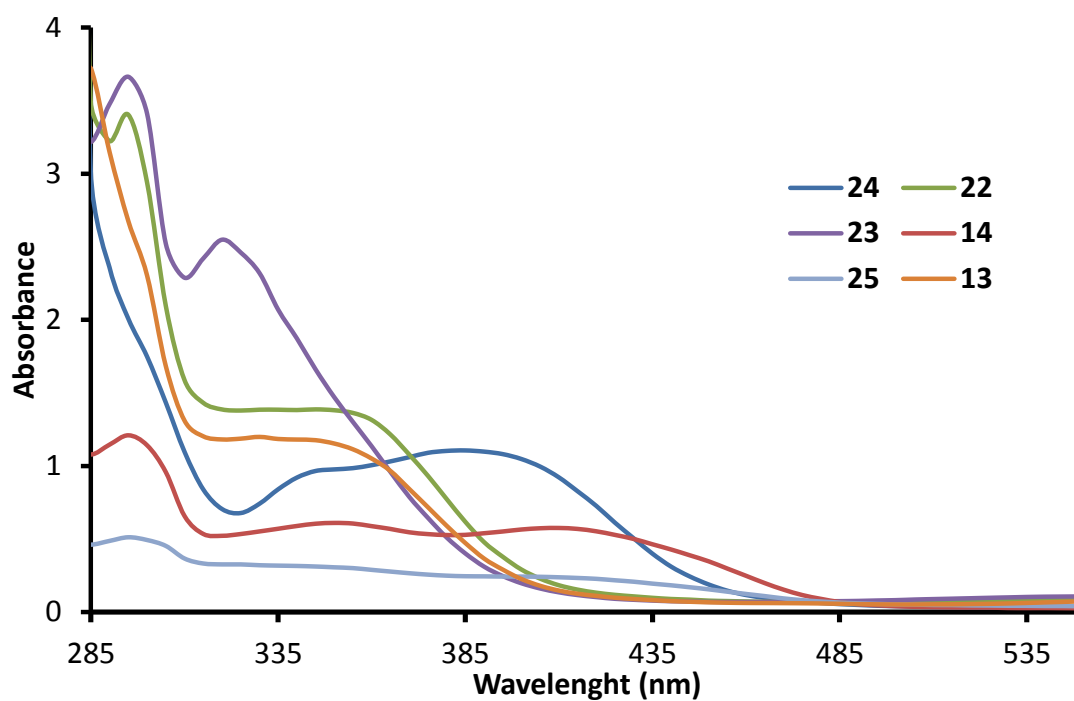
I.2 Experimental

Materials and methods:

All experiments were carried out under an inert N2 (g) atmosphere using standard Schlenk or glovebox techniques. Solvents were purified using a two-column solid-state purification system (Innovative Technology, NJ, USA) and transferred to the glove box without exposure to air. Methanol (99.8%, extra dry, over molecular sieve) was purchased from AcroSeal®. Deuterated solvents were purchased from Cambridge Isotope Laboratories, Inc., and were degassed and stored over activated 3 Å molecular sieves. All other reagents were purchased from commercial sources and were degassed by standard freeze-pump-thaw procedures prior to use. 1H and 31P spectra were recorded at ambient temperature on a Bruker Avance 400 spectrometer. 1H NMR chemical shifts were referenced to residual solvent as determined relative to TMS (δ 0.00ppm). GC-MS measurements were conducted on a Perkin-Elmer Clarus 600 GC equipped with Clarus 600T MS and Agilent J&W GC column, DB-5MS UI 25m, 0.250mm, 0.25 µm. IR measurements were recorded on powder samples at ambient temperature on a Varian 800 FT-IT Scimitar Series spectrometer. Elemental analyses were performed on a Carlo Erba EA 1110 CHN Instrument. HRESI-MS measurements were conducted at EPFL ISIC Mass Spectrometry Service with a Micro Mass QTOF Ultima Spectrometer. UV-Vis-absorption spectra were recorded with a Varian 50 Bio UV-Vis spectrometer.

Synthesis of complex [(^{iPr}PONOP)FeBr$_2$] (29):

0.627g of FeBr$_2$ (0.0029 mol) and 1g of ^{iPr}PONOP (0.0029 mol) were mixed in 30 mL of dry THF in a round-bottom flask in the glovebox and the reaction mixture was stirred overnight. The color turned yellow and then darker. The day after the solution was filtered through a PTFE filter and concentrated. Addition of n-pentane promoted the precipitation of the product as a fine pale yellow powder that was filtered off and washed with additional n-pentane (yield: 75%). Single crystals suitable for X-ray analysis were grown by diffusion of n-pentane in a concentrated solution of complex **29** in THF.

Due to the paramagnetic feature it was not possible to analyze **29** with NMR techniques. Anal. calcd. for C$_{17}$H$_{31}$Br$_2$FeNO$_2$P$_2$: C 36.52%, H 5.59%, N 2.45%. Found: C 36.57%, H 5.62%, N 2.43%. ESI-MS (*m/z, pos*) not detected.

Synthesis of complex [(^{Cy}PONOP)FeBr$_2$] (30):

0.35 g of FeBr$_2$ (0.0016 mol) were suspended in 30 ml of dry THF in a round-bottom flask in the glovebox. Afterwards 0.86g of ^{Cy}PONOP (0.0016 mol) were added and the reaction mixture was stirred for 54h. The color turned yellow and then darker. The reaction mixture was filtered through PTFE filters and concentrated. By addition of n-pentane the product as a fine pale yellow powder precipitated and it was filtered off and washed with additional n-pentane (yield: 72%).

Due to the paramagnetic nature of the compound, it was not possible to analyze **30** with NMR techniques. Anal. calcd. for C$_{29}$H$_{47}$Br$_2$FeNO$_2$P$_2$: C 48.42%, H 6.59%, N 1.95%. Found: C 48.50%, H 6.61%, N 1.97 %. ESI-MS (*m/z, pos*) not detected.

Synthesis of complex [(^{iPr}PONOP)Fe(CO)(H)(PEt$_3$)] (31):

0.1 g of [(^{iPr}PONOP)Fe(CO)(H)(CH$_3$CN)] (**15**) (0.00016 mol) was dissolved in dry THF and 0.05 g of PEt$_3$ (0.0004 mol) were added. The reaction mixture was stirred for 2 days. Successively, the solvent was removed under vacuum and the yellow powder that appeared was dissolved in a minimum amount of THF dry. By addition of an excess of n-pentane the product precipitated as fine yellow powder. The product was collected and washed with additional n-pentane (yield 64%). Crystals were obtained by diffusion of n-pentane in a saturated solution of **31** in THF.

^{1}H NMR (400MHz, CD$_2$Cl$_2$, 20°C): δ 7.75 (t, 1H, ^{3}J$_{HH}$ = 8.0 Hz, aryl-H$_4$), δ 6.76 (d, 2H, ^{3}J$_{HH}$ = 8.0 Hz, aryl-H$_{3,5}$), δ 2.98 (m, 2H, PC*H*(CH$_3$)$_2$), δ 2.86 (m, 2H, PC*H*(CH$_3$)$_2$, δ 1.61 (m, 12H, PCH(C*H$_3$*)$_2$), δ 1.48 (m, 6H, PC*H$_2$*CH$_3$), δ 1.27 (m, 9H, PCH$_2$C*H$_3$*) δ 0.94 (m, 12H, PCH(C*H$_3$*)$_2$), δ -11.81 (dt, 1H, ^{2}J$_{HP}$ = 64Hz Fe-*H*) ppm. ^{31}P-NMR (162MHz, CD$_2$Cl$_2$, 20°C): δ 235.9 (d, *PONOP*), δ 20.21(t, *P*Et$_3$) ppm.

X-ray Crystallography

The diffraction data were measured using Mo Kα radiation on a Bruker APEX II CCD diffractometer equipped with a kappa geometry goniometer. The datasets were reduced by EvalCCD and then corrected for absorption. The data were measured using Cu Kα radiation on an Agilent Technologies SuperNova dual system in combination with an Atlas CCD detector. The data reduction was carried out by Crysalis PRO. The solutions and refinements were performed by SHELX. The crystal structures were refined using full-matrix least-

squares based on F^2 with all non hydrogen atoms anisotropically defined. Hydrogen atoms were placed in calculated positions by means of the "riding" model.

X-ray Structural Analysis of 31:

Crystal Data: $C_{25}H_{47}F_3FeNO_6P_3S$, 0.49 x 0.39 x0.31mm^3, Monoclinic, P 2(1)/c, a=9.5162(5) Å, b=17.925(3) Å, c=20.0006(17)Å, α= 90.0°, β=97.485(6)°, γ=90.0°. T= 100(2) K, V= 3382.5(7) Å^3, Z= 4, ρ_c=1.366 Mg/m^3, μ= 0.702 mm^{-1}.

Data Collection and Processing: 62627 reflections collected, -16 ≤ h ≤ 16, -18 ≤ k ≤ 19, -20 ≤ l ≤ 22, 11681 [R(int) = 0.0451].

Solution and refinement: Refinement method used Full-matrix least-squares on F^2. 11681 data with 0 restraints and 376 parameters. Goodness-of-fit on F^2=1.188, largest diff. peak= 0.649 e.Å^{-3}and hole= -0.443 e.Å^{-3}. Final R indices [I>2σ(I)]: R1 = 0.0439, wR2 = 0.0806, R indices (all data): R1 = 0.0663, wR2 = 0.0902.

Table I.1. Selected bond lengths and angles for **31.**

	Bond length [Å]		Bond angles [°]
P(3)-Fe(1)	2.3290(5)	H(1)-Fe(1)-P(3)	178.2(11)
H(1)-Fe(1)	1.40(3)	C(1)-Fe(1)-N(1)	171.72(7)
Fe(1)-C(1)	1.7533(18)	N(1)-Fe(1)-P(1)	82.09(4)
Fe(1)-N(1)	1.9960(14)	C(1)-Fe(1)-P(1)	96.90(6)
Fe(1)-P(1)	2.1913(5)	N(1)-Fe(1)-P(3)	91.81(4)
Fe(1)-P(2)	2.1906(5)	P(1)-Fe(1)-P(2)	153.45(2)

Curriculum Vitae

Simona MAZZA

Nationality: Italian

✉ Avenue Mon Repos 2, CH-1005 Lausanne, Switzerland

💻 smazza1987@gmail.com

Education

Sep 11 - Sept 15	Ph.D. in Chemistry and Chemical Engineering – Swiss Federal Institute of Technology in Lausanne (EPFL) -Switzerland.
Sep 09 - Jul 11	With Honours Master in Inorganic Chemistry, University of Parma- Italy.
Sep 06 - Sep 09	B.S.Chem. University of Parma- Italy. Grade 107 out of 110.

Research Experience

- **Chemistry and Chemical Engineering Program,** *EPF Lausanne, Switzerland (Sep 2011- Aug 2015)*

Doctoral thesis research conducted with Prof. Hu Xile in the laboratory of Inorganic Synthesis and Catalysis (LSCI). Synthesized novel iron pincer complexes bearing the tridentate PONOP ligand as chemoselective catalyst for hydrogenation and hydrogen transfer reaction of aldehydes. The work resulted in a recent publication in Organometallics.

- **Department of Chemistry**, *University of Parma, Italy (Nov 2010- Jun 2011)*

Master thesis research conducted under the guidance of Dr. Pelagatti Paolo in the laboratory of Inorganic and Coordination Chemistry. Investigated innovative ruthenium based complexes (Wheel-and-Axle Metal-organic frameworks) for gas uptake reactions. The work resulted in 1 publication in Crystal Growth & Design.

- **Department of Chemistry**, *University of Parma, Italy (March 2009- Jun 2011)*

Three-month internship in the laboratory of Inorganic and Coordination Chemistry conducted with Dr. Pelagatti Paolo. Investigated MOF ruthenium based complexes for gas uptake reactions. The work resulted in 1 publication in Crystal Growth & Design.

Research Interests

My research focuses on the activation of small molecules from an organometallic and bioinorganic perspective. In particular, I have been working in hydrogen activation reaction developing synthetic models for the active site of [Fe]-hydrogenase, and well-defined iron-based systems bearing tridentate PONOP ligands. Only few iron complexes are known to activate hydrogen and the iron-PONOP systems synthesized not only activate hydrogen, but also show a catalytic reactivity and great chemoselective in the reduction of aldehydes. Kinetic studies have been performed in order to investigate the mechanism of the reaction. Accurate analytical procedures have been used for product characterization (NMR, HPLC, GC-MS, FT-IR, UV-Vis, ICP).

Teaching experience

- **Teaching assistant**

  During my Ph.D. I was enrolled as teaching assistant for bachelor students completing c.800 teaching hours (c.150 students per semester over 5 semesters). My main duty was to assist them on laboratory practical work and to correct the related reports.

- **Master students' supervisor**

I supervised three master students in their master projects over the past 2 years. I directed their research and assisted them in both the practical work in the laboratory and during the writing process of the final thesis.

Professional qualifications

Sep 14- present   **PRESIDENT - Swiss Young Chemists' Association (Switzerland)**
- Organized the 13th national 2-day "Swiss Snow Symposium" for 60+ people (all Swiss universities attended) and raised funds from leading chemical companies.
- Presented activities of the SYCA for the main board division of Fundamental Research's approval.

Feb 14- present   **SCHOLAR - PreScouter – Technology scouting R&D network**
- Collaborated with an international team proposing a set of potential technologies to improve the product quality, recycling process, and product durability on three R&D projects (each for a F500 company).

Sep 14- Dec 14   **Venture Challenge programme**
- Active participation to the "Venture challenge" course aiming at explaining how to launch a start-up and concluded with the writing of a business plan an oral examination - EPF Lausanne (Switzerland).

Publications

- **Simona Mazza**, Rosario Scopelliti and Xile Hu "Chemoselective hydrogenation and transfer hydrogenation of aldehydes catalysed by iron (II) PONOP pincer complexes" *Organometallics* **2015,** *34,* pp 1538-1545.

- Alessia Bacchi, Susan Bourne, Giulia Cantoni, Silvia A. M. Cavallone, **Simona Mazza**, Gift Mehlana, Paolo Pelagatti, Lara Righi "Reversible Guest Removal and Selective Guest Exchange with a Covalent Dinuclear Wheel-and-Axle Metallorganic Host Constituted by Half-Sandwich Ru(II) Wheels Connected by a Linear Diphosphine Axle" *Cryst. Growth Des.*, **2015,** 15 (4), pp 1876-1888.

- Alessia Bacchi, Giulia Cantoni, Matteo Granelli, **Simona Mazza**, Paolo Pelagatti, Gabriele Rispoli "Hydrogen Bond Optimization via Molecular Design for the Fabrication of Crystalline Organometallic Wheel-and-Axle Compounds Based on Half-Sandwich Ru(II) Units" *Cryst. Growth Des.,* **2011,** 11, pp 5039-5047.

Conferences

- 3rd COST-CARISMA meeting "*Catalytic Routines for Small Molecule Activation*", Tarragona, Spain, 18th-20th March **2015:** Oral presentation
- Swiss Chemical Society Fall Meeting, Zurich, Switzerland, Sept **2014:** Oral presentation
- 13th Swiss Snow Symposium, Saas-Fee, Switzerland, Feb **2015:** Poster presentation

Key skills

Laboratory machinery   Maintenance responsible of a Gas Chromatographer and Mass Spectrophotometer (daily used by c. 12 people) for a period of three year. Tasks include: installation, calibration, replacing spare parts and troubleshooting.

I.T.   **Office**: Word; Excel; Power Point; **Research databases:** SciFinder, Reaxys;
Chemistry software: MestReNova; ChemDraw; Mercury; GCMSsolution, ChemStation.

Language

Fluent: English, Italian (native), French   **Basic:** Spanish